SENSITIVITY ANALYSIS OF FLEXIBLE PAVEMENT RESPONSE

AND AASHTO 2002 DESIGN GUIDE FOR PROPERTIES OF

UNBOUND LAYERS

A Thesis

by

SANAA MASAD

Submitted to the Office of Graduate Studies of
Texas A&M University
in partial fulfillment of the requirements for the degree of

MASTER OF SCIENCE

May 2004

Major Subject: Civil Engineering

SENSITIVITY ANALYSIS OF FLEXIBLE PAVEMENT RESPONSE

AND AASHTO 2002 DESIGN GUIDE FOR PROPERTIES OF

UNBOUND LAYERS

A Thesis

by

SANAA MASAD

Submitted to Texas A&M University
in partial fulfillment of the requirements
for the degree of

MASTER OF SCIENCE

Approved as to style and content by:

Dallas N.Little	Amy Epps Martin
(Chair of Committee)	(Member)
Daren B.H. Cline	Paul N. Roschke
(Member)	(Head of Department)

May 2004

Major Subject: Civil Engineering

ABSTRACT

Sensitivity Analysis of Flexible Pavement Response and AASHTO 2002 Design Guide
for Properties of Unbound Layers. (May 2004)
Sanaa Masad, B.S., Jordan University of Science and Technology
Chair of Advisory Committee: Dr. Dallas N. Little

Unbound granular materials are generally used in road pavements as base and subbase layers. The granular materials provide load distribution through aggregate contacts to a level that can help the subgrade to withstand the applied loads.

Several research studies have shown that unbound pavement layers exhibit anisotropic properties. Anisotropy is caused by the preferred orientation of aggregates and compaction forces. The result is unbound pavement layers that have higher stiffness in the vertical direction than in the horizontal direction. This behavior is not accounted for in the design and analysis procedures included in the proposed AASHTO 2002 design guide.

One of the objectives of this study is to conduct a comparative analysis of flexible pavement response using different models for unbound pavement layers: linear isotropic, nonlinear isotropic, linear anisotropic and nonlinear anisotropic. Pavement response is computed using a finite element program. The computations from nonlinear isotropic and anisotropic models of unbound layers are compared to the AASHO field experimental measurements.

The second objective is to analyze the influence of using isotropic and anisotropic properties for the pavement layers on the performance of flexible pavements calculated using the AASHTO 2002 models.

Finally, a comprehensive sensitivity analysis of the proposed AASHTO 2002 performance models to the properties of the unbound pavement layers is conducted. The sensitivity analysis includes different types of base materials, base layer thicknesses, hot mix asphalt type and thickness, environmental conditions, and subgrade materials.

DEDICATION

This thesis is dedicated to my parents and my brother Eyad (Dr. Masad) for providing me the support that I needed to finish this thesis.

ACKNOWLEDGMENTS

I would like to take this opportunity to thank Dr. Dallas Little for his invaluable guidance, support and encouragement throughout this study. I am grateful to him for allowing me to work on this topic. I would like also to thank Dr. Lytton and Dr. Masad for fruitful discussions on the topic of this study. Special thanks are to Dr. Epps and Dr. Cline for serving as committee members and for their input on the thesis.

Special thanks to Ms. Lois Peters from the Department of Civil Engineering at Texas A&M University, and for Ms. Cathy Bryan and Ms. Pam Kopf from the Texas Transportation Institute for their help on many administrative matters.

I appreciate all the support I received from my family in Jordan, my family in College Station (Lina, Ahmad, Danna and Amr), and my friends. This support was essential to keep me motivated and to achieve this goal.

TABLE OF CONTENTS

LIST OF TABLES

LIST OF FIGURES

CHAPTER I

INTRODUCTION

1.1   Problem Statement

Unbound granular materials are generally used in road pavements as base and subbase layers. The granular materials provide load distribution through aggregate contacts to a level that can be sustained by the subgrade. In pavement design and analysis, the base and subbase layers are often described using the resilient modulus which is the ratio of the dynamic resilient stress to the dynamic resilient strain.

The resilient modulus is often described as a power function of the sum of the principal stresses (*1*). However, it was found that this model has serious limitations as it neglects the effect of shear strain and it can only be used at low strain values in the characterization of granular materials (*2*). May and Witczak (*2*) noted that deviatoric stress should be included in the evaluation of the resilient modulus. Uzan *(3)* developed a model that relates the resilient modulus to the summation of principal stresses and the octahedral stress.

Recent studies have shown that the unbound granular layers exhibit cross-anisotropic properties that are not accounted for in the models used in the practice, and they are not part of the proposed AASHTO 2002 design guide (*4, 5, and 6*).

_____

This thesis follows the style and format of *Transportation Research Record.*

The behavior is caused by the preferred orientation of aggregates in the unbound layers and the compaction forces. The result is base and subbase layers that are stiffer in the vertical direction than in the horizontal direction. The main advantages of using the directional dependency of stiffness are to describe the dilative behaviour of unbound layers and also to reduce/eliminate the unrealistic significant tensile stresses predicted in the granular bases using isotropic models (*7*).   There is a need to further investigate the influence of using different response models (isotropic vs. anisotropic and linear vs. nonlinear) on the performance predictions of asphalt pavements.   In addition, there is an urgent need to evaluate the sensitivity of the proposed AASHTO 2002 guide to the properties of unbound layers prior to the use of this guide in the practice.

1.2   Thesis Organization

The thesis is organized in six chapters. Chapter II includes the literature review related to the resilient properties of unbound aggregate bases with emphasis on the anisotropic properties.

In chapter III, a finite element program capable of isotropic and anisotropic as well as linear and nonlinear analyses of unbound layers is used to calculate the deflections of test sections resembling those used in the AASHO road test.   The computations from nonlinear isotropic and anisotropic models of unbound layers are compared to the AASHO experimental measurements.   A total of 246 sections with different layer thicknesses were analyzed. The applied loads varied from 6000 to 30000 psi (single axle load). The material properties for all layers were obtained from a study by Finn et al, (*8*).

Chapter IV documents the calculations of the permanent deformation and fatigue cracking in typical cross sections of asphalt pavements using the mechanistic-empirical models in the AASHTO 2002. However, the pavements responses that are used in these performance models are calculated using isotropic and anisotropic properties for the unbound layers.

Chapter V presents the sensitivity analysis of the AASHTO 2002 design guide to the characteristics of various base materials. The analysis is conducted for different layer thicknesses, asphalt layer properties, subgrade properties, traffic levels, and environmental conditions. Chapter VI presents the conclusions and recommendations of this research.

1.3   Objectives

The objectives of this study are to:

1.   Conduct comparative analysis of flexible pavement response using different models for unbound pavement layers: nonlinear isotropic and nonlinear anisotropic. The results from the different models will be compared with the experimental measurements from the AASHO road test.

2.   Evaluate the permanent deformation and fatigue cracking calculated using the performance models in the proposed AASHTO 2002 design guide. These distresses are calculated using pavement responses computed from linear isotropic, nonlinear isotropic, linear anisotropic, and nonlinear anisotropic models for the unbound aggregate layers.

3. Conduct sensitivity analysis of the proposed AASHTO 2002 guide to the properties of the unbound pavement layers.

CHAPTER II

LITERATURE REVIEW

2.1   Introduction

Literature review was conducted through information search using electronic databases and documented publications. The information gathered including resilient properties, triaxial testing, resilient models, and permanent deformation models of unbound materials was summarized and documented. This is discussed in this chapter.

Granular materials are commonly used in the unbound bases and subbases of flexible pavements in order to distribute loads, through aggregate contacts and interlocking, such that the subgrade can withstand the applied loads.

The deformation response of granular layers under traffic loading is characterized by recoverable (resilient) deformation and a residual (permanent) deformation. Granular materials are not elastic but the non-recoverable deformation is much smaller than the recoverable deformation. As the number of load repetitions increases the plastic strain due to each load repetition decreases. Therefore, the unbound layers are often described using resilient properties.

The deformation of the granular materials is the result of three mechanisms:

- The consolidation mechanism: The change in the shape and compressibility of particle assemblies,

- Distortion mechanism: characterized by bending, sliding, and rolling of the particles, and

- The crushing and the breaking of the particles which occur when the applied load exceeds the strength of the particles.

2.2 Factors Affecting the Resilient Response of Unbound Layers

It is known that the granular materials and the subgrade soils are nonlinear with an elastic modulus varying with the level of stresses. The resilient response of granular materials is defined by resilient modulus and Poisson's ratio. The factors that influence the behaviour of unbound layers are discussed in this sections (*9*).

Many studies have shown that the resilient modulus is affected by the confining pressure or the sum of principle stresses and the deviatoric stress. The resilient modulus increases with an increase in the confining pressure, and decreases with an increase in the deviatoric stress. In general, the resilient modulus of unbound materials increases with an increase in density.

Aggregate gradation influences the resilient modulus. Some researchers have shown that the resilient modulus decreases with an increase in the amount of fine materials. It was also shown that the resilient modulus increases with an increase in maximum particle size given that the amount of fines and shape of aggregates remain the same. Stiffness tends to increase with an increase in moisture content below the optimum moisture content. However, beyond the optimum moisture content when the material becomes more saturated and excess pore water pressure is developed the stiffness starts to decline. The effect of moisture change increases as the fine content increases. The resilient modulus tends to increase as aggregate particles become more angular and rougher.

2.3 Triaxial Testing of Resilient Properties

The repeated load triaxial test is the method typically used to study the mechanical properties of unbound granular materials. In this test, a deviatoric stress is axially cycled while a constant confining stress is applied. The general relation used to determine the resilient modulus for the unbound granular materials is as follows:

$$M_r = \frac{\Delta(\sigma_1 - \sigma_2)}{\varepsilon_{1,r}} = \frac{\sigma_d}{\varepsilon_{1,r}} \qquad (2.1)$$

$$v = -\frac{\varepsilon_{3,r}}{\varepsilon_{1,r}} \qquad (2.2)$$

Where

σ_1 = major principal stress,

σ_2 = minor principal stress,

σ_d = deviatoric stress,

$\varepsilon_{1,r}$ = resilient strain in the direction of the major principal stress (axial stress),

$\varepsilon_{3,r}$ = deviatoric strain in the direction of the minor principal stress.

If the repeated load triaxial test is applied with variable confining stresses, the resilient modulus and Poisson's ratio are defined as follows:

$$M_r = \frac{\Delta(\sigma_1 - \sigma_3)\Delta(\sigma_1 + 2\sigma_3)}{\varepsilon_{1,r}\Delta(\sigma_1 + \sigma_3) - 2\varepsilon_{3,r}\Delta\sigma_3} \qquad (2.3)$$

$$v = \frac{\Delta\sigma_1\varepsilon_{3,r} - \Delta\sigma_3\varepsilon_{1,r}}{2\Delta\sigma_3\varepsilon_{3,r} - \varepsilon_{1,r}\Delta(\sigma_1 + \sigma_3)} \qquad (2.4)$$

2.4 Models for Resilient Behavior of Unbound Granular Material

Dunlap (10) and Monismith (11) indicated that the resilient modulus increases with an increase in the confining pressure:

$$M_r = K_1 \sigma_3^{K_2}$$

(2.5)

where

K_1 and K_2 = regression constants,

σ_3　　　= the minor principal stress.

Seed (12), Brown and Pell (13) and Hicks (14) found that it is necessary to include the applied axial stress in the analysis so they suggested the following model which is commonly known as K-θ model:

$$M_r = K_1 \theta^{K_2}$$

(2.6)

where

θ = sum of principal stresses.

The K-θ model is simple and has been widely used for analysis of stress dependence of material stiffness. However, the model neglects the effect of the shear stress and is therefore applicable only in the range of low strain values. Uzan *(3)* noticed that the resilient modulus is a function not only of bulk stress but also of the shear stress. Uzan *(3)* included deviatoric stress and expressed the resilient modulus as follows:

$$M_r = K_1 P_a \left(\frac{I_1}{P_a} \right)^{K_2} \left(\frac{\tau_{oct}}{P_a} \right)^{K_3}$$

(2.7)

Where

τ_{oct} = octahedral shear stress,

I_1 = sum of principal stress (θ),

P_a = atmospheric pressure,

K_1, K_2, and K_3 = regression coefficients that depend on material properties.

Elliot and Lourdesnathan (*15*) noticed that the Uzan model fits the data very well for pre failure stresses but when the stresses exceeded the static failure the predictions were poor. So they suggested adding the failure term for the previous model:

$$M_r = k_1 \frac{\theta^{K_2}}{10^{A I_1}}$$

(2.8)

where

A = failure term.

Several models have been proposed for the resilient behavior based on decomposing both stresses and strains into volumetric and shear components. Boyce (*16*) assumed the material to be nonlinear isotropic and proposed the following equations for the volumetric (ε_v) and shear (ε_s) strains:

$$\varepsilon_v = p^A \frac{1}{K} \left[1 - \beta \frac{\sigma_d^2}{p^2} \right]$$

(2.9)

$$\varepsilon_s = p^A \frac{1}{3G} \left(\frac{\sigma_d}{p} \right)$$

(2.10)

Where

p = hydrostatic stress,

G = shear modulus,

K = bulk modulus.

Brown and Pappin (*17*) proposed the following relationships for the volumetric and shear strains:

$$\varepsilon_v = \delta\left[\left(\frac{p}{A}\right)^B\left(1 - C\left(\frac{\sigma_d}{p}\right)^2\right)\right] \tag{2.11}$$

$$\varepsilon_s = \delta D\left[\frac{\sigma_d}{P+E}\right]\left[\frac{\sqrt{P^2_r} + \sigma_d^2}{p_m}\right]^F \tag{2.12}$$

Where

ε_v = recoverable volumetric strain,

ε_s = shear strain,

P = mean normal stress,

σ_d = deviatoric Stress.

Several studies (Tutumluer, (*4*); Tutumluer and Thompson, (*18*), Hornych et al. (*19*) suggested that the use of anisotropic models better represent the behaviour of granular materials.

The Boyce model was modified by Hornych (*19*) in order to account for the effect of anisotropy. The mathematical expressions of the anisotropic model are as follows:

$$\varepsilon_v = \frac{P^{*A}}{P_0^{A-1}}\left[\frac{\gamma+2}{3K_1} + \frac{A-1}{18G_1}(\gamma+2)\left(\frac{q^*}{p^*}\right)^2 + \frac{\gamma-1}{3G_1}\left(\frac{q^*}{p^*}\right)\right] \tag{2.13}$$

$$\varepsilon_s = \frac{2}{3}\frac{P^{*A}}{P_0^{A-1}}\left[\frac{\gamma-1}{3K_1} + \frac{A-1}{18G_1}(\gamma-1)\left(\frac{q^*}{p^*}\right)^2 + \frac{2\gamma+1}{6G_1}\left(\frac{q^*}{p^*}\right)\right] \tag{2.14}$$

Triaxial testing was conducted using a machine capable of applying dynamic loads in the axial and radial directions *(18)*. The results obtained from this test showed definite directional dependency (anisotropy) of aggregate moduli. The resilient moduli in the vertical and radial directions varied with the applied stress states. It was noticed that the vertical modulus in the vertical direction is more than that for horizontal direction for unbound materials. However, this relationship was reversed in the case of sandy gravel with high fines content and if the specimen was compacted at the wet side of optimum.

Five cross-anisotropic material properties are needed to define an anisotropic material under conditions of axial symmetry: the horizontal resilient modulus ($M_R{}^H$), the vertical dynamic modulus ($M_R{}^v$), the shear modulus (G_R), the horizontal Poisson's ratio (v_H), and the vertical Poisson's ratio (v_V). These properties are defined as follows:

$$M_R^V = \frac{\sigma_d}{\varepsilon_{vertical}} \qquad (2.15)$$

$$M_R^H = \frac{\sigma_3}{\varepsilon_{horizontal}} \qquad (2.16)$$

$$G_R = \frac{\sigma_d}{2\left(\varepsilon_{vertical} - \varepsilon_{horizontal}\right)} \qquad (2.17)$$

$$v_H = -\frac{\varepsilon_{horizontal\_2}}{\varepsilon_{horizontal\_1}} \qquad (2.18)$$

$$v_V = -\frac{\varepsilon_{horizontal}}{\varepsilon_{vertical}} \qquad (2.19)$$

$\varepsilon_{horizontal\_1}$ is the applied horizontal strain, and $\varepsilon_{horizontal\_2}$ is the measured horizontal strain 90° from the applied horizontal strain.

$$M_R^V = K_1 P_a \left(\frac{I_1}{P_a} \right)^{K_2} \left(\frac{\sigma_d}{P_a} \right)^{K_3} \qquad (2.20)$$

$$M_R^H = K_4 P_a \left(\frac{I_1}{P_a} \right)^{K_5} \left(\frac{\sigma_d}{P_a} \right)^{K_6} \qquad (2.21)$$

$$G_R = K_7 P_a \left(\frac{I_1}{P_a} \right)^{K_8} \left(\frac{\sigma_d}{P_a} \right)^{K_9} \qquad (2.22)$$

As it was mentioned before the advantage of modeling granular materials using cross anisotropic nonlinear elasticity is to predict the dilative granular material behaviour (*20*). Figure (2.1) shows the variation of principal strain ratios with increasing major to minor principal stress ratios. Any value less than 2 for the stress ratio corresponds to the case of elastic dilation. The nonlinear anisotropic model matches very well the experimental values. On the other hand, under the assumption of linear isotropy, modeling of the dilative behavior could be achieved when the Poisson's ratio is more than 0.5.

2.5 Models for Permanent Deformation of Unbound Granular Material

The deformational response of the granular materials can be defined under repeated, traffic-type loading by a resilient response which is important for load carrying ability and permanent strain response which characterizes the long-term performance of the pavement and rutting phenomenon. Few studies have been conducted to model the permanent deformation of granular materials.

Several factors affect the plastic behavior in the unbound granular materials, these factors include, stress, principal stress reorientation, number of load applications, moisture content, stress history, density and fine contents, grading and aggregate type (*21*).

There are several models used to characterize the permanent deformation properties and to predict the permanent strain in the unbound granular materials.

Barksdale (*22*) found by using the repeated load triaxial tests with 10^5 load applications that the accumulation of permanent axial stain was proportional to the logarithm of the number of load cycles and expressed as follows:

$$\varepsilon_{1,P} = a + b\log(N) \tag{2.23}$$

where

N   = number of load repetitions,

$\varepsilon_{1,P}$ = permanent strain,

a and b = regression parameters.

Bonaquist and Witczak (*23*) developed a model based on the flow theory of plasticity. This model defines the magnitude of the permanent strain occurring during the first cycle of loading. Under repeated loading the permanent strain at any load cycle can be expressed as a power function of permanent strain during the first load cycle. The total permanent strain will be the sum of the permanent strain in each cycle.

$$\varepsilon_{1,P} = \sum \varepsilon_N = \sum \frac{1}{N^h} \varepsilon_i \tag{2.24}$$

where

ε_i = permanent strain in the first load cycle,

ε_N = permanent strain for load cycle N.

The Hyperbolic model developed by Duncan and Chang (*24*) is used to predict the plastic strain by using static triaxial tests. The results from this test are then used to relate the permanent axial strain to the ratio of repeated deviator stress and constant confining pressure. The model is expressed as:

$$\varepsilon_{1,p} = \frac{\sigma_d / a\sigma_3^{\,b}}{1 - \left[\dfrac{\left(R_{fq}\right)/2\left(C\cos\phi + \sigma_3\,\sin\phi\right)}{\left(1 - \sin\phi\right)}\right]}$$ (2.25)

where

ε_p = the axial plastic strain,

C = cohesion,

ϕ = angle of internal friction,

R = the ratio of measured strength to ultimate hyperbolic strength.

Models developed by Tseng and Lytton (*25*) are used to estimate the permanent deformation of asphalt, base and subgrade materials. The basic relationship is:

$$\delta_a(N) = \left(\frac{\varepsilon_0}{\varepsilon_r}\right) e^{-\left(\frac{\rho}{N}\right)^{\beta}} \varepsilon_v h$$ (2.26)

where

δ_a = permanent deformation for layer/sublayer,

ε_v = average vertical resilient strain in the layer/sublayer as obtained from the primary response model,

h = thickness of layer/sublayer,

ε_r = resilient strain imposed in laboratory test to obtain material properties ε_0, ρ and β.

The ratio $\dfrac{\varepsilon_0}{\varepsilon_r}$, β and ρ are estimated according to the type of materials investigated. For granular base, the ratio can be estimated using the following form:

$$\log\left(\frac{\varepsilon_0}{\varepsilon_r}\right) = .80978 - .06626 W_C - .003077 \sigma_\theta + .000003 E_r \tag{2.27}$$

$$\log \beta = -.919 + .03105 W_C + .001806 \sigma_\theta - .0000015 E_r \tag{2.28}$$

$$\log \rho = -1.78667 + 1.45062 W_C + .003784 \sigma^2{}_\theta - .002074 W_C{}^2 \sigma_\theta - .0000105 E_r \tag{2.29}$$

For subgrade, the model parameters can be estimated using the following relationships:

$$\log\left(\frac{\varepsilon_0}{\varepsilon_r}\right) = -1.69867 + .09121 W_C - .11921 \sigma_d + .91219 \log E_r \tag{2.30}$$

$$\log \beta = -.973 - .0000278 W_c{}^2 \sigma_d + .017165 \sigma_d - .00000338 W_C{}^2 \sigma_\theta \tag{2.31}$$

$$\log \rho = 11.009 + .0000681 W_c{}^2 \sigma_d - .4026 \sigma_d + .00000545 W_C{}^2 \sigma_\theta \tag{2.32}$$

The above equations are modified from the ones published by Tseng and Lytton. It was found, based on discussion with Dr.Lytton that sign errors where in the paper by Tseng and Lytton.

Some researchers developed computational procedures for pavement analysis based on the Shakedown theory (*26*). According to the Shakedown theory, if the applied load exceeds a limiting value called a shakedown load the pavement will show a progressive accumulation of plastic strains under repeated loading. On the other hand if the applied loads are lower that the shakedown limit, the pavement will be able to adapt

the loads. So the response for the pavement will be totally resilient under the load applications.

The Vesys computer program is used to predict the rut depth based on the assumption that the permanent strain is proportional to the resilient strain by

$$\varepsilon_p(N) = \varepsilon \mu N^{-\alpha} \tag{2.33}$$

where

$\varepsilon_p(N)$ = permanent or plastic strain due to a single load application at Nth application,

ε = elastic or resilient strain at the 200th repetition,

N   = load application number,

μ = permanent deformation representing the constant of proportionality between permanent and elastic strain,

α = the permanent deformation indicating the rate of decrease in permanent strain with number of load applications.
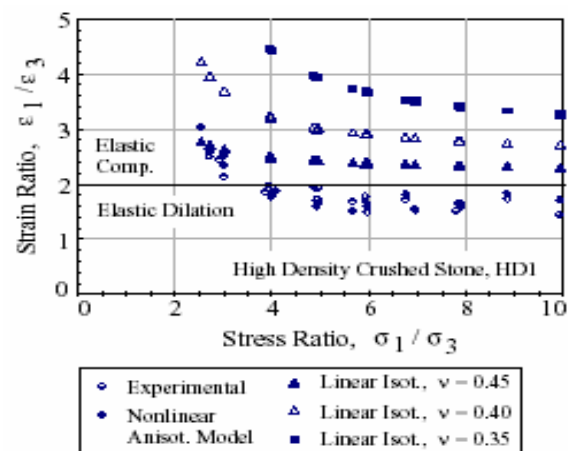
FIGURE 2.1 Variation of principal strain ratios with principal stress ratios for the HD1 material.

CHAPTER III

SENSITIVITY ANALYSIS OF PAVEMENT RESPONSE USING DIFFERENT STRUCTURAL MODELS AND COMPARISON WITH AASHO ROAD MEASUREMENTS

3.1 Introduction

This chapter includes a comparison between the pavement deflections calculated using isotropic and anisotropic nonlinear models for the unbound layers and the field deflection measurements in the AASHO road test. The comparison is conducted based on deflection measurements rather than the measured performance in order to the comparison not to be affected by the assumptions made in the empirical transfer functions typically used in performance predictions.

The asphalt layer is assumed to be linear isotropic while the base and subbase layer are modeled using nonlinear isotropic and nonlinear anisotropic properties. The subgrade is modeled using nonlinear isotropic properties. The analysis includes a total of 246 sections with different layer thicknesses. The applied loads in the AASHO test varied from 6000 to 30000psi (single axle load). The material properties for all layers are obtained from the experimental measurements by Finn et al. (8).

3.2 AASHO Road Test

3.2.1 Background about the AASHO Road Test

The AASHO Road test near Ottawa, Illinois, was performed over a two year period to develop a design methodology for asphalt and concrete pavements (*27, 28*). The test

facilities consisted of 4 major loops numbered from 3 through 6 and two smaller loops. All vehicles had the same axle arrangements-axle load combinations to any one traffic lane of loops 2 through 6. The same materials were used in all the major loops as listed in Table 3.1.

TABLE 3.1 Description of Materials Used in the Major Loops of the AASHO Road Test

Layer	Material
Hot Mix Asphalt	• Crushed limestone coarse aggregate • Natural siliceous coarse sand • Mineral filler which was limestone dust • Penetration Grade asphalt cement (85-100 pen)
Base	Crushed Dolomitic Limestone
Subbase	Sand-Gravel mixture
Subgrade	A-6

The loops were subjected to traffic for more than two years. The traffic was operated at 35 mph on the test sections over 18 hrs with periods of 40 minutes each day for 6 days a week. The traffic was extended to 7 days a week during the first 6 months of 1960.

The major loops included a total of 468 sections. Each test section was 12-ft wide, and most of them were 100 or 160 ft long. Each loop included pavement sections with three different thicknesses of asphalt concrete surfacing, three different thicknesses of crushed limestone base, and three different thicknesses of sand-gravel subbase.

The applied axle load over the test sections ranged from a 2000 lb single axle load in one lane and a 6000 lb single axle load in the other lane in loop 2. Loop 6 was subjected to a 30000 lb single axle load in one lane and a 48000 lb tandem axle load in the other. Table 3.2 summarizes the variables in the major sections.

TABLE 3.2 Materials and Loads Used in the AASHO Test

Item	Loop					
	1	2	3	4	5	6
Test axle loading (Ib)	No traffic	2,000 S	12,000 S	18,000 S	22,400 S	30,000 S
		6,000 S	24,000 T	32,000 T	40,000 T	48,000 T
Factorial test sections	48	44	60	60	60	60
Special study sections	16	24	24	24	24	24
Asphalt Concrete Surfacing Thicknesses (in)	1,3,5	0,1,2,3	2,3,4	3,4,5	3,4,5	4,5,6
Base thicknesses (in)	0,6	0,3,6	0,3,6	0,3,6	3,6,9	3,6,9
Subbase thicknesses (in)	0,8,16	0,4	0,4,8	4,8,12	4,8,12	8,12,16

3.2.2 Field Deflection Measurements and Material Properties

3.2.2.1 Field Deflection Measurements

Deflection measurements of the pavement surface are important for the evaluation of the performance of a flexible pavement structure and rigid pavement load transfer. The surface deflection is a function of many factors used in the design of the pavement such as traffic (type and volume), pavement structural section, temperature, and moisture. Thus, many characteristics of a flexible pavement can be determined by measuring its

deflection in response to load. The advantage of using deflection to compare with analytical solutions is that no empirical transfer functions are used in this comparison as is the case in performance predictions.

Surface deflection is measured as a pavement surface's vertical deflected distance as a result of an applied (either static or dynamic) load. In the AASHO test, the deflection of a pavement surface was measured using the Benkelman beam under vehicle wheels moving at creep speeds (approximately 2mph). The Benkelman Beam consists of a simple lever arm supported by 3 legs (Figure 3.1). The Benkelman Beam was used with a loaded truck - typically 80 kN (18,000 lb) on a single axle with dual tires inflated to 480 to 550 kPa (70 to 80 psi). Tip of measuring arm was placed between the dual tires of a truck. As the truck moved at the creep speed, the device recorded the rebound deflection of the pavement surface. The measured deflection for each test consisted of the mean of four measurements; two in the inner and two in the outer wheel path.
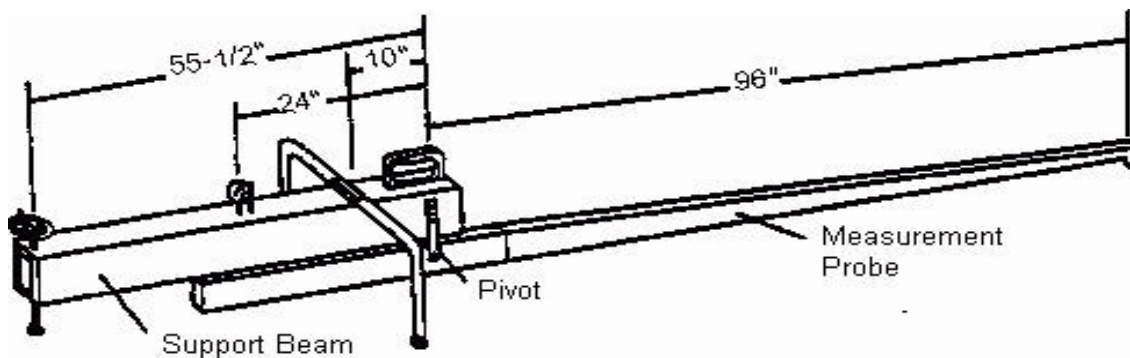
FIGURE 3.1 A schematic of the Benkelman beam.

Two series of deflection measurements were conducted in the AASHO road test. The first series included the deflections in the fall of 1958, while the second series included the deflections in the spring of 1959. The fall period was selected because the highway was completed and opened to traffic at that time. The spring period was selected because there was a big chance of the distress occurrence that time due to the higher moisture contents of the base and subbase that existed in the spring. Table 3.3 shows the loads used in the deflection measurements.

TABLE 3.3 Loads Used in Deflection Studies

Loop	Lane	Single Axle Load (Kips)
2	1	-
	2	6
3	1	12
	2	12
4	1	12,18
	2	12
5	1	12,22.4
	2	12
6	1	12,30
	2	12

3.2.2.2   Seasonal Material Characterization

Since the performance of the pavements varies from season to season, it was necessary to analyze the AASHO road test pavement in different seasons (*29*). Finn et al. (*8*) characterized the properties of the materials used in the AASHO road test including the asphalt surfacing, base, subbase and subgrade. The evaluation of the seasonal material properties was conducted using laboratory triaxial testing. The resilient moduli for the base and subbase materials were expressed as function of the first stress invariant, while the subgrade materials were modeled as a function of the deviatoric stress.

The modulus of the asphalt concrete was measured at the average temperature of the AASHO road test location during the traffic testing. The resilient moduli of the base materials were measured at density values representing the construction values, and using three different water contents to take into account the seasonal variation (water content = 4.2%, 5.6%, and 1.5%).

The subbase material modulus was measured at the optimum water content (3.8%) and at the saturation water content (6.4%).   The subgrade modulus was determined using a trial and error procedure such that the calculated surface deflections using a linear elastic program had the best match with field measurements. The material moduli are shown in Table 3.4. The Poisson's ratio was assumed constant for each material, and the values in Table 3.5 were assigned for the different layers.

TABLE 3.4 Elastic Moduli of AASHO Road Test Materials

Seasons	Material Moduli			
	Asphalt concrete	Base	Subbase	Subgrade
	psi (kPa)	psi (kPa)	psi (kPa)	psi (kPa)
Spring	0.71×10^6 (4.9×10^6)	$3200\,\theta^{0.6}$ $(6900\,\theta^{0.6})$	$4600\,\theta^{0.6}$ $(10000\,\theta^{0.6})$	$8000\,\sigma_d^{-1.06}$ $(427000\,\sigma_d^{-1.06})$
Fall	0.45×10^6 (3.1×10^6)	$4000\,\theta^{0.6}$ $(8700\,\theta^{0.6})$	$5400\,\theta^{0.6}$ $(11700\,\theta^{0.6})$	$27000\,\sigma_d^{-1.06}$ $(1440000\,\sigma_d^{-1.06})$
Summer	0.23×10^6 (1.6×10^6)	$3600\,\theta^{0.6}$ $(7800\,\theta^{0.6})$	$5000\,\theta^{0.6}$ $(10800\,\theta^{0.6})$	$18000\,\sigma_d^{-1.06}$ $(960000\,\sigma_d^{-1.06})$
Winter	1.7×10^6 (11.7×10^6)	50000 (34500)	50000 (345000)	50000 (345000)

TABLE 3.5 Poisson's Ratio of AASHO Road Test Material

Material	Poisson's ratio
Asphalt	0.3
Granular base	0.4
Granular subbase	0.4
Fine grained subgrade	0.45

3.3 Pavement Analysis

A finite element program was used to calculate the deflections at the surface of the pavement by using the materials properties given in Tables 3.4 and 3.5. Two models were used in the finite element program to describe the base and subbase layers; nonlinear isotropic and nonlinear anisotropic. The results were compared with the experimental deflection measurements.

The finite element program allows the computation of the resilient response of flexible pavement, such as stress, strain and deformation at any location in the pavement. The program accounts for nonlinear and anisotropic elastic properties of all pavement layers. The program uses a typical axisymmetric finite element mesh as shown in Figure 3.2. The mesh used in this analysis has 50 in width with 9 columns while the length is 100 in with 16 rows. The total number of elements is 144. Each element has 8 nodes. The applied pressure is 75 psi which is equivalent to the pressure used in the Benkelman device in the AASHO road test to measure the surface deflection. The loading radius depends on the applied load which was different for the different loops.

It is known that the modulus of the unbound granular materials is stress sensitive and changes through the layer so the modulus of the untreated materials at any point in the layer is a function of stress. The properties are the same in all directions (isotropic). The resilient modulus is calculated as:

$$M_r = K_1 P_a \left(\frac{I_1}{P_a}\right)^{K_2} \left(\frac{\tau_{oct}}{P_a}\right)^{K_3} \tag{3.1}$$

where

I_1 = first stress invariant (Sum of principal stresses),

τ_{oct} = octahedral shear stress,

P_a = atmospheric pressure.

$K_1,$ K_2 and K_3 used in the finite element model are calculated based on the measured material properties given in Table 3.4 for the spring and fall seasons.

In the anisotropic model, equations similar to Eq. 3.1 are used to express the vertical modulus, horizontal modulus, and shear modulus. The moduli are modeled from the triaxial stress states using the following equations:

$$M_R^V = K_1 P_a \left(\frac{I_1}{P_a}\right)^{K_2} \left(\frac{\sigma_d}{P_a}\right)^{K_3} \tag{3.2}$$

$$M_R^H = K_4 P_a \left(\frac{I_1}{P_a}\right)^{K_5} \left(\frac{\sigma_d}{P_a}\right)^{K_6} \tag{3.3}$$

$$G_R = K_7 P_a \left(\frac{I_1}{P_a}\right)^{K_8} \left(\frac{\sigma_d}{P_a}\right)^{K_9} \tag{3.4}$$
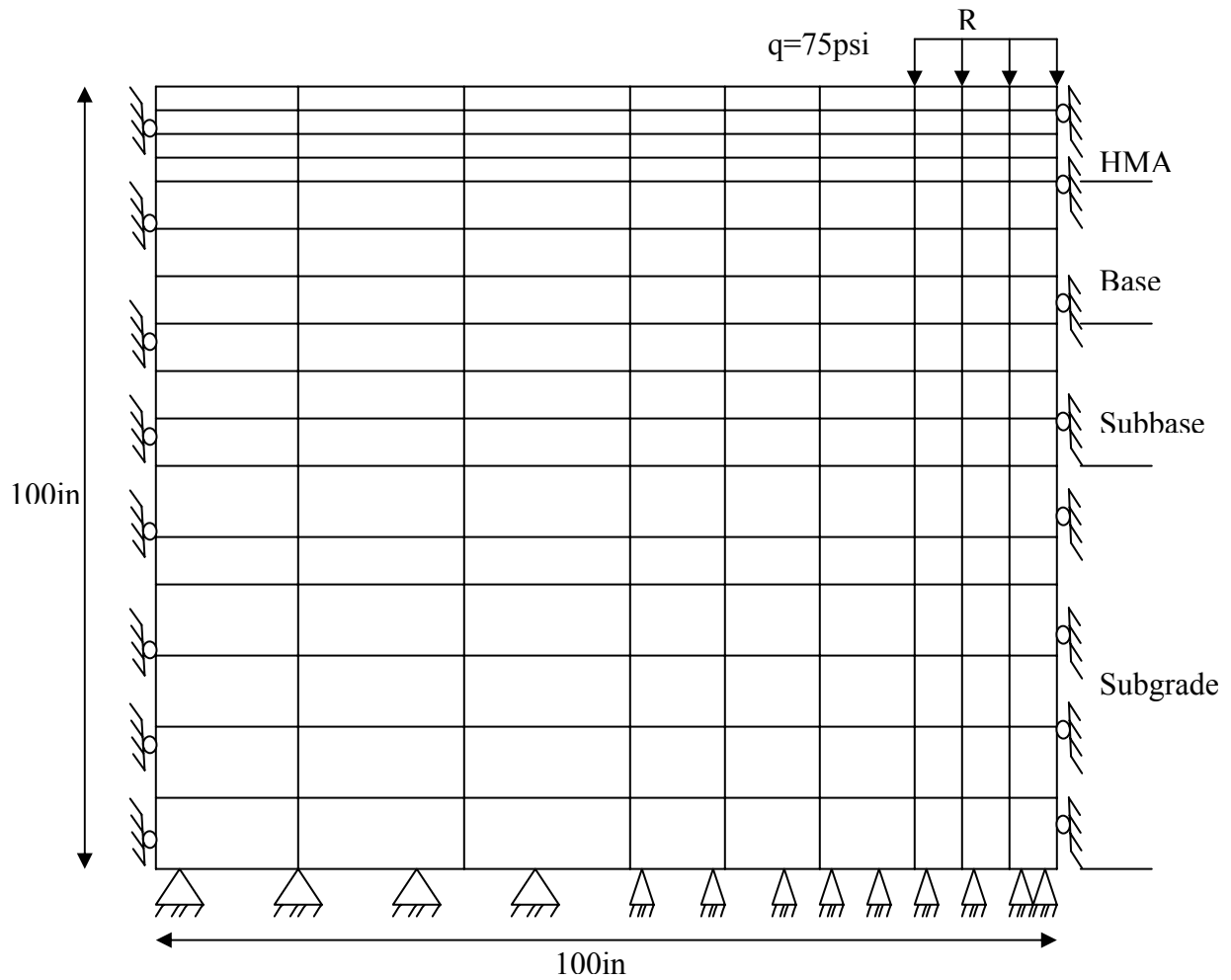
FIGURE 3.2 Finite element mesh for pavement analysis.

The finite element program requires the K_1, K_2, K_3, n, m and μ parameters:

$$n = \frac{M_R^H}{M_R^V} \tag{3.5}$$

$$m = \frac{G_{xy}}{M_R^V} \tag{3.6}$$

$$\mu = \frac{v_{xx}}{v_{xy}} \tag{3.7}$$

v_{xx} is the horizontal Poisson's ratio, and v_{xy} is the vertical Poisson's ratio.

In this study, the base and subbase layer are assumed to be either nonlinear isotropic or nonlinear anisotropic. In the isotropic approach, the modular ratios (n and μ) are set to 1. In the anisotropic analysis, the n value is taken to be 0.5, 0.4 and 0.3, while μ is set to 1.5. These values are selected to represent experimental measurements for a wide range of aggregates at the Texas Transportation Institute (*5, 30*). By assuming the Poisson's ratio in the base and subbase layer to be equal 0.4, the m value can be determined by using the following equation.

$$m = \frac{1}{2\left(1 + v_{xy}\right)} \tag{3.8}$$

The asphalt layer is modeled as linear isotropic, and the materials properties K_2 and K_3 are set to zero. The subgrade is modeled by nonlinear isotropic properties. Table 3.6 shows a summary of the input data used in the FEM

TABLE 3.6 A Summary of the Input Data Used in the FEM Program (LIS: Linear Isotropic, NIS: Nonlinear Isotropic, NAN: Nonlinear Anisotropic, NIS: Nonlinear Isotropic)

Season	Layer	AASHO Road Modulus	Model	FEM Parameters						
				K_1	K_2	K_3	n	m	μ	v_{xy}
Spring	HMA	0.71×10^6	LIS	48965.5	0	0	1	0.38	1	0.3
Fall		0.45×10^6		31034.5	0	0	1	0.38	1	0.3
Spring	Base	$32000\theta^{0.6}$	NIS	1098	0.6	0	1	0.36	1	0.4
			NAN	1098	0.6	0	0.5 0.4 0.3	0.36	1.5	0.4
Fall		$40000\theta^{0.6}$	NIS	1372.5	0.6	0	1	0.36	1	0.4
			NAN	1372.5	0.6	0	0.5 0.4 0.3	0.36	1.5	0.4
Spring	Subbase	$46000\theta^{0.6}$	NIS	1578.4	0.6	0	1	0.36	1	0.4
			NAN	1578.4	0.6	0	0.5 0.4 0.3	0.36	1.5	0.4
Fall		$54000\theta^{0.6}$	NIS	1852.9	0.6	0	1	0.36	1	0.4
			NAN	1852.9	0.6	0	0.5 0.4 0.3	0.36	1.5	0.4
Spring	Subgrade	$3000\sigma_d^{-1.06}$	NIS	32.41	0	1.06	1	0.34	1	0.45
Fall		$2700\sigma_d^{-1.06}$		109.4	0	1.06	1	0.34	1	0.45

3.4   Comparison Between the FEM Calculations and Measurements

A comparative analysis was conducted between the finite element predictions and the measured deflections in the AASHO road sections. The finite element program was used to calculate the deflections at the surface of 246 different pavement sections. The material properties for 134 sections represented the fall season, while the remaining 112 sections represented the spring season. These predicted deflections were then compared with the deflections measured in the AASHO Road test. The sections used for this study were from loop 2 through loop 6 with single axle loads that ranged from 6 to 30 kip.

Figures 3.3-3.6 show the relationships between the field measurements in the fall season and the finite element results using either isotropic or anisotropic material properties. The comparisons with the measurements from the spring season are shown in Figures 3.7-3.10, and the results combined for both seasons are shown in Figures 3.11-3.14. Deflections calculated using isotropic material properties tend to be smaller than the experimental measurements. As the anisotropy increases (n value decreases), the calculated deflections become closer to the measurements and the accuracy of the prediction increases. In general, the finite element predictions are closer to measurements in the fall season than in the spring season.
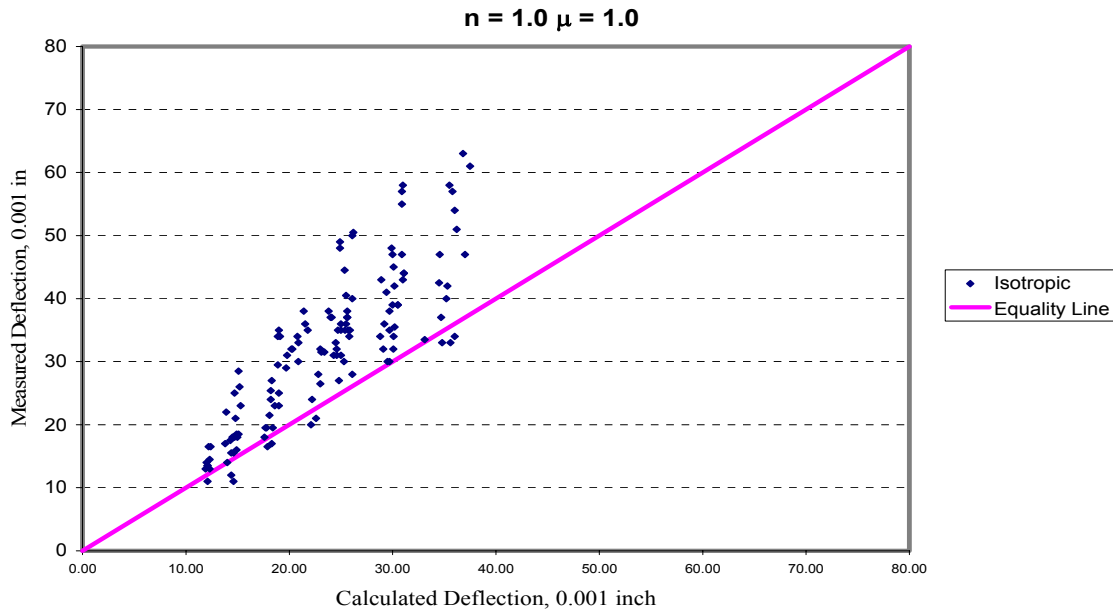
FIGURE 3.3 Measured versus calculated deflections for the fall season using isotropic properties.
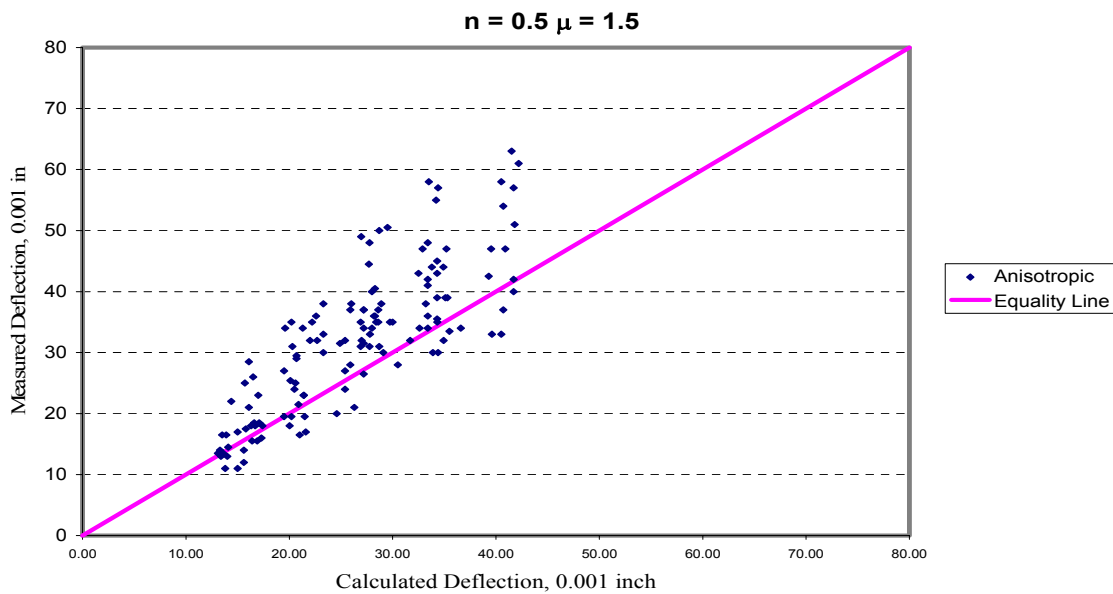
FIGURE 3.4 Measured versus calculated deflections for the fall season using anisotropic properties with n = 0.5.
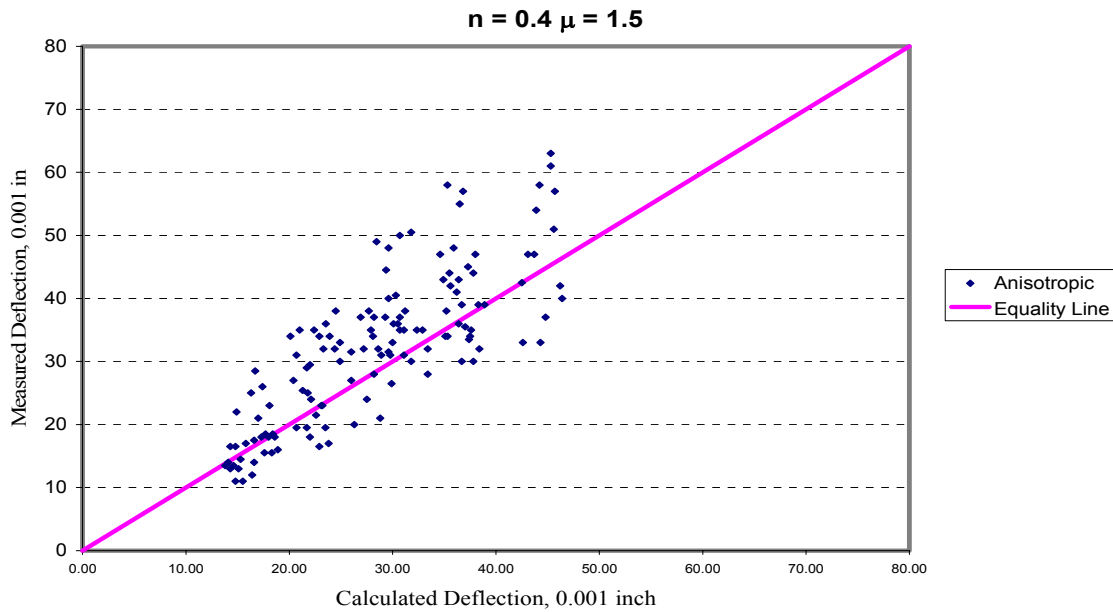
FIGURE 3.5 Measured versus calculated deflections for the fall season using anisotropic properties with n = 0.4.
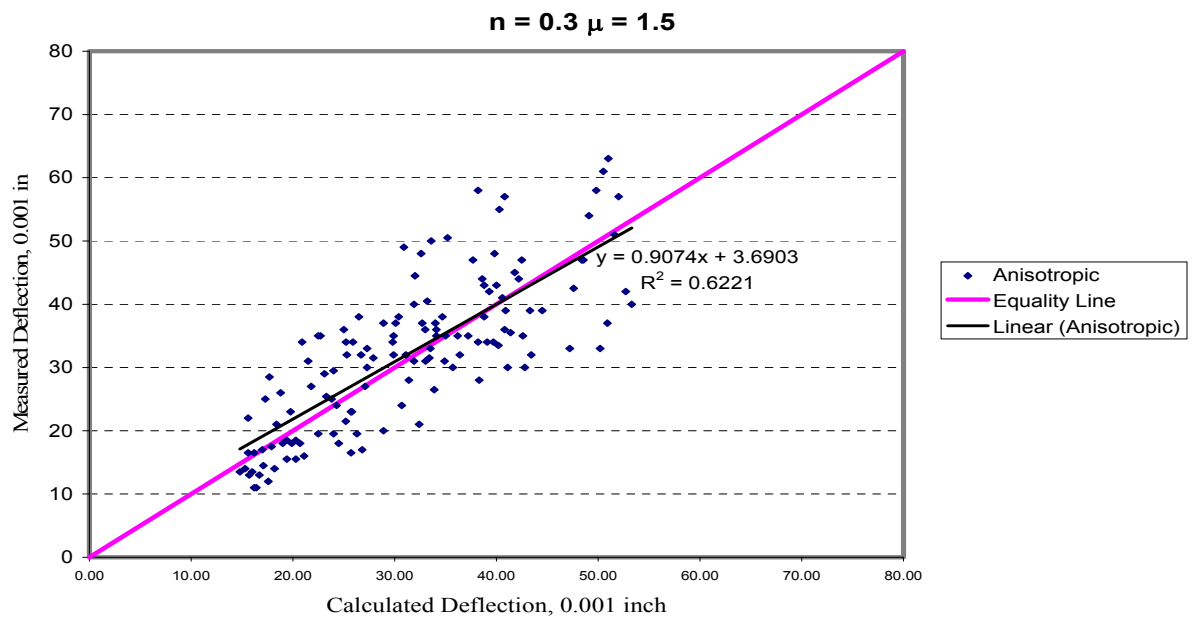
FIGURE 3.6 Measured versus calculated deflections for the fall season using anisotropic properties with n = 0.3.
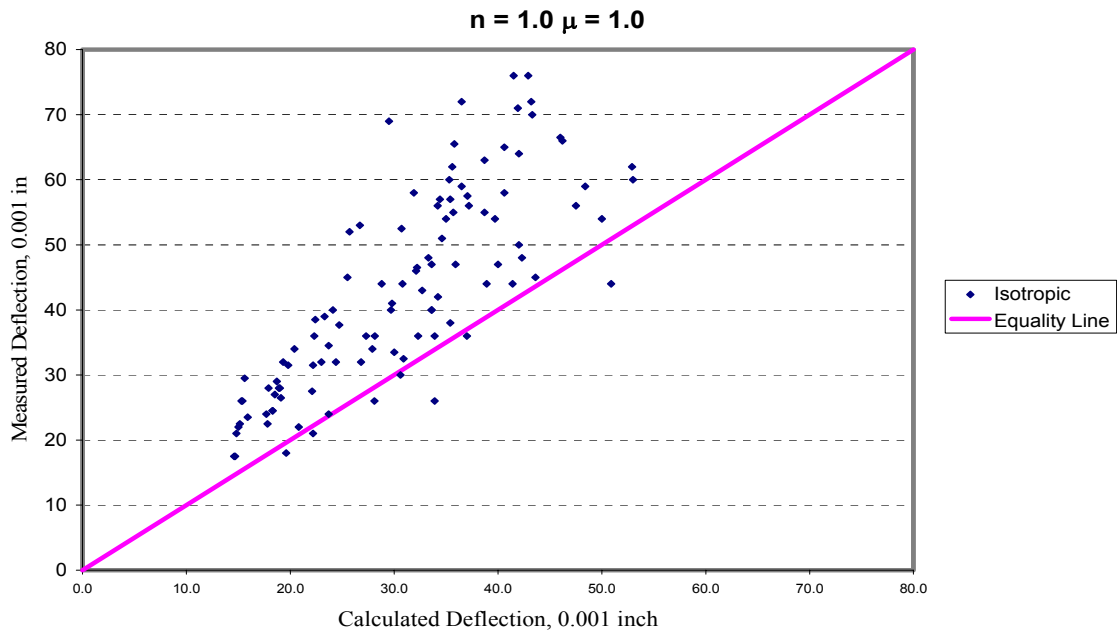
FIGURE 3.7 Measured versus calculated deflections for the spring season using isotropic properties.
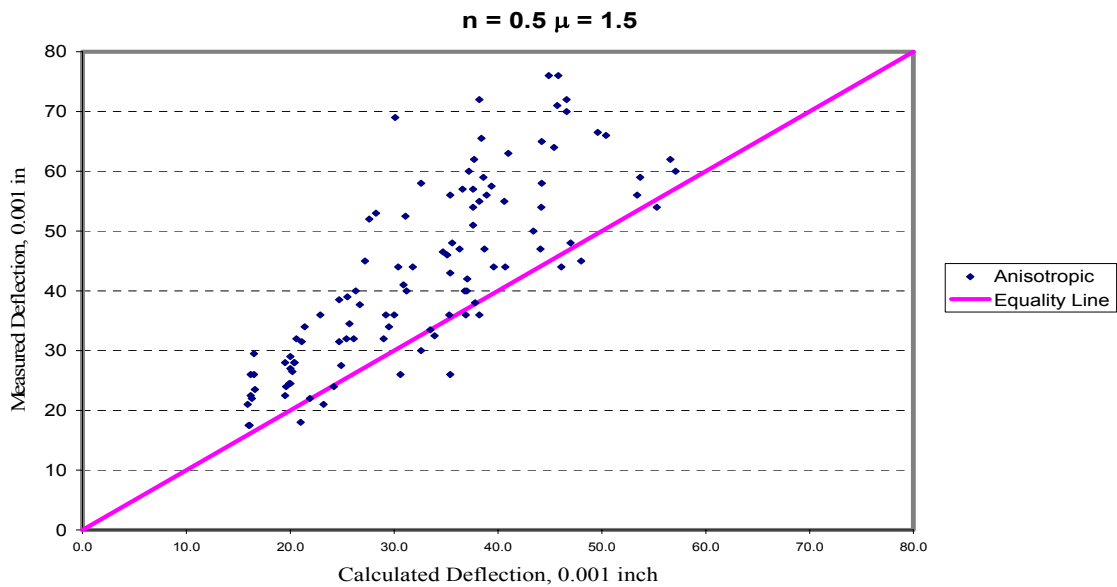
FIGURE 3.8 Measured versus calculated deflections for the spring season using anisotropic properties with n = 0.5.
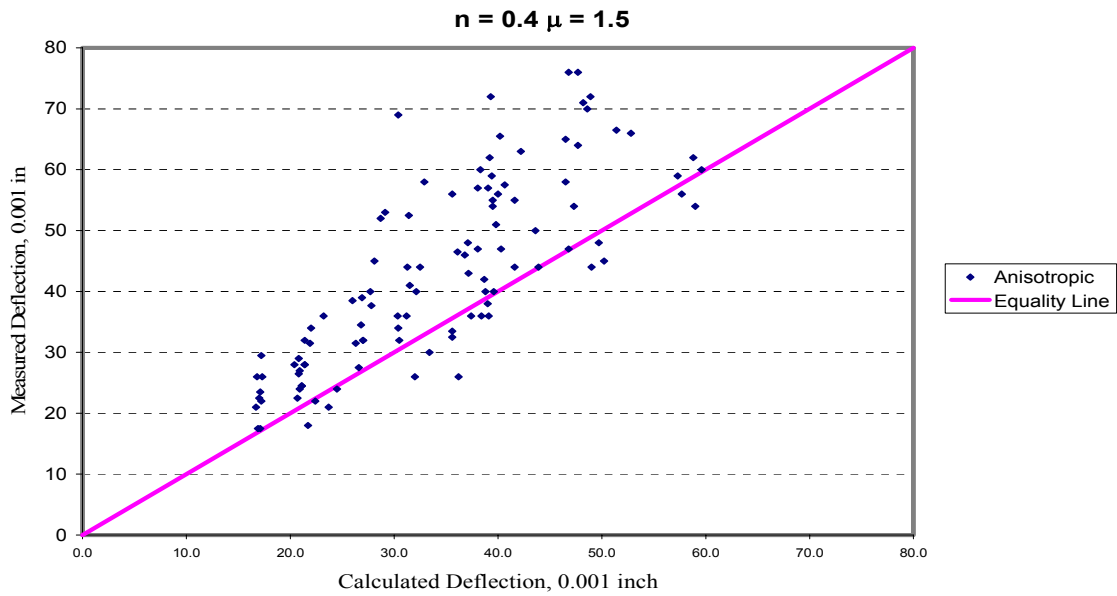
FIGURE 3.9 Measured versus calculated deflections for the spring season using anisotropic properties with n = 0.4.
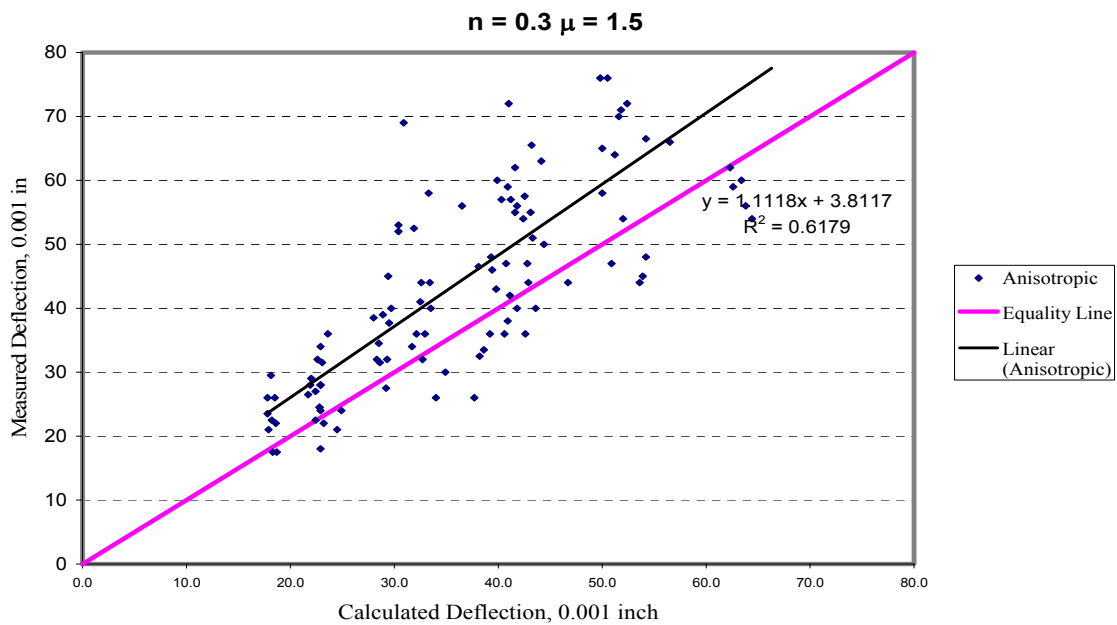
FIGURE 3.10 Measured versus calculated deflections for the spring season using anisotropic properties with n = 0.3.
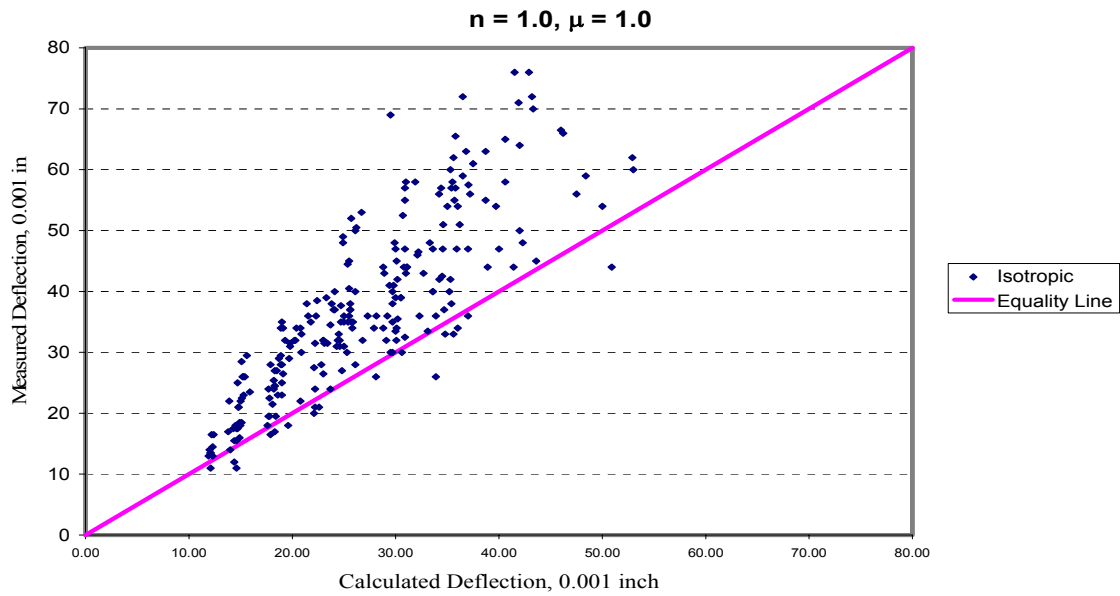
FIGURE 3.11 Measured versus calculated deflections for the spring and fall seasons using isotropic properties.
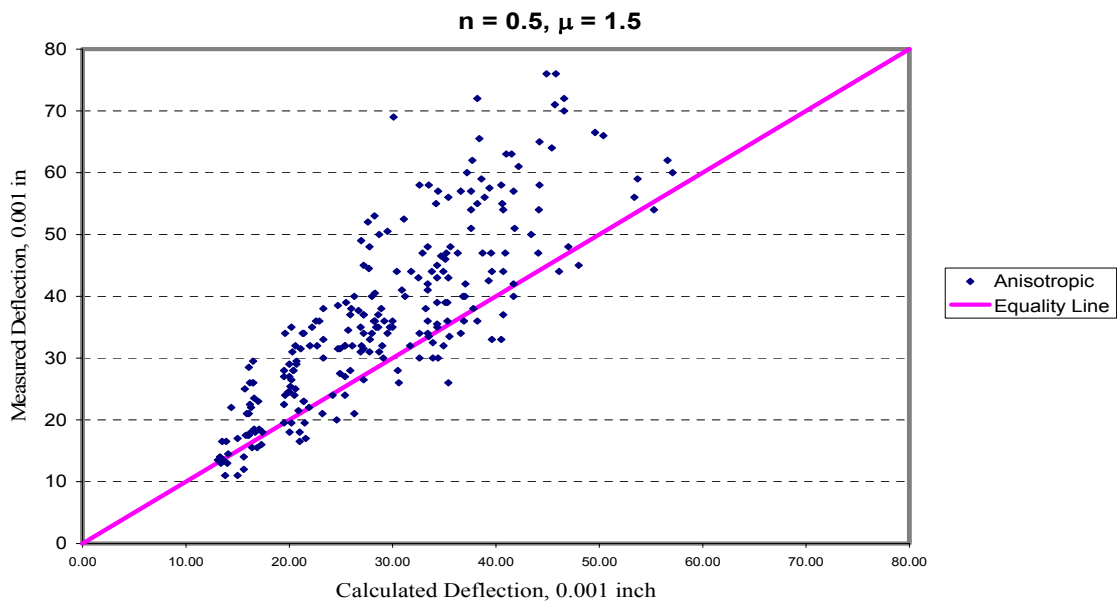
FIGURE 3.12 Measured versus calculated deflections for the spring and fall season using anisotropic properties with n = 0.5.
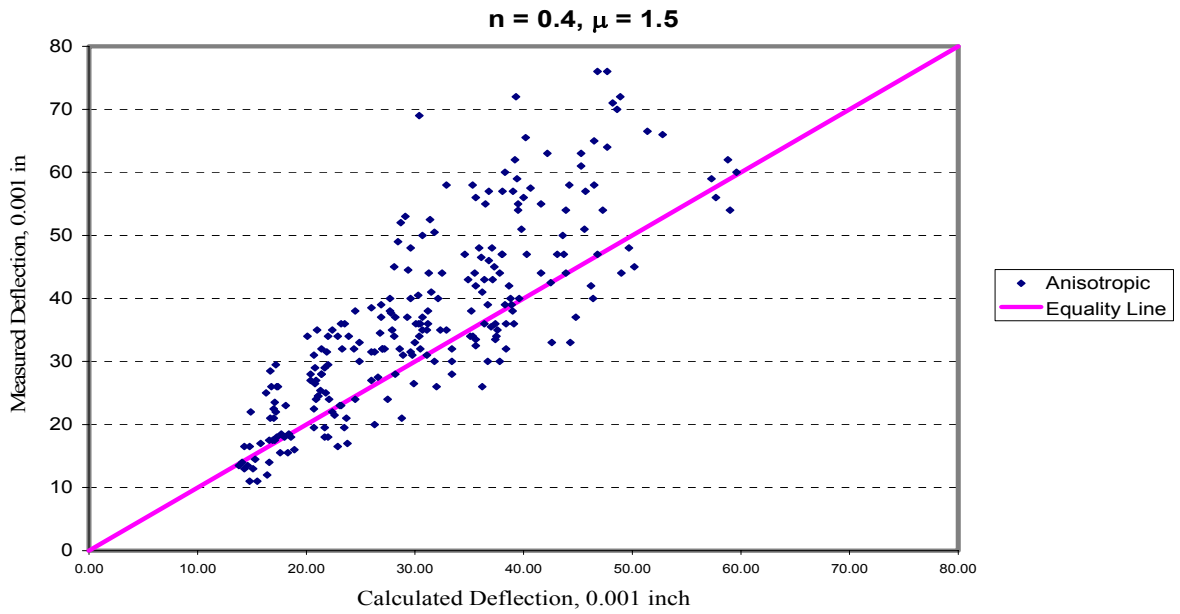
FIGURE 3.13 Measured versus calculated deflections for the spring and fall season using anisotropic properties with n = 0.4.
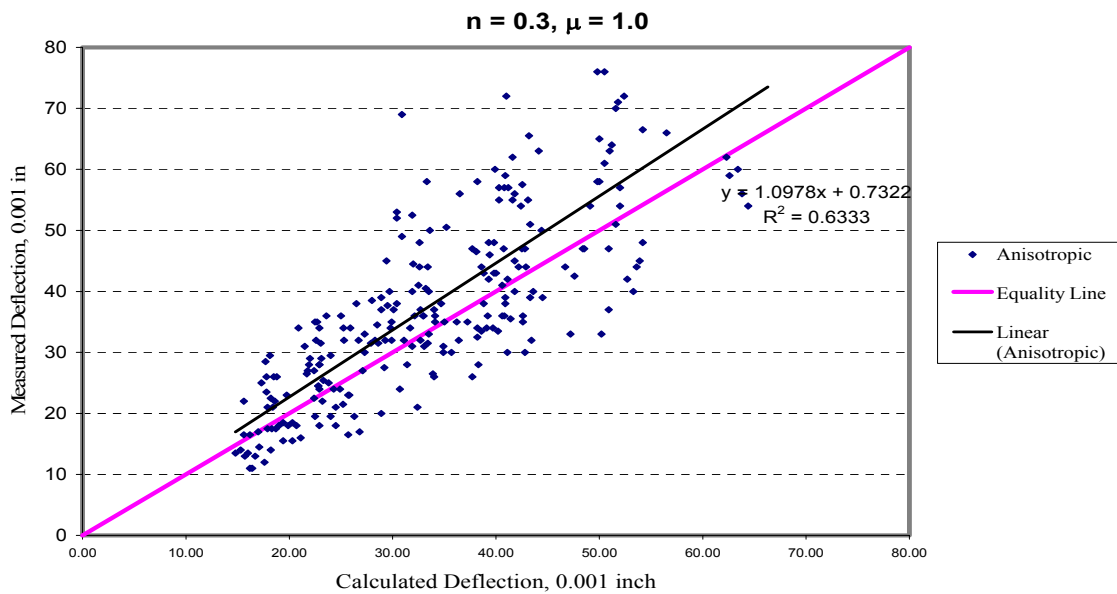
FIGURE 3.14 Measured versus calculated deflections for the spring and fall season using anisotropic properties with n = 0.3.

The accuracy of the calculations in predicting the measurements was studied by calculating the percentage of error which is the absolute difference between the calculated and measured values divided by the measured value. The cumulative distribution function of errors is shown in Figures 3.15-3.17. The y axis represents the percentage of data points with an error equal to or less than the corresponding value on the x axis. The results clearly show that the anisotropic model reduces the percentage of errors. This point can also be shown in Figures 3.18-3.20, which show the number of data points that belong to different error levels. Again, it can be seen that the number of data points shift from high error ranges to small error ranges as anisotropy increases.
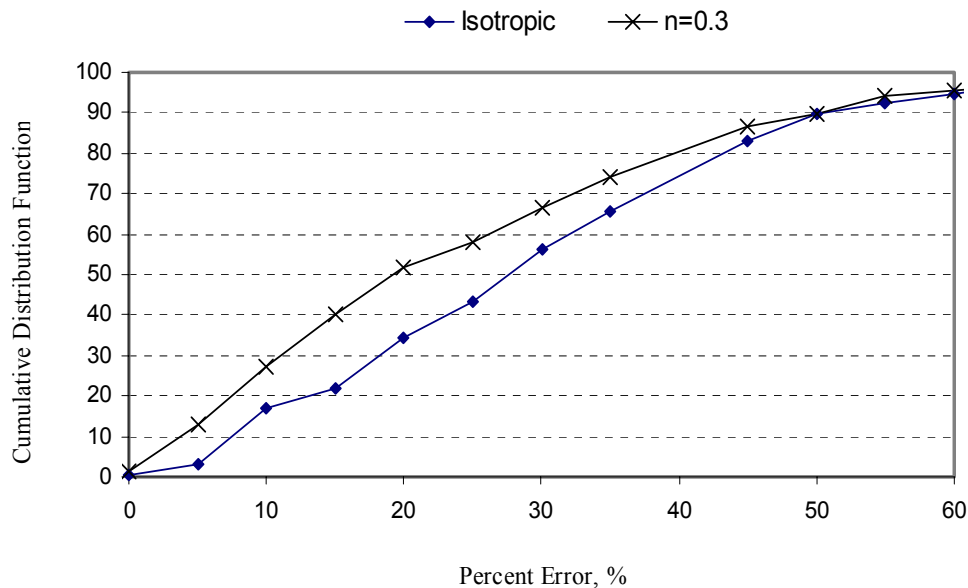
FIGURE 3.15 Percentage error for isotropic and anisotropic (n=0.3) predictions for the fall season.
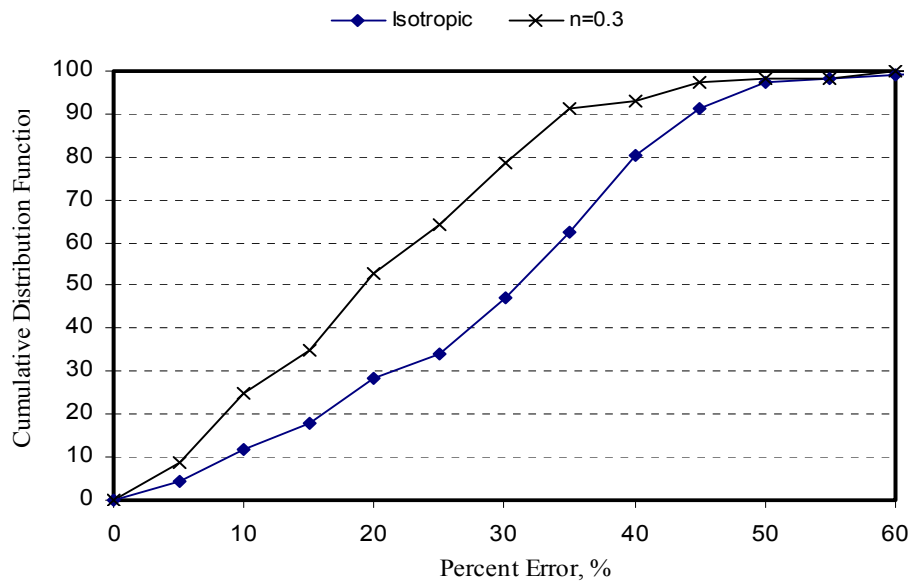
FIGURE 3.16 Percentage error for isotropic and anisotropic (n=0.3) predictions for the spring season.
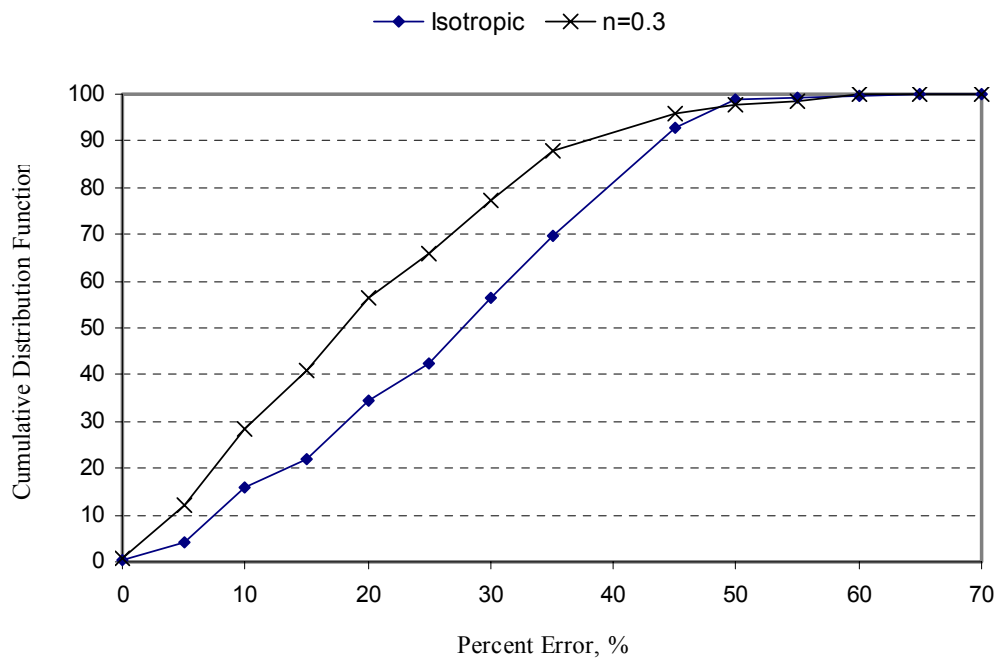
FIGURE 3.17 Percentage error for isotropic and anisotropic (n=0.3) predictions for the fall and spring seasons.
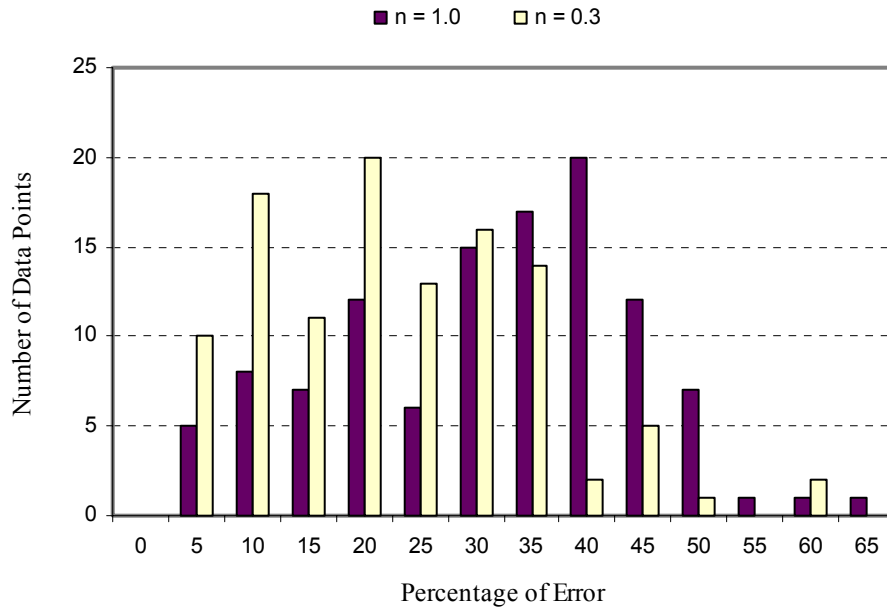
FIGURE 3.18 Number of points within a certain range of percent of error for the spring season.
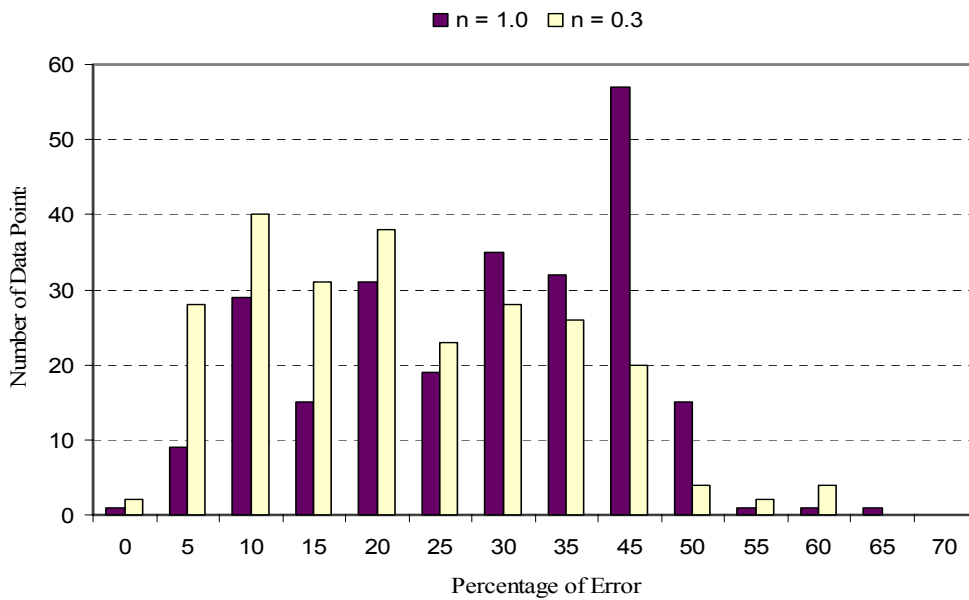
FIGURE 3.19 Number of points within a certain range of percent of error for the spring and fall seasons.
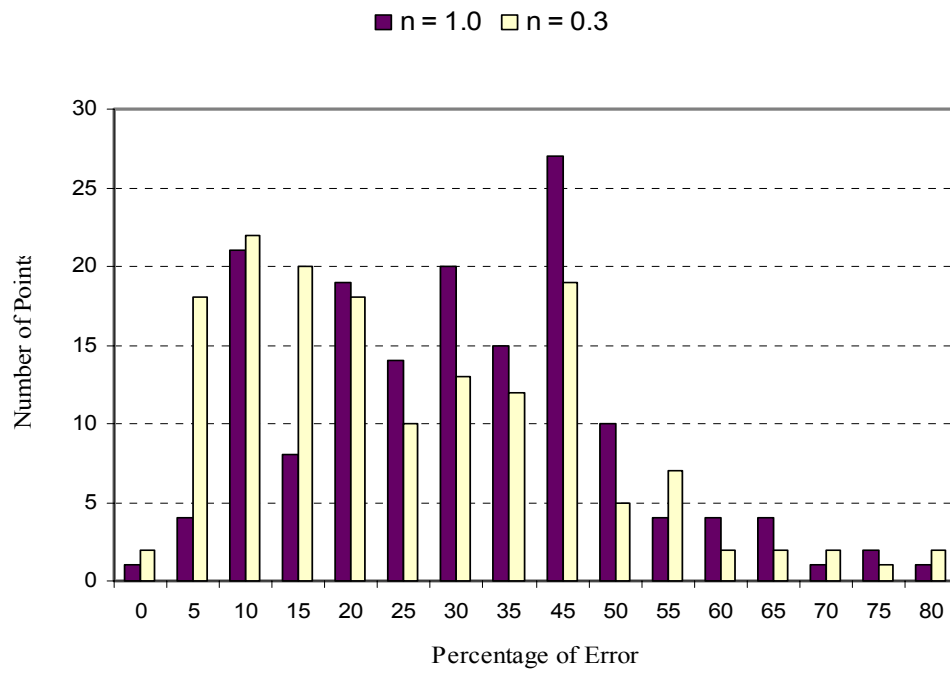
FIGURE 3.20 Number of points within a certain range of percent of error for the fall season.

3.5   Summary of Findings

In this chapter, a finite element program was used to calculate deflections of sections resembling the AASHO road test. These calculations were compared to the field experimental measurements. The following points summarize the findings:

- Anisotropy was modeled by the ratio of the horizontal modulus to vertical modulus. The percentage of error between predictions and measurements decreased as the anisotropy increased.

- The FEM predictions correlated the best with the experimental measurements when the horizontal modulus was about 30% of the vertical modulus.

- The predictions matched the AASHO measurements in the fall season better that the measurements in the spring season. As reported in the AASHO experiment, distresses were detected in the spring season that might have caused the response to deviate from the elastic solutions used in the FEM.

CHAPTER IV

ANALYSIS OF FLEXIBLE PAVEMENT RUTTING AND FATIGUE CRACKING USING ISOTROPIC AND ANISOTROPIC RESPONSE MODELS

4.1   Introduction

This chapter presents predictions of permanent deformation and fatigue cracking based on the mechanistic-empirical models used in the AASHTO 2002. These models utilize elastic stress and strain values, which are calculated in this chapter using a finite element program with the base course represented by linear isotropic, nonlinear isotropic, linear cross-anisotropic or nonlinear cross-anisotropic properties. Comparisons between the performance predictions of rutting and fatigue cracking using these different models are reported in this chapter.

4.2   Fatigue Cracking Models in the AASHTO 2002 Guide

Fatigue cracking is one of the most important distresses occurring in flexible pavements. The repeated traffic induces tensile and shear stresses in the bound layer. The repeated load initiates cracks at the point of critical tensile stress. The location of the critical tensile stress depends on the stiffness of the layer.

It is typically assumed that the fatigue cracking normally occurs at the bottom of the asphalt layer and propagates to the surface. In order to predict the allowable number of load repetitions for fatigue cracking to occur in the flexible pavement, the tensile strain at the bottom of the HMA layer is considered as the critical strain. This type of

cracking (bottom up cracking) is actually due the bending action of the pavement layer. However most recent studies show that fatigue cracking may initiate from the top and propagate down (top-down). The top-down cracking is caused by large contact pressures at the tire edge-pavement interface where the top layer of the pavement has been oxidized (*6*). In this case, the critical point for the tensile strain will be at the surface of the layer or at 0.5in from the top (*6*). The different versions of the AASHTO 2002 released until the point of the preparation of this thesis included two models for fatigue which are discussed herein.

The model used to find the allowable number of load repetition has the following form:

$$N_f = Ck_1 \left(\frac{1}{\varepsilon_t}\right)^{k_2} \left(\frac{1}{E}\right)^{k_3} \tag{4.1}$$

$$= Ck_1 \left(\varepsilon_t\right)^{-k_2} \left(E^*\right)^{-K_3} \tag{4.2}$$

where

N_f = number of repetitions to fatigue cracking,

ε_t = tensile strain at the critical location,

E = stiffness of the material,

k_1, k_2, k_3 = laboratory calibration parameters,

C   = laboratory to field adjustment factor.

The fatigue model in the AASHTO 2002 design guide released on December 2002 is based on the Shell Oil fatigue model. The most important terms in this model

are the stiffness of the asphalt layer and the tensile strain at the point of critical location. The critical location may be at the top of the layer for the top-down cracking or at the bottom for the bottom-up cracking.

Two types of controlled loading are used in the laboratory for fatigue cracking the constant stress and constant stain. Constant stress loading is considered applicable when the thickness of the layer is more than 8 inches, while constant strain is applicable for thin layers less than two inches. Shell Oil has developed equations to predict fatigue cracking for these two cases. These equations are summarized below:

Constant Strain: $N_f = A_f \left[0.17PI - 0.0085PI(V_b) + 0.0454V - 0.112 \right]^5 \varepsilon_t^{-5} E^{-1.8}$ (4.3)

Constant Stress: $N_f = A_f \left[0.0252PI - .00126PI(V_b) + 0.00673V_b - 0.0167 \right]^5 \varepsilon_t^{-5} E^{-1.4}$ (4.4)

where

PI = penetration index,

V_b = volume of bitumen.

Since the thickness for the asphalt layer could be between 2 and 8 inches which is not included in these equations, a new equation is developed in the AASHTO 2002 design guide to take into account the intermediate thickness (between 2 and 8 inches) based on equations 4.3 and 4.4. The generalized Shell Oil fatigue equation is as follows:

$$N_f = C \left(1 + \frac{13909E^{-0.4} - 1}{1 + \exp^{(1.354h_{ac} - 5.408)}} \right) \left(0.0252PI - 0.00126PI(V_b) + 0.00673V_b - 0.0167 \right)^5 \left(\frac{1}{\varepsilon_t} \right) \left(\frac{1}{E^*} \right)^{-1.4}$$ (4.5)

$$F'' = 1 + \frac{13909E^{-0.4} - 1}{1 + \exp^{(1.354h_{ac} - 5.408)}}$$ (4.6)

$$K_{1\alpha} = \left[0.0252PI - 0.00126PI(V_b) + 0.00673V_b - 0.0167 \right]^5$$ (4.7)

where

C = laboratory to field adjustment factor; with a default value of 1.0,

h_{ac} = thickness of the asphalt layer,

ε_t = tensile strain,

E = stiffness of the material,

PI = penetration index,

V_b = volume of bitumen.

The fatigue model used in the AASHTO 2002 design guide released in November 2003 was based on the Asphalt institute method. However, the equations were modified using calibration factors based on data collected from 82 LTPP sections located in 24 states, and to accommodate pavements with different thicknesses. The model has the form in Equations 4.8 – 4.12:

$$N_f = \beta_{f1} k_1 (\varepsilon_t)^{-\beta_{f2} k_2} (E^*)^{-\beta_{f3} k_3} \tag{4.8}$$

$$N_f = 0.00432 * k_1' * C \left(\frac{1}{\varepsilon_t}\right)^{3.9492} \left(\frac{1}{E}\right)^{1.281} \tag{4.9}$$

$$C = 10^M \tag{4.10}$$

$$M = 4.84 \left(\frac{V_b}{V_a + V_b} - 0.69\right) \tag{4.11}$$

$$k_1' = \frac{1}{0.000398 + \dfrac{0.003602}{1 + e^{(11.02 - 3.49 * h_{ac})}}} \tag{4.12}$$

where

$\beta_{f1}, \beta_{f2}, \beta_{f3}$ = calibration parameters,

V_a = percent air voids,

V_b = effective binder content,

h_{ac} = total thickness of the asphalt layer,

k_1' = correction for different asphalt layer thickness effects.

4.3   Analysis of Fatigue Cracking Using Isotropic and Anisotropic Models

The base layer and the asphalt mix are modeled using linear isoptropic, nonlinear isotropic, linear cross-anisotropic or nonlinear cross anisotropic properties.   The parameters K_1, K_2, K_3, n, m and μ in Eqs. 3.2-3.8 for the different pavement layers are shown in Table 4.1. v_{xx} is the horizontal Poisson's ratio, and v_{xy} is the vertical Poisson's ratio.   The linear isotropic properties are determined by taking K_2 and K_3 to be zero, while n and m are assigned to unity. Six sections are used in the analysis. Sketches of these sections are shown in Figure 4.1.

Table 4.1 Pavement Material Properties

HMA Layer (2, 4, 6 in)			
LIS $K_1 = 28000$ $K_2=0$ $K_3= 0$ $\quad$ n=1.0 m=0.38 $\quad$ μ=1.0 υ_{xy}=0.35	**NIS** $K_1 = 28000$ K_2=0.1 $K_3= 0$ $\quad$ n=1.0 m=0.38 $\quad$ μ=1.0 υ_{xy}=0.35	**LAN** $K_1 = 28000$ K_2=0 $K_3= 0$ $\quad$ n=0.5 m=0.38 $\quad$ μ=1.5 υ_{xy}=0.35	**NAN** $K_1 = 28000$ K_2=0.1 $K_3= 0$ $\quad$ n=0.5 m=0.38 $\quad$ μ=1.5 υ_{xy}=0.35
Base Layer (12, 18 in)			
LIS $K_1 = 2069$ K_2=0 $K_3= 0$ $\quad$ n=1.0 m=0.38 $\quad$ μ=1.0 υ_{xy}=0.35	**NIS** $K_1 = 2069$ K_2=0.455 $K_3= 0.295$ n=1.0 m=0.38 $\quad$ μ=1.0 υ_{xy}=0.35	**LAN** $K_1 = 2069$ K_2=0 $K_3= 0$ $\quad$ n=0.5 m=0.38 $\quad$ μ=1.5 υ_{xy}=0.35	**NAN** $K_1 = 2069$ K_2=0.455 $K_3= 0.295$ n=0.5 m=0.38 $\quad$ μ=1.5 υ_{xy}=0.35

Subgrade	
LIS $K_1 = 345$ K_2=0 K_3=0 n=1.0 m=0.38 μ=1.0 υ_{xy}=0.4	**NIS** $K_1 = 345$ K_2=0 K_3=-0.3 n=1.0 m=0.38 μ=1.0 υ_{xy}=0.4

\

400,000psi	υ=0.35	2in
30,000psi	υ=0.35	12in
5000psi	υ=0.4	

Section (A)   Section (B)   Section (C)

400,000psi	υ=0.35	2in
30000PSI	υ=0.35	18in
5000psi	υ=0.4	

Section (D)   Section (E)   Section (F)
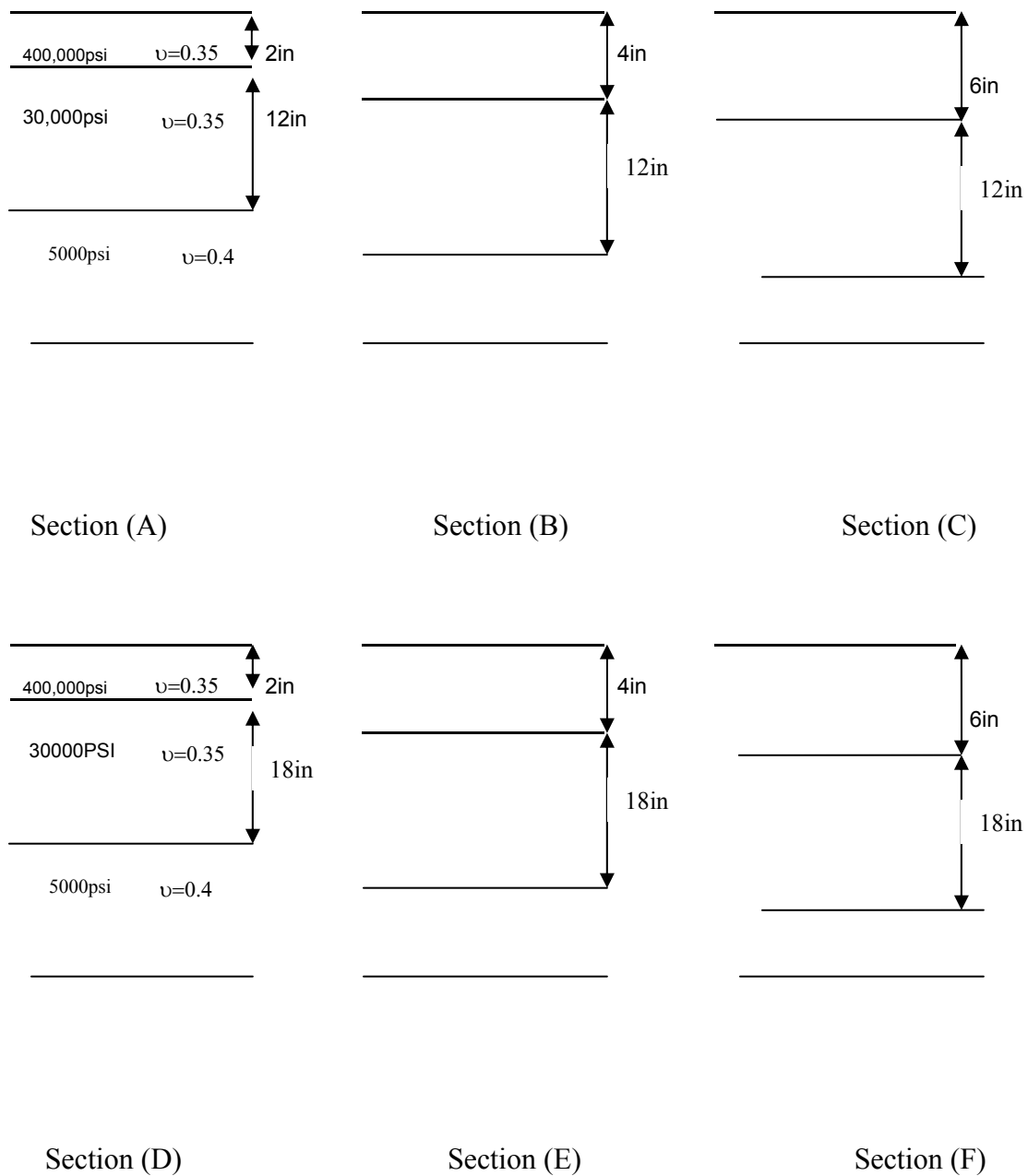
FIGURE 4.1 The sections used in the analysis.

   The fatigue analysis is conducted using the Shell model and Asphalt Institute model calibrated in the AASHTO 2002 design guide. The tensile strain at the bottom of the HMA layer was considered as the critical strain for bottom-top cracking.

The Shell equation was used with typical values for the penetration index (0.934) and volume of bitumen (11%). Figures 4.2 and 4.3 show the fatigue life using the isotropic and anisotropic material properties.
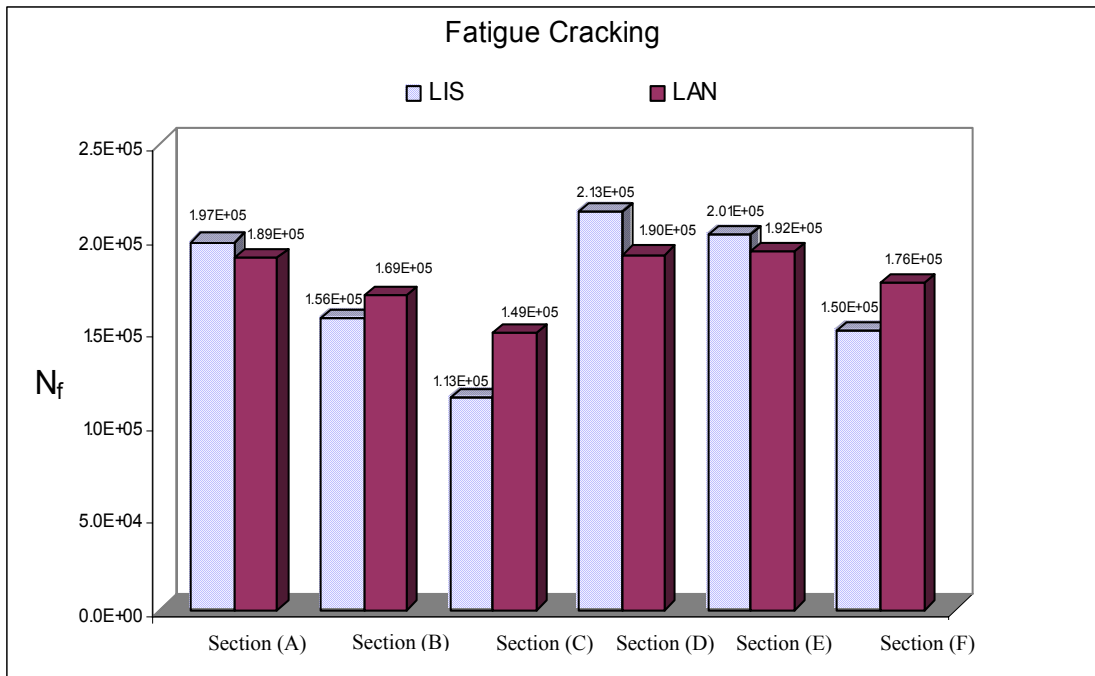
FIGURE 4.2 Comparison between linear isotropic and linear anisotropic models of the allowable number of load repetitions using the Shell method.
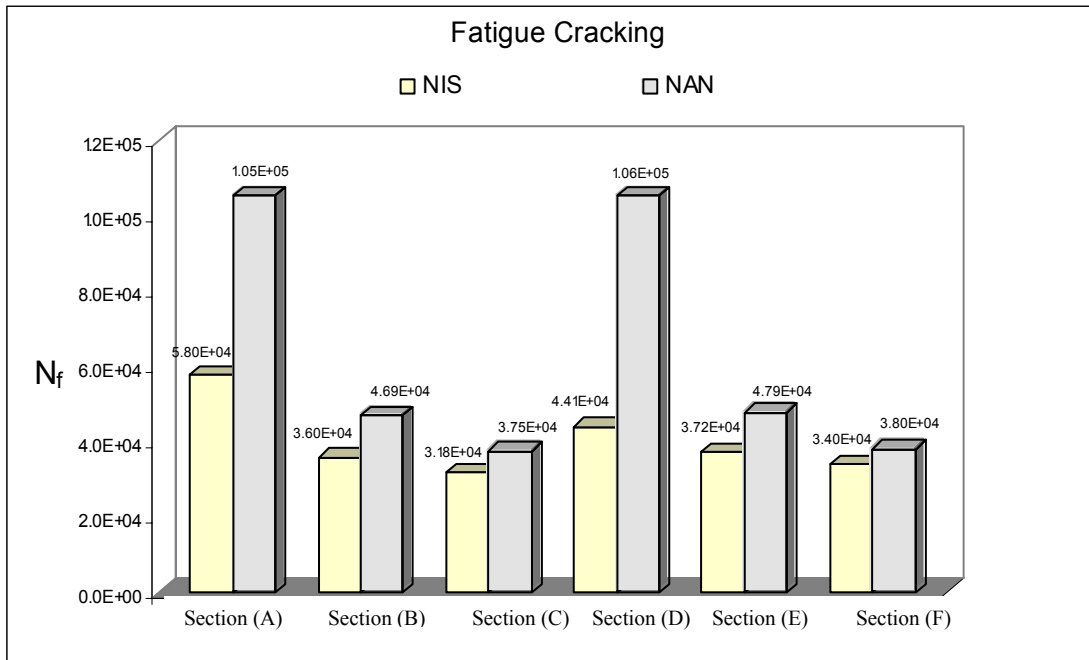
FIGURE 4.3 Comparison between non-linear isotropic and non-linear anisotropic models of the allowable number of load repetitions using the Shell method.

It can be seen form Figure 4.2 that the anisotropic model starts to give higher number of load repetitions than the isotropic models when the thickness of the HMA layer increases in the linear analysis. In the case of nonlinear analysis, it can be seen that the anisotropic model gives longer fatigue life than the isotropic model. These results can explain part of the shift factor between the laboratory fatigue life and the field fatigue life. It is clear that using anisotropic properties predicts longer fatigue life and less shift factor.

Figures 4.4 and 4.5 show a comparison between the linear isotropic and linear anisotropic models based on the tensile strain distribution across the depth of the asphalt and base layer. It can be seen from this figure that the tensile strain at the bottom of HMA for the isotropic model is more than that for the anisotropic model. Appendix A

includes the strain profiles for the sections in Figure 4.1 calculated using the different

models in Table 4.1.

FIGURE 4.4 The tensile strain profiles in the asphalt and base layers of section C using linear isotropic and anisotropic properties.
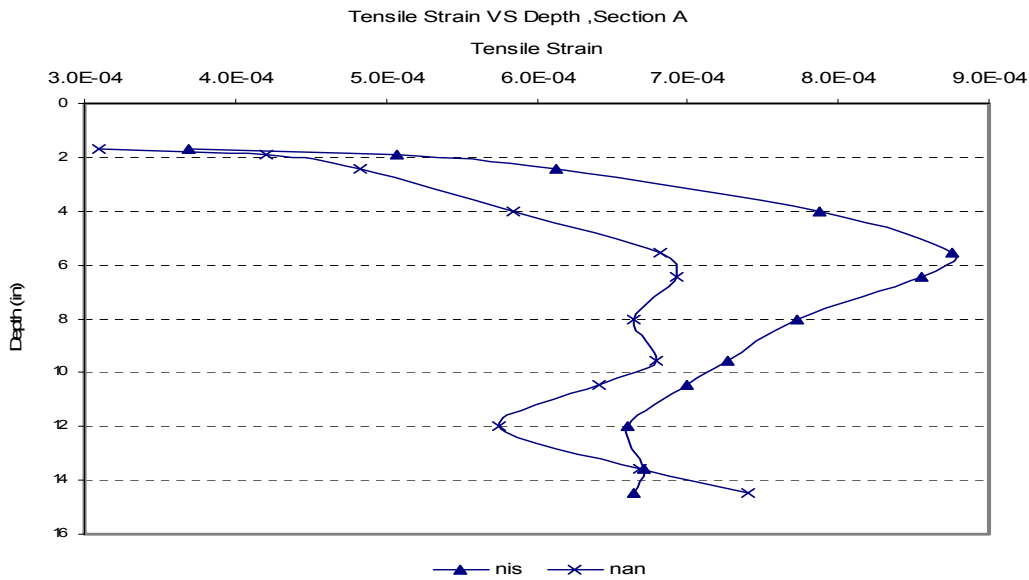
FIGURE 4.5 The tensile strain profiles in the asphalt and base layers of section A using nonlinear isotropic and anisotropic properties.

The Asphalt Institute equation (Eq.4.9) was also used to determine the fatigue life using a volume of bitumen of 11 % and percentage air voids in the asphalt mix equal to about 7.5%. Figure 4.6 and Figure 4.7 show comparisons in fatigue life using isotropic and anisotropic material properties. The results are in accordance with those from the Shell method. More specifically, the nonlinear anisotropic analysis predicts longer fatigue life than the nonlinear isotropic analysis.
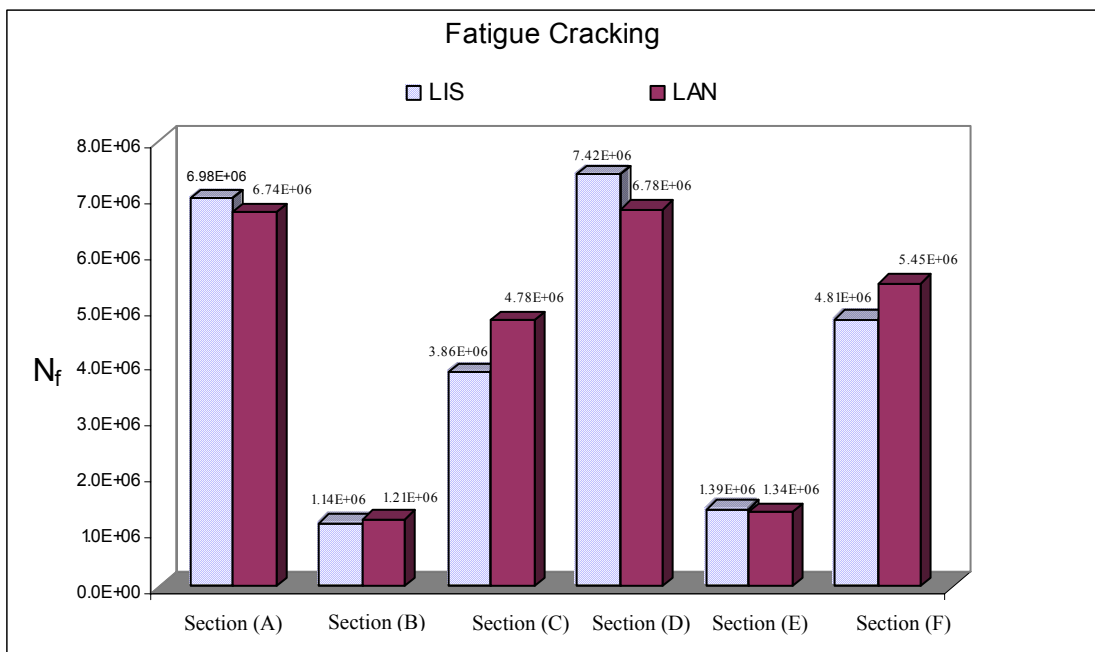
FIGURE 4.6 Comparison between linear isotropic and linear anisotropic models of the allowable number of load repetitions using the Asphalt Institute method.
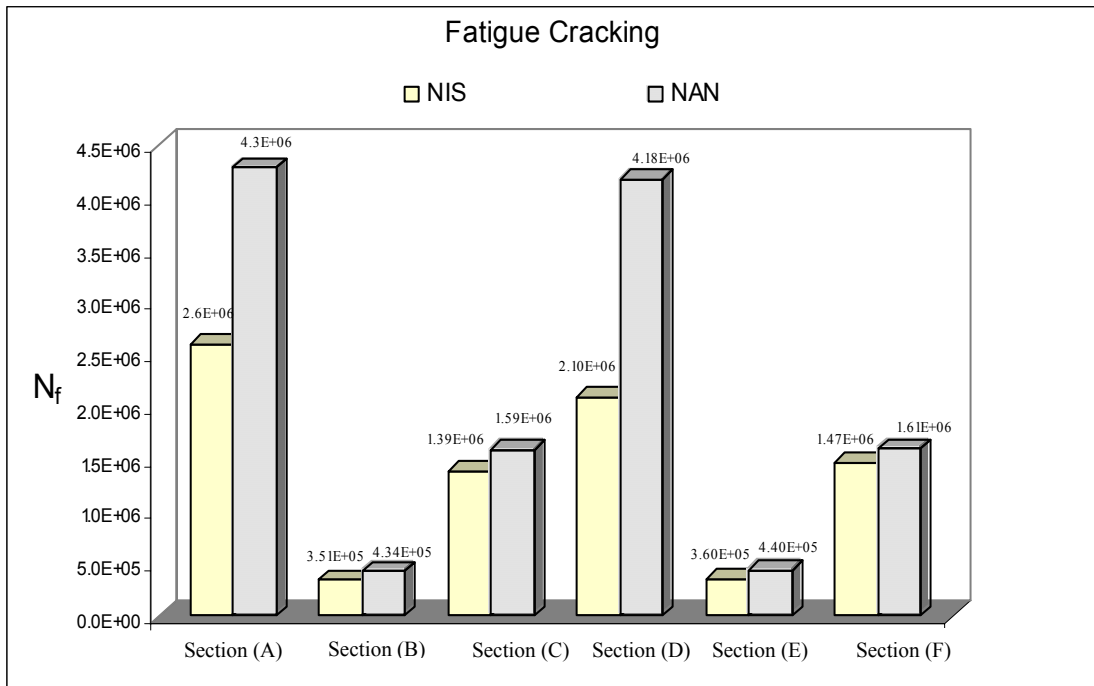
FIGURE 4.7 Comparison between nonlinear isotropic and nonlinear anisotropic models of the allowable number of load repetitions using the Asphalt Institute method.

The fatigue life predicted by the Asphalt Institute model is much longer than that predicted by the Shell model. This is attributed to the fact that the Asphalt Institute method was calibrated with field data, while the Shell method was not. It is interesting to note that the results show that thin pavements can have longer fatigue life than the thick pavements. This is consistent with the findings by the AASHTO 2002 team that it is not necessary that the magnitude of tensile strain increases proportionally to a decrease in HMA thickness.

4.4   Permanent Deformation Models in the AASHTO 2002 Guide

Permanent deformation is one of the most important distresses occurring in the flexible pavement. It is associated with rutting in the wheel path and develops gradually as the

number of load repetitions increase. For many years it was assumed that the permanent deformation is related to the vertical compressive strain at the top of subgrade so the rutting can be reduced by limiting the vertical compressive strain at the top of subgrade. The AASHTO 2002 considers the total permanent deformation in all layers in the pavement structure.

The Tseng and Lytton model is used to predict the permanent deformation in the asphalt, base and subgrade layers. The model has three parameters ($\varepsilon_0, \beta\ and\ \rho$), and it describes the relationship between the permanent strains and the number of load repetitions (*24*). Many factors affect the permanent deformation of the pavement layers; stress state, density, moisture content, asphalt content, temperature, and other material and environmental characteristics. The three parameters in the asphalt layer are sensitive to resilient modulus, deviatoric stress, asphalt content and temperature, while the three parameters in the granular base material are functions of resilient modulus, confining pressure and the water content. In addition to the factors used in the equations for the granular materials, it was found that the deviatoric stress is also a significant factor which affects the values of the parameters in the subgrade soil. In the model, the three parameters are used as a fractional increase of total strains for each layer in the pavement.

In this study, the vertical resilient strains were calculated at the middle of each layer (or sublayer) using the finite element program. The permanent deformation is taken as the summation of the permanent deformations in all sublayers.

For a single axle load, the permanent Deformation, δ_a, is given by

$$\delta_a(N) = \sum_{i=1}^{n} \left\{ \left(\frac{\varepsilon_{0i}}{\varepsilon_{ri}} \right) e^{-\left(\frac{\rho_i}{N}\right)^{\beta_i}} \int_{h_{i-1}}^{h_i} \varepsilon_v(Z) dz \right\} \tag{4.13}$$

where

δ_a = permanent deformation for layer/sublayer,

ε_v = average vertical resilient strain in the layer/sublayer as obtained from the primary

response model,

h = thickness of the layer/sublayer,

ε_r = resilient strain imposed in laboratory test to obtain material properties ε_0, ρ and β,

ε_0, β and ρ = material properties.

The equations of the three parameters are (some of the signs in these equations are

modified here based on discussion with Dr.Lytton):

<u>Asphalt Layer</u>

$$\log \beta = -5.04349 + 0.01812 A_c + 0.011045 A_c^2 + 0.01127 T - 0.203249 \log \sigma_d + 1.12228 \log E_r \tag{4.14}$$

$$\log \beta = -2.51475 + 0.60816 A_c - 0.05282 A_c^2 - 0.00214 T + 0.16597 \log \sigma_d - 0.0000002 E_r \tag{4.15}$$

$$\log \rho = 8.105675 - 4.241965 A_c + 0.54159 A_c^2 + 0.03865 T - 0.01487 \sigma_d + 0.000005 E_r \tag{4.16}$$

<u>Granular Material</u>

$$\log\left(\frac{\varepsilon_0}{\varepsilon_r}\right) = 0.80978 - 0.06626 W_C + 0.003077 \sigma_\theta + 0.000003 E_r \tag{4.17}$$

$$\log \beta = -0.919 + 0.03105 W_C + 0.001806 \sigma_\theta - 0.0000015 E_r \tag{4.18}$$

$$\log \rho = -1.78667 + 1.45062 W_C + 0.003784 \sigma^2_\theta - 0.002074 W_C^2 \sigma_\theta - 0.0000105 E_r \quad (4.19)$$

Subgrade

$$\log \left(\frac{\varepsilon_0}{\varepsilon_r} \right) = -1.69867 + 0.09121 W_C - 0.11921 \sigma_d + 0.91219 \log E_r \qquad (4.20)$$

$$\log \beta = -0.973 - 0.0000278 W_c^2 \sigma_d + 0.017165 \sigma_d - 0.00000338 W_C^2 \sigma_\theta \qquad (4.21)$$

$$\log \rho = 11.009 + 0.0000681 W_c^2 \sigma_d - 0.4026 \sigma_d + 0.00000545 W_C^2 \sigma_\theta \qquad (4.22)$$

where

W_C = water content(%),

σ_d = deviatoric stress (psi),

σ_θ = bulk stress (psi),

E_r = resilient modulus of the layer/sublayer(psi).

The form of the Tseng and Lytton model was modified in the AASHTO 2002 to include a calibration factor:

$$\delta_a(N) = \beta_1 \left(\frac{\varepsilon_0}{\varepsilon_r} \right) e^{-\left(\frac{\rho}{N} \right)^\beta} \varepsilon_v h \qquad (4.23)$$

where

β_1 = calibration factor for the unbound granular and subgrade materials; equal to 2.2 for the base layer while it is equal to 8.0 for the subgrade soil.

The equations used to get the three parameters ε_0, β and ρ in the base and subgrade layers in the AASHTO 2002 are different than the ones proposed by Tseng and

Lytton. The stress term is eliminated from the equations in the AASHTO 2002. The relationships for the base and subgrade are as follows:

$$\log \beta = -0.61119 - 0.017638 W_c \tag{4.24}$$

$$\log\left(\frac{\varepsilon_0}{\varepsilon_r}\right) = \frac{\left(e^{(\rho)^\beta} * a_1 E_r^{b_1}\right) + \left(e^{\left(\frac{\rho}{10^7}\right)^\beta} * a_7 E_r^{b_7}\right)}{2} \tag{4.25}$$

$$C_0 = \ln\left[\frac{\left(a_1 E_r^{b_1}\right)}{a_7 E_r^{b_7}}\right] \tag{4.26}$$

$$\rho = 10^7 \left[\frac{C_0}{\left(1-\left(10^7\right)^\beta\right)}\right]^{\frac{1}{\beta}} \tag{4.27}$$

$$W_c = 51.712\left[\left(\frac{E_r}{2555}\right)^{\frac{1}{0.64}}\right]^{-0.3586*GWT^{0.1192}} \tag{4.28}$$

Where:

W_c = water content (%),

E_r = resilient Modulus of the layer/sublayer (psi),

GWT = ground water table depth (ft),

a1   = 1.0942e-18,

b1   = 3.520049,

a7   = 0.03162278,

b7   = 0.5.

The relationship used in the AASHTO 2002 to predict the permanent deformation in the Asphalt layer is based on the statistical analysis of laboratory repeated load permanent deformation tests.

The final equation conducted by Leahy, Ayers and Kaloush to predict the permanent deformation is as follows:

$$\frac{\varepsilon_p}{\varepsilon_r} = K_1 * 10^{-3.51108} N^{.0.479244} T^{1..5606} \tag{4.29}$$

$$C_1 = -0.1039 * H_{ac}^2 + 2.4868 * H_{ac} - 17.342 \tag{4.30}$$

$$C_2 = 0.0172 * H_{ac}^2 - 1.7331 * H_{ac} + 27.428 \tag{4.31}$$

where

ε_r = the vertical resilient strain at any depth (obtained from the primary response model),

N = allowable number of load repetitions,

T = temperature (F),

ε_p = plastic strain,

k_1 = function of total asphalt layer thickness and depth to computational point, to correct for the confining pressure at different depths.

The rut depth for each sublayer in the AC layer can be found from

$$\Delta R_{di} = \varepsilon_{pi.} \Delta h_i \tag{4.32}$$

The summation for all incremental ΔR_d, the total layer rut depth can be obtained from

$$R_d = \sum_{i=1} \Delta R_{di} \tag{4.33}$$

4.5   Analysis of Permanent Deformation Using Isotropic and Anisotropic Models

It was found that the permanent strain calculated using anisotropic properties is higher than that using isotropic properties in the asphalt layer. An example of the results is shown in Figure 4.8.   This is attributed to the higher compressive strain in the anisotropic model compared with the isotropic model, although the deviatoric stress is less for the anisotropic model. Examples of the results are shown in Figures 4.9 and 4.10. The results for the other sections are given in Appendix A
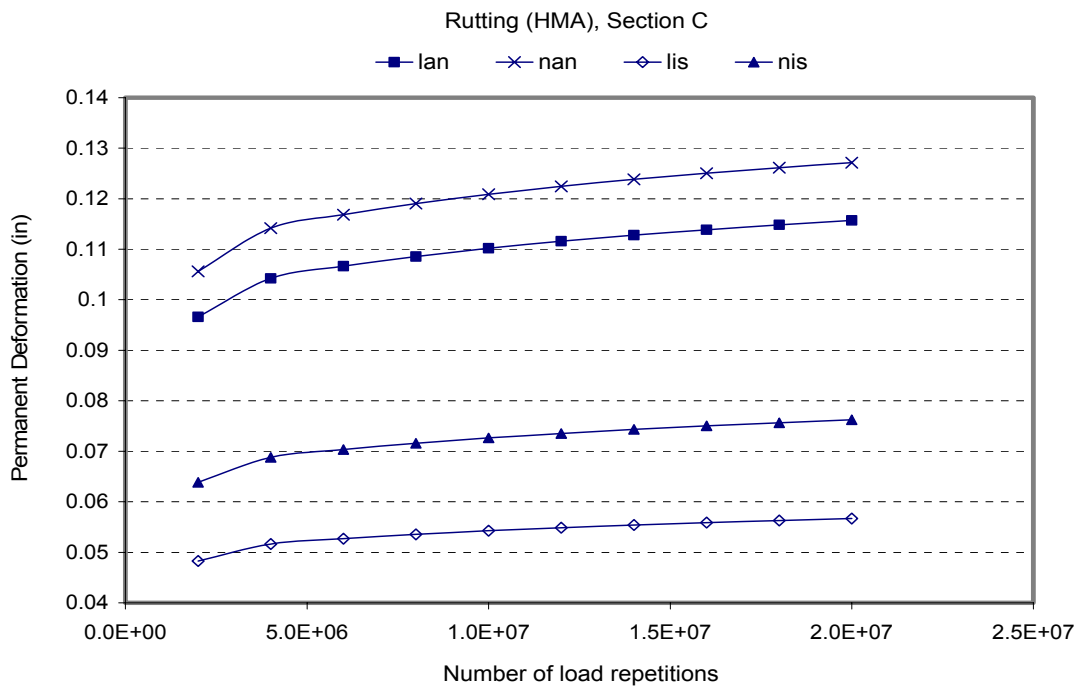
FIGURE 4.8 HMA permanent deformation in section C using the Tseng and Lytton model.
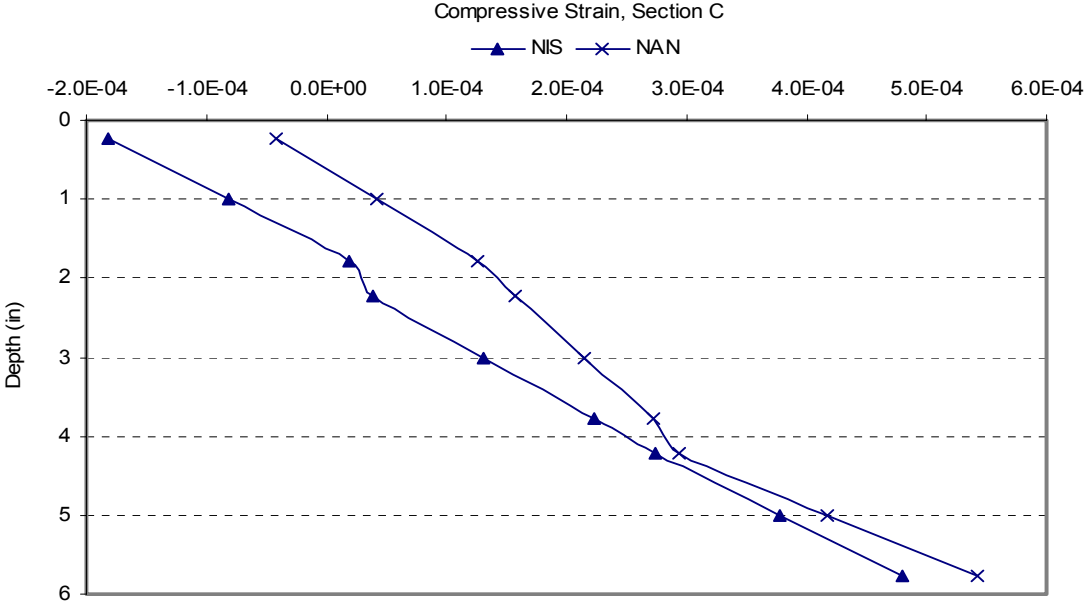
FIGURE 4.9 The compressive strain profiles in the asphalt layer of section C using non-linear isotropic and anisotropic properties.
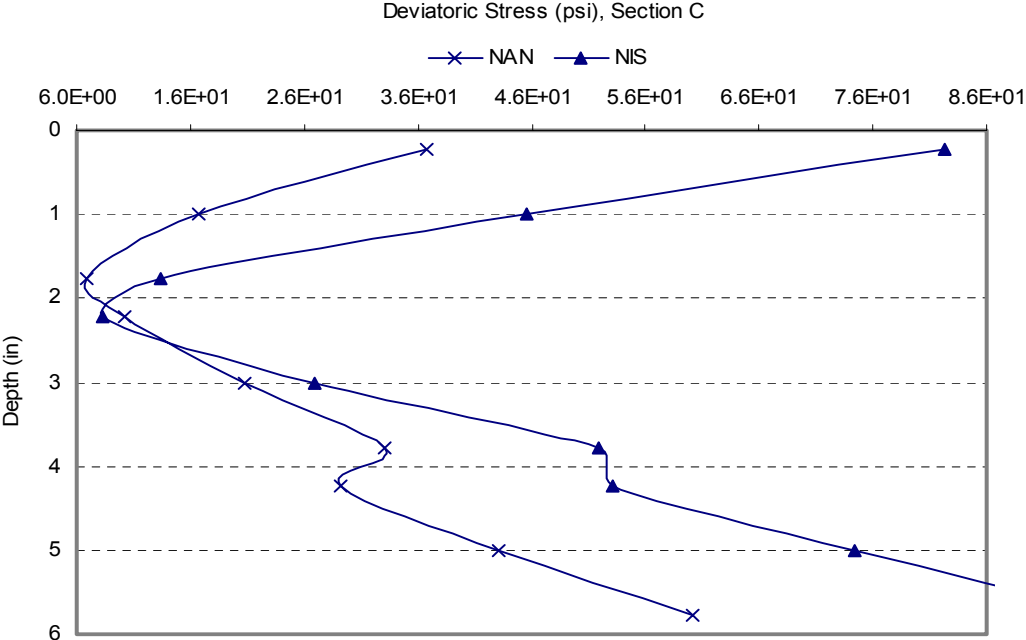
FIGURE 4.10 The deviatoric stress profiles in the asphalt layer of section C using non-linear isotropic and anisotropic properties.

Figure 4.11 shows that the permanent deformation in the base layer obtained by using anisotropic properties is always more than the isotropic model. This is caused by the higher compressive strain in the base layer for the case of using anisotropic properties (Figure 4.12). It should be noticed that the bulk stress is higher for the anisotropic model (Figure 4.13). The results indicate that the compressive strain rather than the bulk stresses is more dominant the design in terms of permanent deformation. The results for the other sections are shown in Appendix A.
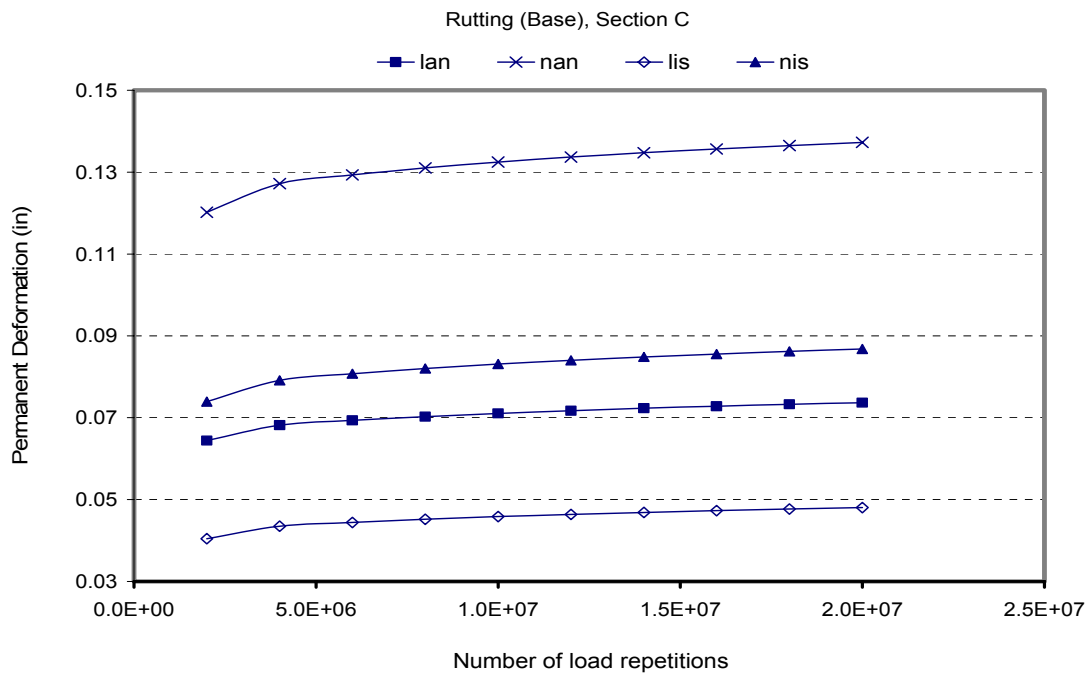
FIGURE 4.11 Permanent deformation in the base of section C using the Tseng and Lytton model.
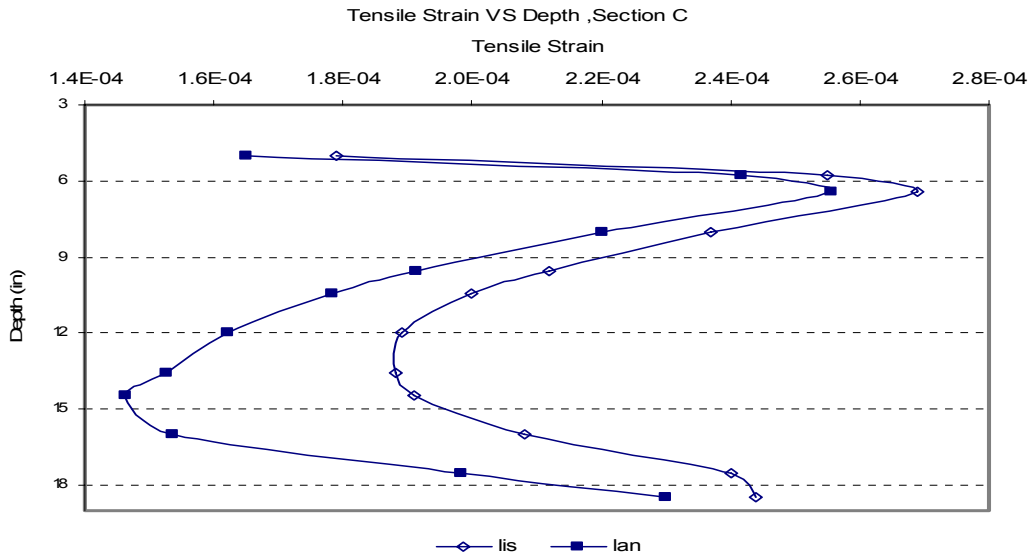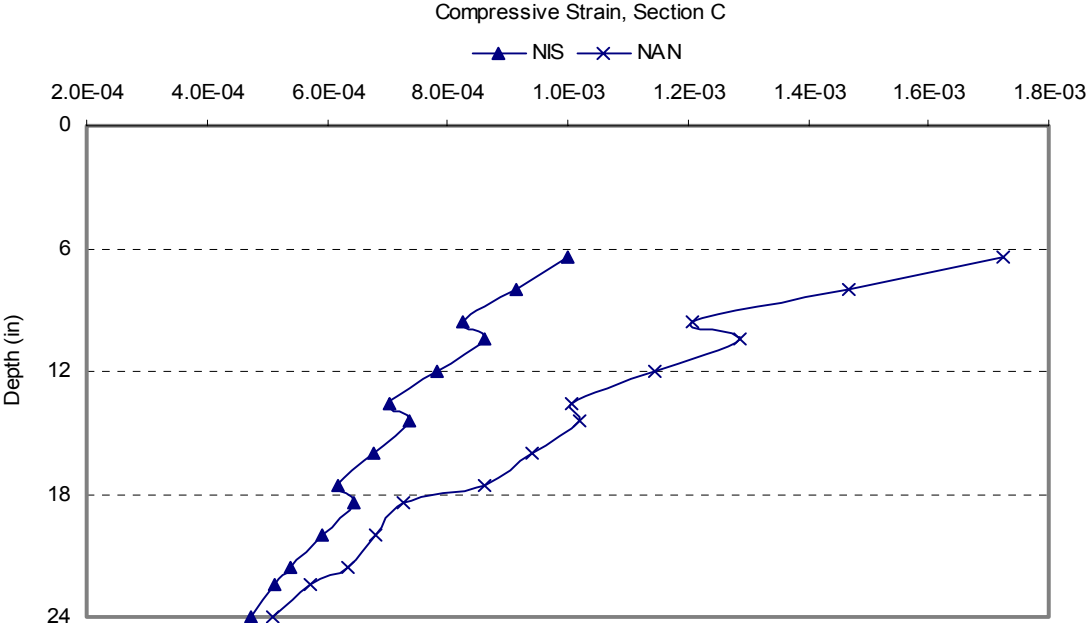
FIGURE 4.12 Compressive strain profiles in the base layer of section C using non-linear isotropic and anisotropic properties.
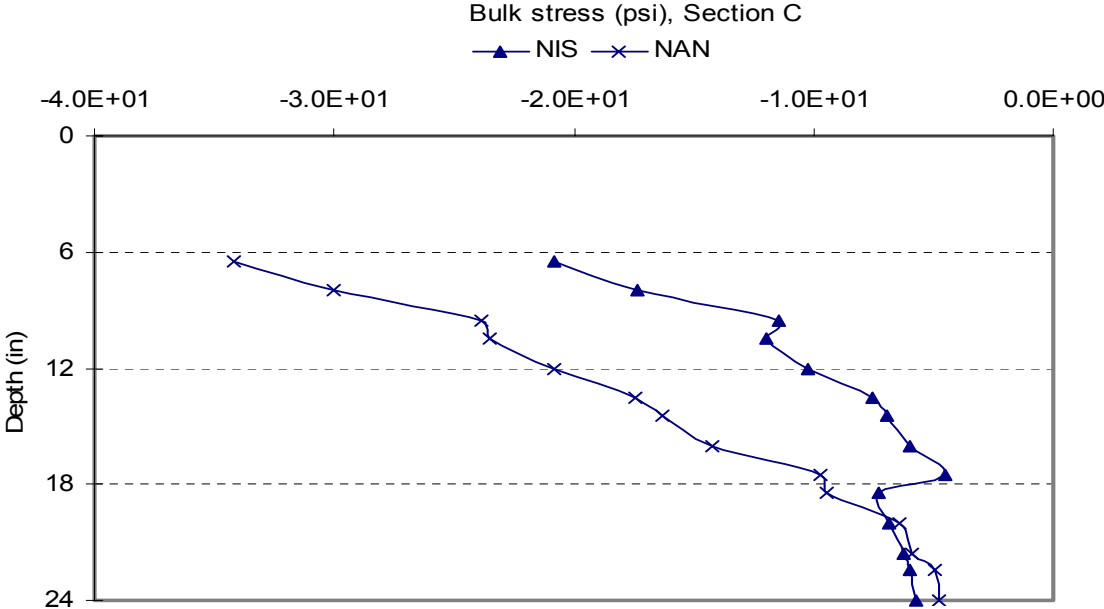
FIGURE 4.13 The bulk stress profiles in the base layer of section C using non-linear isotropic and anisotropic properties.
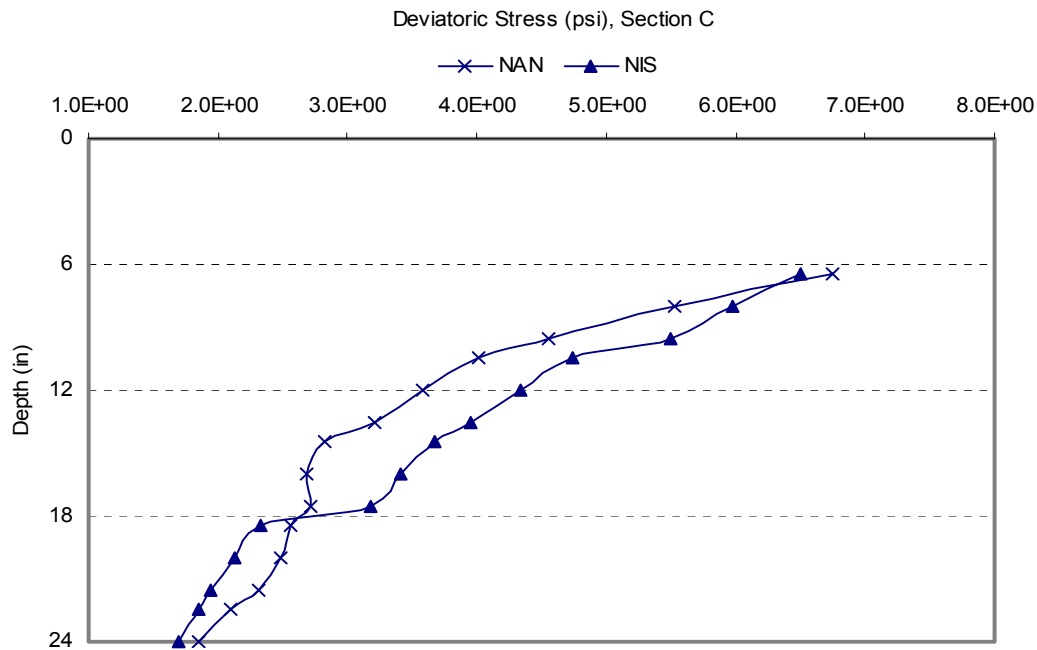
FIGURE 4.14 The deviatoric stress profiles in the base layer of section C using non-linear isotropic and anisotropic properties.

The bulk stress at the top of subgrade is higher for the anisotropic model as can be seen from Figure 4.13.   The deviatoric stress (Figure 4.14) and the vertical compressive strain for the anisotropic model can be higher or lower than those of the isotropic. However, the resultant of the effects of the bulk stress, deviatoric stress and the vertical strain give less permanent deformation using the anisotropic properties (Figure 4.15).

Figure 4.16 shows the total rutting in section C. The results show that the permanent deformation for the nonlinear isotropic model is more than that for the nonlinear anisotropic model.

Rutting (Subgrade), Section C

■ lan   ✕ nan   ◇ lis   ▲ nis
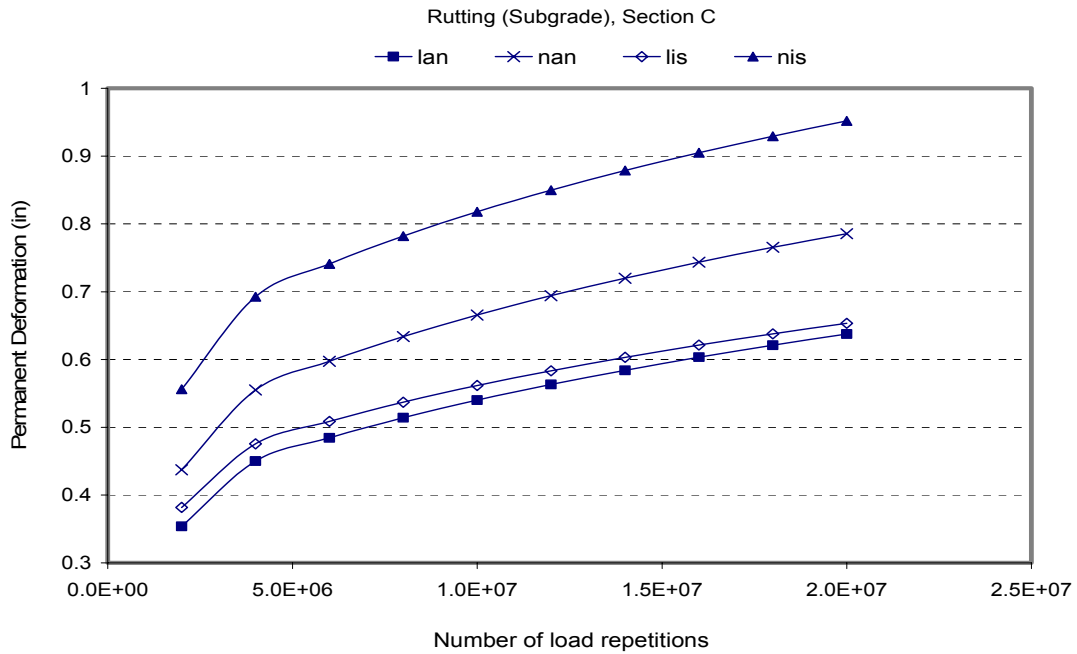
FIGURE 4.15 Subgrade permanent deformation in section C using the Tseng and Lytton model.

Rutting (Total), Section C

■ lan   ✕ nan   ◇ lis   ▲ nis
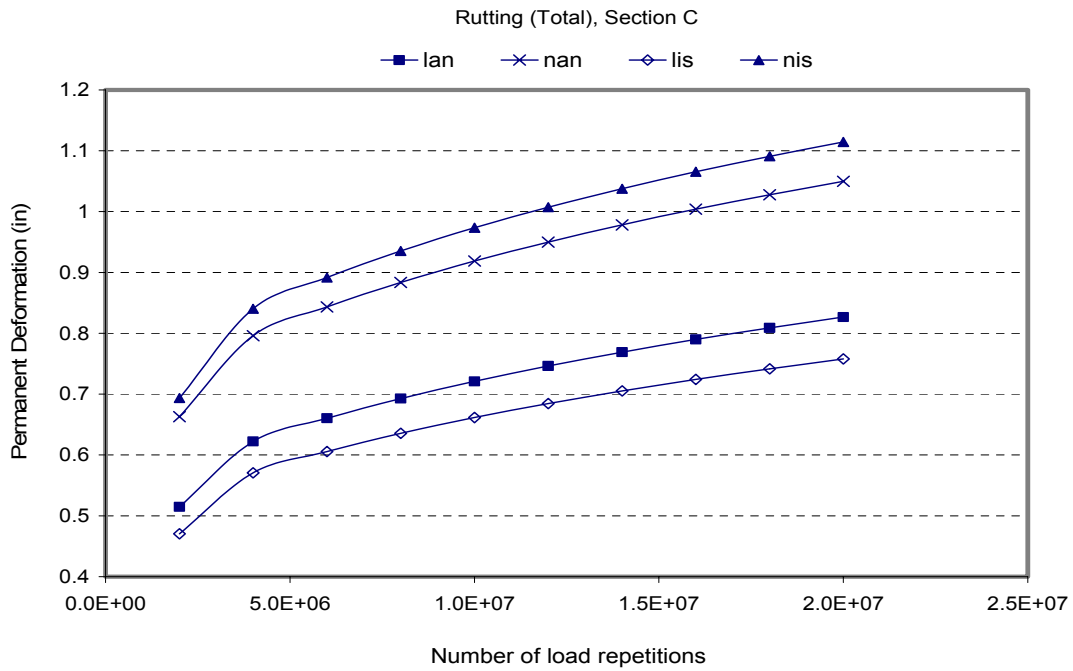
FIGURE 4.16 Total permanent deformation in section C using the Tseng and Lytton model.

The permanent deformation was also calculated in the pavement layers using the regression equations implemented in the AASHTO 2002 guide. The permanent deformation for the anisotropic model is more than that for the isotropic model (Figure 4.17).
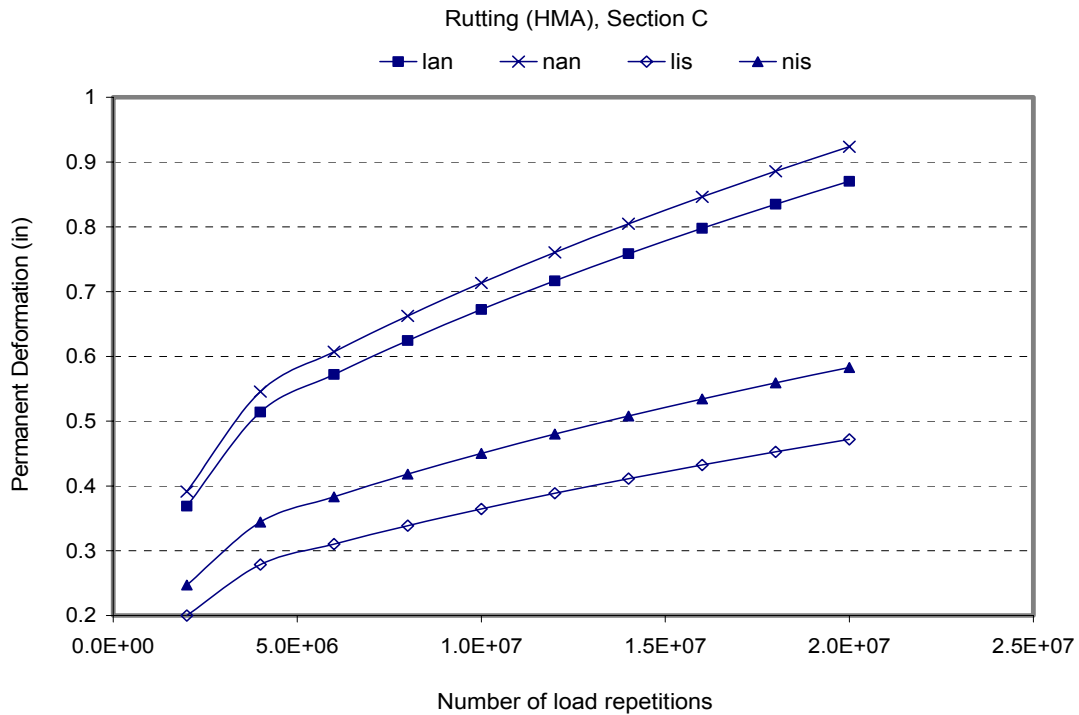
FIGURE 4.17 HMA permanent deformation in section C using the AASHTO 2002 model.

It can be seen from Figure 4.18 that the permanent deformation in the base layer obtained using the anisotropic model is always more than the isotropic model. For the subgrade, the permanent deformation obtained by using isotropic model can be more or less than that calculated using the anisotropic model depending on the section and the material properties. An example of the subgrade permanent deformation is in Figure

4.19. Figure 4.20 shows that the total rutting for the anisotropic model is always more than that for isotropic model.

Rutting (Base), Section C
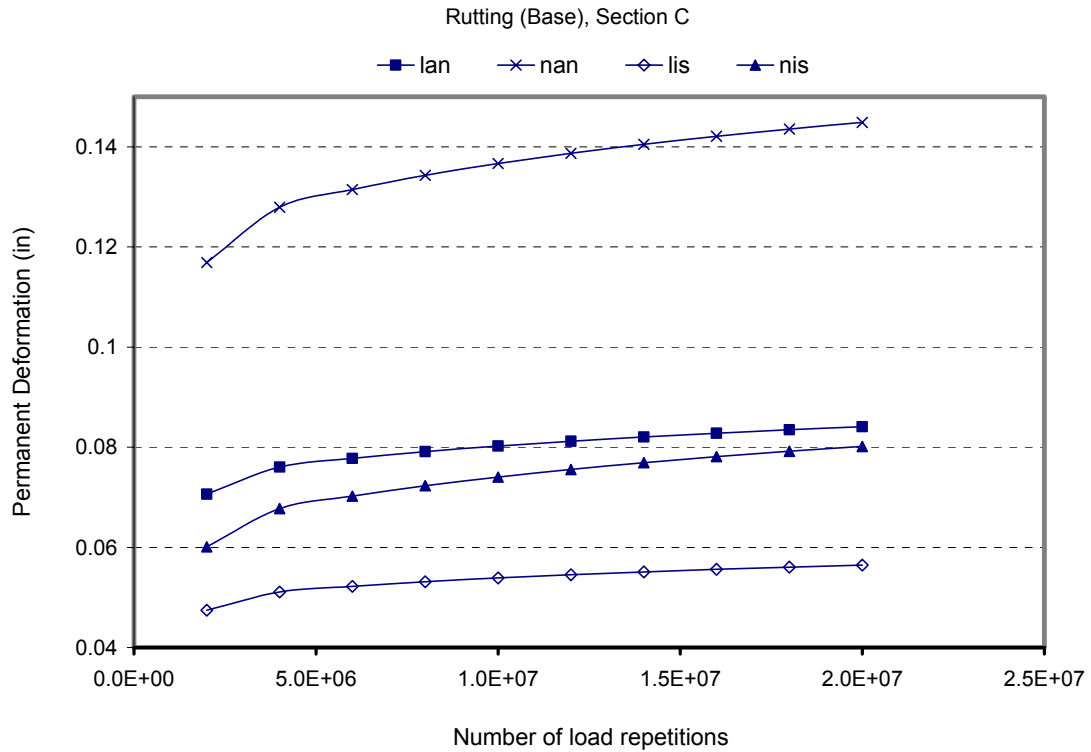
FIGURE 4.18 Base permanent deformation in section C using the AASHTO 2002 model.
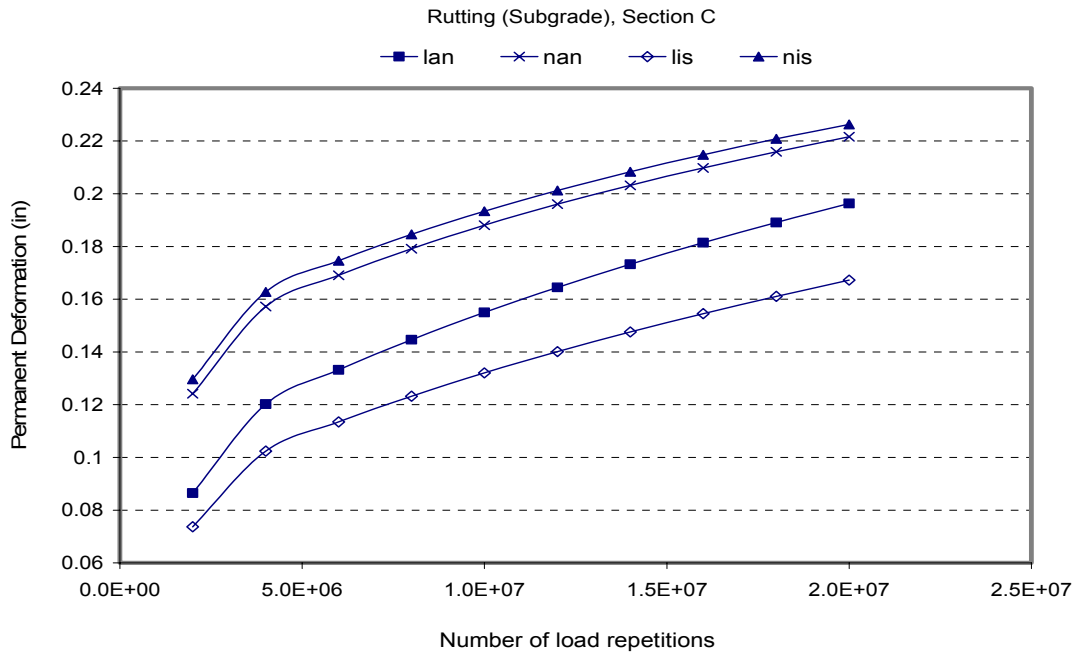
FIGURE 4.19 Subgrade permanent deformation in section C using the AASHTO 2002 model.
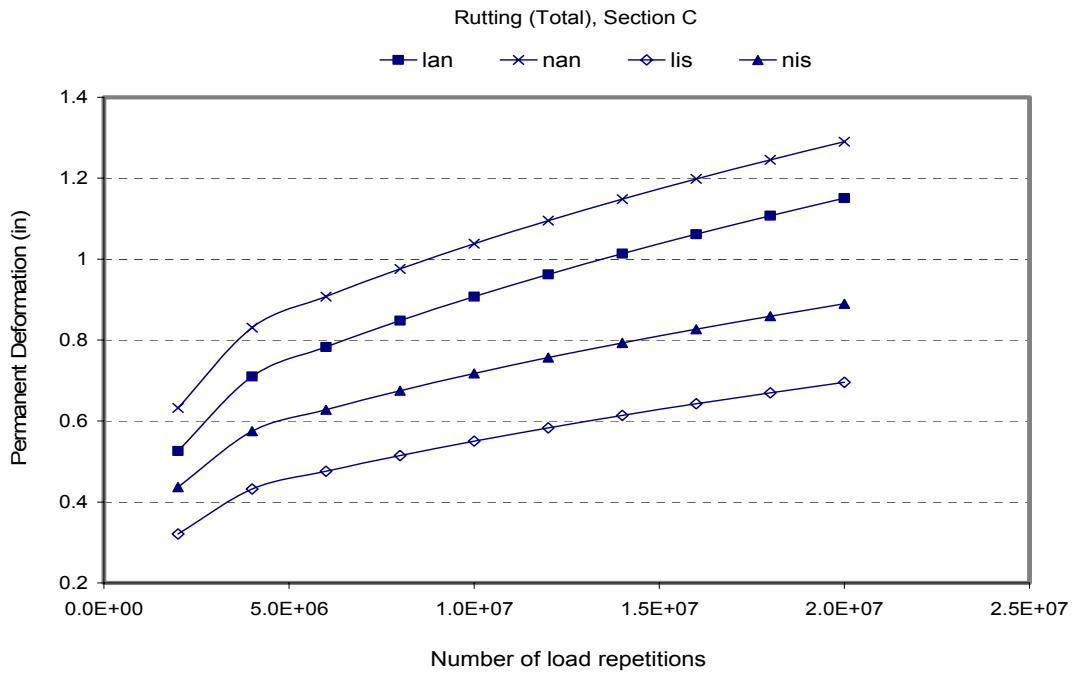
FIGURE 4.20 Total permanent deformation in section C using the AASHTO 2002 model.

4.6   Summary of Findings

In this chapter the permanent deformation and fatigue cracking were calculated based on the mechanistic-empirical models used in AASHTO 2002 with isotropic and anisotropic material properties. The following points summarize the results:

- For the base and Asphalt layer, the permanent deformation obtained using the anisotropic model is always more than that with the isotropic model.

- The permanent deformation in the subgrade obtained using the isotropic model is more than that for the anisotropic model when the regression equations from Tseng and Lytton are used. However, the permanent deformation using the isotropic model can be more or less than that calculated using the anisotropic model when the regression equations used in the AASHTO 2002 are used.

- The total permanent deformation using the isotropic model can be more or less than that for anisotropic model when the regression equations from Tseng and Lytton are used. However, the total permanent deformation using the anisotropic model is more than that calculated using the isotropic model when the AASHTO 2002 equations are used.

- The fatigue life predicted using the nonlinear anisotropic approach is higher than the life predicted using the nonlinear isotropic approach. This can explain part of the high shift factor typically found between the laboratory fatigue life calculated using the isotropic analysis, and field fatigue life. This shift factor is reduced when anisotropic properties are used.

CHAPTER V

SENSITIVITY ANALYSIS OF THE AASHTO 2002 DESIGN GUIDE

5.1   Introduction

This chapter documents the results of the sensitivity analysis of the AASHTO 2002 design guide to the characteristics of the materials used in the unbound pavement layers. The sensitivity analysis includes two asphalt binder grades, two asphalt layer thicknesses, three thicknesses for the base layer, five stiffness moduli for the base layer, three stiffness moduli for the subgrade layer, and three geographic locations representing different environmental conditions.

5.2   Background on the AASHTO 2002 Design Guide

The previous AASHTO guide for the design of pavement for both flexible and rigid pavement was developed based on the AASHO road test experiment about 35 years ago. There are several limitations of this design procedure such as (*6*):

1) Pavement rehabilitation design procedures did not exist at the AASHO road test.

2) The AASHTO road test did not take into accounts the effects of differences in the climate.

3) One type of subgrade was used.

4) There is a big difference between the traffic used in 1950 and the traffic in modern pavements.

5) Aging was not addressed because the duration of the road test was just 2 years.

The 2002 design guide is developed based on the mechanistic empirical design approach that accounts for the climate, aging, and modern vehicle loading. Analysis of the sensitivity of the AASHTO 2002 flexible pavement design procedure design to the base properties is presented in this chapter. The material properties used in the analysis are discussed in the following sections.

5.3   Input for the Sensitivity Analysis

Three traffic levels are used in the analysis based on the default values in the AASHTO 2002 guide. The traffic parameters are as follows:

- Two way average annual daily truck traffic = 1500, 3000, 5000

- Number of lanes in the design direction = 2

- Percent of trucks in design direction = 50%

- Percent of trucks in design lane = 95%

- Optional speed limit = 55 mph

- Design life = 10 years

- Traffic growth = 4%

The environmental conditions have a significant effect on the performance of the flexible pavement. There are two methods to generate the climatic data in the AASHTO 2002 software. The first method is by using the data available in the software since the design guide software includes a database for over 400 cities in the U.S. The next method is by providing the following inputs: pavement location latitude and longitude and the elevation besides the water table depth. Then the climatic data are interpolated

to the actual project location. In this analysis, three locations were selected to represent different climatic regions: Houston-Texas, Pullman-Washington State, and New York City. Table 5.1 summarizes all the variables used in the sensitivity analysis. The results presented in this chapter are from the analysis of the Texas site. The results from the other two sites followed the same trends and, their results are included in Appendix C.

Different pavement sections were analyzed to represent a wide spectrum of structural designs. The material properties used for the different layers are shown in Tables 5.2 and 5.3.

TABLE 5.1 Values for All of the Variables Used in the Sensitivity Analysis

Input Category	Variables		Source of Data	Number of Variables
Climate	Texas, Washington State, and New York city		ICE Climate Database	3
Asphalt Concrete	Type of Mix	• PG 58-28 • PG 72-22	FHWA Reports on ALF mixes *(31,32)*	2
	Thickness	• 4 inches • 8 inches		2
Base Layer	Type	• A-1-a (42,000 psi) • A-1-b (38,000 psi) • A-2-4 (35,000 psi) • A-2-4 (31,500 psi) • A-2-5 (28,000 psi)	AASHTO 2002 Design Guide	5
	Thickness	• 10 inch • 12 inch • 15 inch		3
Subgrade	Type	• A-2-5 (28,000 psi) • A-6 (18,000 psi) • A-7-6 (8,000 psi)	AASHTO 2002 Design Guide	3

TABLE 5.2 Asphalt Mix Properties

Asphalt Mix Property	Value
Average Tensile Strength	1600 psi.
Void in Mineral Aggregate	15%
Percent Air Voids	8.5%
Poisson's ratio	0.35
Thermal conductivity	0.67 BTU/(hr.ft.^{o}F)
Heat capacity asphalt	0.23 BTU/(Ib.^{o}F)
Effective Binder Content	4.8%

TABLE 5.3 Unbound Layer Properties

Modulus (psi) Gradation	42,000	38,000	35,000	31,500	28,000	18000	8,000
PI	1	1	2	2	2	25	40
P_{200}	3	3	20	20	20	80	90
P_4	20	40	80	80	80	95	99
D_{60}	8	2	0.1	0.1	0.1	0.01	0.01

5.4 Analysis and Results

The sensitivity analysis was conducted based on the main distresses which may occur in
the pavement. The main distresses include roughness, rutting, and fatigue cracking (top
down and bottom up cracking). All figures are presented as the percent change in a
certain distress as a function of change in the base material type and thickness with
respect to reference values. The results are shown in Tables 5.4- 5.15.

TABLE 5.4 Percent Change in Different Types of Distresses by Changing the Thickness of the Base Layer Using A-2-5 Subgrade (28 ksi) and PG58-28 Binder in the HMA

Thickness (in)		Base Type	% Change on Rutting	% Change on Longitudinal Cracking		% Change on Alligator Cracking	% Change on IRI
HMA	Base			Surface	Depth=0.5in		
4	15	A-1-a(42ksi)	0.000	0.000	0.000	0.000	0.000
4	12	A-1-a	-5.198	12.621	20.698	0.000	-1.765
4	10	A-1-a	4.733	13.592	19.535	0.346	1.506
8	15	A-1-a	0.000	0.000	0.000	0.000	0.000
8	12	A-1-a	-7.337	-0.121	0.277	-6.218	-4.403
8	10	A-1-a	-16.932	1.568	2.774	0.518	0.116
4	15	A-1-b(38ksi)	0.000	0.000	0.000	0.000	0.000
4	12	A-1-b	19.738	5.128	7.283	0.227	0.490
4	10	A-1-b	5.127	9.402	13.386	0.227	0.833
8	15	A-1-b	0.000	0.000	0.000	0.000	0.000
8	12	A-1-b	-14.679	-0.932	-0.921	-12.174	-4.363
8	10	A-1-b	-32.025	-0.350	-0.132	-11.739	-4.248
4	15	A-2-4(35ksi)	0.000	0.000	0.000	0.000	0.000
4	12	A-2-4	8.181	2.128	4.831	-0.439	-3.941
4	10	A-2-4	4.853	4.255	6.602	0.000	-0.205
8	15	A-2-4	0.000	0.000	0.000	0.000	0.000
8	12	A-2-4	-6.908	-0.568	-0.631	-6.557	-4.530
8	10	A-2-4	-16.665	0.341	0.631	-0.410	0.000
4	15	A-2-4(31.5)	0.000	0.000	0.000	0.000	0.000
4	12	A-2-4	19.695	0.610	1.202	-0.108	-0.454
4	10	A-2-4	5.086	1.220	2.003	-0.108	-0.984
8	15	A-2-4	0.000	0.000	0.000	0.000	0.000
8	12	A-2-4	-14.472	-1.544	-2.169	-14.915	-5.222
8	10	A-2-4	-31.952	-1.544	-2.048	-14.915	-5.222
4	15	A-2-5(28ksi)	0.000	0.000	0.000	0.000	0.000
4	12	A-2-5	19.655	-1.036	-1.106	-0.106	-1.022
4	10	A-2-5	5.026	-2.073	-2.434	-0.213	-2.142
8	15	A-2-5	0.000	0.000	0.000	0.000	0.000
8	12	A-2-5	-14.340	-1.728	-2.448	-15.455	-5.773
8	10	A-2-5	-32.048	-1.836	-2.564	-16.061	-5.773

TABLE 5.5 Percent Change in Different Types of Distresses by Changing the Thickness of the Base Layer Using A-6 Subgrade (18 ksi) and PG58-28 Binder in the HMA

Thickness (in)		Base Type	% Change on Rutting	% Change on Longitudinal Cracking		% Change on Alligator Cracking	% Change on IRI
HMA	Base			Surface	Depth=0.5in		
4	15	A-1-a(42ksi)	0.000	0.000	0.000	0.000	0.000
4	12	A-1-a	3.787	21.359	28.217	0.897	4.281
4	10	A-1-a	5.915	45.631	60.948	1.794	9.400
8	15	A-1-a	0.000	0.000	0.000	0.000	0.000
8	12	A-1-a	-9.674	1.548	2.950	0.851	-3.469
8	10	A-1-a	2.316	5.806	9.783	11.489	1.189
4	15	A-1-b(38ksi)	0.000	0.000	0.000	0.000	0.000
4	12	A-1-b	3.885	18.852	25.421	0.768	4.921
4	10	A-1-b	5.994	39.344	52.523	1.427	9.802
8	15	A-1-b	0.000	0.000	0.000	0.000	0.000
8	12	A-1-b	1.652	2.128	3.693	5.645	0.715
8	10	A-1-b	2.806	4.255	7.238	10.887	1.226
4	15	A-2-4(35ksi)	0.000	0.000	0.000	0.000	0.000
4	12	A-2-4	3.810	16.197	20.912	0.541	4.328
4	10	A-2-4	5.873	33.099	43.396	1.081	8.834
8	15	A-2-4	0.000	0.000	0.000	0.000	0.000
8	12	A-2-4	-9.541	0.359	0.826	-1.384	-3.582
8	10	A-2-4	2.373	3.349	5.785	8.304	1.162
4	15	A-2-4(31.5)	0.000	0.000	0.000	0.000	0.000
4	12	A-2-4	3.796	13.095	17.013	0.426	4.111
4	10	A-2-4	5.797	26.190	35.065	0.745	8.571
8	15	A-2-4	0.000	0.000	0.000	0.000	0.000
8	12	A-2-4	1.711	1.174	1.867	4.348	0.598
8	10	A-2-4	2.852	2.230	3.867	7.692	1.097
4	15	A-2-5(28ksi)	0.000	0.000	0.000	0.000	0.000
4	12	A-2-5	3.763	10.553	13.709	0.210	3.999
4	10	A-2-5	5.715	20.603	26.461	0.526	7.336
8	15	A-2-5	0.000	0.000	0.000	0.000	0.000
8	12	A-2-5	-9.402	-0.451	-0.625	-3.390	-3.936
8	10	A-2-5	2.450	1.691	2.875	5.650	1.031

TABLE 5.6 Percent Change in Different Types of Distresses by Changing the Thickness of the Base Layer Using A-7-6 Subgrade (8 ksi) and PG58-28 Binder in the HMA

Thickness (in)		Base Type	% Change on Rutting	% Change on Longitudinal Cracking		% Change on Alligator Cracking	% Change on IRI
HMA	Base			Surface	Depth=0.5in		
4	15	A-1-a(42ksi)	0.000	0.000	0.000	0.000	0.000
4	12	A-1-a	4.267	46.829	62.771	1.435	8.488
4	10	A-1-a	6.942	111.382	154.545	2.649	18.557
8	15	A-1-a	0.000	0.000	0.000	0.000	0.000
8	12	A-1-a	1.408	9.600	17.974	11.808	1.326
8	10	A-1-a	2.362	21.600	40.523	22.878	2.653
4	15	A-1-b(38ksi)	0.000	0.000	0.000	0.000	0.000
4	12	A-1-b	4.372	42.674	56.623	1.190	9.303
4	10	A-1-b	7.052	96.658	134.106	2.165	19.361
8	15	A-1-b	0.000	0.000	0.000	0.000	0.000
8	12	A-1-b	1.409	7.394	14.096	10.891	1.483
8	10	A-1-b	2.380	16.197	30.319	20.462	2.880
4	15	A-2-4(35ksi)	0.000	0.000	0.000	0.000	0.000
4	12	A-2-4	4.360	36.601	49.608	0.961	8.762
4	10	A-2-4	6.999	82.482	114.621	1.708	19.118
8	15	A-2-4	0.000	0.000	0.000	0.000	0.000
8	12	A-2-4	1.411	5.591	10.431	9.281	1.463
8	10	A-2-4	2.368	11.981	22.449	17.665	2.926
4	15	A-2-4(31.5)	0.000	0.000	0.000	0.000	0.000
4	12	A-2-4	4.384	31.667	43.232	0.632	9.057
4	10	A-2-4	7.013	70.000	102.020	1.263	18.755
8	15	A-2-4	0.000	0.000	0.000	0.000	0.000
8	12	A-2-4	1.429	4.094	7.632	8.401	1.609
8	10	A-2-4	2.419	8.918	16.438	15.447	3.133
4	15	A-2-5(28ksi)	0.000	0.000	0.000	0.000	0.000
4	12	A-2-5	4.376	27.152	36.476	0.521	8.901
4	10	A-2-5	6.989	57.616	79.289	0.938	18.905
8	15	A-2-5	0.000	0.000	0.000	0.000	0.000
8	12	A-2-5	1.432	2.842	5.326	7.108	1.658
8	10	A-2-5	2.408	6.225	11.684	12.990	3.151

TABLE 5.7 Percent Change in Different Types of Distresses by Changing the Type of the Base Layer Using A-2-5 Subgrade (28 ksi) and PG58-28 Binder in the HMA

Thickness (in)		Base Type	% Change on Rutting	% Change on Longitudinal Cracking		% Change on Alligator Cracking	% Change on IRI
HMA	Base			Surface	Depth=0.5in		
4	10	A-1-a(42ksi)	0.000	0.000	0.000	0.000	0.000
4	10	A-1-b(38ksi)	-9.004	9.402	12.062	1.724	5.320
4	10	A-2-4(35ksi)	1.179	25.641	28.794	4.713	24.348
4	10	A-2-4(31.5)	-7.591	41.880	48.638	6.092	33.811
4	10	A-2-5(28ksi)	-6.773	61.538	71.595	7.701	51.867
8	10	A-1-a	0.000	0.000	0.000	0.000	0.000
8	10	A-1-b	-11.152	1.544	2.429	4.639	-3.472
8	10	A-2-4	-0.676	4.869	7.557	25.258	2.199
8	10	A-2-4	-11.736	6.057	9.717	29.381	-1.273
8	10	A-2-5	-11.997	7.957	12.821	42.784	0.116
4	12	A-1-a	0.000	0.000	0.000	0.000	0.000
4	12	A-1-b	14.501	6.034	5.010	2.076	8.457
4	12	A-2-4	15.327	24.138	25.434	4.614	23.679
4	12	A-2-4	16.282	42.241	46.050	6.459	39.006
4	12	A-2-5	17.340	64.655	72.254	8.189	58.721
8	12	A-1-a	0.000	0.000	0.000	0.000	0.000
8	12	A-1-b	-0.028	2.657	4.149	11.602	0.970
8	12	A-2-4	-0.537	5.676	8.852	25.967	2.182
8	12	A-2-4	-0.551	7.850	12.310	38.674	3.394
8	12	A-2-5	-0.551	9.903	15.768	54.144	4.848
4	15	A-1-a	0.000	0.000	0.000	0.000	0.000
4	15	A-1-b	-9.344	13.592	18.140	1.845	6.023
4	15	A-2-4	1.064	36.893	44.419	5.075	26.480
4	15	A-2-4	-7.901	59.223	74.186	6.574	37.175
4	15	A-2-5	-7.033	87.379	110.233	8.304	57.529
8	15	A-1-a	0.000	0.000	0.000	0.000	0.000
8	15	A-1-b	8.575	3.498	5.409	19.171	0.927
8	15	A-2-4	-0.995	6.152	9.847	26.425	2.317
8	15	A-2-4	7.745	9.409	15.118	52.850	4.287
8	15	A-2-5	7.579	11.701	19.001	70.984	6.373

TABLE 5.8 Percent Change in Different Types of Distresses by Changing the Type of the Base Layer Using A-6 Subgrade (18 ksi) and PG58-28 Binder in the HMA

Thickness (in)		Base Type	% Change on Rutting	% Change on Longitudinal Cracking		% Change on Alligator Cracking	% Change on IRI
HMA	Base			Surface	Depth=0.5in		
4	10	A-1-a(42ksi)	0.000	0.000	0.000	0.000	0.000
4	10	A-1-b(38ksi)	0.998	13.333	14.446	1.762	11.618
4	10	A-2-4(35ksi)	1.820	26.000	27.910	2.974	22.751
4	10	A-2-4(31.5)	2.843	41.333	45.863	4.185	38.483
4	10	A-2-5(28ksi)	4.018	60.000	66.900	5.286	56.999
8	10	A-1-a	0.000	0.000	0.000	0.000	0.000
8	10	A-1-b	-10.856	1.585	2.687	4.962	-2.938
8	10	A-2-4	-0.370	5.366	8.628	19.466	2.351
8	10	A-2-4	-11.133	6.220	10.184	22.901	-0.686
8	10	A-2-5	-0.832	10.000	16.407	42.748	5.583
4	12	A-1-a	0.000	0.000	0.000	0.000	0.000
4	12	A-1-b	1.019	16.000	18.134	2.000	11.892
4	12	A-2-4	1.883	32.000	35.387	3.333	23.445
4	12	A-2-4	2.966	52.000	58.627	4.778	39.314
4	12	A-2-5	4.191	76.000	88.380	5.889	59.585
8	12	A-1-a	0.000	0.000	0.000	0.000	0.000
8	12	A-1-b	-0.157	3.685	5.882	10.549	1.232
8	12	A-2-4	-0.279	6.607	10.407	20.253	2.259
8	12	A-2-4	-0.454	9.530	15.234	31.646	3.593
8	12	A-2-5	-0.663	12.198	19.910	44.304	5.236
4	15	A-1-a	0.000	0.000	0.000	0.000	0.000
4	15	A-1-b	0.923	18.447	20.767	2.130	11.209
4	15	A-2-4	1.860	37.864	43.567	3.700	23.389
4	15	A-2-4	2.958	63.107	73.815	5.269	39.541
4	15	A-2-5	4.216	93.204	112.415	6.614	60.018
8	15	A-1-a	0.000	0.000	0.000	0.000	0.000
8	15	A-1-b	-11.281	3.097	5.124	5.532	-2.973
8	15	A-2-4	-0.425	7.871	12.733	22.979	2.379
8	15	A-2-4	-11.596	9.935	16.460	27.234	-0.595
8	15	A-2-5	-0.961	14.452	24.224	50.638	5.748

TABLE 5.9 Percent Change in Different Types of Distresses by Changing the Type of the Base Layer Using A-7-6 Subgrade (8 ksi) and PG58-28 Binder in the HMA

Thickness (in)		Base Type	% Change on Rutting	% Change on Longitudinal Cracking		% Change on Alligator Cracking	% Change on IRI
HMA	Base			Surface	Depth=0.5in		
4	10	A-1-a(42ksi)	0.000	0.000	0.000	0.000	0.000
4	10	A-1-b(38ksi)	1.234	17.692	20.238	1.505	13.147
4	10	A-2-4(35ksi)	2.290	34.615	39.796	2.473	26.521
4	10	A-2-4(31.5)	3.635	56.923	70.068	3.441	44.647
4	10	A-2-5(28ksi)	5.157	83.077	97.279	4.194	68.240
8	10	A-1-a	0.000	0.000	0.000	0.000	0.000
8	10	A-1-b	-0.107	8.553	13.953	9.610	1.550
8	10	A-2-4	-0.260	15.296	25.581	18.018	3.015
8	10	A-2-4	-0.382	22.533	38.372	27.928	4.910
8	10	A-2-5	-0.565	29.112	51.163	38.438	7.149
4	12	A-1-a	0.000	0.000	0.000	0.000	0.000
4	12	A-1-b	1.231	22.924	25.798	1.741	13.229
4	12	A-2-4	2.326	45.072	52.394	2.938	26.245
4	12	A-2-4	3.682	74.972	88.564	4.026	45.164
4	12	A-2-5	5.221	112.625	134.840	5.005	68.385
8	12	A-1-a	0.000	0.000	0.000	0.000	0.000
8	12	A-1-b	-0.123	11.314	18.837	10.891	1.483
8	12	A-2-4	-0.262	20.620	34.903	20.462	2.880
8	12	A-2-4	-0.416	29.927	52.355	32.013	4.712
8	12	A-2-5	-0.586	38.686	69.806	44.224	6.981
4	15	A-1-a	0.000	0.000	0.000	0.000	0.000
4	15	A-1-b	1.129	26.504	30.736	1.987	12.384
4	15	A-2-4	2.235	55.935	65.801	3.422	25.926
4	15	A-2-4	3.566	95.122	114.286	4.857	44.406
4	15	A-2-5	5.111	145.528	180.087	5.960	67.747
8	15	A-1-a	0.000	0.000	0.000	0.000	0.000
8	15	A-1-b	-0.125	13.600	22.876	11.808	1.326
8	15	A-2-4	-0.266	25.200	44.118	23.247	2.741
8	15	A-2-4	-0.438	36.800	66.993	36.162	4.421
8	15	A-2-5	-0.610	47.800	90.196	50.554	6.631

TABLE 5.10 Percent Change in Different Types of Distresses by Changing the Thickness of the Base Layer Using A-2-5 Subgrade (28 ksi) and PG76-22 Binder in the HMA

Thickness (in)		Base Type	% Change on Rutting	% Change on Longitudinal Cracking		% Change on Alligator Cracking	% Change on IRI
HMA	Base			Surface	Depth=0.5in		
4	15	A-1-a(42ksi)	0.000	0.000	0.000	0.000	0.000
4	10	A-1-a	6.034	13.497	17.587	0.324	2.641
8	15	A-1-a	0.000	0.000	0.000	0.000	0.000
8	10	A-1-a	-22.506	0.921	1.536	1.587	0.117
4	15	A-2-4(35)	0.000	0.000	0.000	0.000	0.000
4	10	A-2-4	5.953	4.545	5.455	0.000	0.000
8	15	A-2-4	0.000	0.000	0.000	0.000	0.000
8	10	A-2-4	-22.194	0.221	0.361	0.338	0.000
4	15	A-2-5(28ksi)	0.000	0.000	0.000	0.000	0.000
4	10	A-2-5	5.740	-1.718	-1.961	-0.104	-2.161
8	15	A-2-5	0.000	0.000	0.000	0.000	0.000
8	10	A-2-5	-22.734	-0.108	-0.345	-1.729	-0.333

TABLE 5.11 Percent Change in Different Types of Distresses by Changing the Thickness of the Base Layer Using A-6 Subgrade (18 ksi) and PG76-22 Binder in the HMA

Thickness (in)		Base Type	% Change on Rutting	% Change on Longitudinal Cracking		% Change on Alligator Cracking	% Change on IRI
HMA	Base			Surface	Depth=0.5in		
4	15	A-2-4(35)	0.000	0.000	0.000	0.000	0.000
4	10	A-2-4	7.032	27.111	35.714	0.521	10.486
8	15	A-2-4	0.000	0.000	0.000	0.000	0.000
8	10	A-2-4	3.440	1.769	3.075	7.649	1.552
4	15	A-2-5(28ksi)	0.000	0.000	0.000	0.000	0.000
4	10	A-2-5	6.801	16.225	22.013	0.309	8.531
8	15	A-2-5	0.000	0.000	0.000	0.000	0.000
8	10	A-2-5	3.447	0.904	1.498	5.172	1.317
4	15	A-1-a(42ksi)	0.000	0.000	0.000	0.000	0.000
4	10	A-1-a	7.243	39.053	50.498	1.060	11.601
8	15	A-1-a	0.000	0.000	0.000	0.000	0.000
8	10	A-1-a	3.503	2.981	5.225	10.458	1.690

TABLE 5.12 Percent Change in Different Types of Distresses by Changing the Thickness of the Base Layer Using A-7-6 Subgrade (8 ksi) and PG76-22 Binder in the HMA

Thickness (in)		Base Type	% Change on Rutting	% Change on Longitudinal Cracking		% Change on Alligator Cracking	% Change on IRI
HMA	Base			Surface	Depth=0.5in		
4	15	A-1-a(42ksi)	0.000	0.000	0.000	0.000	0.000
4	12	A-1-a	5.803	38.532	51.770	0.735	11.117
4	10	A-1-a	9.417	86.239	121.239	1.364	24.099
8	15	A-1-a	0.000	0.000	0.000	0.000	0.000
8	12	A-1-a	2.024	3.711	7.365	9.896	2.101
8	10	A-1-a	3.388	10.575	19.830	18.490	4.202
4	15	A-2-4(35ksi)	0.000	0.000	0.000	0.000	0.000
4	12	A-2-4	5.710	29.630	39.082	0.517	11.138
4	10	A-2-4	9.244	62.963	87.761	0.826	23.715
8	15	A-2-4	0.000	0.000	0.000	0.000	0.000
8	12	A-2-4	1.985	1.875	3.863	7.675	2.195
8	10	A-2-4	3.349	5.625	10.730	14.221	4.309
4	15	A-2-5(28ksi)	0.000	0.000	0.000	0.000	0.000
4	12	A-2-5	5.591	20.921	28.696	0.306	10.525
4	10	A-2-5	8.974	43.096	60.870	0.511	21.769
8	15	A-2-5	0.000	0.000	0.000	0.000	0.000
8	12	A-2-5	1.966	0.822	1.730	5.709	2.260
8	10	A-2-5	3.312	2.740	5.363	10.236	4.287
4	15	A-1-b(38ksi)	0.000	0.000	0.000	0.000	0.000
4	12	A-1-b	5.830	35.075	46.287	0.624	12.033
4	10	A-1-b	9.426	75.373	103.800	1.145	24.610
8	15	A-1-b	0.000	0.000	0.000	0.000	0.000
8	12	A-1-b	2.005	2.862	5.825	8.916	2.231
8	10	A-1-b	3.368	7.912	14.806	16.386	4.298
4	15	A-2-4(31.5ksi)	0.000	0.000	0.000	0.000	0.000
4	12	A-2-4	5.670	24.873	34.361	0.308	11.402
4	10	A-2-4	9.138	52.284	74.009	0.616	22.804
8	15	A-2-4	0.000	0.000	0.000	0.000	0.000
8	12	A-2-4	1.986	1.312	2.682	6.526	2.231
8	10	A-2-4	3.331	4.082	7.854	12.211	4.303

TABLE 5.13 Percent Change in Different Types of Distresses by Changing the Type of the Base Layer Using A-2-5 Subgrade (28 ksi) and PG76-22 Binder in the HMA

Thickness (in)		Base Type	% Change on Rutting	% Change on Longitudinal Cracking		% Change on Alligator Cracking	% Change on IRI
HMA	Base			Surface	Depth=0.5in		
4	10	A-1-a(42ksi)	0.000	0.000	0.000	0.000	0.000
4	10	A-2-4(35)	1.284	24.324	26.638	2.153	24.175
4	10	A-2-5(28ksi)	3.075	54.595	63.755	3.767	57.521
8	10	A-1-a	0.000	0.000	0.000	0.000	0.000
8	10	A-2-4	-0.572	3.307	5.170	16.016	2.222
8	10	A-2-5	-0.990	5.929	9.206	33.203	4.912
4	15	A-1-a	0.000	0.000	0.000	0.000	0.000
4	15	A-2-4	1.361	34.969	41.207	2.484	27.455
4	15	A-2-5	3.361	78.528	96.406	4.212	65.253
8	15	A-1-a	0.000	0.000	0.000	0.000	0.000
8	15	A-2-4	-0.972	4.028	6.402	17.460	2.342
8	15	A-2-5	-0.699	7.020	11.268	37.698	5.386

TABLE 5.14 Percent Change in Different Types of Distresses by Changing the Type of the Base Layer Using A-6 Subgrade (18 ksi) and PG76-22 Binder in the HMA

Thickness (in)		Base Type	% Change on Rutting	% Change on Longitudinal Cracking		% Change on Alligator Cracking	% Change on IRI
HMA	Base			Surface	Depth=0.5in		
4	10	A-1-a(42ksi)	0.000	0.000	0.000	0.000	0.000
4	10	A-2-4(35)	1.862	21.702	25.620	1.259	23.395
4	10	A-2-5(28ksi)	4.123	49.362	60.331	2.308	57.185
8	10	A-1-a	0.000	0.000	0.000	0.000	0.000
8	10	A-2-4	-0.198	4.101	6.345	12.426	2.346
8	10	A-2-5	-0.396	7.720	12.138	26.331	5.279
4	15	A-1-a	0.000	0.000	0.000	0.000	0.000
4	15	A-2-4	2.062	33.136	39.303	1.803	24.640
4	15	A-2-5	4.554	78.698	97.761	3.075	61.631
8	15	A-1-a	0.000	0.000	0.000	0.000	0.000
8	15	A-2-4	-0.136	5.342	8.563	15.359	2.485
8	15	A-2-5	-0.341	9.938	16.255	32.680	5.666

TABLE 5.15 Percent Change in Different Types of Distresses by Changing the Type of the Base Layer Using A-7-6 Subgrade (8 ksi) and PG76-22 Binder in the HMA

Thickness (in)		Base Type	% Change on Rutting	% Change on Longitudinal Cracking		% Change on Alligator Cracking	% Change on IRI
HMA	Base			Surface	Depth=0.5in		
4	10	A-1-a(42ksi)	0.000	0.000	0.000	0.000	0.000
4	10	A-1-b(38ksi)	1.343	15.764	18.000	0.621	13.447
4	10	A-2-4 (35.0ksi)	2.522	30.049	35.000	1.035	27.409
4	10	A-2-4(31.5 ksi)	3.933	47.783	58.000	1.449	44.831
4	10	A-2-5(28ksi)	5.509	68.473	85.000	1.863	67.257
8	10	A-1-a	0.000	0.000	0.000	0.000	0.000
8	10	A-1-b	-0.060	7.550	11.820	6.154	1.774
8	10	A-2-4	-0.120	13.423	21.986	11.209	3.468
8	10	A-2-4	-0.200	19.799	33.097	17.143	5.565
8	10	A-2-5	-0.280	25.839	43.972	23.077	7.903
4	12	A-1-a	0.000	0.000	0.000	0.000	0.000
4	12	A-1-b	1.361	19.868	23.469	0.729	13.914
4	12	A-2-4	2.594	39.073	45.773	1.354	27.829
4	12	A-2-4	4.067	62.914	77.843	1.771	61.753
4	12	A-2-5	5.726	91.391	115.743	2.292	69.549
8	12	A-1-a	0.000	0.000	0.000	0.000	0.000
8	12	A-1-b	-0.061	9.302	15.040	7.109	1.811
8	12	A-2-4	-0.121	16.637	27.704	13.033	3.457
8	12	A-2-4	-0.182	24.329	41.425	19.905	5.597
8	12	A-2-5	-0.263	31.664	55.145	27.251	7.984
4	15	A-1-a	0.000	0.000	0.000	0.000	0.000
4	15	A-1-b	1.335	22.936	28.097	0.839	12.982
4	15	A-2-4	2.684	48.624	59.071	1.574	27.805
4	15	A-2-4	4.199	80.734	100.885	2.204	46.358
4	15	A-2-5	5.938	119.266	154.425	2.728	70.457
8	15	A-1-a	0.000	0.000	0.000	0.000	0.000
8	15	A-1-b	-0.041	10.204	16.714	8.073	1.681
8	15	A-2-4	-0.083	18.738	32.011	15.365	3.361
8	15	A-2-4	-0.145	27.273	47.875	23.698	5.462
8	15	A-2-5	-0.207	35.436	63.739	32.292	7.815

5.4.1 Roughness

Smoothness can be defined as "the variation in surface elevation that induces vibrations in traversing vehicles" (*6*). Rough roads not only lead to user discomfort but also to increased travel times and higher vehicle operating costs. The IRI is one of the ways to measure the smoothness. The designer has to choose the terminal IRI values that should not be exceeded at the design level of reliability. Typical values range from 63 to 1260 in/mi (*6*). Figure 5.1 shows the change in the IRI as the base modulus changes from 42,000 psi to 28,000 psi for different thicknesses for the base layer. The y axis represents the percentage change in the IRI as the base modulus changes from 42,000 psi to another value where the data point is plotted. It can be seen that the IRI value increases as the base modulus gets smaller irrespective of the base thickness. As can be seen in Figure 5.2, the effect of the change in the base modulus on IRI becomes smaller as the HMA thickness becomes larger. The influence of base thickness on IRI increases as the HMA thickness decreases and as the subgrade stiffness decreases, (Figure 5.3). These results are almost the same for PG 58-22 and PG 72-22 mixes.

FIGURE 5.1 Percent change in IRI for different thicknesses of the base layer at 8in HMA and 8 ksi subgrade.
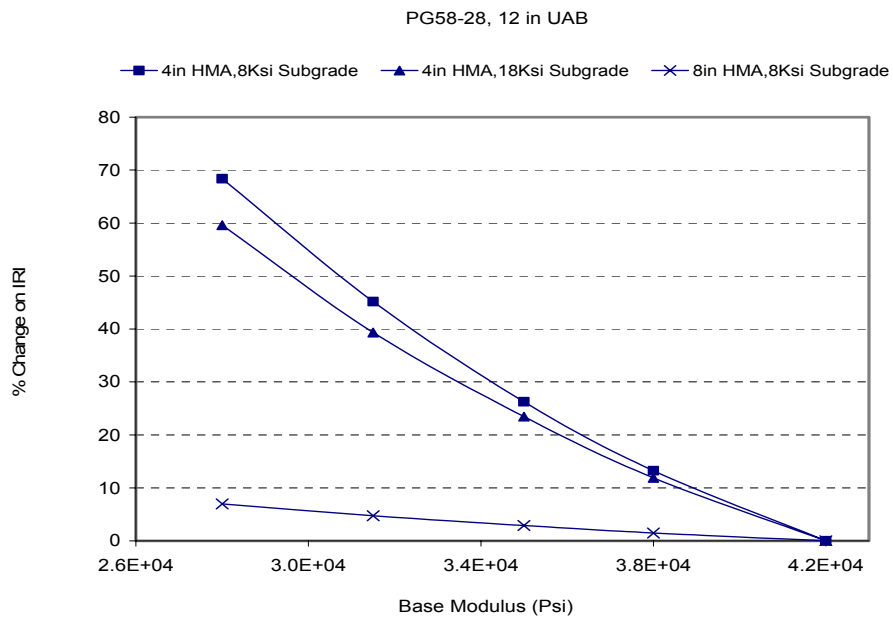
FIGURE 5.2 Percent change in IRI at two different thicknesses of HMA and at two types of subgrade by changing the base modulus.

PG58-28 , A-1-b (38Ksi)
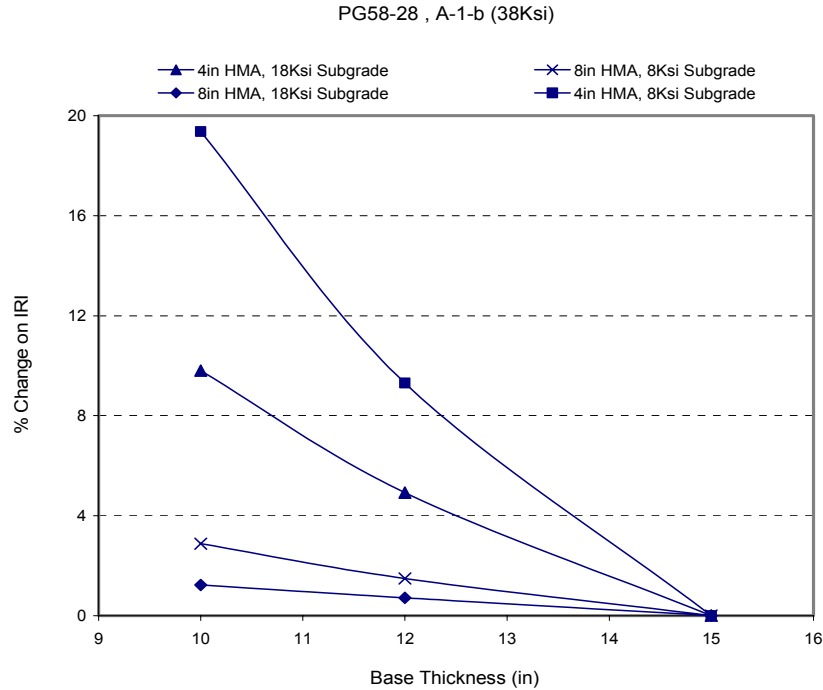
FIGURE 5.3 Percent change in IRI at two different thicknesses of HMA and at two
types of subgrade by changing the base thickness.

5.4.2   Surface-Down Fatigue Cracking (Longitudinal Cracking)

Surface down fatigue cracking is defined as longitudinal cracking at the edge of the
wheel paths. Surface-down cracking can cause loss of smoothness and permits water
infiltration into the underlying pavement layers which can be a reason for structural
failure of the pavement. The performance criterion for surface down fatigue cracking is
defined as the maximum allowable length of longitudinal cracking per mile of pavement
that is permitted to occur at the end of the design life. Typical values of allowable
surface down fatigue cracking are on the order of 500 to 2000 ft/mi of pavement (6).
The longitudinal cracking is calculated by considering the critical tensile stress at the
surface and at 0.5 inch below the surface.

The base type has significant influence on longitudinal cracking as shown in Figure 5.4. Longitudinal cracking increases up to 190% when the base modulus decreases from 42,000 psi to 28,000 psi in a pavement with PG 58-28 binder, 8000 psi subgrade, and 15in base thickness. The influence of base modulus on longitudinal cracking decreases as the base thickness decreases (Figure 5.4), and as the HMA thickness increases (Figures 5.4 and 5.5). Also, comparing Figures 5.4 and 5.5 with Figures 5.6-5.8 reveals that the influence of the base modulus on fatigue cracking decreases as the subgrade modulus increases. Figures 5.9 – 5.11 show clearly that the longitudinal cracking increases as the base thickness decreases. The relationship between base thickness and longitudinal cracking is sensitive to subgrade stiffness and HMA thickness as shown in Figures 5.9-5.12.

FIGURE 5.4 Percent change in longitudinal cracking for different thickness of the base layer at 4 in HMA and 8 ksi subgrade.
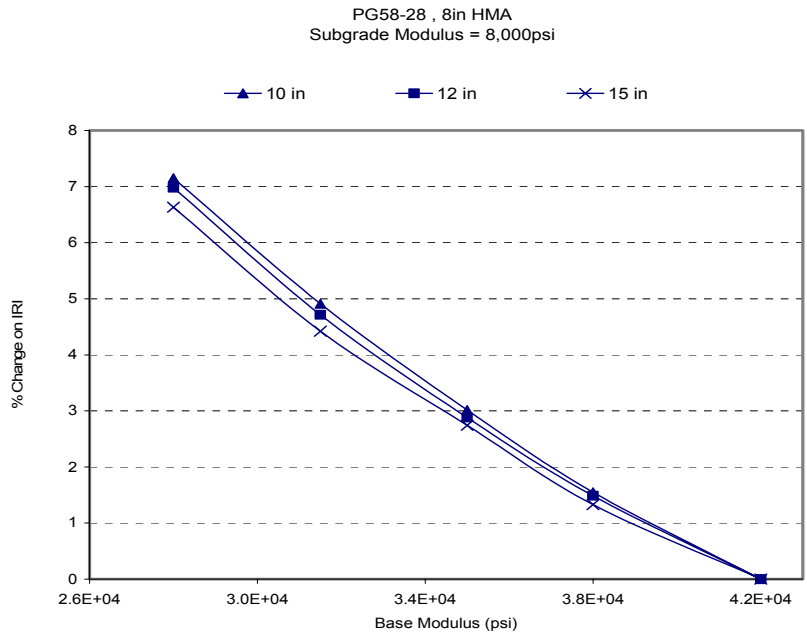
FIGURE 5.5 Percent change in longitudinal cracking for different thickness of the base layer at 8 in HMA and 8 ksi subgrade.
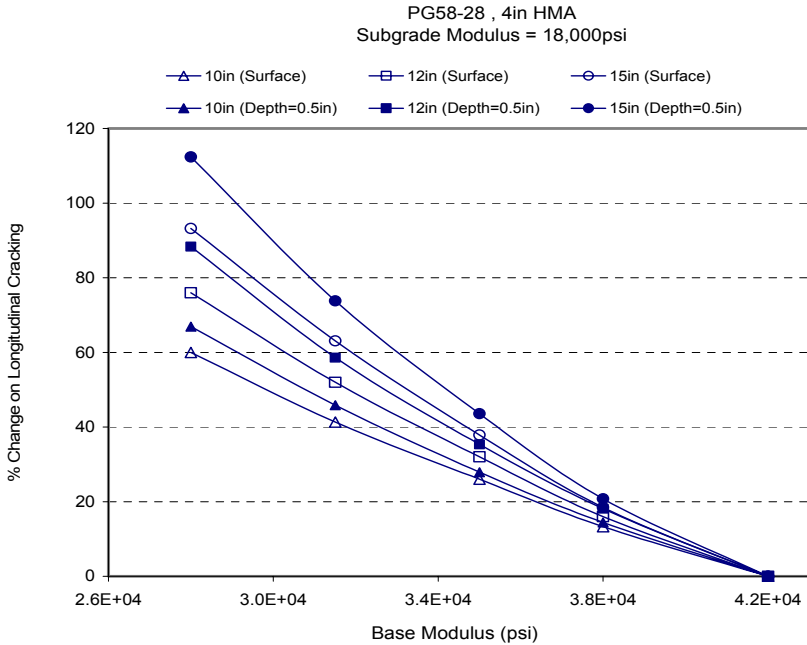
FIGURE 5.6 Percent change in longitudinal cracking for different thickness of the base layer at 4 in HMA and 18 ksi subgrade.
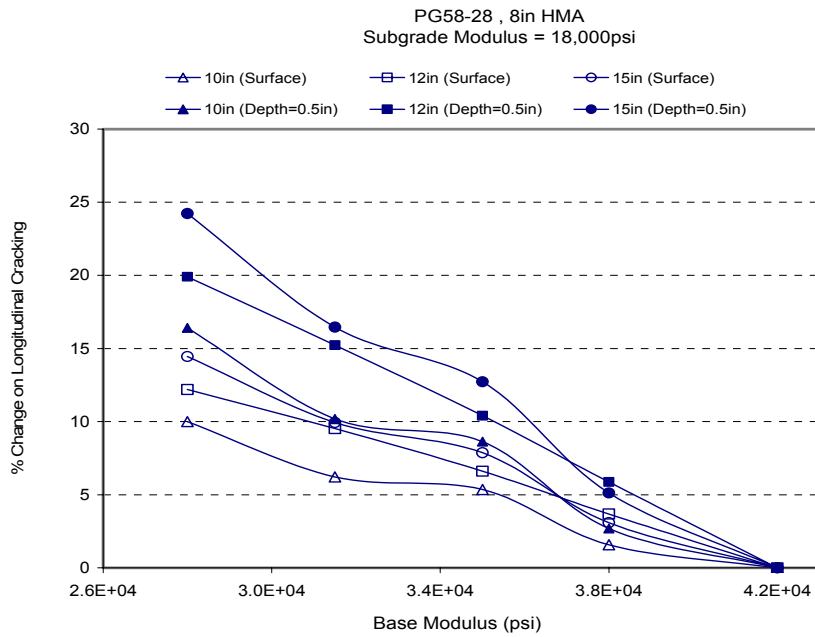
FIGURE 5.7 Percent change in longitudinal cracking for different thickness of the base layer at 8 in HMA and 18 ksi subgrade.
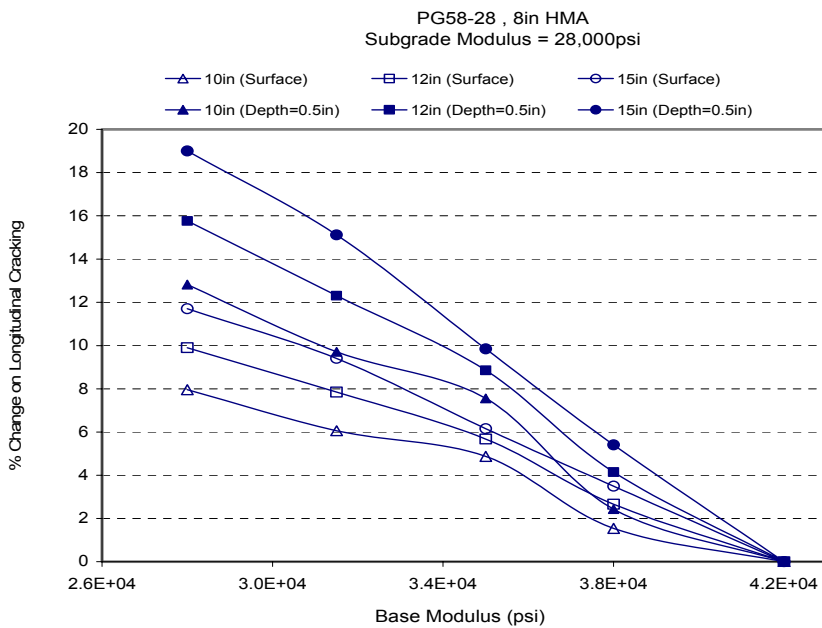
FIGURE 5.8 Percent change in longitudinal cracking for different thickness of the base layer at 8 in HMA and 28 ksi subgrade.

FIGURE 5.9 Percent change in longitudinal cracking for different types of the base layer at 4 in HMA and 8 ksi subgrade.

FIGURE 5.10 Percent change in longitudinal cracking at different types of the base layer for 8 in HMA and 8 ksi subgrade.

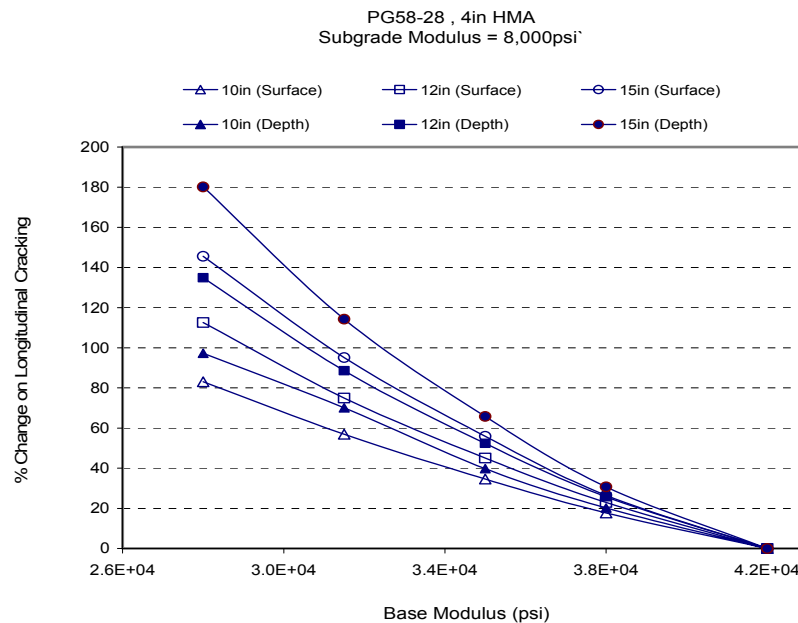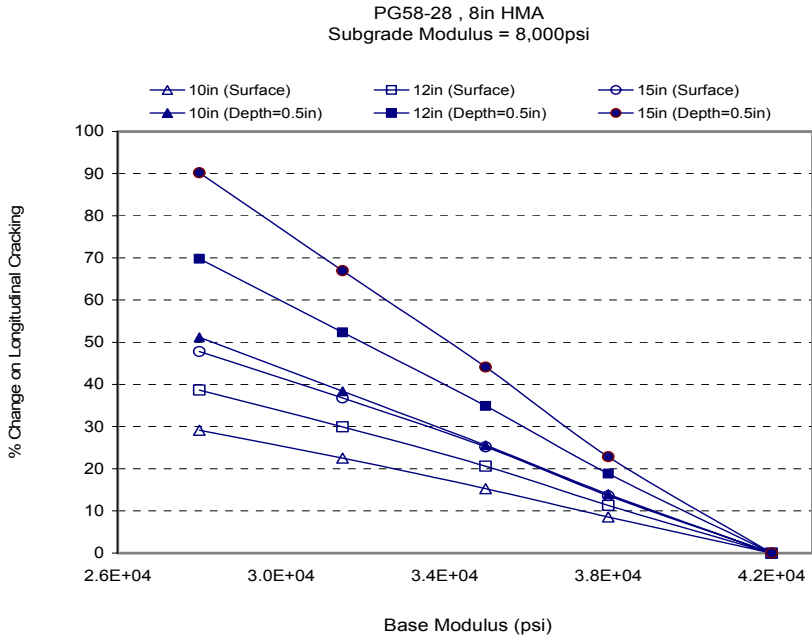FIGURE 5.11 Percent change in longitudinal cracking for different type of the base layer at 4 in HMA and 18 ksi subgrade.

FIGURE 5.12 Percent change in longitudinal cracking for different types of the base layer at 8 in HMA and 18 ksi subgrade.
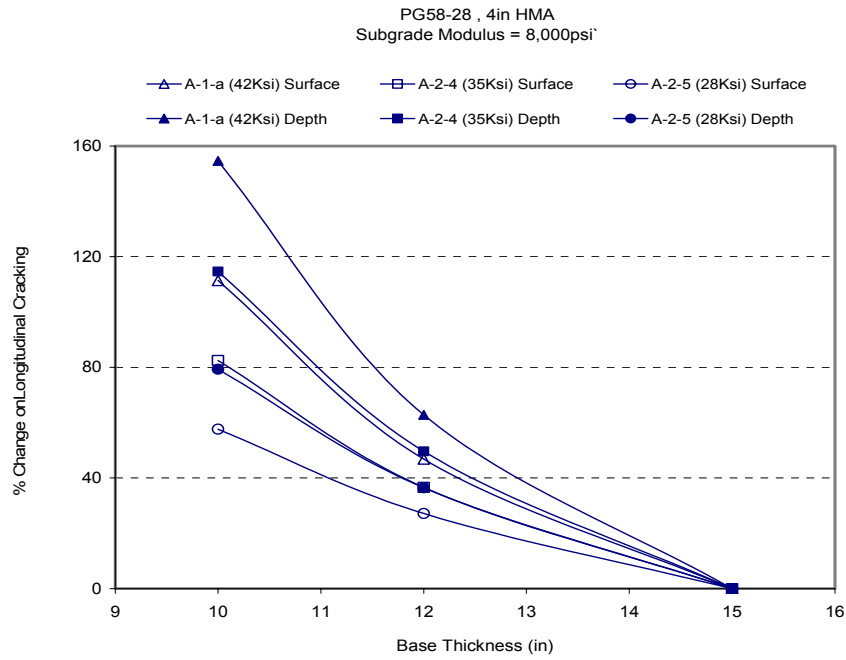
5.4.3   Bottom-Up Fatigue Cracking

This type of cracking starts from the bottom of the layer and propagates to the top so the critical fatigue depth location is at the bottom of the asphalt layer. Bottom-up fatigue cracking appears as alligator cracking within the wheel paths (*6*). Bottom-up cracking has an effect on the smoothness which can cause loss of smoothness and can permit water infiltration into the underlying pavement layers that can cause structural failure of the pavement. The performance criterion for bottom-up fatigue cracking is defined as the percentage of the cracking per total lane area that may occur over the design period. Typical values of allowable surface down fatigue cracking are on the order of 25 to 100% of pavement (*6*). The alligator cracking is calculated by considering the critical tensile stress at the bottom of the pavement.

The base type has significant influence on alligator cracking as shown in Figure 5.13. Alligator cracking increases by about 50% when the base modulus decreases from 42,000 psi to 28,000 psi in a pavement with PG 58-28 binder, 8000 psi subgrade, and 15in base thickness. The influence of base modulus on alligator cracking decreases as the base thickness decreases (Figure 5.13) and as the HMA thickness decreases (Figures 5.13 and 5.14). Also, comparing Figures 5.13 and 5.14 with Figures 5.15 and 5.16 indicates that the influence of the base modulus on fatigue cracking is the same irrespective of the subgrade type. Figures 5.17 and 5.20 show clearly that the base thickness has significant influence on alligator cracking. The relationship between base thickness and alligator cracking depends on subgrade stiffness and HMA thickness as shown in Figures 5.17-5.20.

PG58-28 , 8in HMA
Subgrade Modulus = 8,000psi

FIGURE 5.13 Percent change in alligator cracking for different thicknesses of the base layer at 8 in HMA and 8 ksi subgrade.

PG58-28 , 4in HMA
Subgrade Modulus = 8,000psi

FIGURE 5.14 Percent change in alligator cracking for different thicknesses of the base layer at 4 in HMA and 8 ksi subgrade.
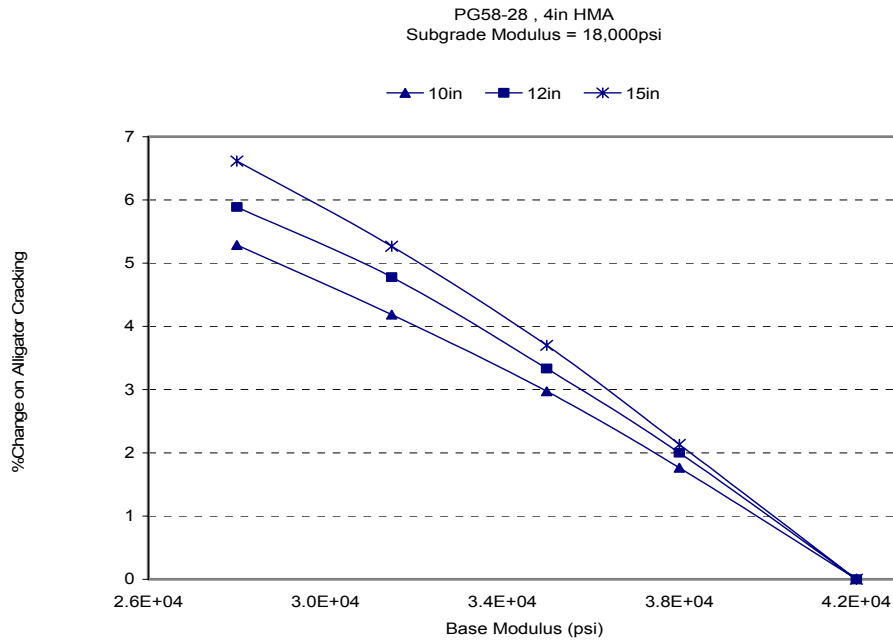
FIGURE 5.15 Percent change in alligator cracking for different thicknesses of the base layer at 4 in HMA and 18 ksi subgrade.
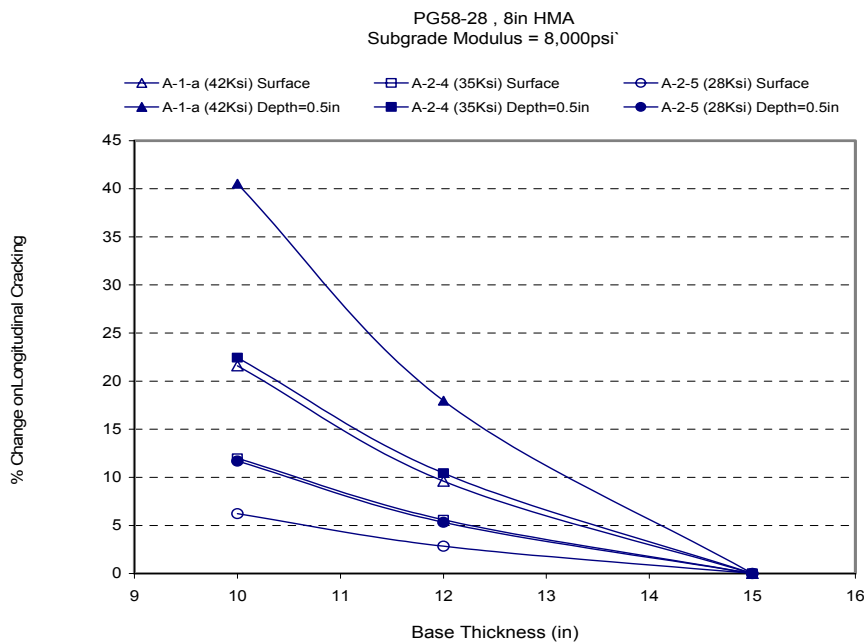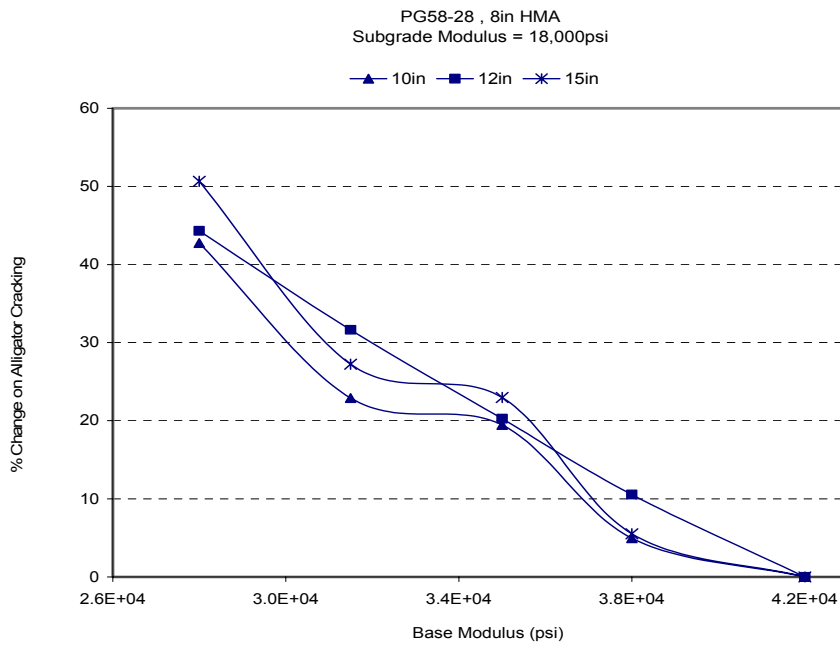

FIGURE 5.16 Percent change in alligator cracking for different thicknesses of the base layer at 8 in HMA and 18 ksi subgrade.
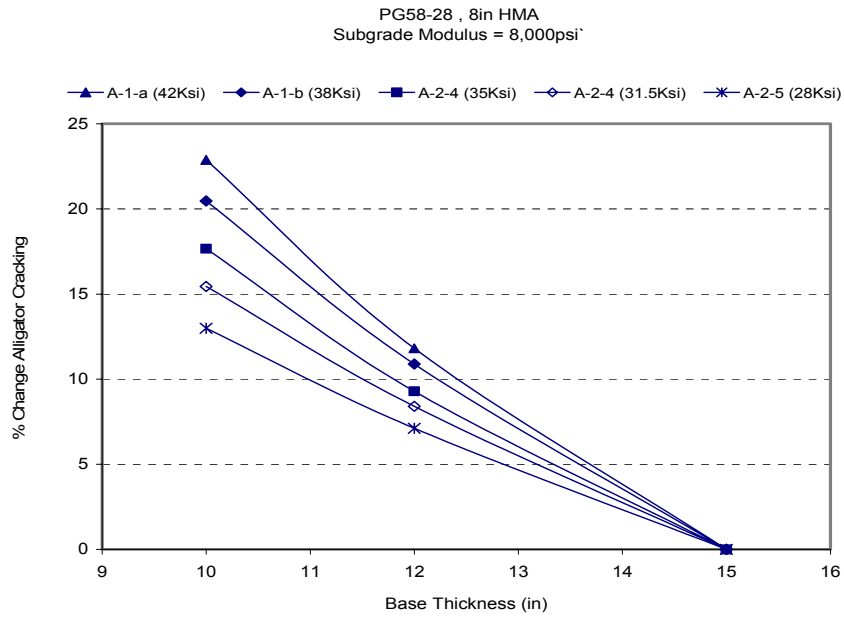
FIGURE 5.17 Percent change in alligator cracking for different types of the base layer at 8 in HMA and 8 ksi subgrade.
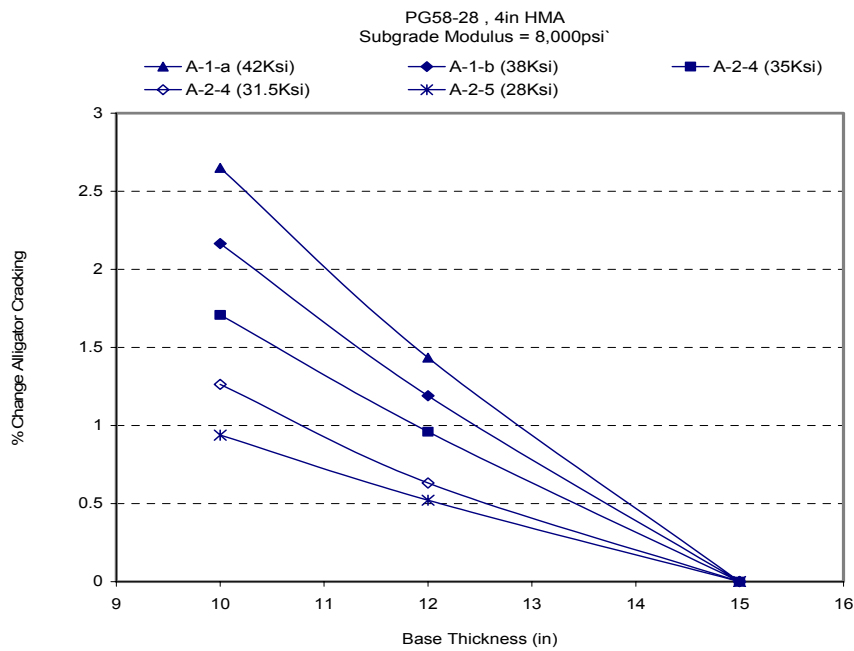
FIGURE 5.18 Percent change in alligator cracking for different types of the base layer at 4 in HMA and 8 ksi subgrade.
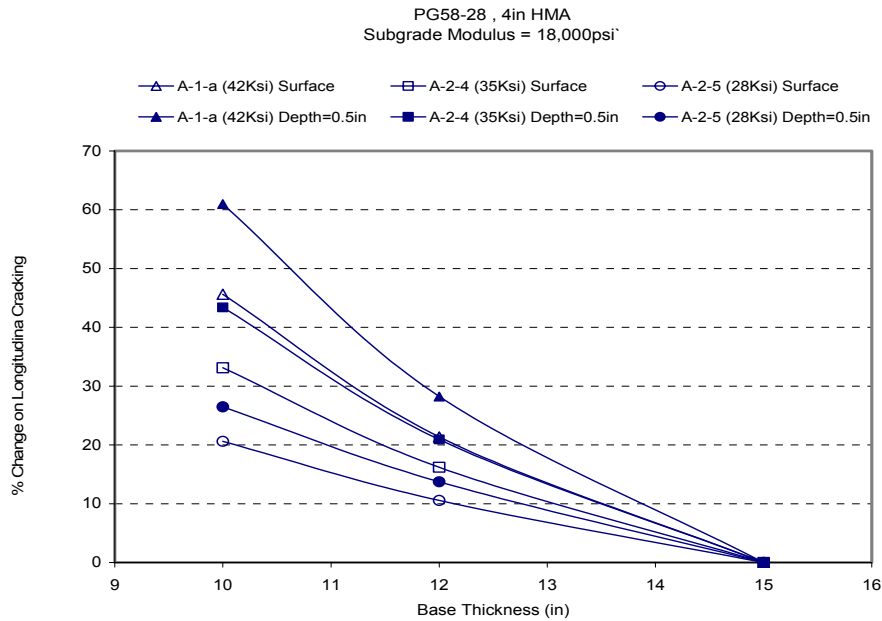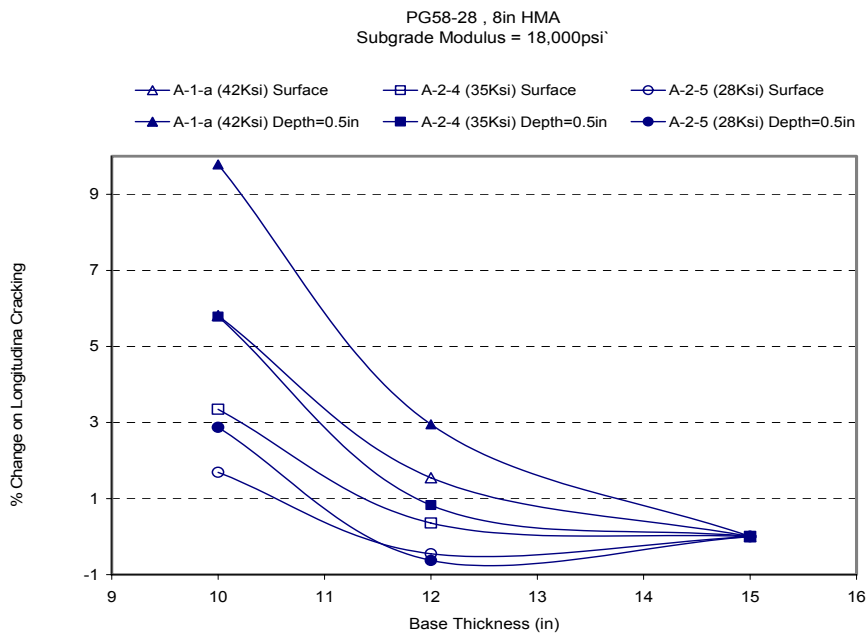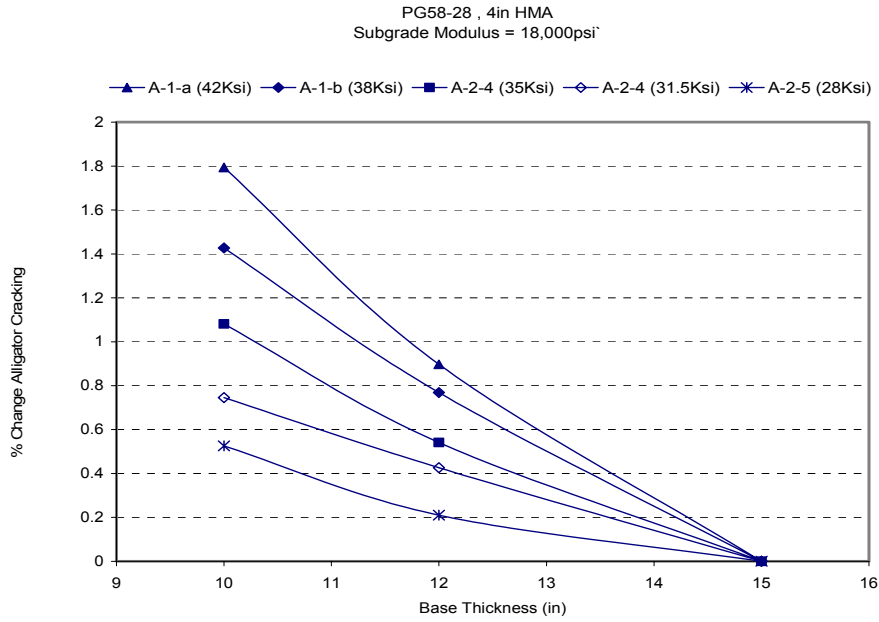
FIGURE 5.19 Percent change in alligator cracking for different types of the base layer at 4 in HMA and 18 ksi subgrade.
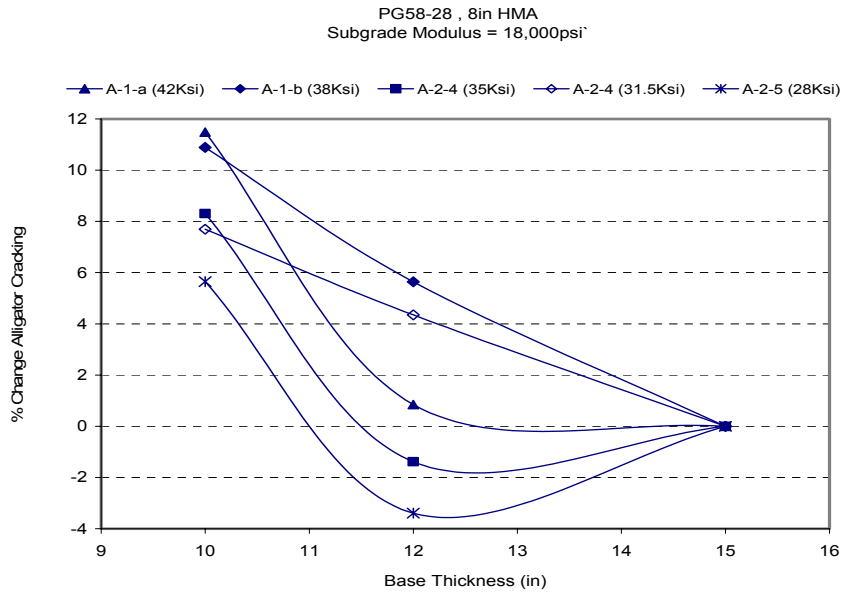
FIGURE 5.20 Percent change in alligator cracking for different types of the base layer at 8 in HMA and 18 ksi subgrade.

5.4.4 Permanent Deformation

Permanent deformation is one of the most important types of distresses in flexible pavements. Water can accumulate in traffic lanes and reduce skid resistance of the surface and cause unsafe traffic conditions. In AASHTO 2002 Design guide, the permanent deformation is calculated at the middepth of each sublayer within the pavement so the overall permanent deformation is the summation of the permanent deformation for all the layers. The performance criterion for total permanent deformation is defined in terms of the maximum rut depth in the wheel path. A typical maximum rut depth for total permanent deformation is about 3 in (*6*).

All the results from the permanent deformation analysis show that the base properties have almost no influence on permanent deformation (Figures 5.21-5.26). This is a surprising result given that the main function of the base layer is the distribution of applied loads to reduce permanent deformation. The analysis in chapter IV of this thesis showed that the permanent deformation models are sensitive to the base properties. This indicates that the implementation of these models in the AASHTO 2002 should be carefully reviewed.
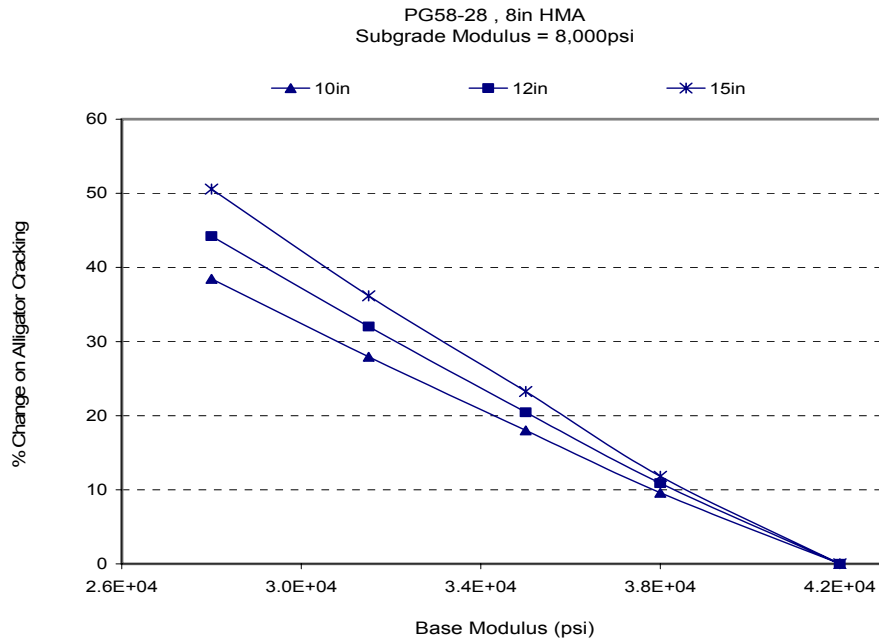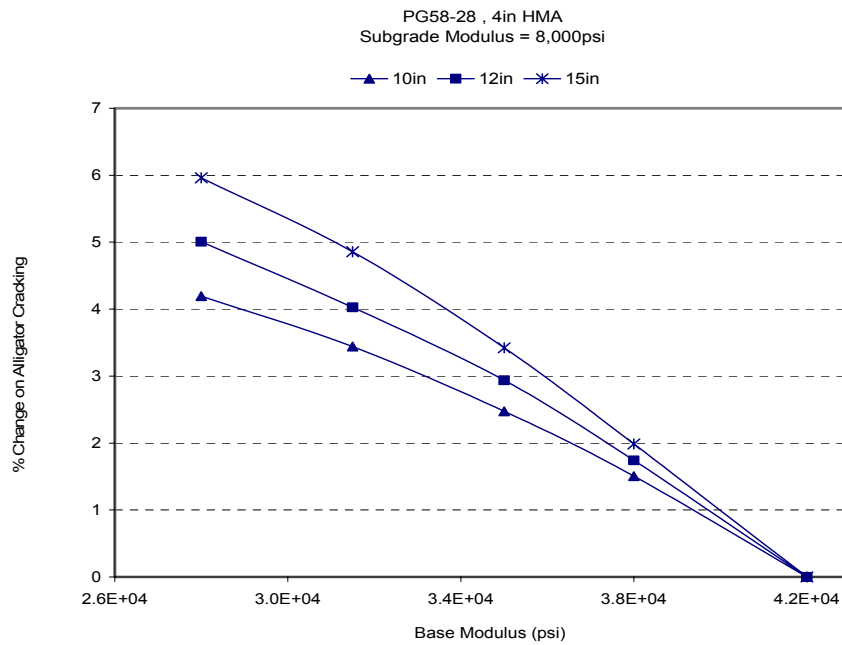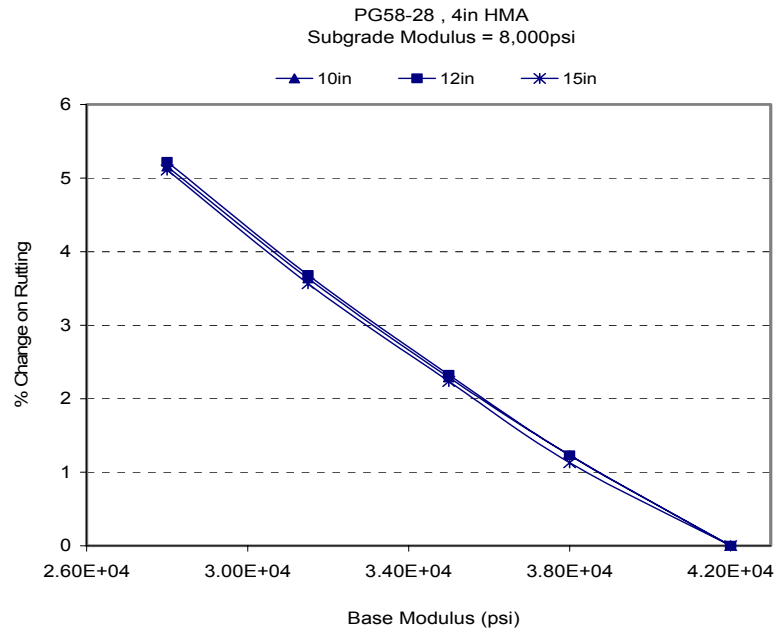
FIGURE 5.21 Percent change in rutting for different thicknesses of the base layer at 4 in HMA and 8 ksi subgrade.
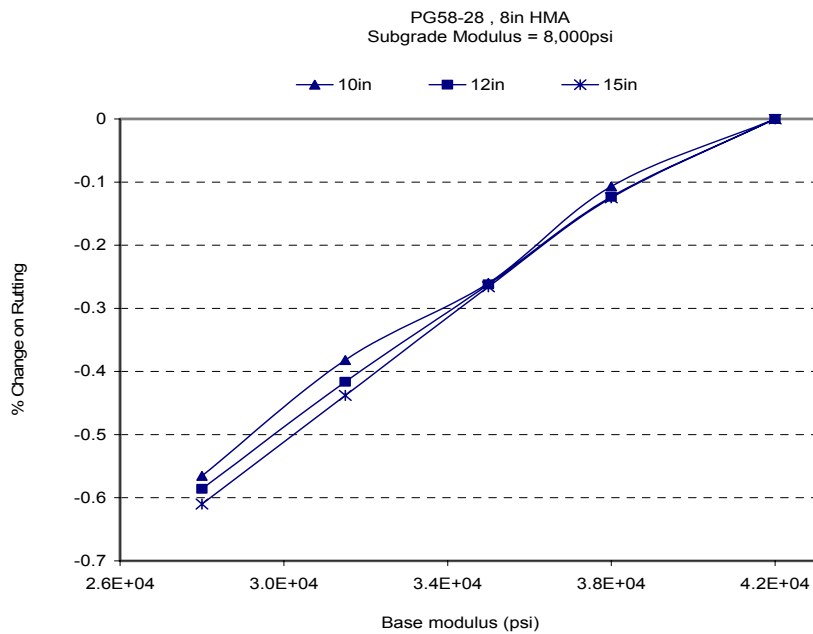
FIGURE 5.22 Percent change on rutting for different thicknesses of the base layer at 8 in HMA and 8 ksi subgrade.

PG58-28 , 4in HMA
Subgrade Modulus = 18,000psi
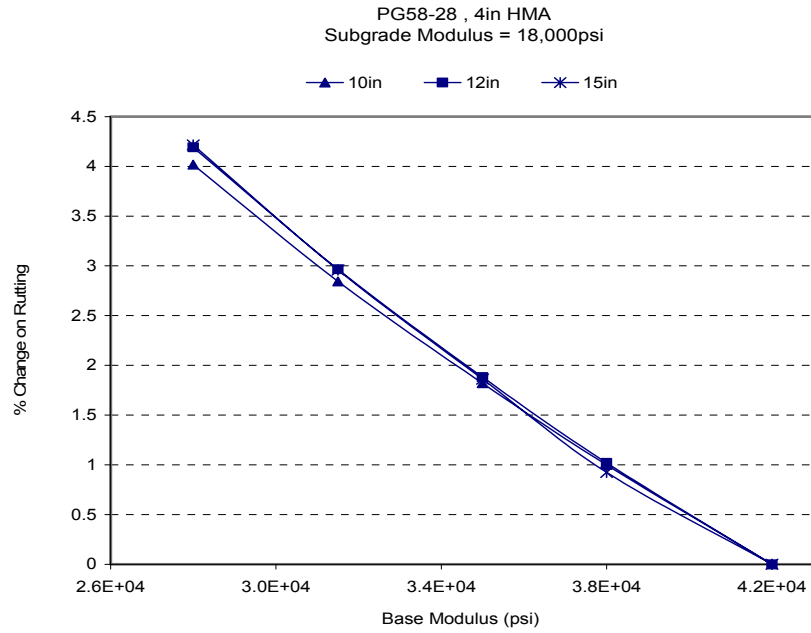
FIGURE 5.23 Percent change on rutting for different thicknesses of the base layer at 4 in HMA and 18 ksi subgrade.

PG58-28 , 4in HMA
Subgrade Modulus = 8,000psi`
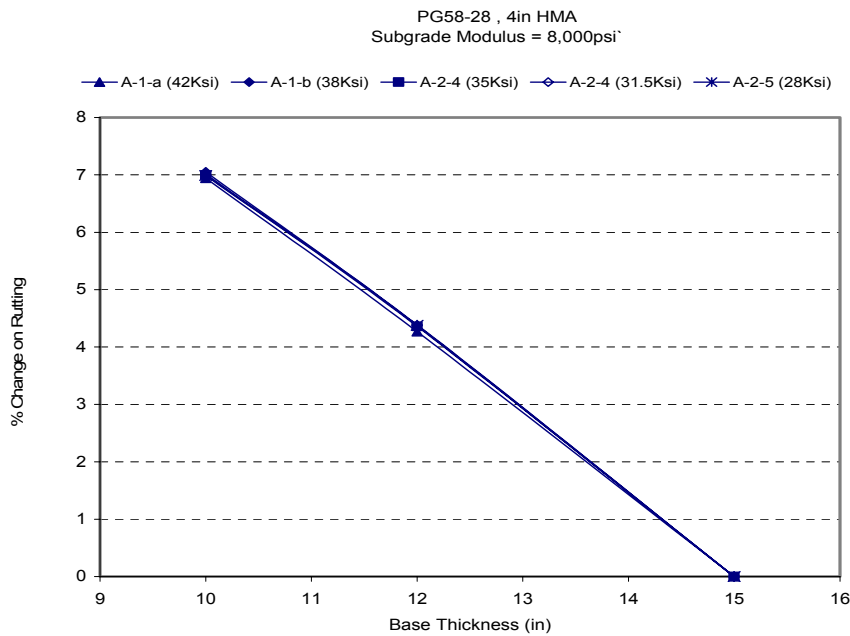
FIGURE 5.24 Percent change on rutting for different types of the base layer at 4 in HMA and 8 ksi subgrade.

PG58-28 , 8in HMA
Subgrade Modulus = 8,000psi`

—▲—A-1-a (42Ksi) —◆—A-1-b (38Ksi) —■—A-2-4 (35Ksi) —◇—A-2-4 (31.5Ksi) —✳—A-2-5 (28Ksi)
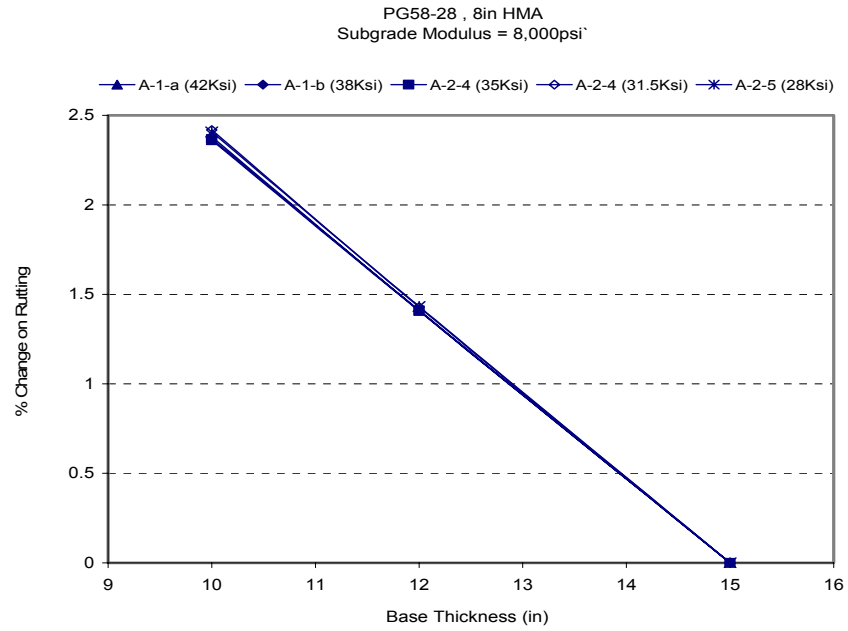
FIGURE 5.25 Percent change on rutting for different types of the base layer at 8 in HMA and 8 ksi subgrade.

PG58-28 , 4in HMA
Subgrade Modulus = 18,000psi`

—▲—A-1-a (42Ksi) —◆—A-1-b (38Ksi) —■—A-2-4 (35Ksi) —◇—A-2-4 (31.5Ksi) —✳—A-2-5 (28Ksi)
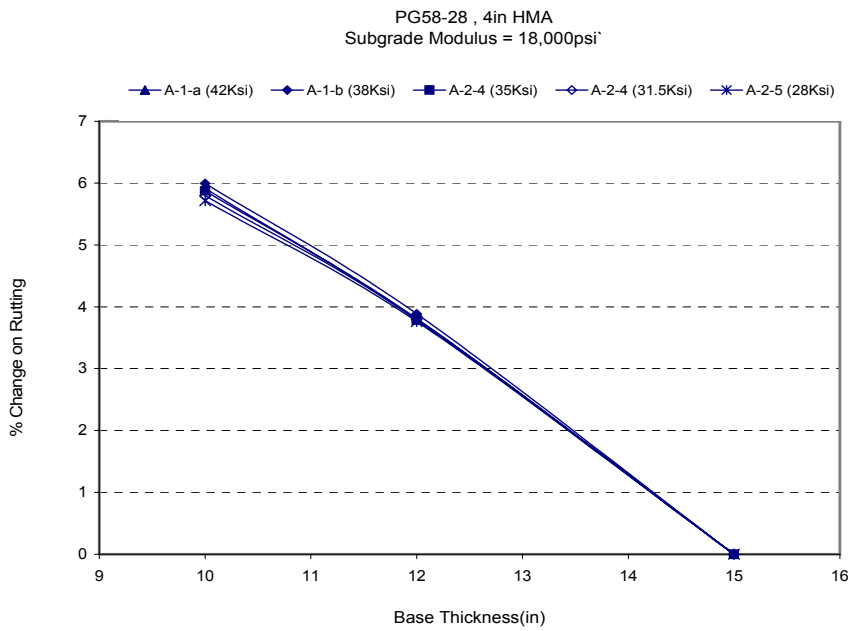
FIGURE 5.26 Percent change on rutting for different types of the base layer at 4 in HMA and 18 ksi subgrade.

5.5   Summary of Findings

The sensitivity analysis results show that the base modulus and thickness have significant influence on the international roughness index and the longitudinal cracking. The influence of base properties on alligator cracking is about half of the influence of base properties on longitudinal cracking. All the results show that the base properties have almost no influence on permanent deformation. These findings are applicable to the three climatic zones, the two asphalt binder grades, and three traffic levels used in this study.

CHAPTER VI

CONCLUSIONS

It is evident from the literature that there is a need to compare the calculated response of isotropic and anisotropic pavement models based on field experimental sections. This was achieved in this thesis by comparing the models predictions with the AASHO deflection measurements. The analysis included sections with different profiles and materials properties. Anisotropy was modeled by the ratio of the horizontal modulus to vertical modulus. The percentage of error between predictions and measurements decreased as the anisotropy increased. The predictions correlated the best with the experimental measurements when the horizontal modulus was about 30% of the vertical modulus. The predictions matched the AASHO measurements in the fall season better than the measurements in the spring season. As reported in the AASHO experiment, distresses were detected in the spring season that might have caused the response to deviate from the elastic solutions used in the FEM.

A critical review was conducted for the models used in the AASHTO 2002 design guide. The review focused on the differences between these models and the original models on which the AASHTO 2002 models were developed. It was found that the original models (Asphalt Institute Shell model for fatigue and Tseng and Lytton model for permanent deformation) were modified based on calibration with field data mainly from the LTPP database. The predictions from the original models can differ from the predictions of the AASHTO 2002 models.

The permanent deformation and fatigue cracking were calculated based on the mechanistic-empirical models used in AASHTO 2002 using isotropic and anisotropic material properties. The permanent deformation in the asphalt and base layers obtained using the anisotropic model is always more than that from the isotropic model. The permanent deformation in the subgrade obtained using the isotropic model is more than that for the anisotropic model when the regression equations from Tseng and Lytton are used. However, the permanent deformation using the isotropic model can be more or less than that calculated using the anisotropic model when the regression equations used in the AASHTO 2002 are used. The total permanent deformation using the isotropic model can be more or less than that for the anisotropic model when the regression equations from Tseng and Lytton are used. However, the total permanent deformation using the anisotropic model is more than that calculated using the isotropic model when the AASHTO 2002 equations are used.

The fatigue life predicted using the nonlinear anisotropic approach is higher than the life predicted using the nonlinear isotropic approach. This can explain the high shift factor typically found between the laboratory fatigue life calculated using the isotropic analysis, and the field fatigue life. This shift factor can be reduced when anisotropic properties are used.

The sensitivity analysis of the AASHTO 2002 model shows that the base modulus and thickness have significant influence on the international roughness index and the longitudinal cracking. The influence of base properties on alligator cracking is about half of the influence of base properties on longitudinal cracking. Surprisingly, all

the results show that the base properties have almost no influence on permanent deformation. These findings are applicable to all the material properties, pavement profiles, and environmental conditions used in this study. The implementation of the AASHTO 2002 guide to the permanent deformation model should be carefully reviewed to address this discrepancy.

REFERENCES

1. Hicks, R.G., and C. L. Monismith. Factors Influencing the Resilient Properties of Granular Materials. In *Transportation Research Record 345,* TRB*,* National Research Council, Washington DC, 1971, pp. 15-31.

2. May, R. W., and M.W. Witczak. Effective Granular Modulus to Model Pavement Responses. In *Transportation Research Record 810*, TRB, Washington, DC, 1981, pp. 1-9.

3. Uzan, J. Characterization of Granular Material. In *Transportation Research Record 1022*, TRB, National Research Council, Washington DC, 1985, pp. 52-59.

4. Tutumluer, E. *Predicting Behavior of Flexible Pavements with Granular Bases*. Ph.D. Dissertation. Georgia Institute of Technology, Atlanta, 1995.

5. Adu-Osei, A. *Characterization of Unbound Granular Layers in Flexible Pavements*. Ph.D. Dissertation. Department of Civil Engineering, Texas A&M University, College Station, 2000.

6. ERES. 2002 Design Guide, *Design of New and Rehabilitated Pavement Structures*, Draft Final Report. National Cooperative Highway Research Program, Washington DC, 2002.

7. Tutumluer, E. Anisotropic Behavior of Unbound Aggregate Bases - State of the Art Summary. *Proceedings 6th Annual Symposium of the International Center for Aggregate Research (ICAR)*, St. Louis, Missouri. 1998.

8. Finn, F., C. Saraf, R. Kulkarni, K. Nair, W. Smith, and A. Abdullah. The use of Distress Prediction Subsystems for the Design of Pavement Structures. *Proceedings 4rd International Conference on Structural Design of Asphalt Pavements*, Univ. of Michigan, Ann Arbor. 1977.

9. Lekarp, F., U. Isaacson, and A. Dawson. State of the Art. II: Resilient Response of Unbound Aggregate. *Journal of Transportation Engineering*, ASCE, Vol.126, No.1, 2000, pp. 66-75.

10. Dunlap, W. A. *A Report on Mathematical Model Describing the Deformation Characteristics of Granular Materials*. Tech.Rep.No.1, Pro.2-8-62-27, Texas Transportation Institute, Texas A&M University, College Station, 1963.

11. Monismith, C. L., H.B. Seed, F.G. Mitry, and C.K. Chan. Prediction of Pavement Deflection from Laboratory Tests. *Proc., 2nd International Conference on Structural Design of Asphalt Pavements*, University of Michigan, Ann Arbor, 1967, pp.109-140.

12. Seed, H. B., F.G. Mitry, C.L. Monismith, and C.K. Chan. *NCHRP Report 35: Prediction of Flexible Pavement Deflections from Laboratory Repeated Load Tests*. National Cooperative Highway Research Program, Washington, DC, 1967.

13. Brown, S. F., and P.S. Pell. An experimental Investigation of the Stresses, Strain and Deflections in a Layered Pavement Structure Subjected to Dynamic Loads. *Proc., 2nd International Conference on Structural Design of Asphalt Pavements*, University of Michigan, Ann Arbor, 1967, pp. 487-504.

14. Hicks, R.G. *Factors Influencing the Resilient Properties of Granular Materials*. Ph.D .Dissertation. University of California, Berkeley, 1970.

15. Elliot, R. P., and D. Lourdesnathan. Improved Characterization Model for Granular Bases. In *Transportation Research Record 1227*, TRB, Washington, DC, 1989, pp.128-133.

16. Boyce, H. R. A Non-linear Model for the Elastic Behavior of Granular Materials Under Repeated Loading. *Proc., Int. Symp. On Soils under Cyclic and Transient Loading*, Swansea, UK, 1980, pp.285-294.

17. Brown, S. F., and J.W. Pappin. Modeling of Granular Materials in Pavements. In *Transportation Research Record 1022,* TRB, Washington, DC, 1985, pp. 45-51.

18. Tutumluer, E. and M.R. Thompson. Anisotropic Modeling of Granular Bases In Flexible Pavements. In *Transportation Research Record 1577,* TRB, National Research Council, Washington DC, 1997.

19. Hornych, P., A. Kazai, and J.M. Piau. Study of the Resilient Behavior of Unbound Granular Materials. *Proc., 5th International Conference on the Bearing Capacity of Roads and Airfields* (R.S. Nordal and G. Rafsdal, eds), 1998, Vol.3, pp. 1277-1287.

20. Tutumluer, E. Nonlinear Anisotropic Modeling of Dilative Granular Material Behavior, *Proceedings of the Ninth International Conference of the Association for Computer Methods and Advances in Geomechanics*, IACMAG 97, Wuhan, China, 1997.

21. Lekarp, F., U. Isaacson, and A. Dawson. State of the Art. II: Permanent Strain Response of Unbound Aggregate. *Journal of Transportation Engineering*, ASCE, Vol.126, No.1, 2000, pp. 76-83.

22. Barksdale, R.D. Laboratory Evaluation of Rutting in Base Course Materials. *Proc., 3rd International Conference on Structural Design of Asphalt Pavements,* University of Michigan, Ann Arbor,1972, pp. 161-174.

23. Bonaquist, R. F., and M.W. Witczak. A Comprehensive Constitutive Model for Granular Materials in Flexible Pavement Structures. *Proc., 8th International Conference on Structural Design of Asphalt Pavements,* 1997, Vol. 1, pp. 783-802.

24. Duncan, J. M., and C.Y. Chang. Nonlinear Analysis of Stress and Strain in Soils. *J. Soil Mech. And Found. Div.*, ASCE, Vol.96, No.5, 1970, pp. 1629-1653.

25. Tseng, K.-H. and R.L. Lytton. *Prediction of Permanent Deformation in Flexible Pavements Materials*, Implication of Aggregates in The Design, Construction, and Performance of Flexible Pavements, ASTM STP 1016 (H.G.Schreuders and C.R. Marek, eds), American Society for Testing and Materials, Philadelphia 1989, pp.154-172.

26. Lekarp, F., and A. Dawson. Modeling Permanent Deformation Behavior of Unbound Granular Materials. *Constr. and Build. Mat.*, Vol.12, No.1, 1998, pp. 9-18.

27. The AASHO Road test: Report 5, Pavement Research. *Highway Research Board* Special Report 61E, Washington, DC, 1962.

28. The AASHO Road test: Report 7, Summary Report. *Highway Research Board* Special Report 61G, Washington, DC, 1962.

29. David R. Luhr and B. Frank McCullough. Structural Analysis of AASHO Road Test Flexible Pavements for Performance Evaluation, In *Transportation Research Record 888,* TRB, National Academy of Science, Washington DC, 1982.

30. Adu-Osei, A., D.N. Little, and R.L. Lytton. Cross-Anisotropic Characterization of Unbound Granular Materials. In *Transportation Research Record 1757,* TRB, National Academy of Science, Washington, DC, 2001, pp. 82-91.

31. Witczak, M, E., and T. K. Pellinen. *NCHRP Report 9-19: Superpave Support and Performance Models Management,* Task C-Simple Performance Test FHWA

ALF Experimental Site, Team Report SPT-ALF-2(J-K). National Research Council, Washington, DC, May 2000.

32. Witczak, M, E., and R.Bonaquist. *NCHRP 9-19 Report 9-19: Superpave Support and Performance Models Management, Binder Characterization,* Team Report BC-4. National Research Council, Washington, DC, May 2000.

APPENDIX A

Rutting (HMA), Section A

FIGURE A1 HMA permanent deformation in section A using the Tseng and Lytton model.

Rutting (Base), Section A

FIGURE A2 Permanent deformation in the base of section A using the Tseng and Lytton model.

FIGURE A3 Permanent deformation in the subgrade of section A using the Tseng and Lytton model.

FIGURE A4 Total permanent deformation in section A using the Tseng and Lytton model.

FIGURE A5 Bulk stress profiles in the base layer of section A using non-linear isotropic and anisotropic properties.

FIGURE A6 Deviatoric stress profiles in the base layer of section A using non-linear isotropic and anisotropic properties.

FIGURE A7 Compressive strain profiles in the base layer of section A using non-linear isotropic and anisotropic properties.

FIGURE A8 Compressive strain profiles in the asphalt layer of section A using non-linear isotropic and anisotropic properties.

FIGURE A9 Deviatoric stress profiles in the asphalt layer of section A using non-linear isotropic and anisotropic properties.

FIGURE A10 Bulk stress profiles in the base layer of section A using linear isotropic and anisotropic properties.

FIGURE A11 Deviatoric stress profiles in the base layer of section A using linear isotropic and anisotropic properties.

FIGURE A12 Compressive strain profiles in the base layer of section A using linear isotropic and anisotropic properties.

FIGURE A13 Compressive strain profiles in the asphalt layer of section A using linear isotropic and anisotropic properties.

FIGURE A14 Deviatoric stress profiles in the asphalt layer of section A using linear isotropic and anisotropic properties.

FIGURE A15 Tensile strain profiles in the asphalt and base layers of section A using nonlinear isotropic and anisotropic properties.
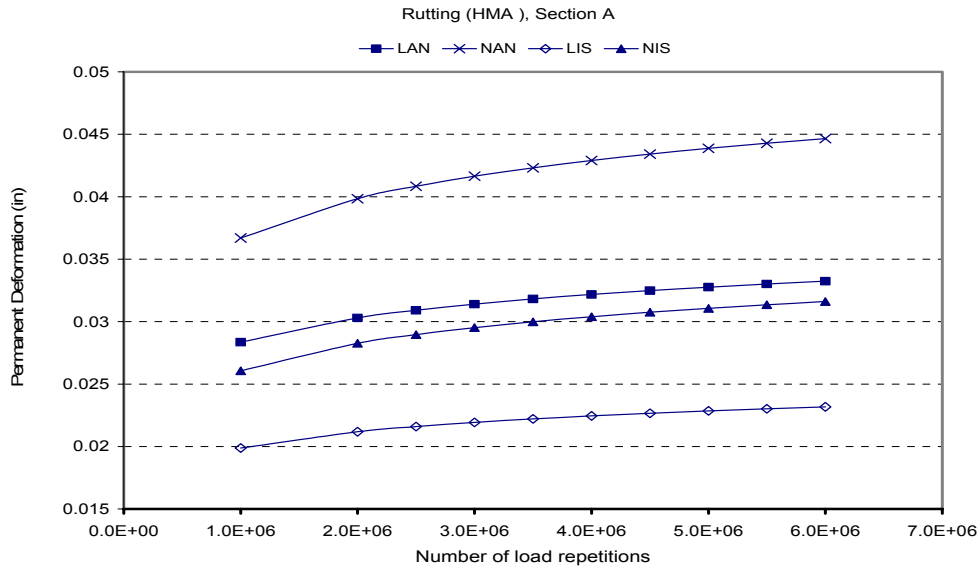

FIGURE A16 HMA permanent deformation in section B using the Tseng and Lytton model.
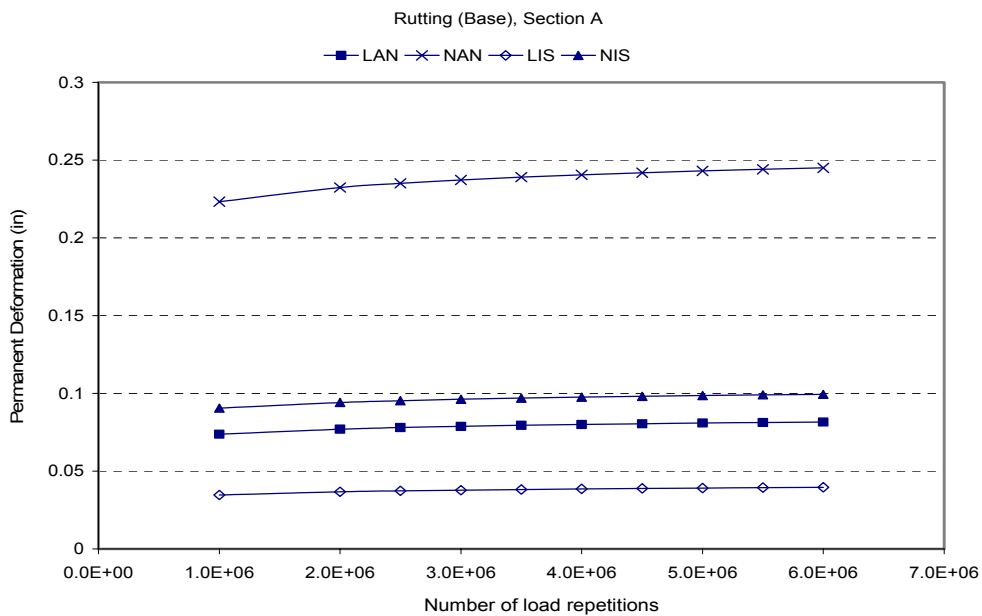
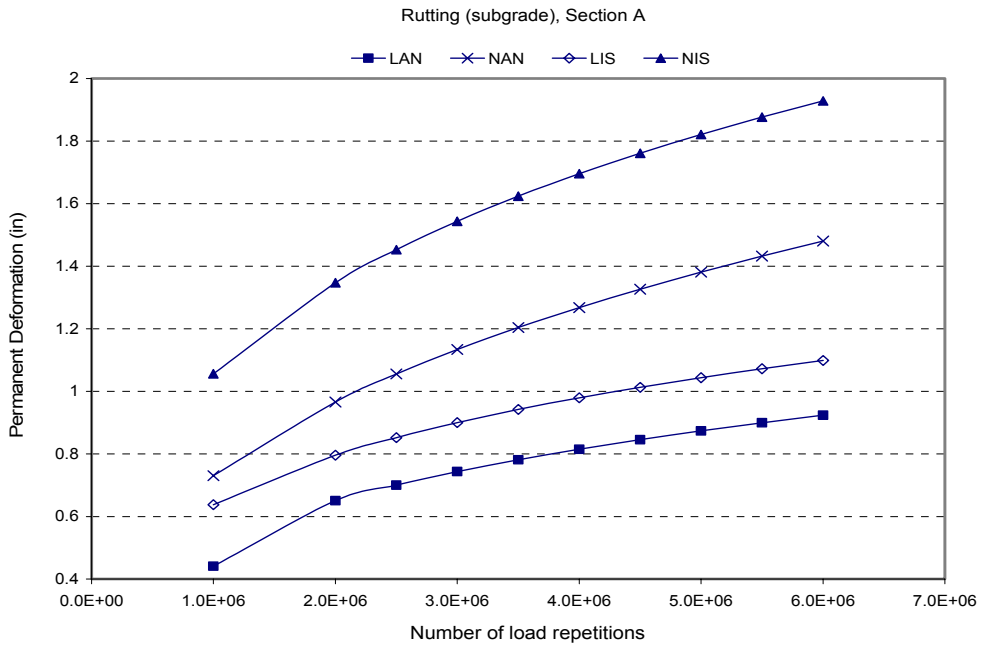FIGURE A17 Permanent deformation in the base of section B using the Tseng and Lytton model.

FIGURE A18 Permanent deformation in the subgrade of section B using the Tseng and Lytton model.
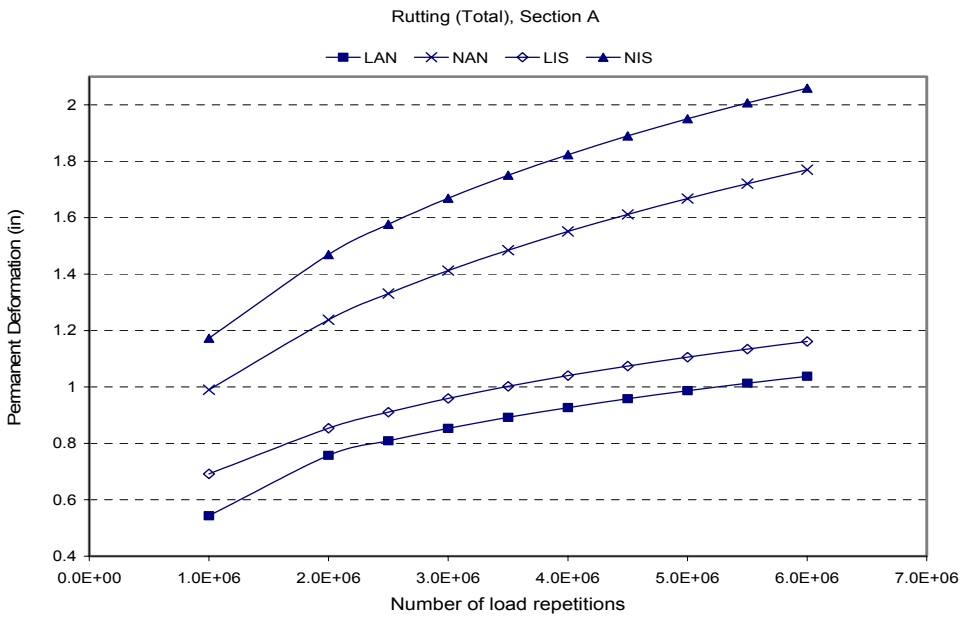
FIGURE A19 Total permanent deformation in section B using the Tseng and Lytton model.
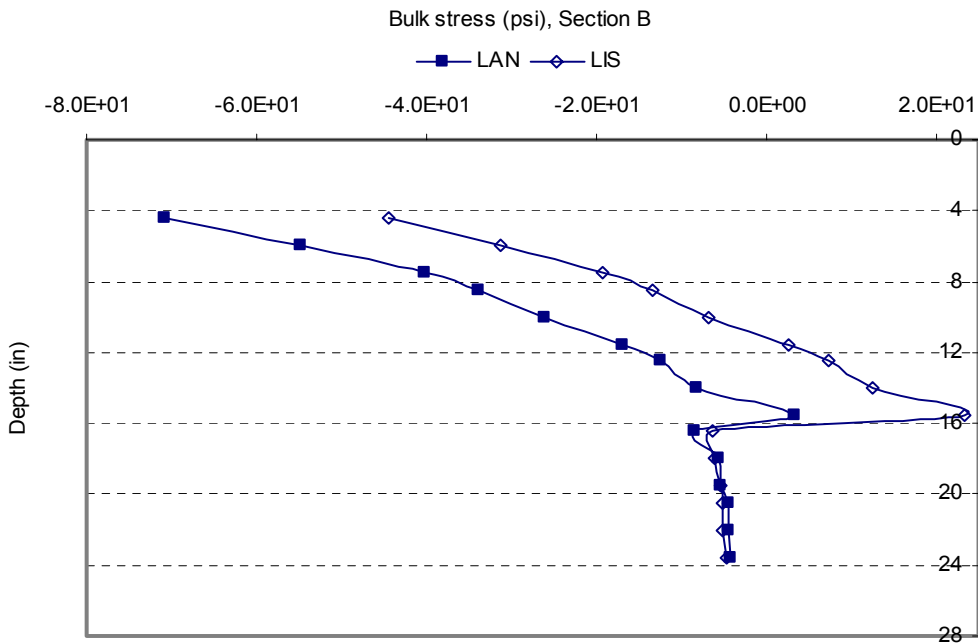
FIGURE A20 Bulk stress profiles in the base layer of section B using linear isotropic and anisotropic properties.

Deviatoric Stress (psi) ,Section B
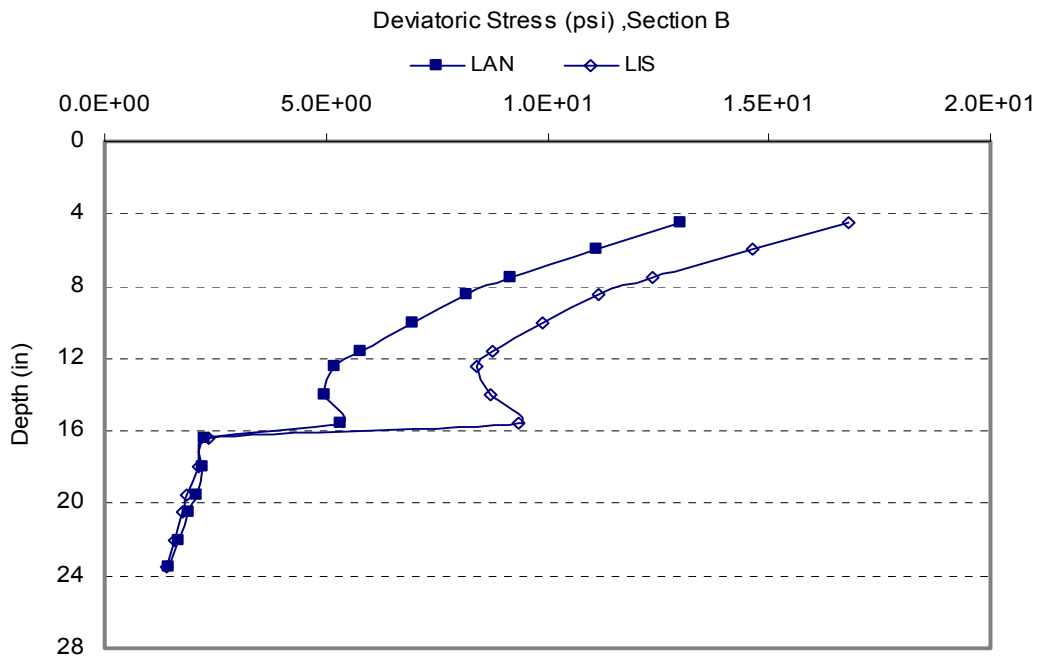
FIGURE A21 Deviatoric stress profiles in the base layer of section B using linear isotropic and anisotropic properties.

Compressive Strain, Section B
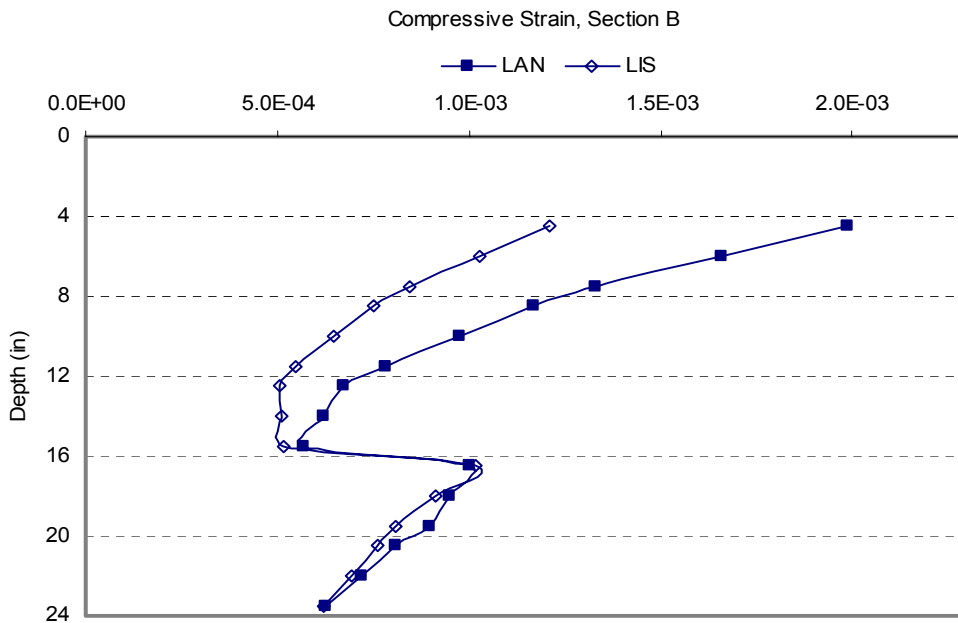
Figure A22 Compressive strain profiles in the base layer of section B using linear isotropic and anisotropic properties.
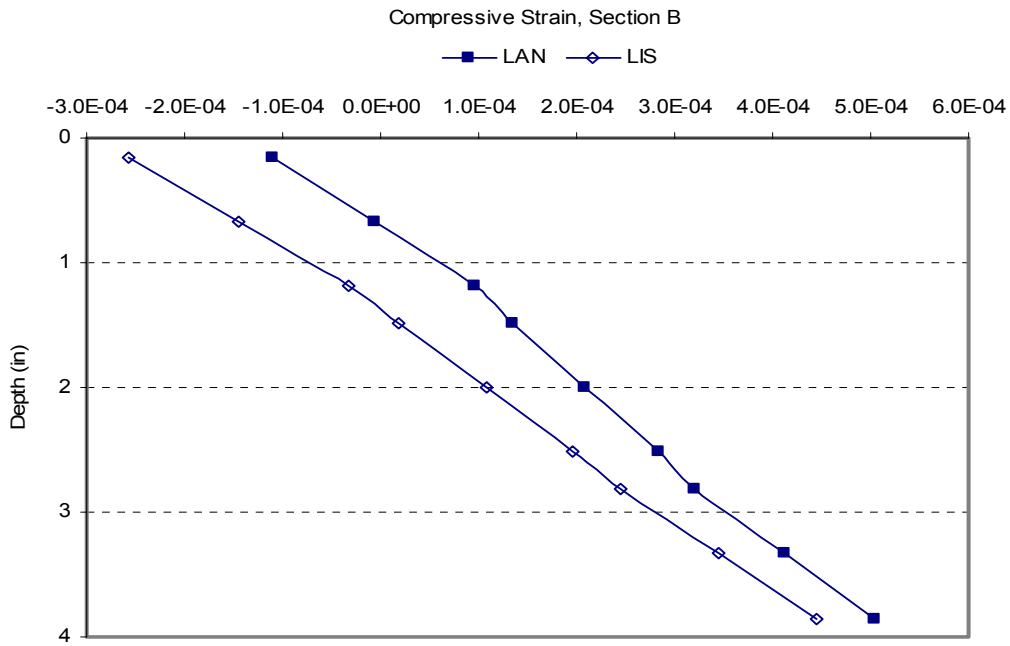
FIGURE A23 Compressive strain profiles in the asphalt layer of section B using linear isotropic and anisotropic properties.
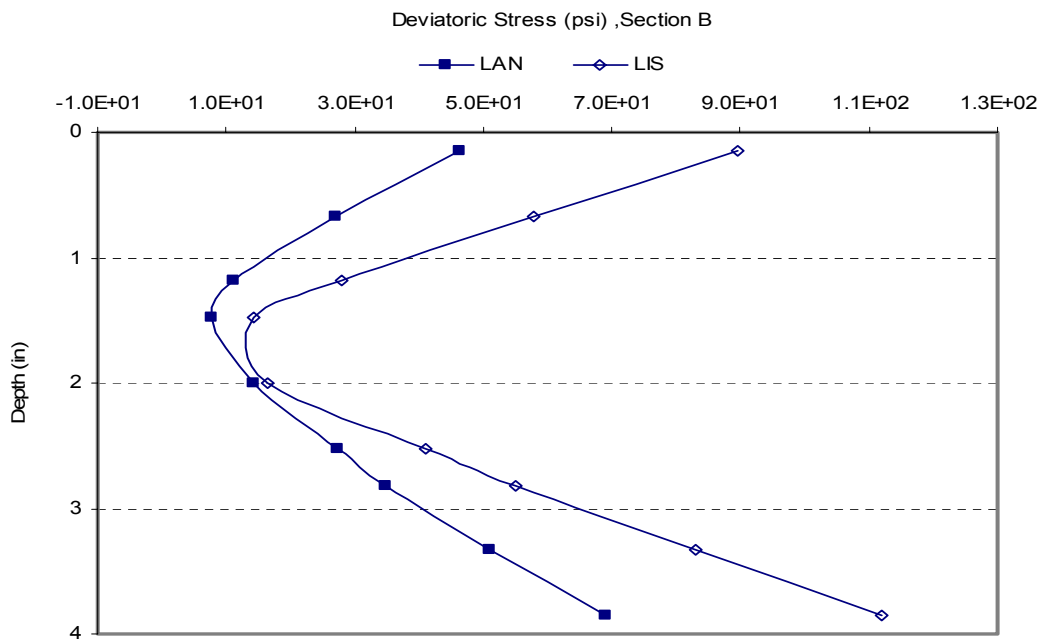
FIGURE A24 Deviatoric stress profiles in the asphalt layer of section B using linear isotropic and anisotropic properties.
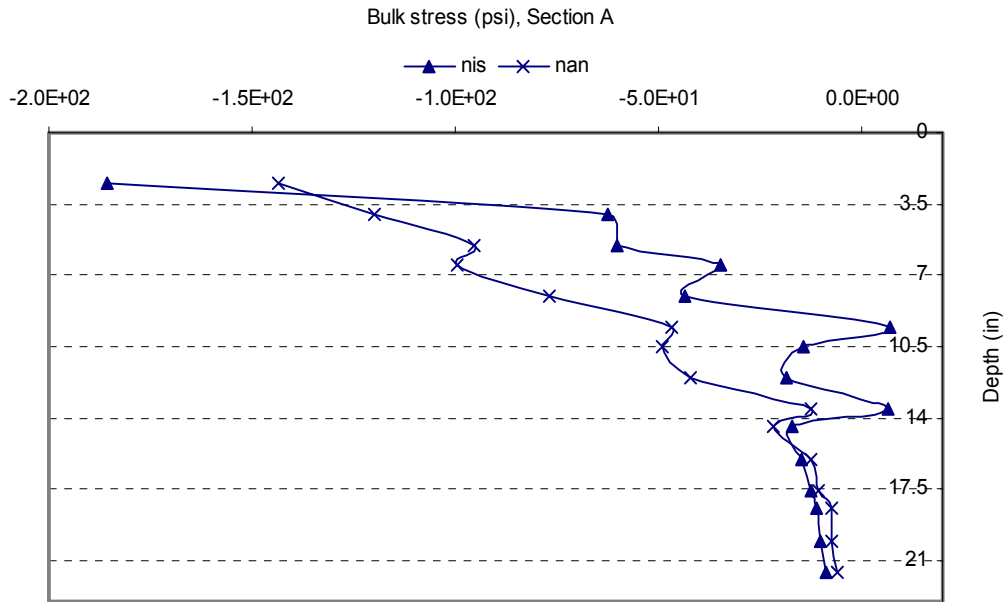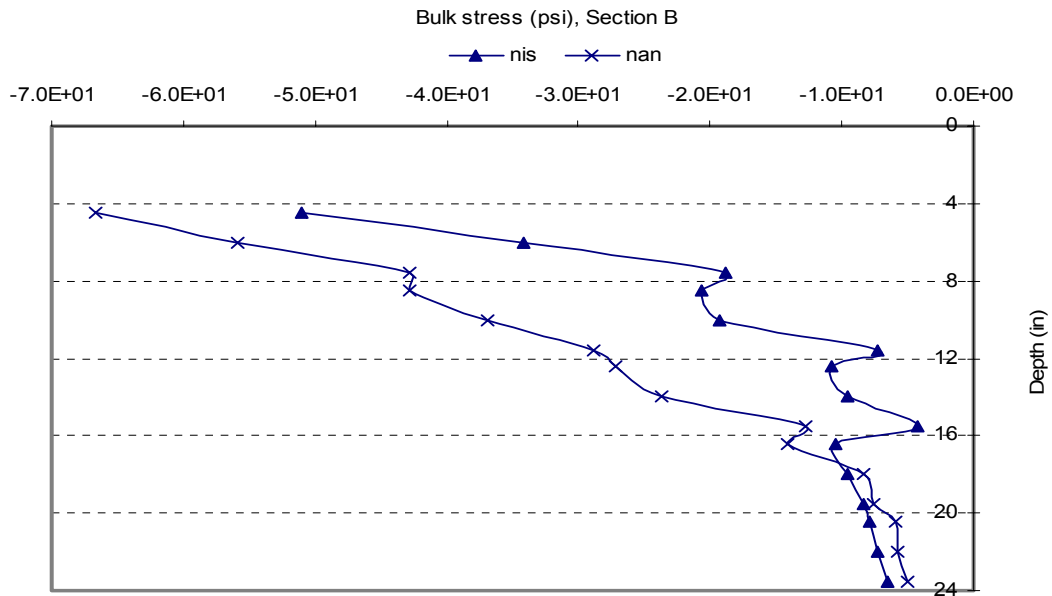
FIGURE A25 Bulk stress profiles in the base layer of section B using non-linear isotropic and anisotropic properties.
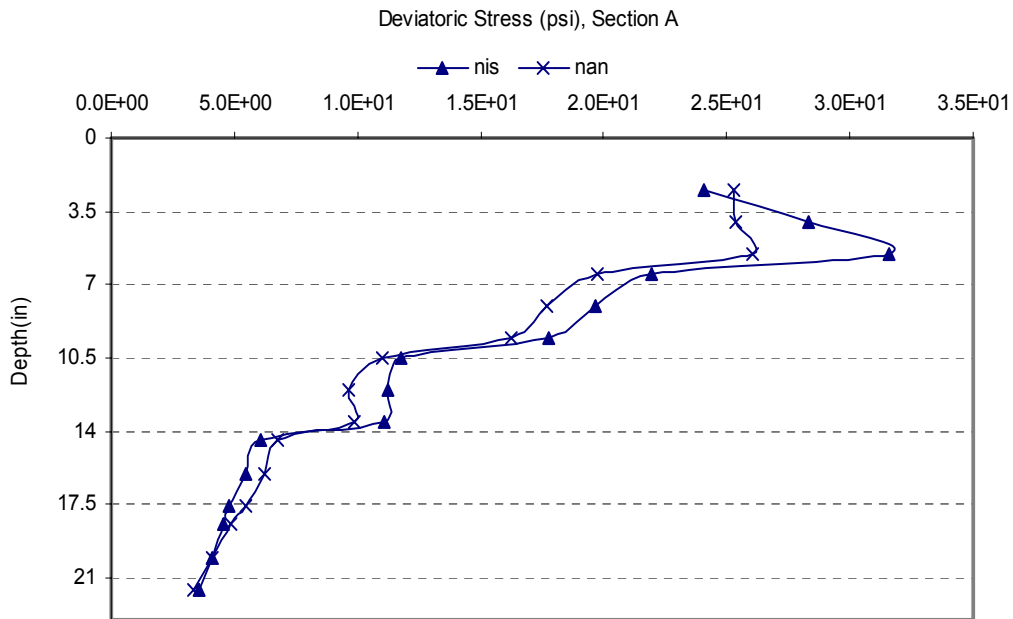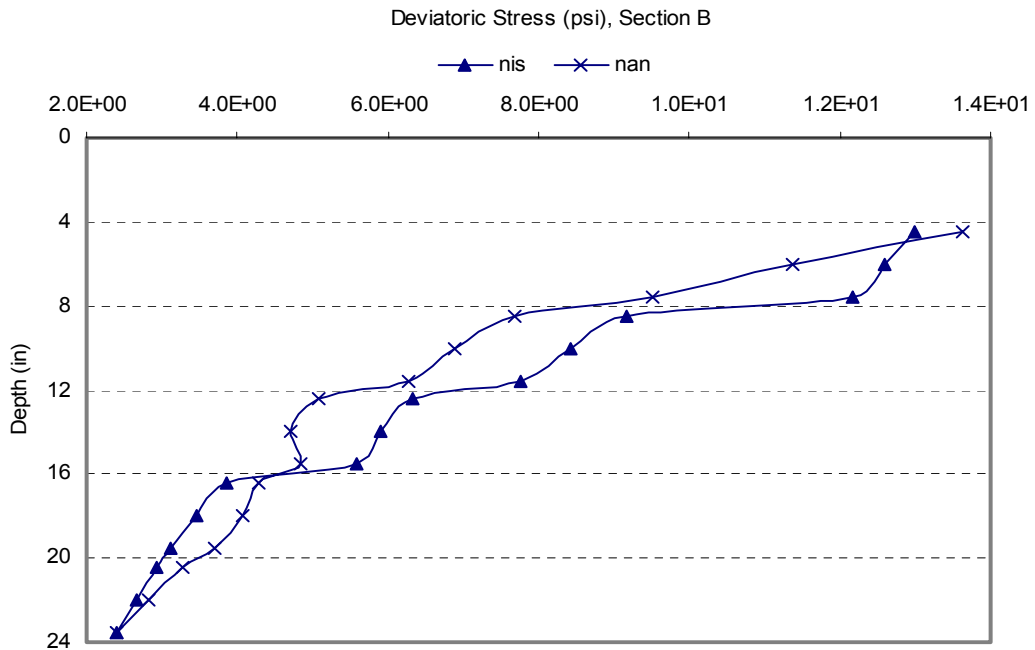

FIGURE A26 Deviatoric stress profiles in the base layer of section B using non-linear isotropic and anisotropic properties.
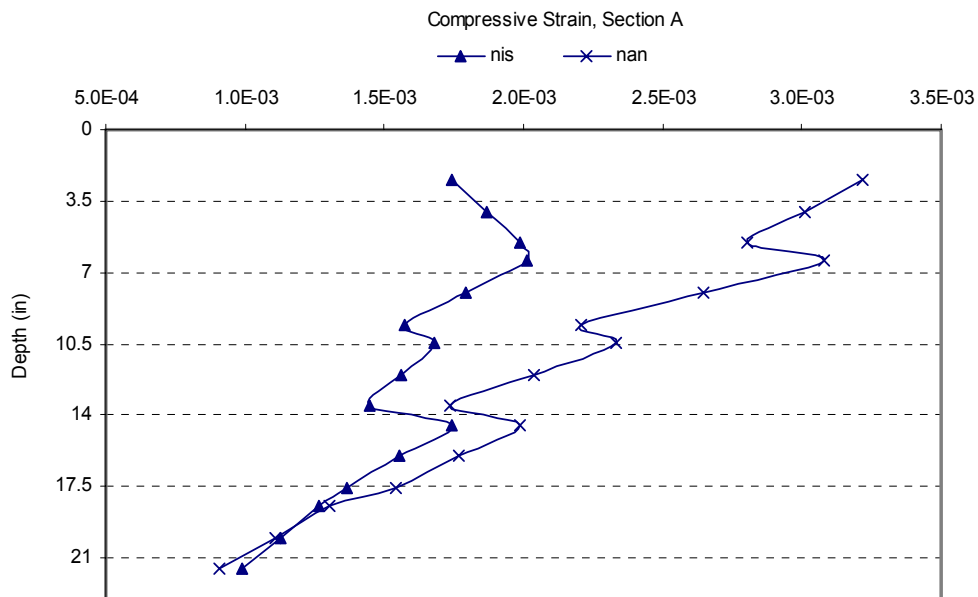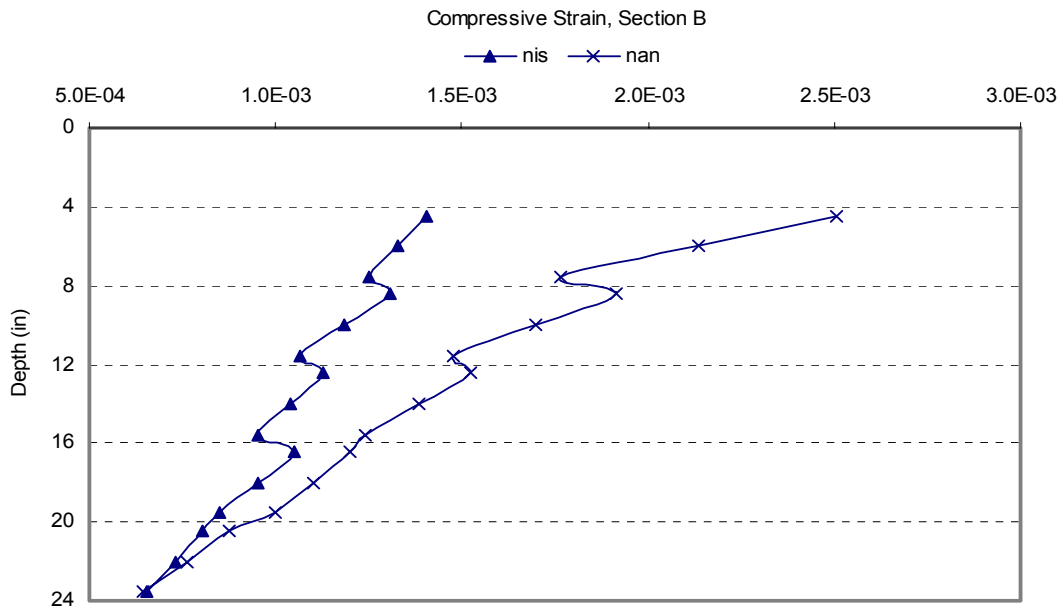
FIGURE A27 Compressive strain profiles in the base layer of section B using non-linear isotropic and anisotropic properties.
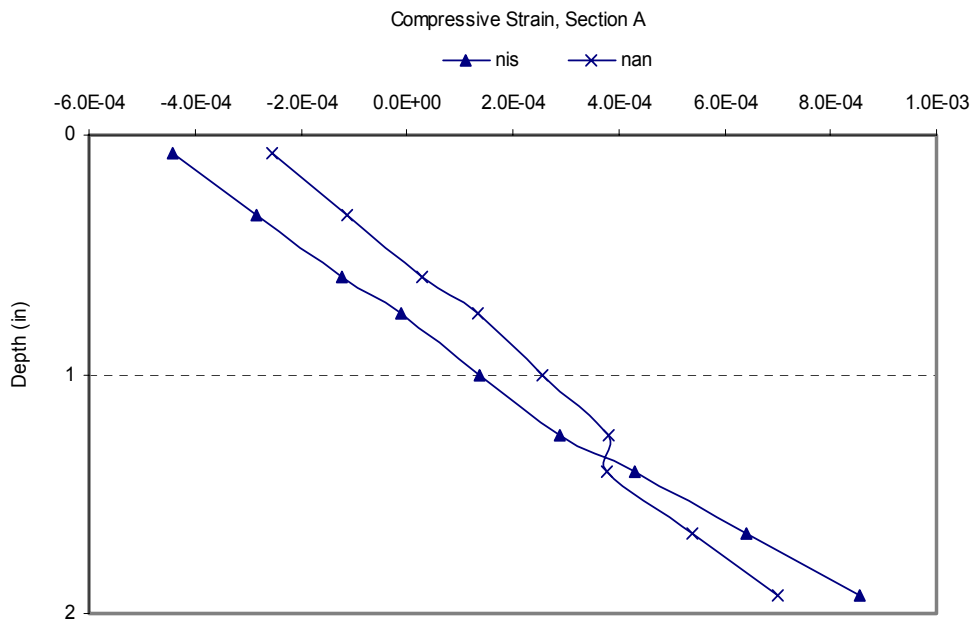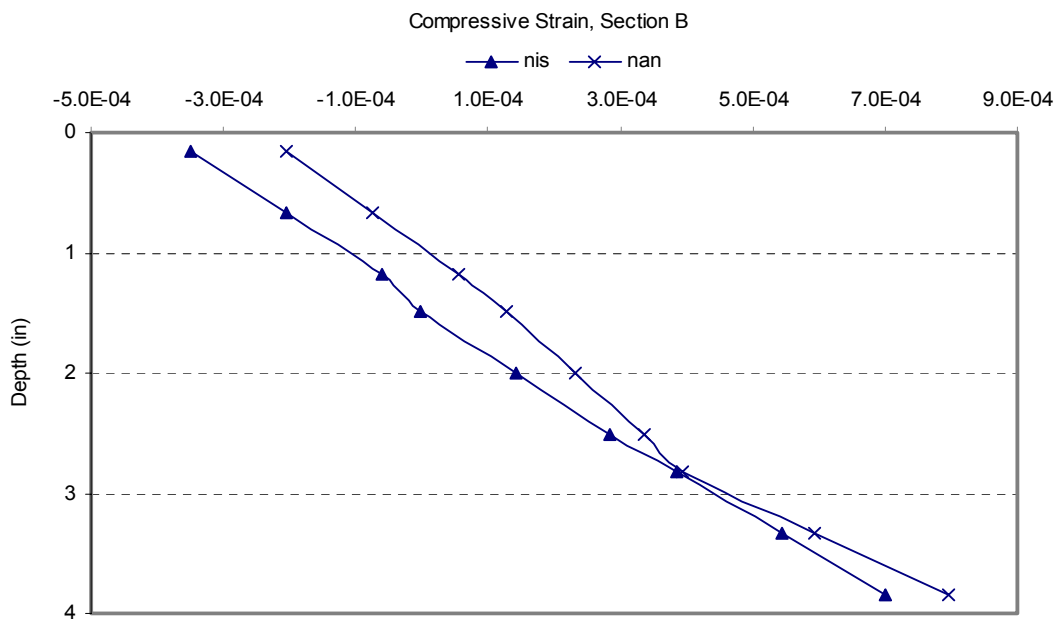

FIGURE A28 Compressive strain profiles in the asphalt layer of section B using non-linear isotropic and anisotropic properties.
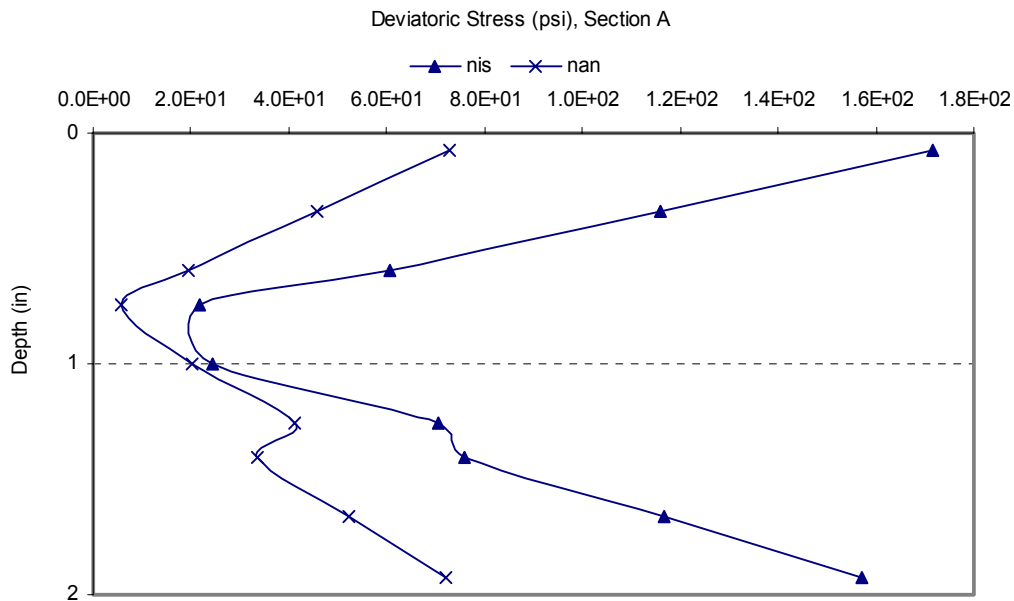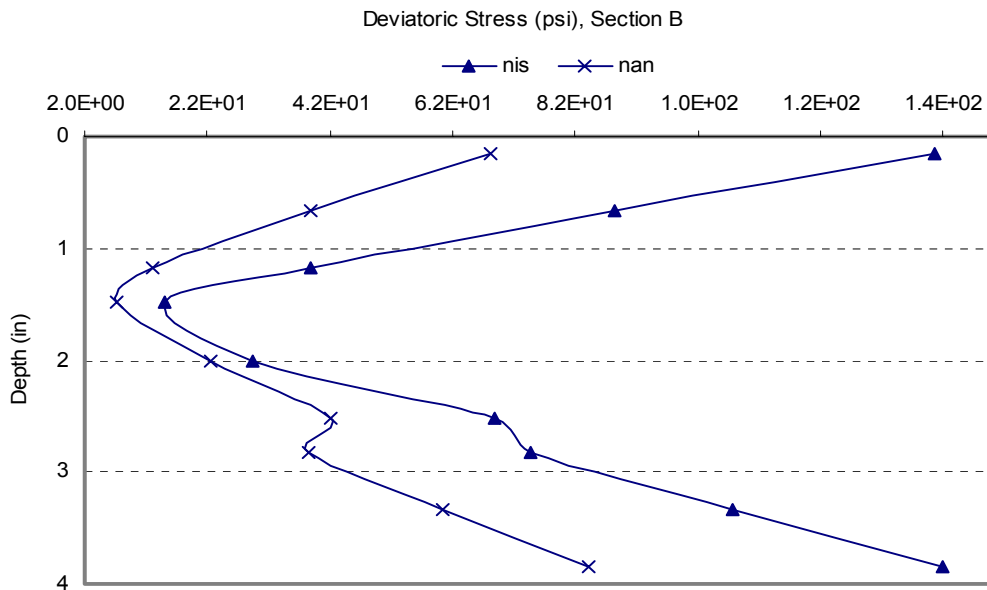
FIGURE A29 Deviatoric stress profiles in the asphalt layer of section B using non-linear isotropic and anisotropic properties.
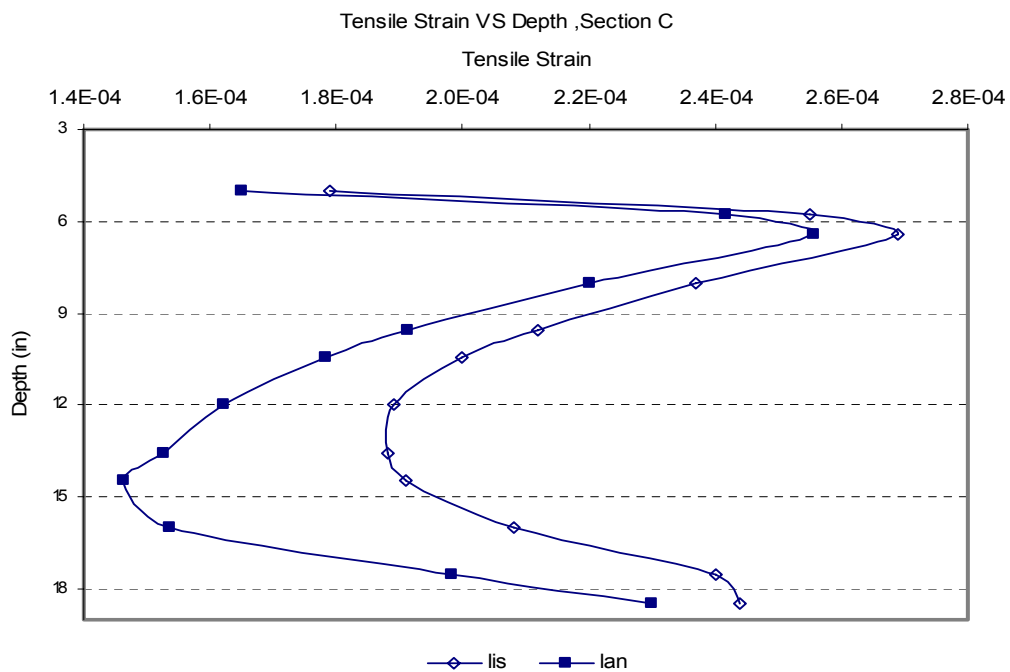
FIGURE A30 Tensile strain profiles in the asphalt and base layers of section C using linear isotropic and anisotropic properties.

Rutting (HMA), Section D

⊗— NAN ▲— NIS ◇— LIS ■— Ian
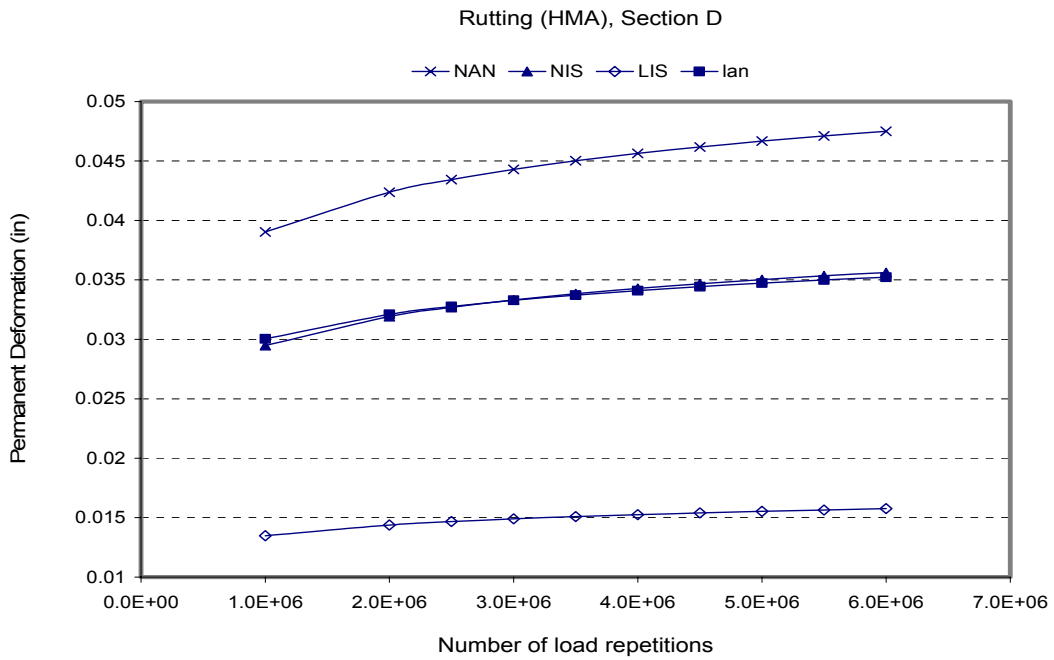
FIGURE A31 HMA permanent deformation in section D using the Tseng and Lytton model.

Rutting (Base), Section D

⊗— NAN ▲— NIS ◇— LIS ■— Ian
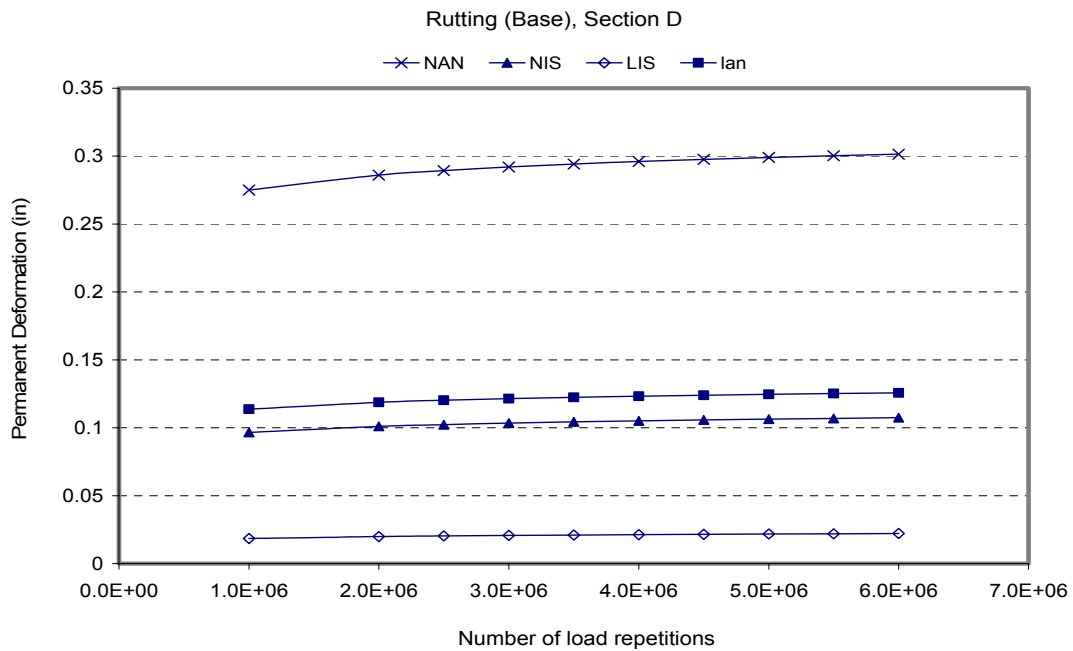
FIGURE A32 Permanent deformation in the base of section D using the Tseng and Lytton model.

Rutting (Subgrade), Section D
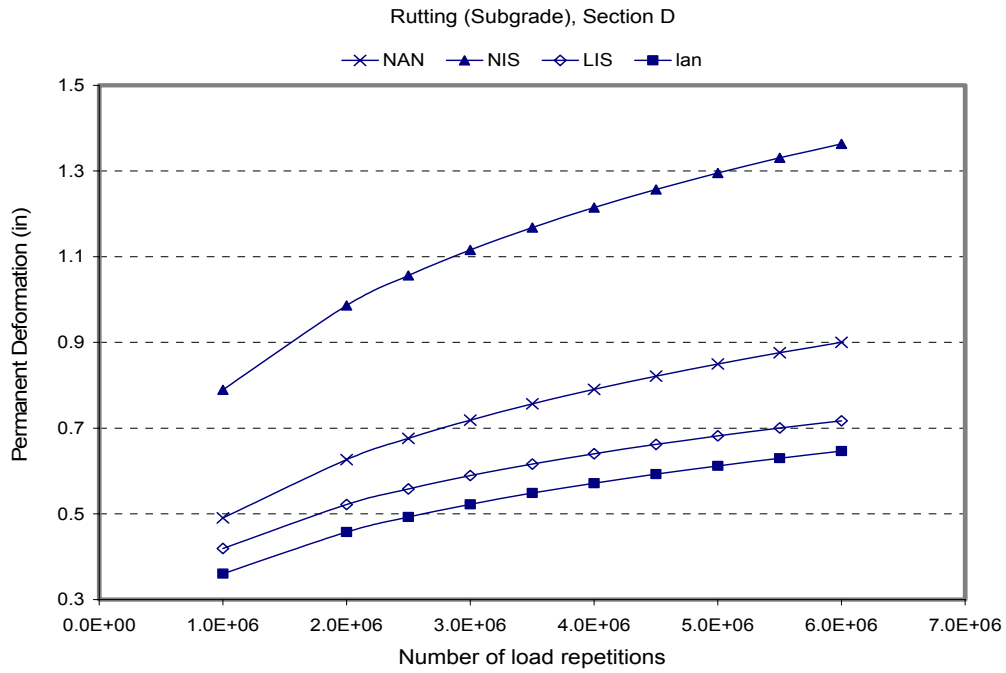
FIGURE A33 Permanent deformation in the subgrade of section D using the Tseng and Lytton model.

Rutting (Total), Section D
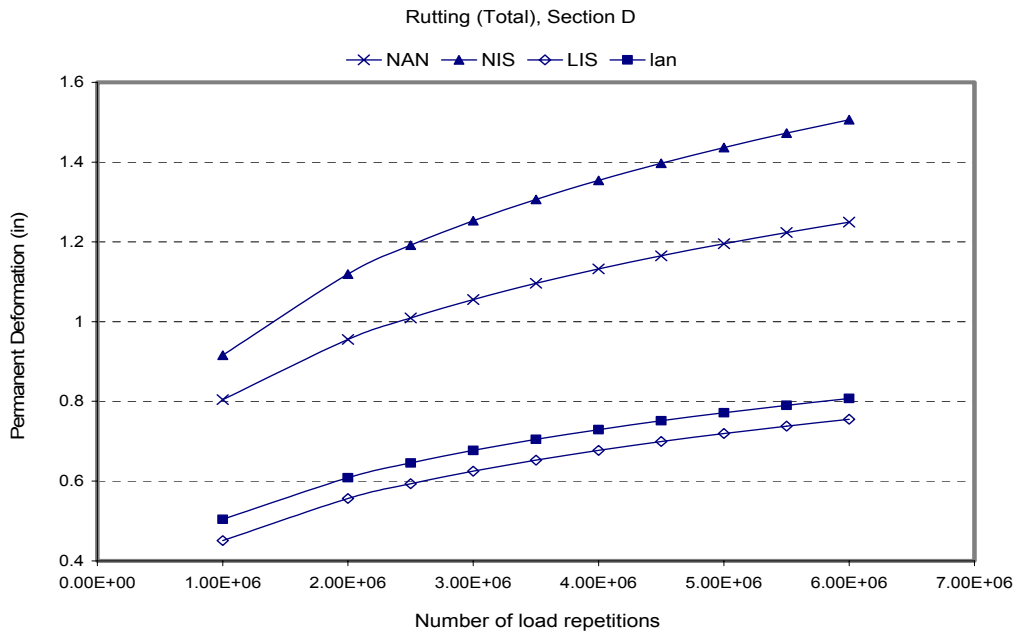
FIGURE A34 Total permanent deformation in section D using the Tseng and Lytton model.
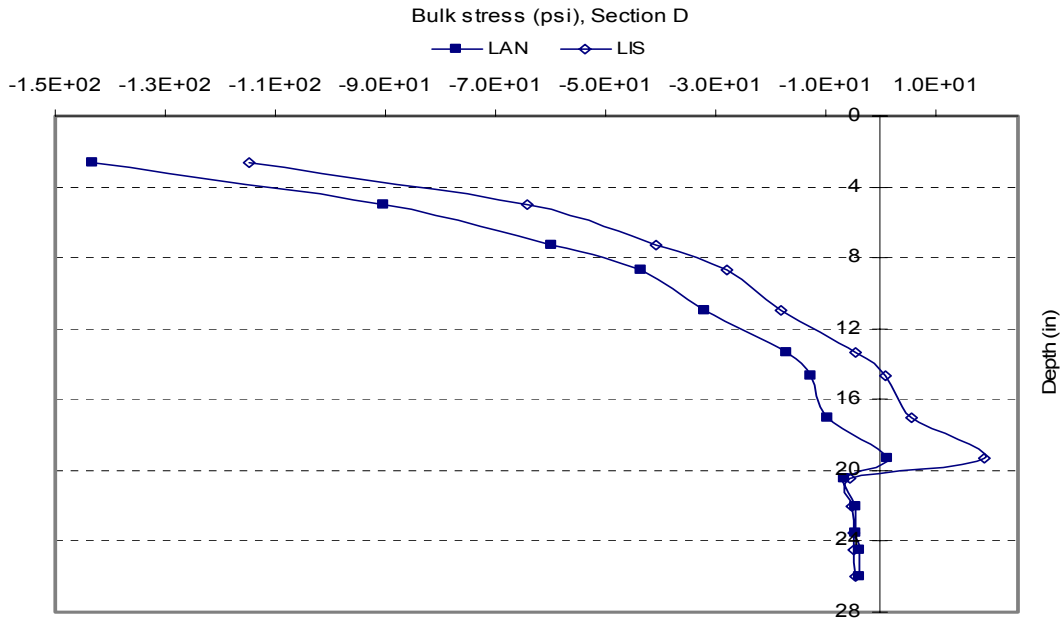
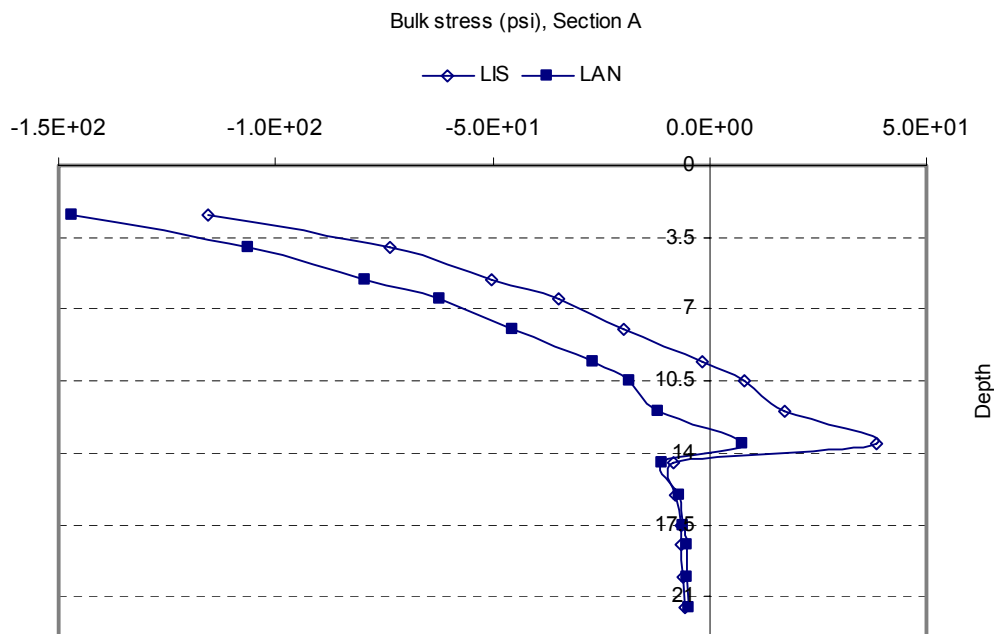FIGURE A35 The bulk stress profiles in the base layer of section D using linear isotropic and anisotropic properties.
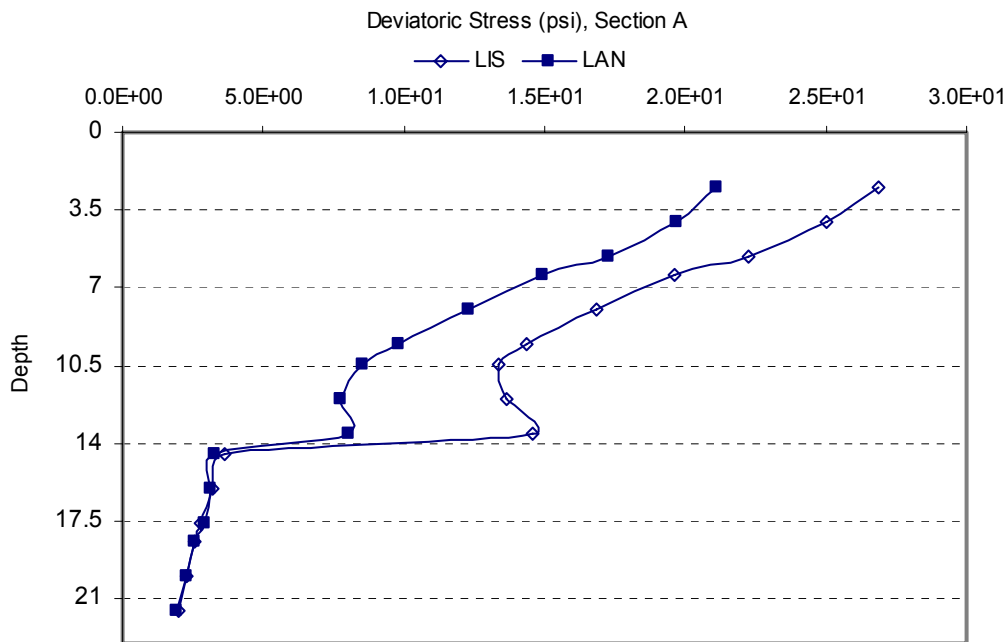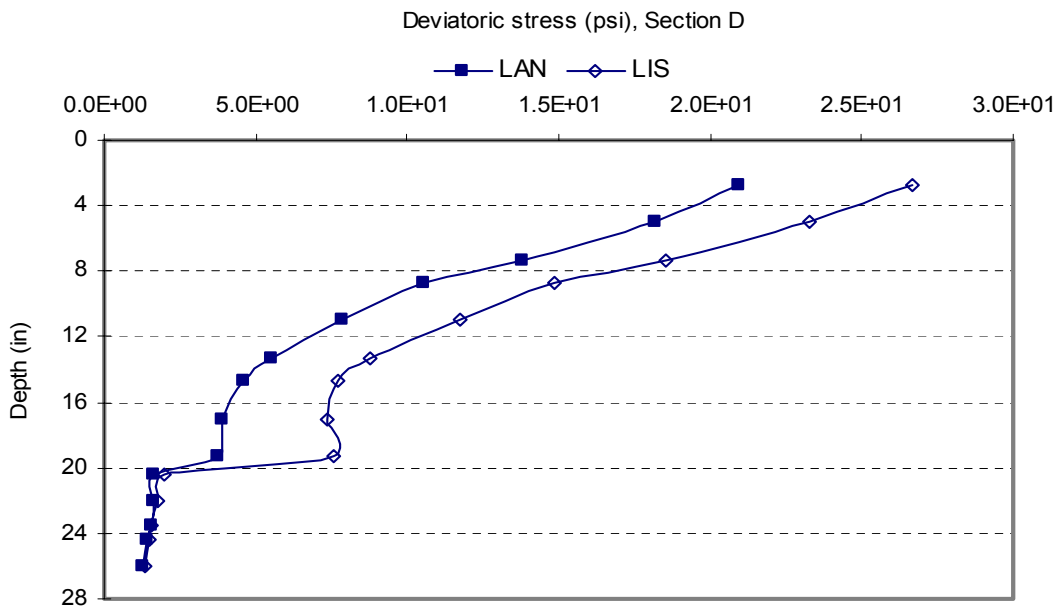

FIGURE A36 Deviatoric stress profiles in the base layer of section D using linear isotropic and anisotropic properties.
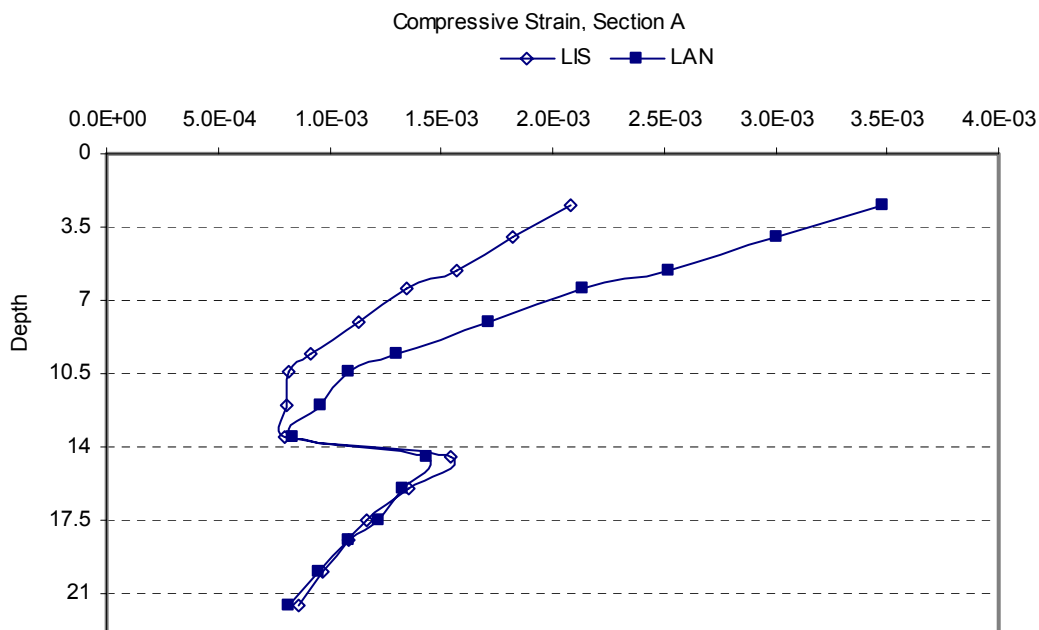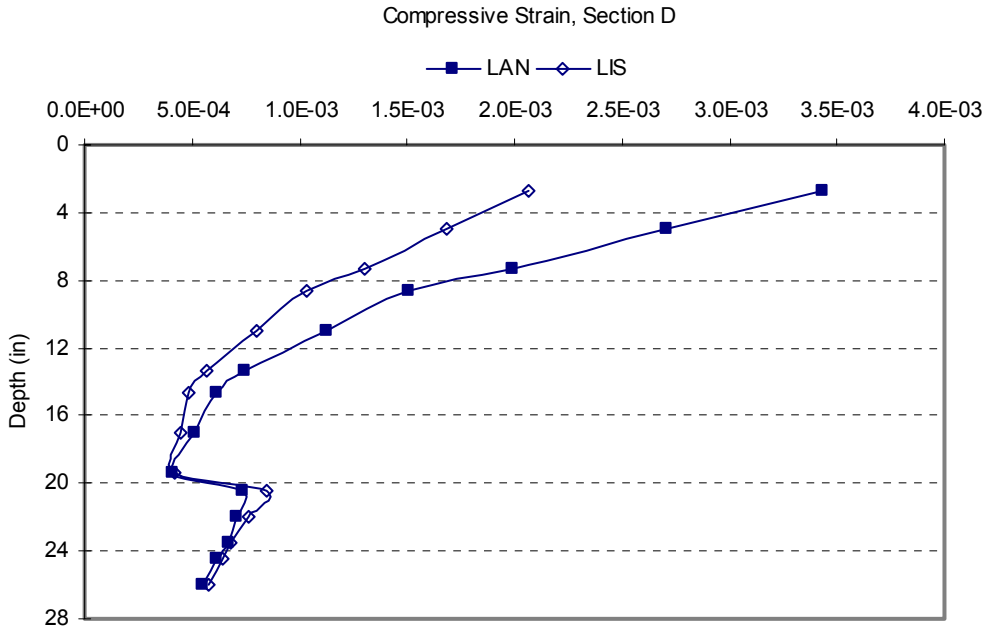
FIGURE A37 Compressive strain profiles in the base layer of section D using linear isotropic and anisotropic properties.
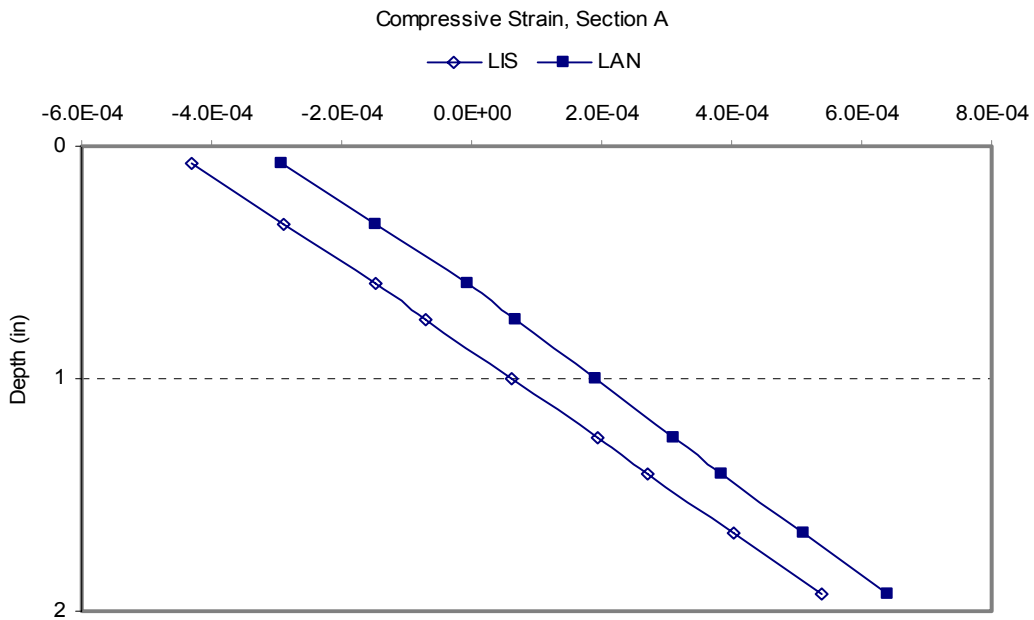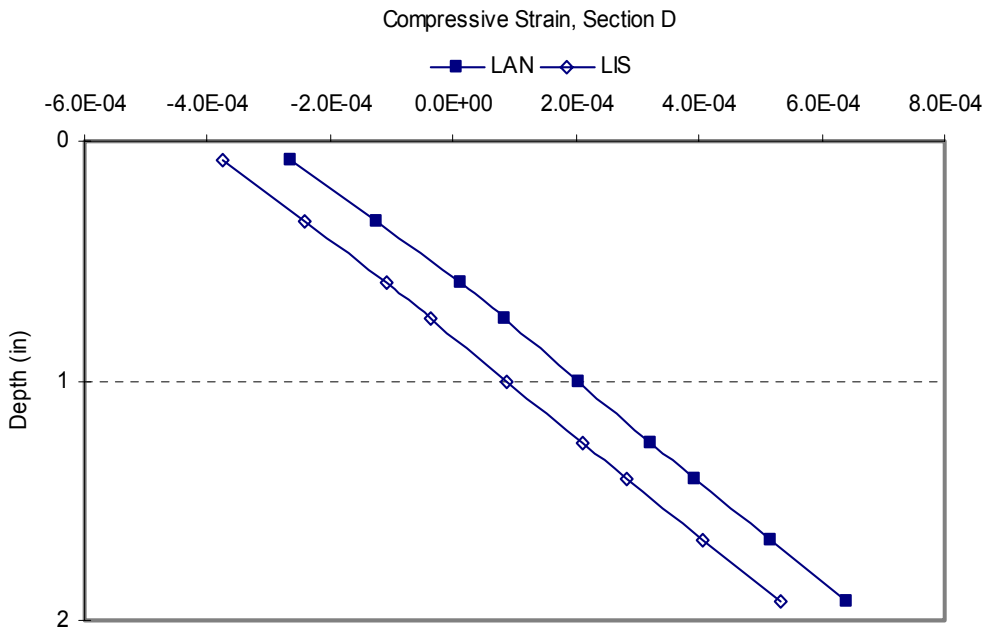

FIGURE A38 Compressive strain profiles in the asphalt layer of section D using linear isotropic and anisotropic properties.
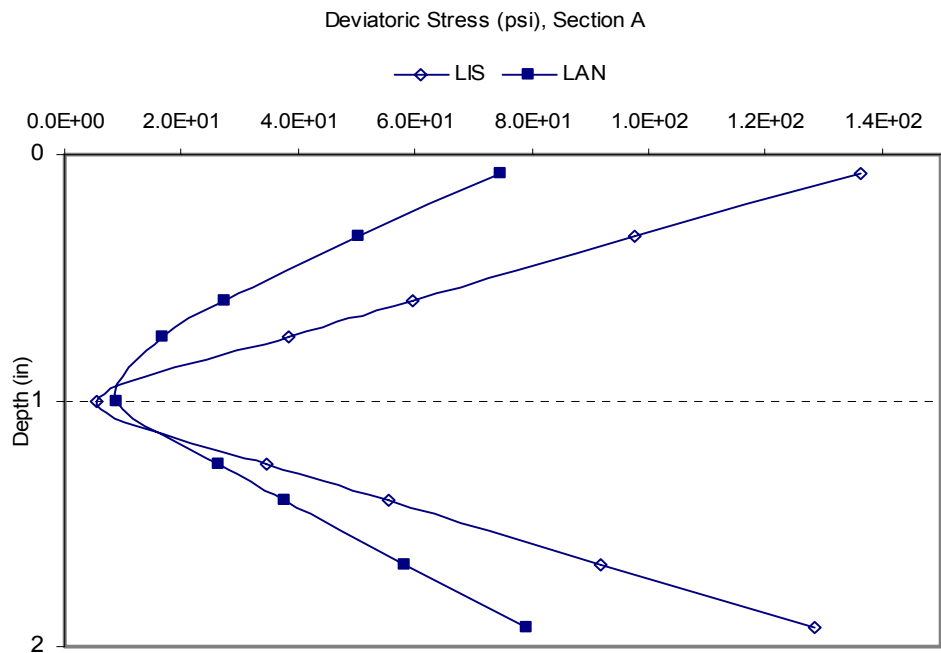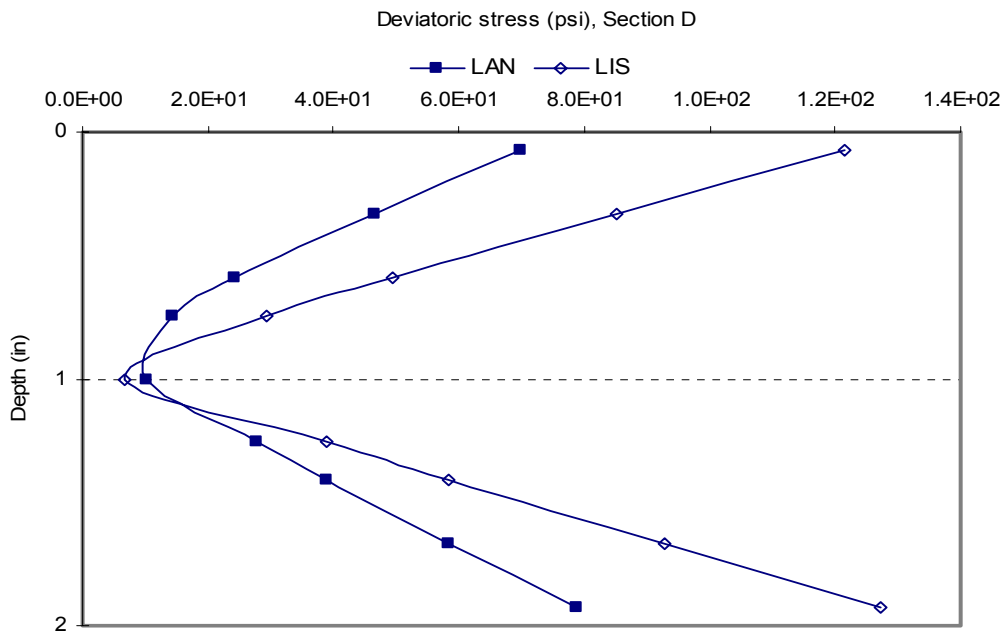
FIGURE A39 Deviatoric stress profiles in the asphalt layer of section D using linear isotropic and anisotropic properties.
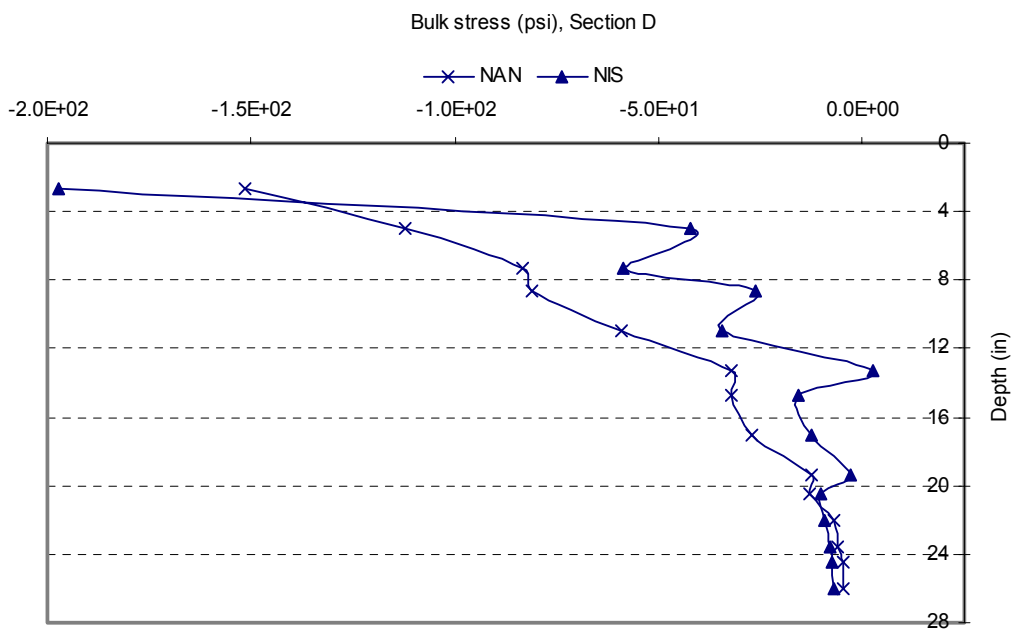
FIGURE A40 Bulk stress profiles in the base layer of section D using non-linear isotropic and anisotropic properties.
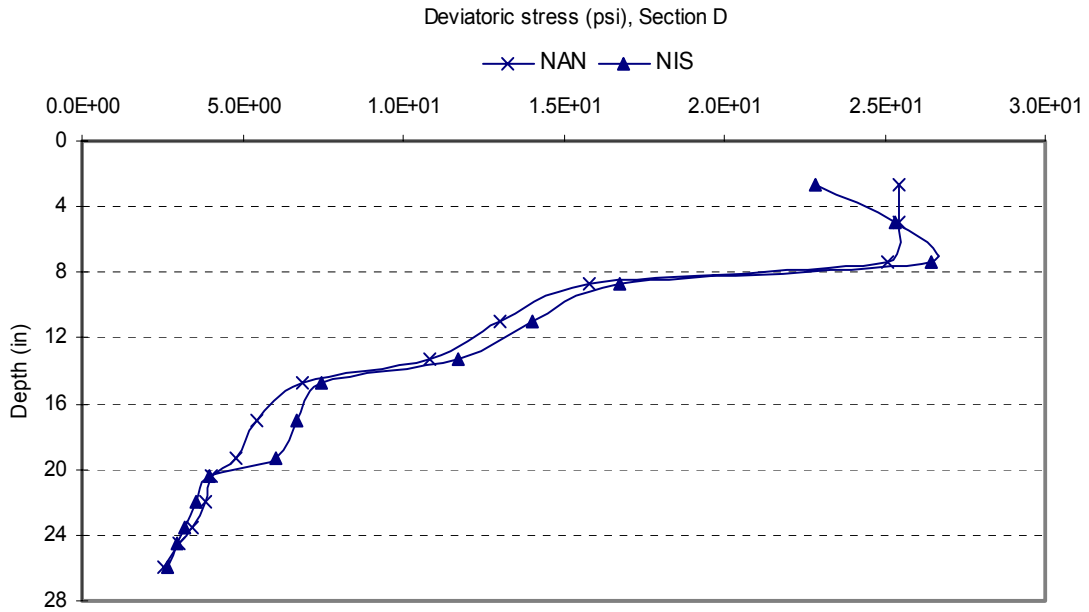
FIGURE A41 Deviatoric stress profiles in the base layer of section D using non-linear isotropic and anisotropic properties.
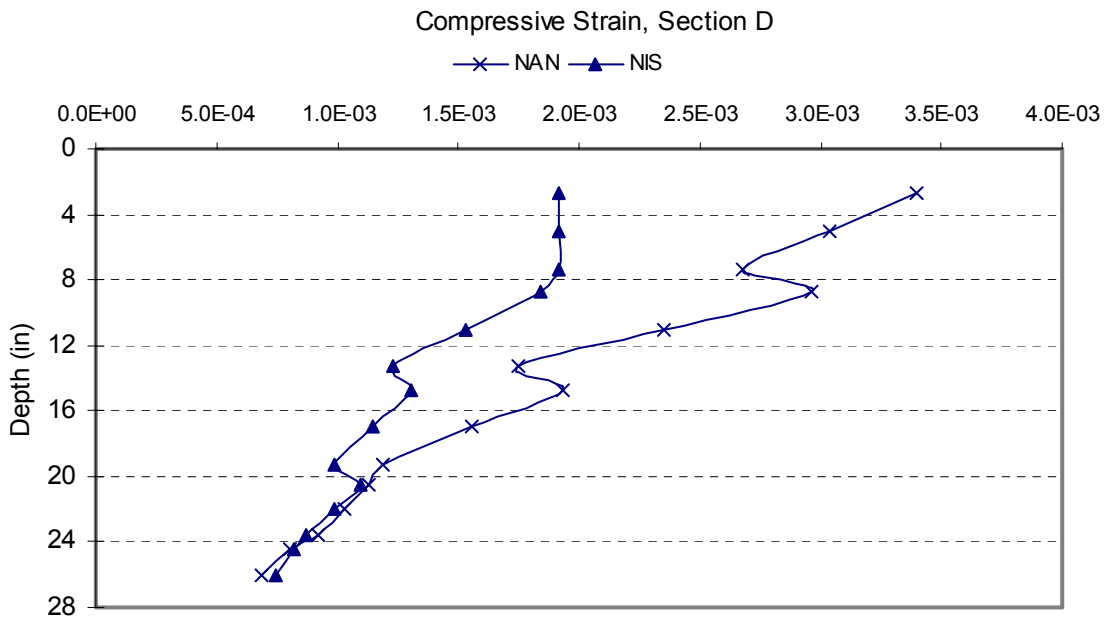
FIGURE A42 Compressive strain profiles in the base layer of section D using non-linear isotropic and anisotropic properties.

Compressive Strain, Section D

NAN NIS
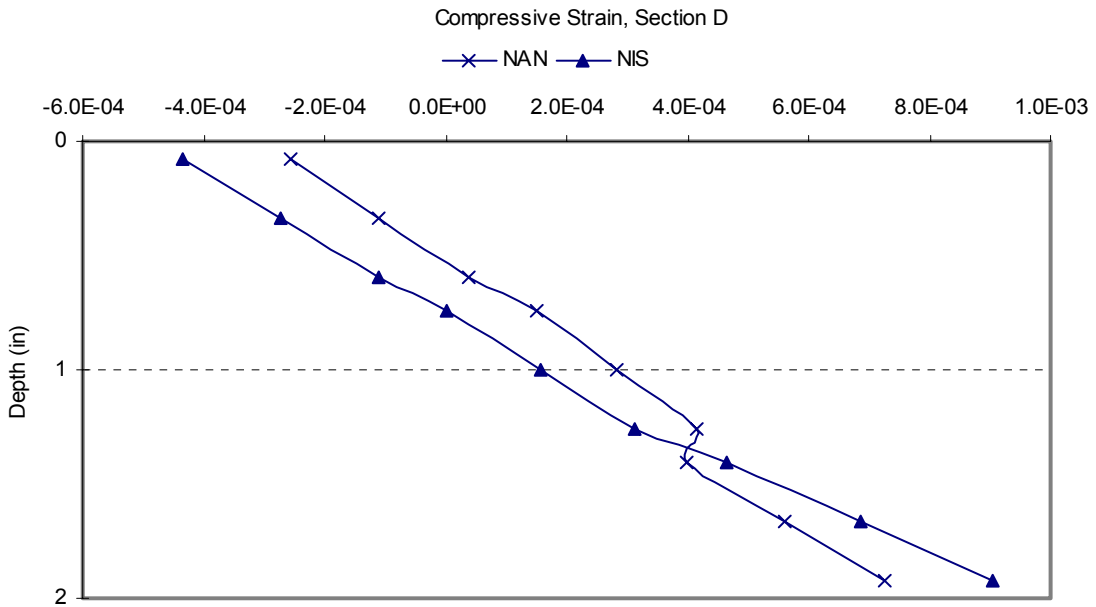
FIGURE A43 Compressive strain profiles in the asphalt layer of section D using non-linear isotropic and anisotropic properties.

Deviatoric stress (psi), Section D

NAN NIS
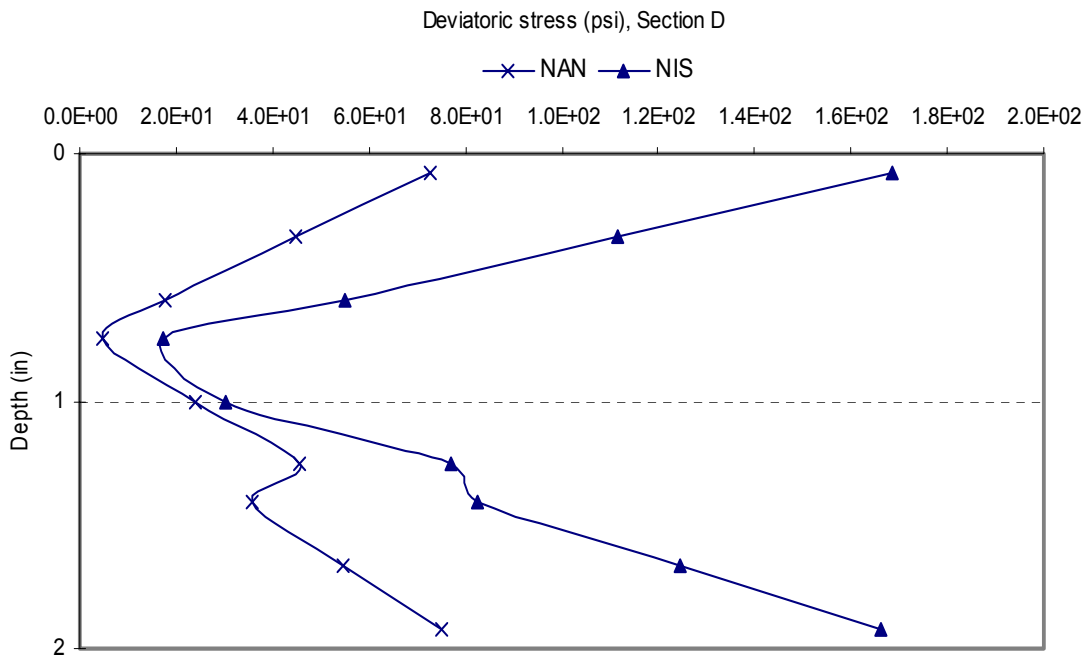
FIGURE A44 Deviatoric stress profiles in the asphalt layer of section D using non-linear isotropic and anisotropic properties.
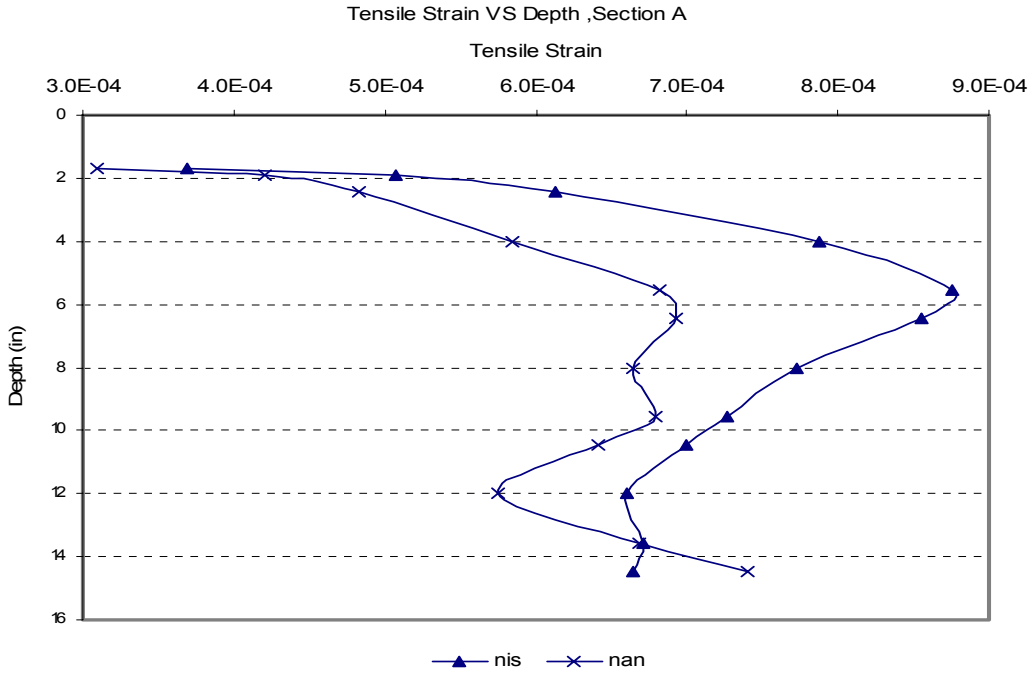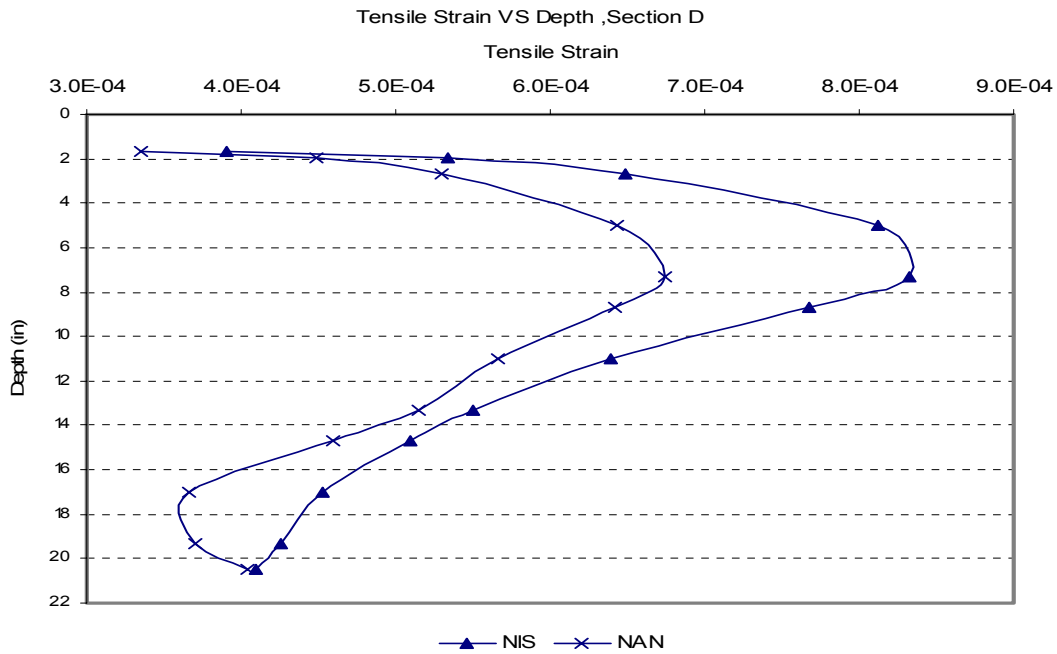
FIGURE A45 Tensile strain profiles in the asphalt and base layers of section D using nonlinear isotropic and anisotropic properties.
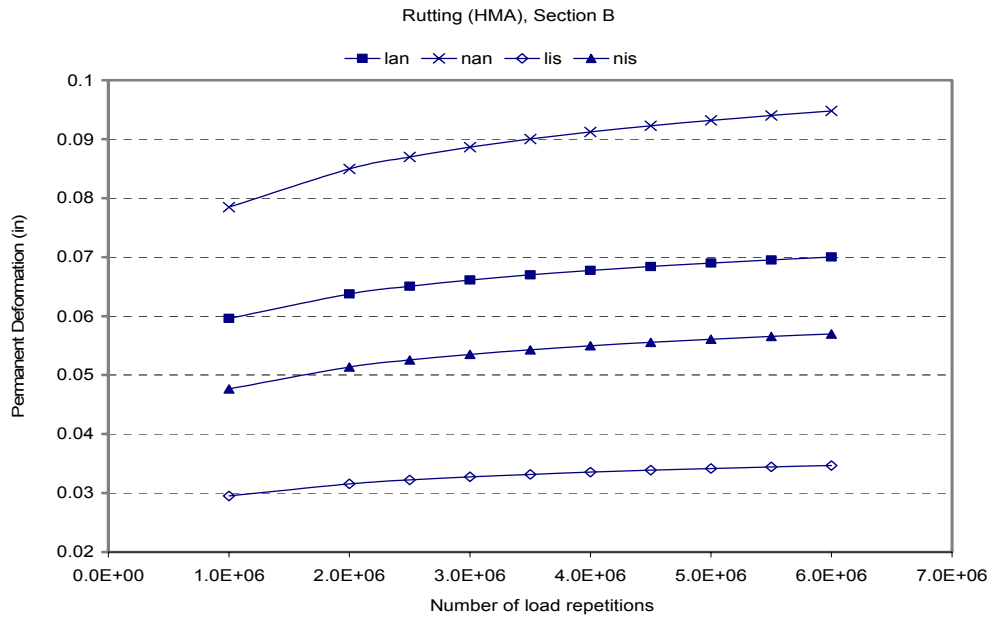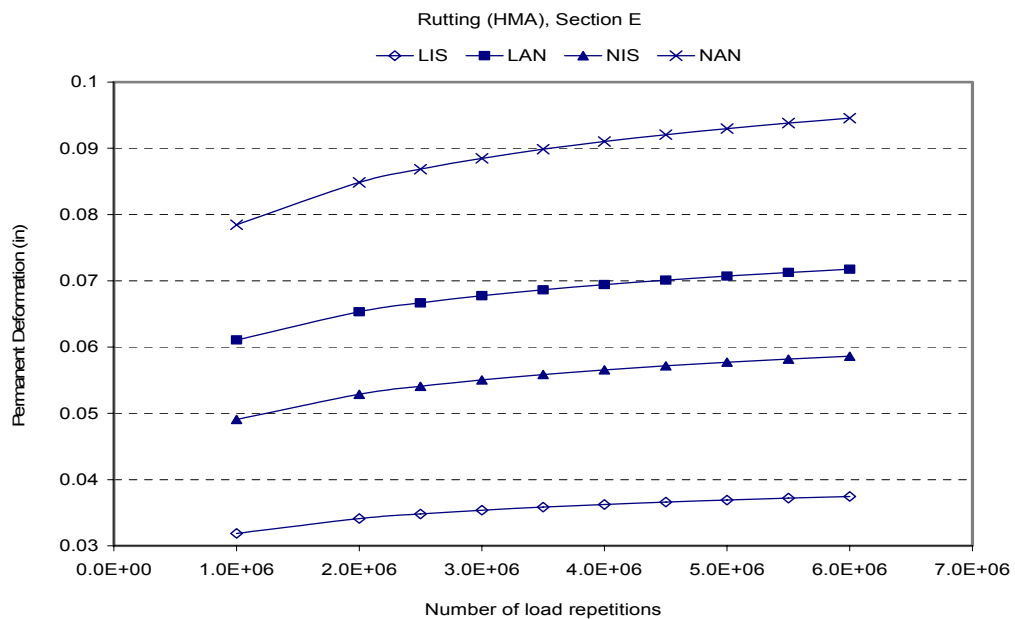

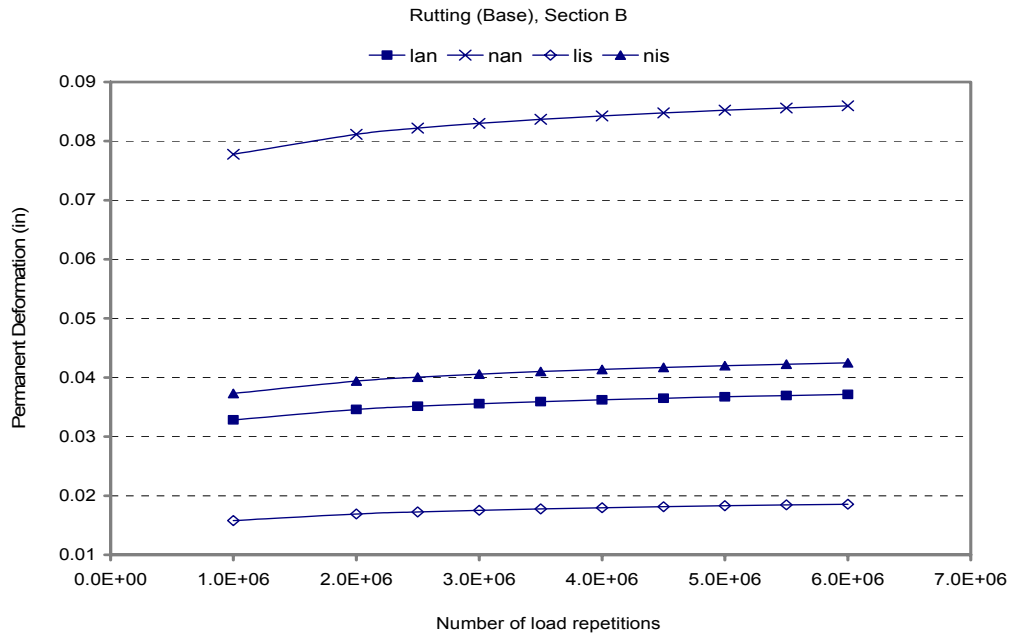FIGURE A46 HMA permanent deformation in section E using the Tseng and Lytton model.

Rutting (Base), Section E

◇ LIS ■ LAN ▲ NIS ✕ NAN
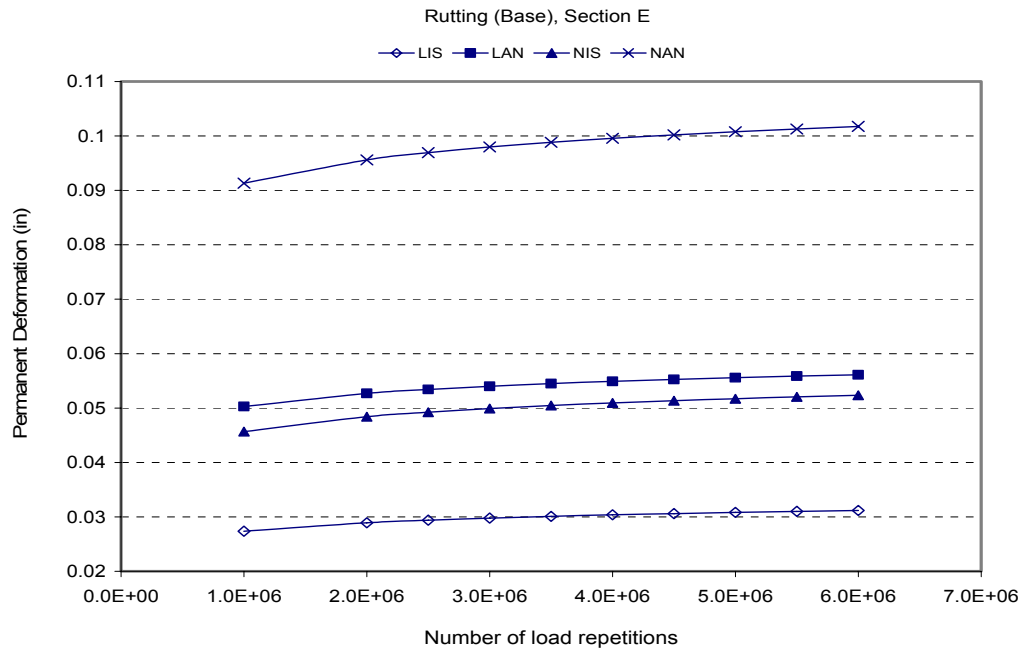
FIGURE A47 Permanent deformation in the base of section E using the Tseng and Lytton model.

Rutting (Subgrade), Section E

◇ LIS ■ LAN ▲ NIS ✕ NAN
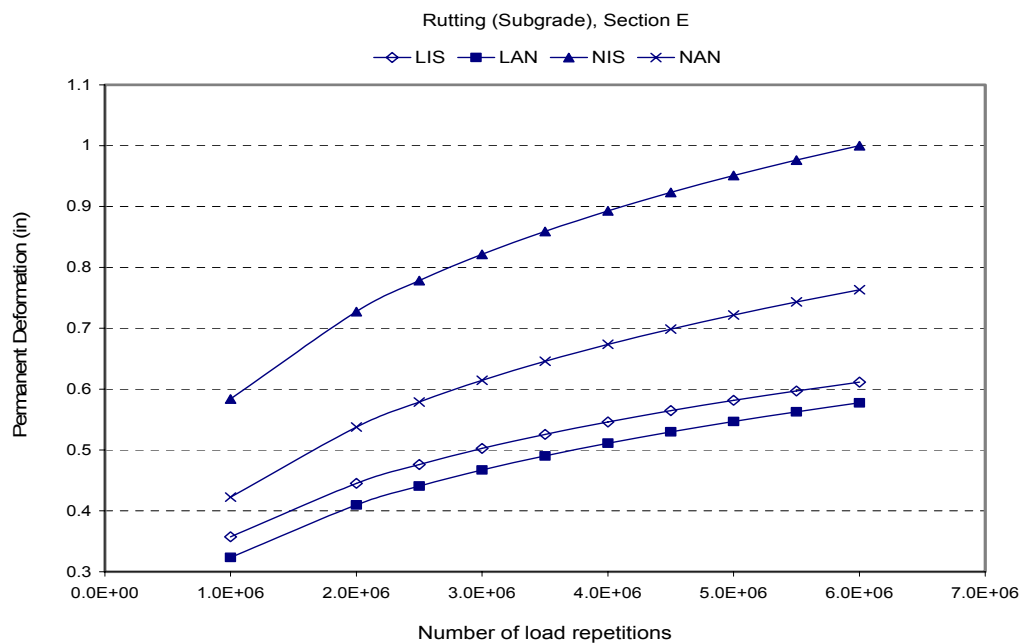
FIGURE A48 Permanent deformation in the subgrade of section E using the Tseng and Lytton model.
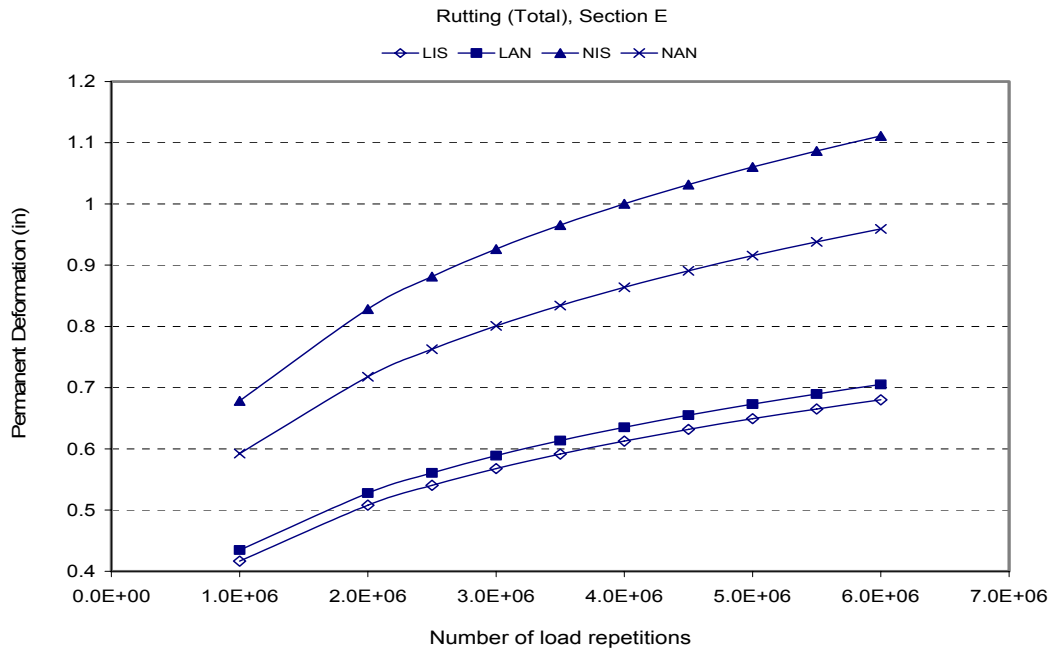
FIGURE A49 Total permanent deformation in section E using the Tseng and Lytton model.
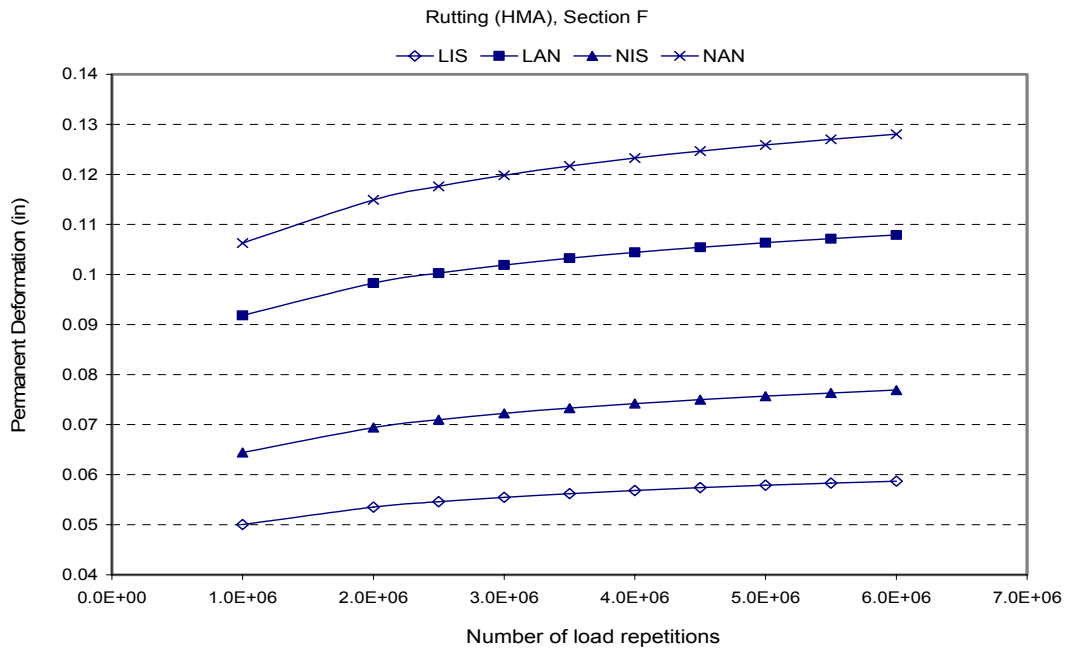
FIGURE A50 HMA permanent deformation in section F using the Tseng and Lytton model.
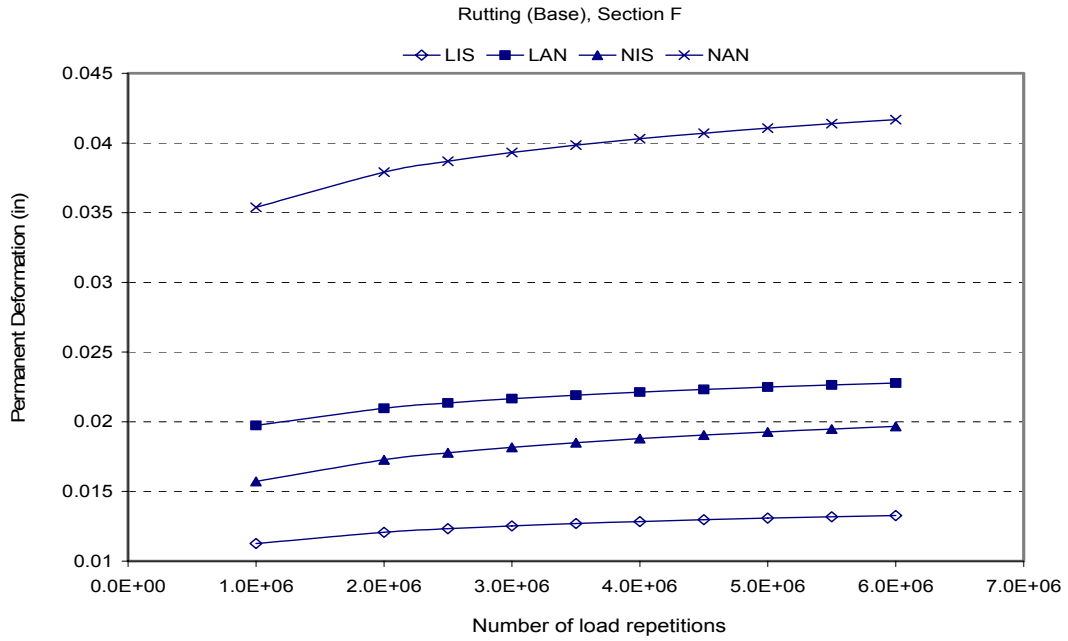
FIGURE A51 Permanent deformation in the base of section F using the Tseng and Lytton model.
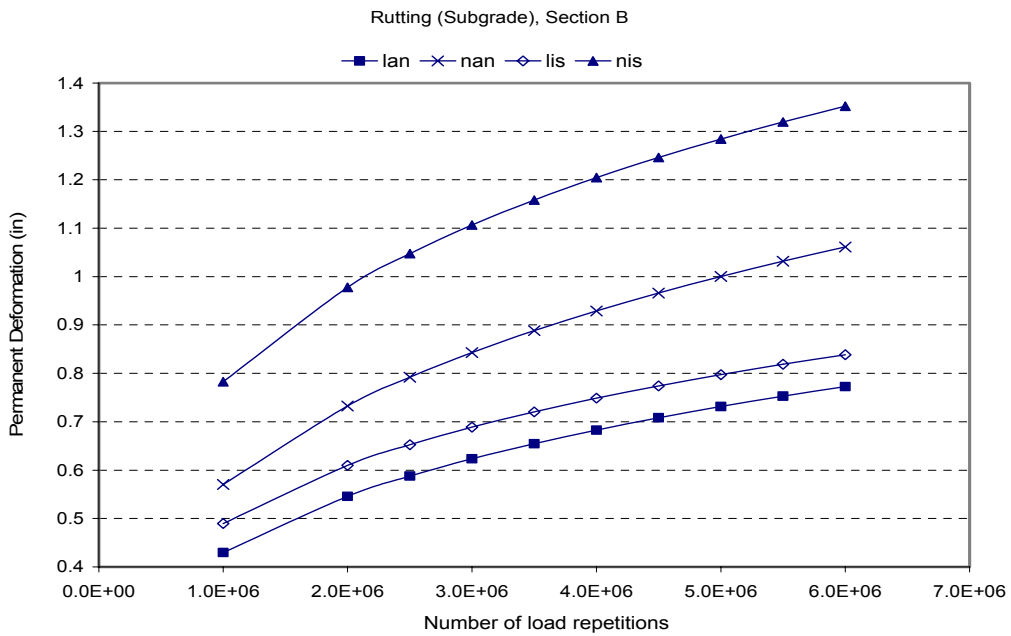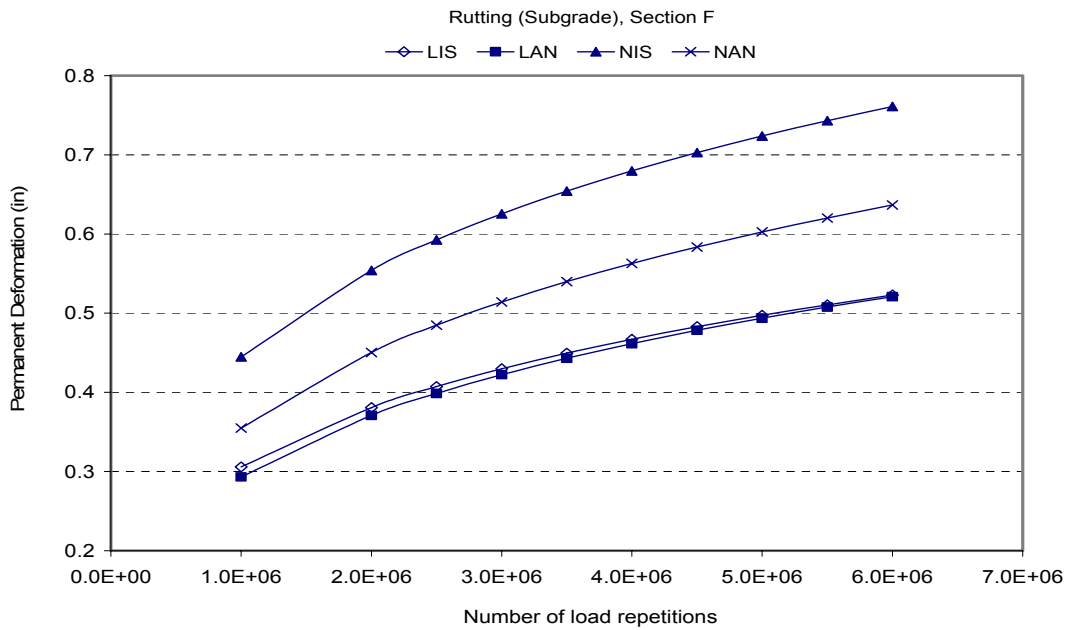

FIGURE A52 Permanent deformation in the subgrade of section F using the Tseng and Lytton model.
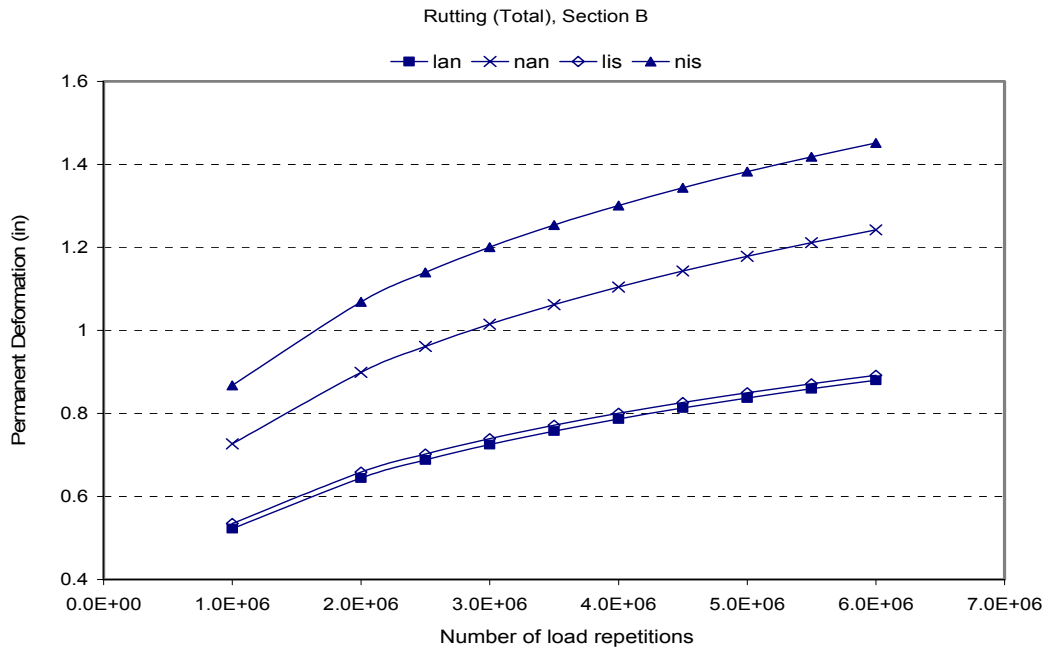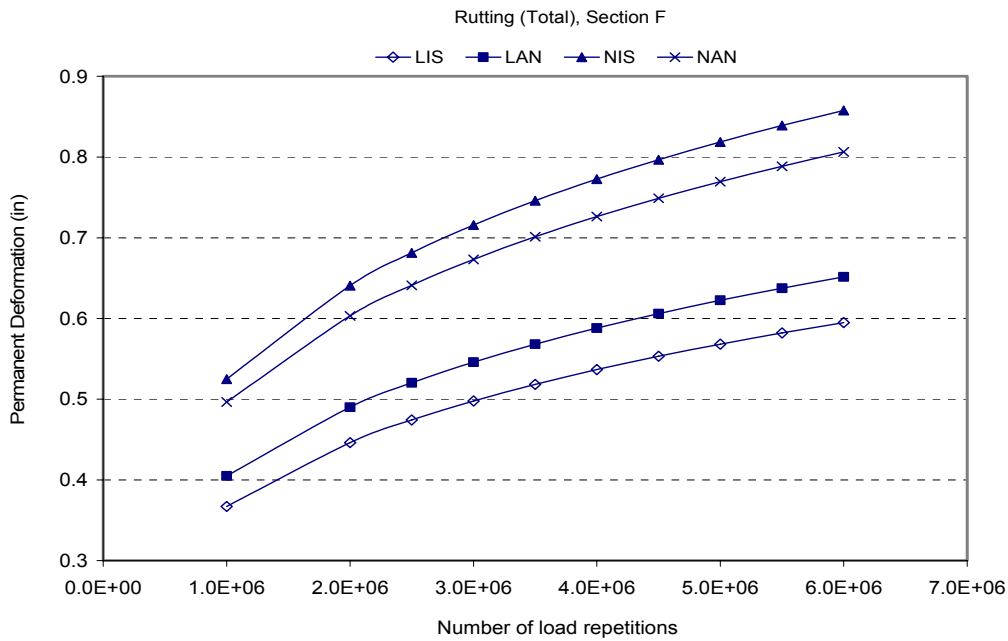
FIGURE A53 Total permanent deformation in section F using the Tseng and Lytton model.
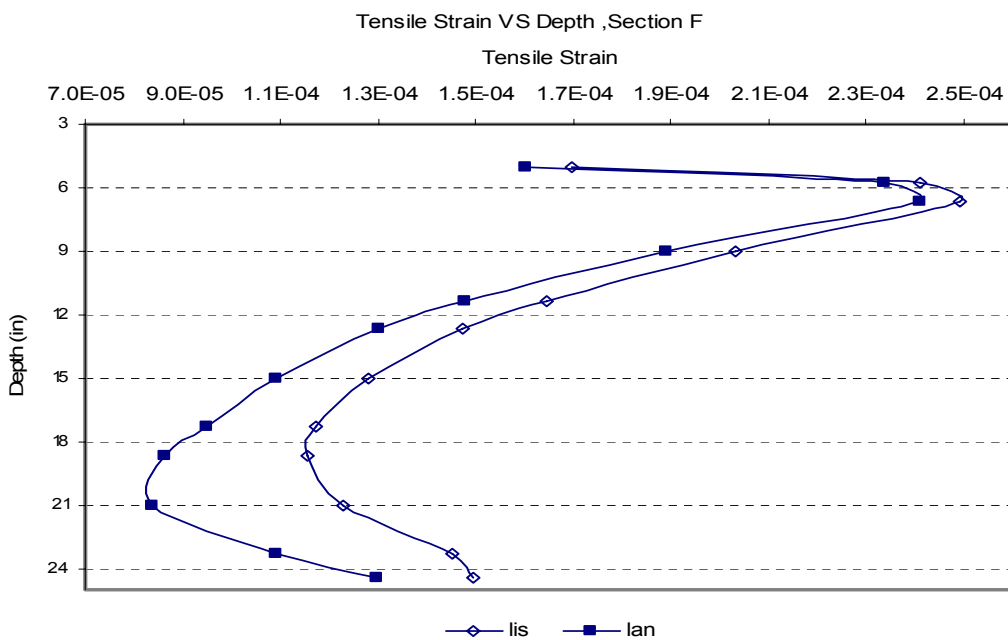
FIGURE A54 Tensile strain profiles in the asphalt and base layers of section D using linear isotropic and anisotropic properties.

APPENDIX B
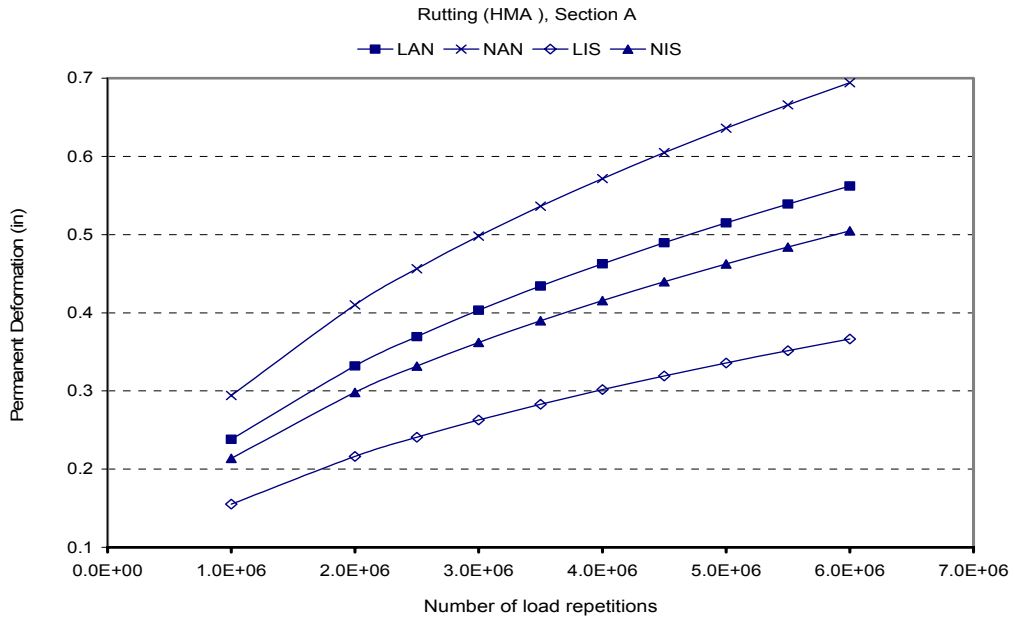
FIGURE B1 HMA permanent deformation in section A using the AASHTO 2002 model.
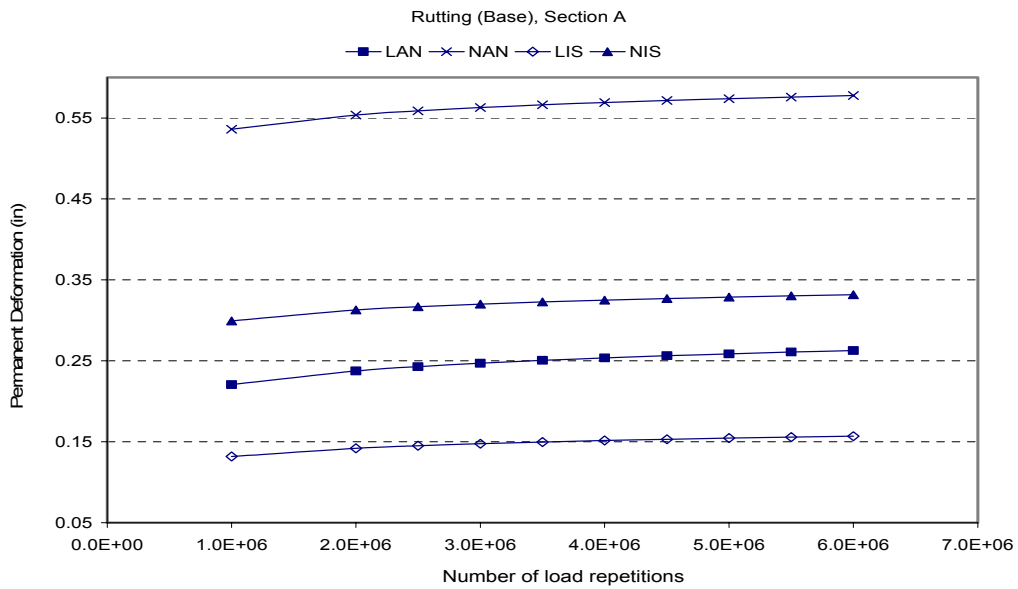
FIGURE B2 Base permanent deformation in section A using the AASHTO 2002 model.
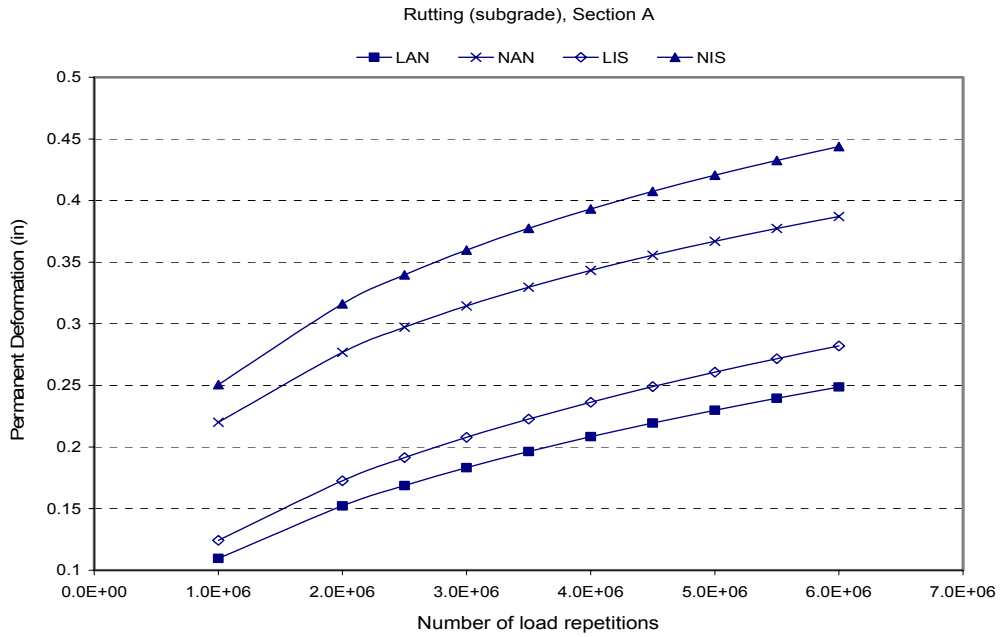
FIGURE B3 Subgrade permanent deformation in section A using the AASHTO 2002 model.
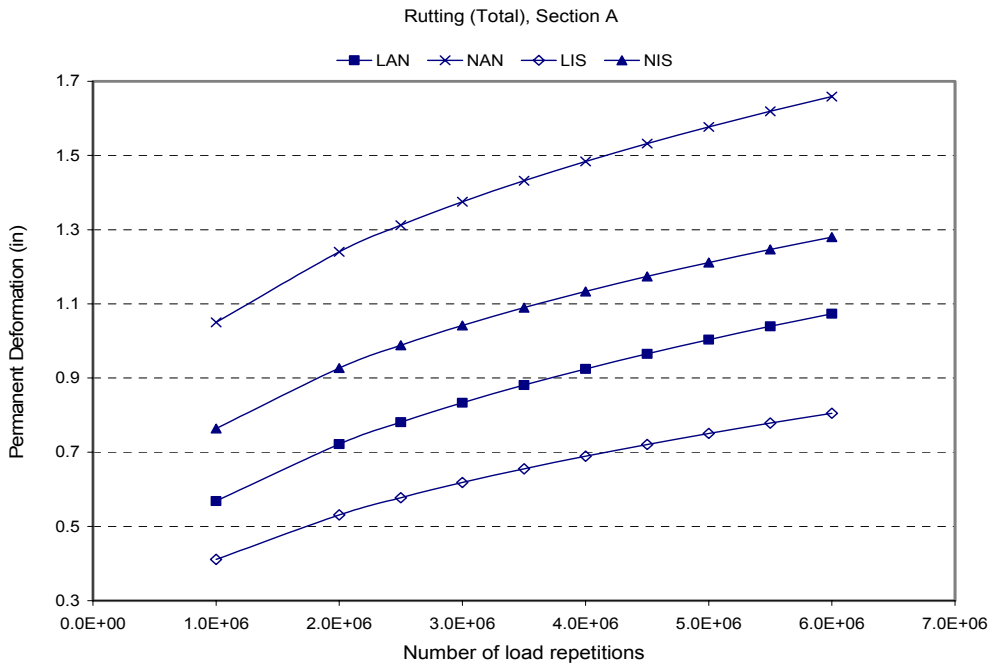
FIGURE B4 Total permanent deformation in section A using the AASHTO 2002 model.

Rutting (HMA), Section B

■ lan ✕ nan ◇ lis ▲ nis
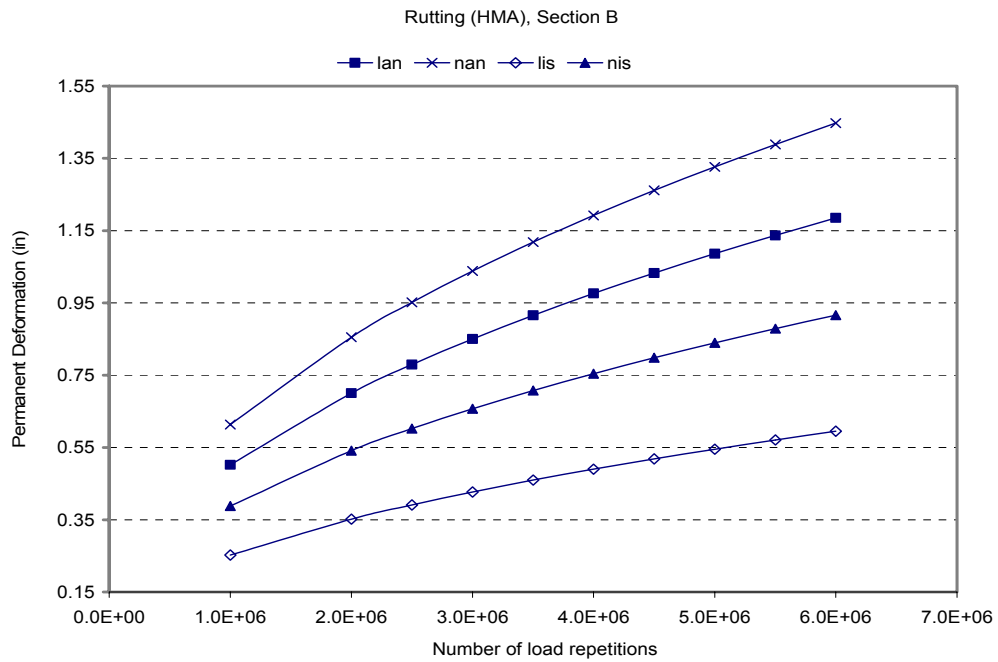
FIGURE B5 HMA permanent deformation in section B using the AASHTO 2002 model.

Rutting (Base), Section B

■ lan ✕ nan ◇ lis ▲ nis
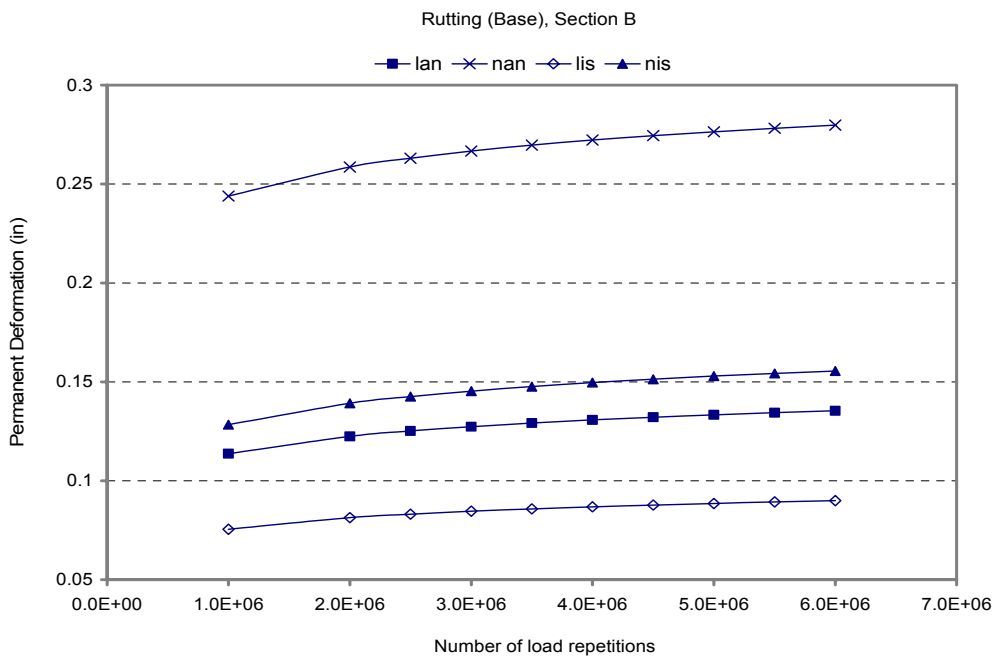
FIGURE B6 Base permanent deformation in section B using the AASHTO 2002 model.

Rutting (Subgrade), Section B
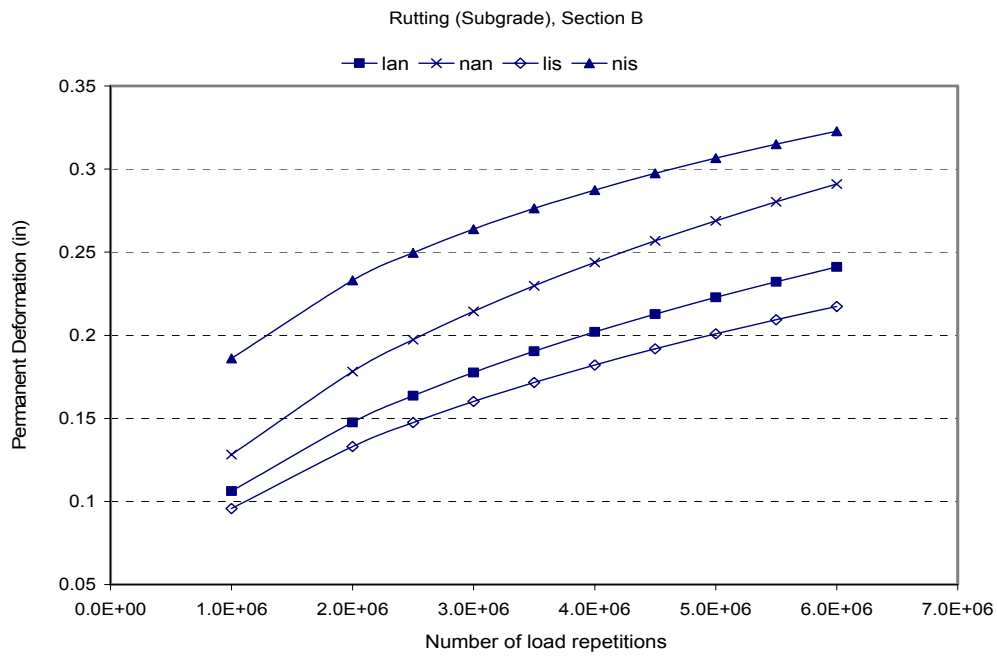
FIGURE B7 Subgrade permanent deformation in section B using the AASHTO 2002 model.

Rutting (Total), Section B
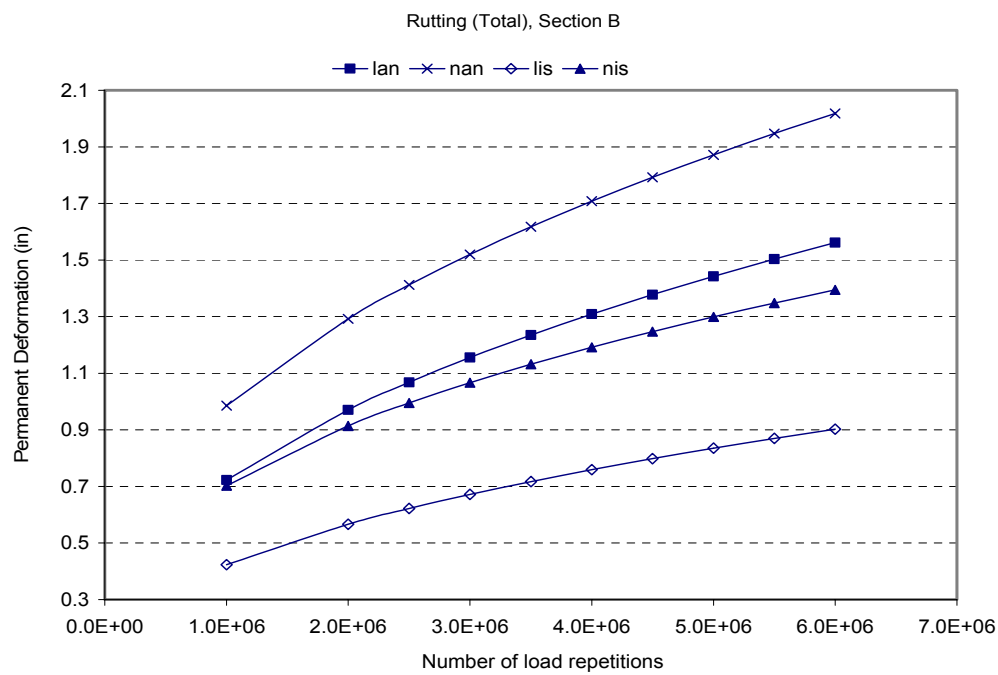
FIGURE B8 Total permanent deformation in section B using the AASHTO 2002 model.
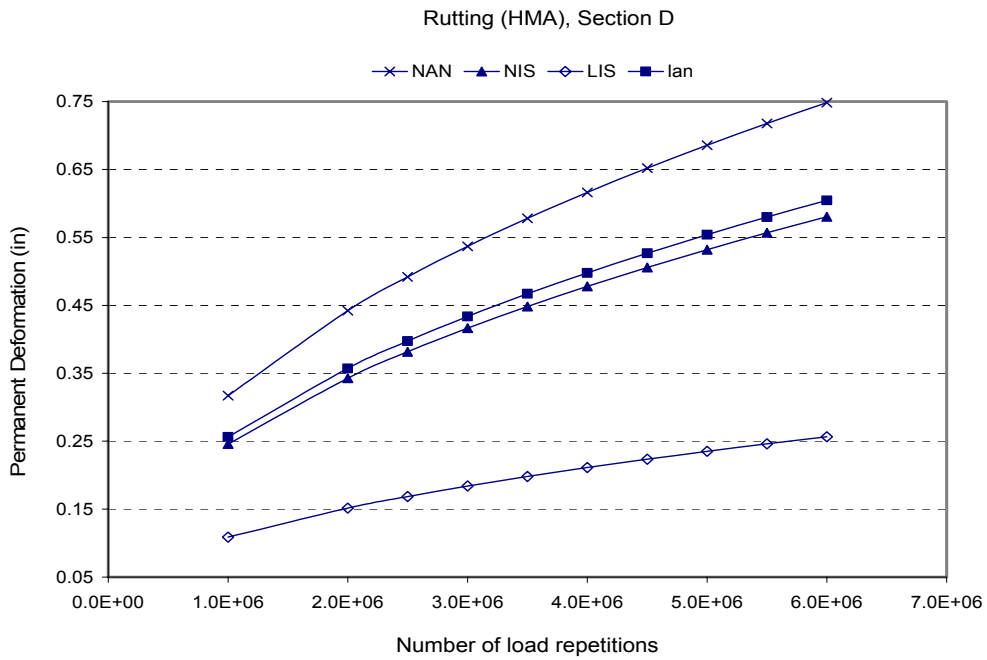
FIGURE B9 HMA permanent deformation in section D using the AASHTO 2002 model.
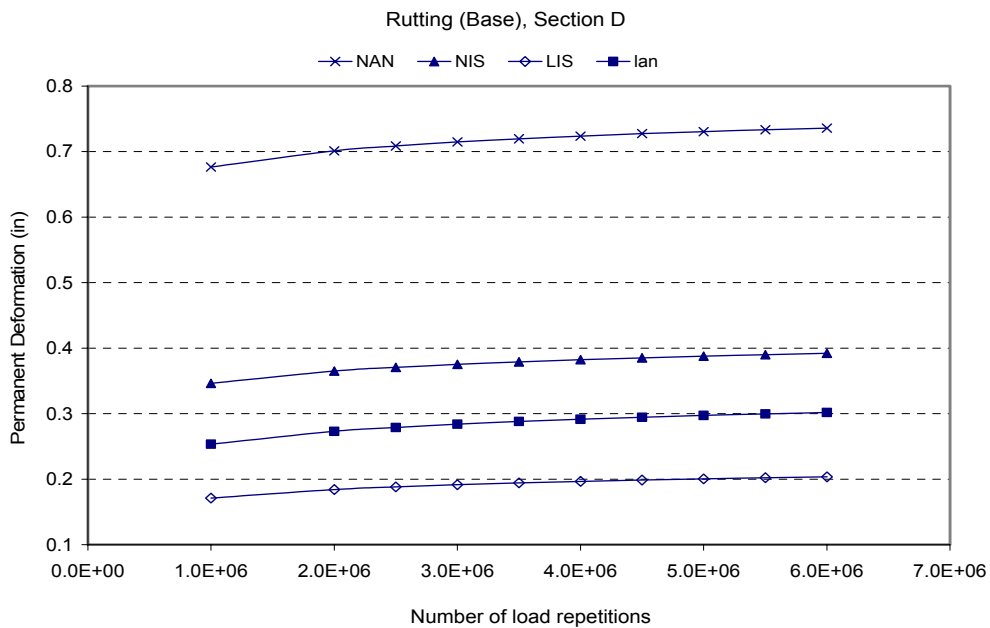
FIGURE B10 Base permanent deformation in section D using the AASHTO 2002 model.
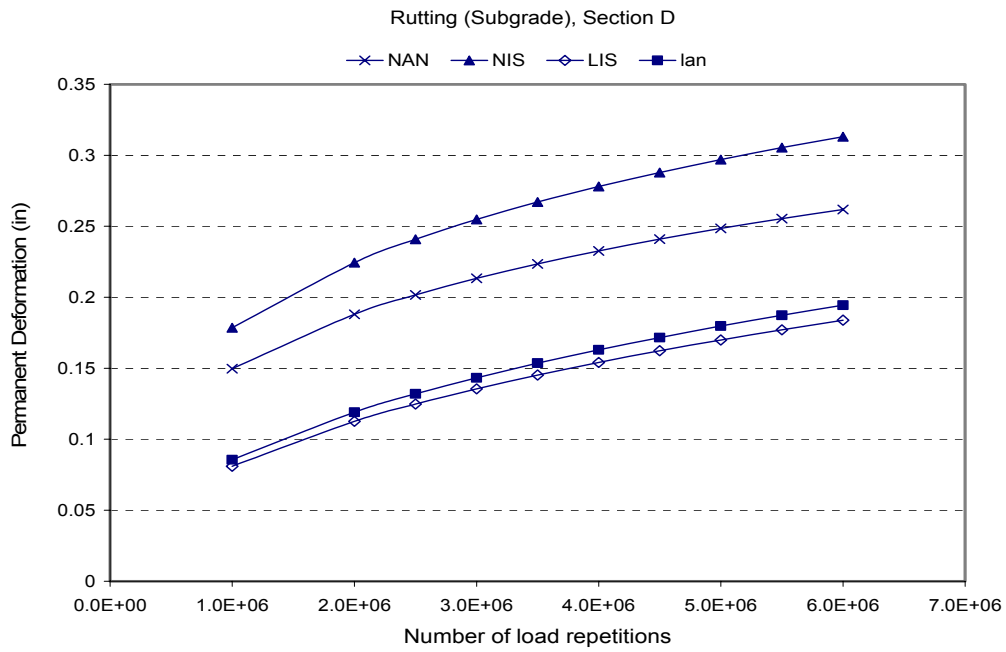
FIGURE B11 Subgrade permanent deformation in section D using the AASHTO 2002 model.
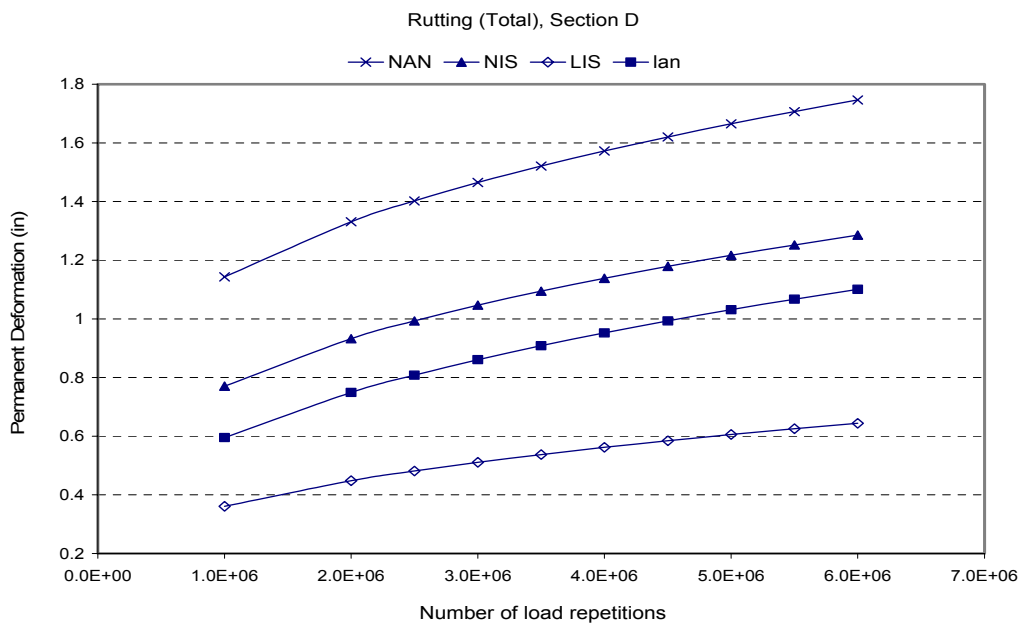
FIGURE B12 Total permanent deformation in section D using the AASHTO 2002 model.
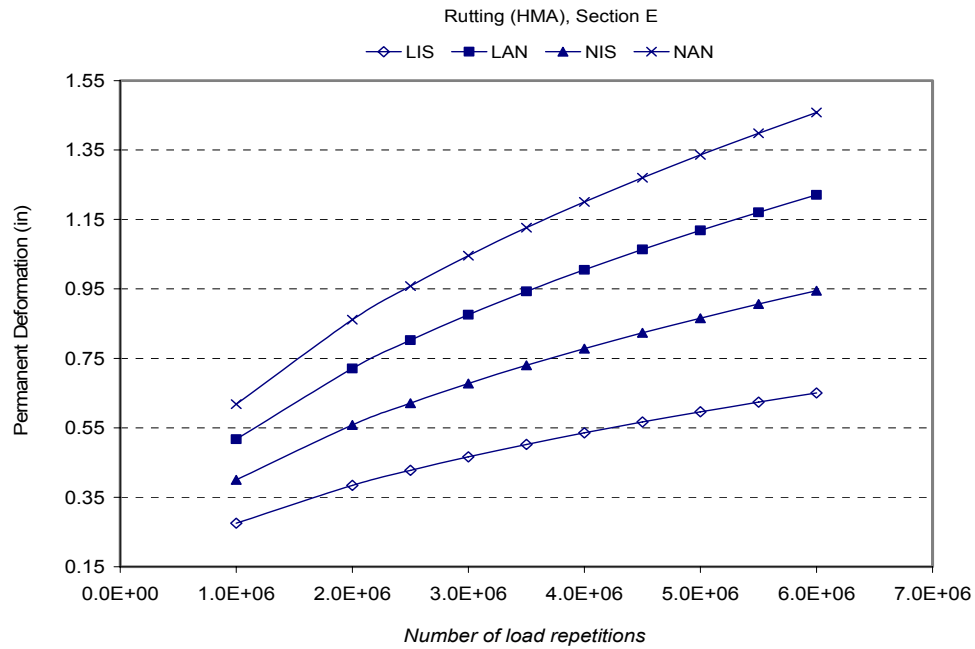
FIGURE B13 HMA permanent deformation in section E using the AASHTO 2002 model.
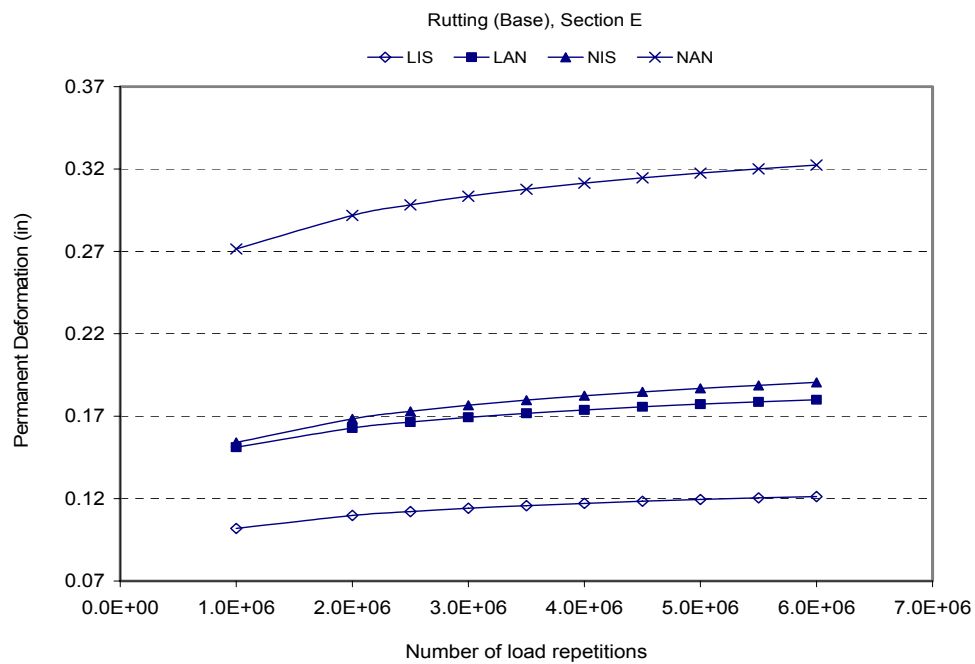
FIGURE B14 Base permanent deformation in section E using the AASHTO 2002 model.
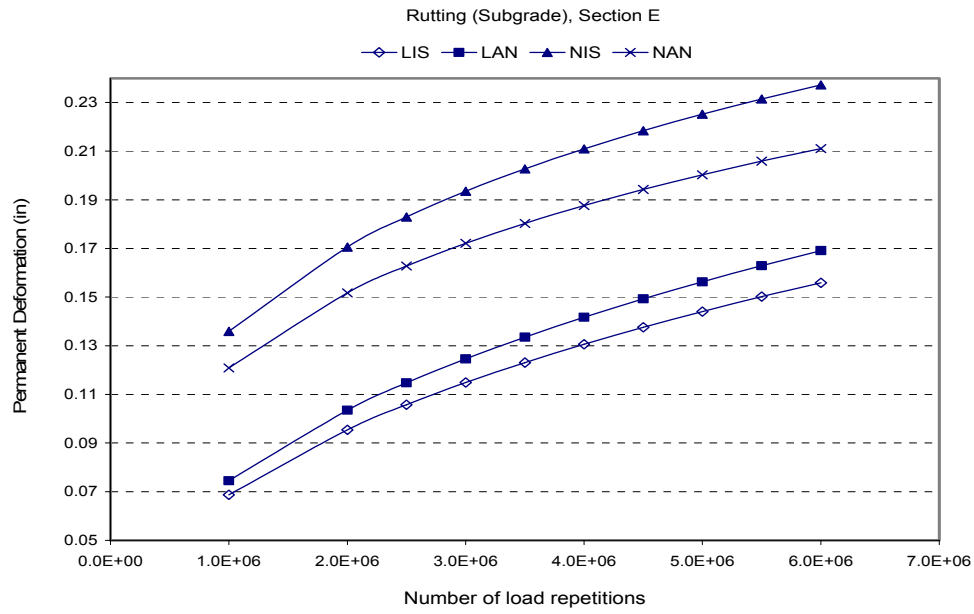
FIGURE B15 Subgrade permanent deformation in section E using the AASHTO 2002 model.
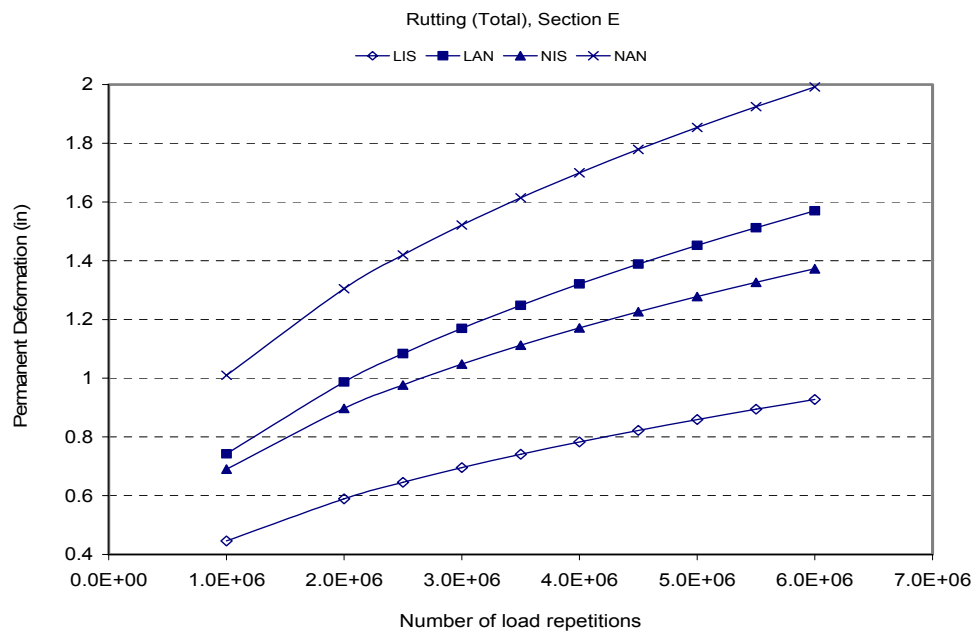
FIGURE B16 Total permanent deformation in section E using the AASHTO 2002 model.
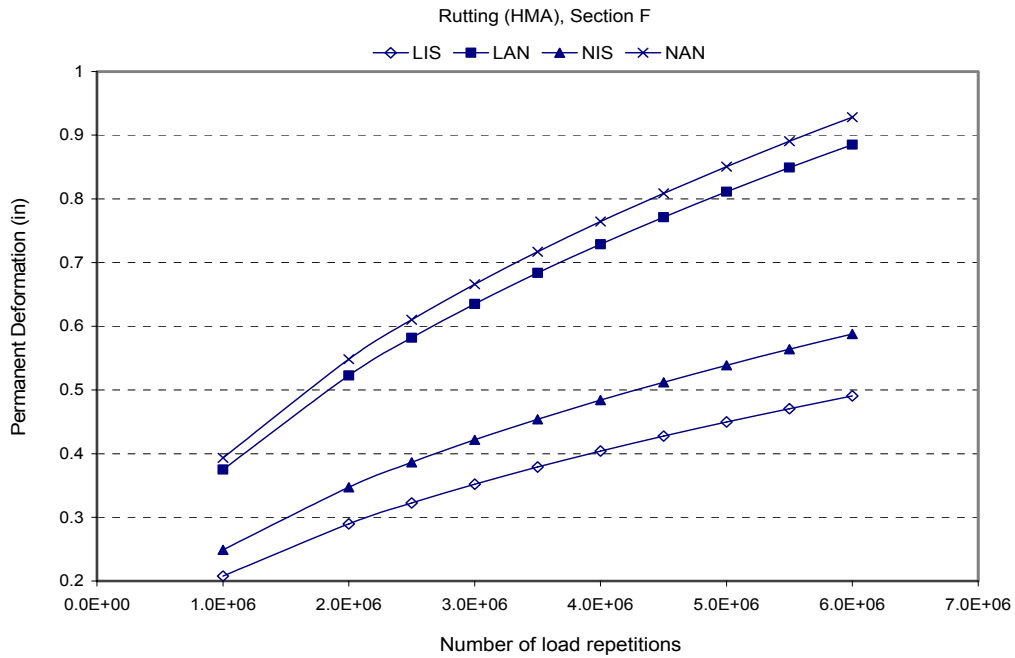
FIGURE B17 HMA permanent deformation in section F using the AASHTO 2002 model.
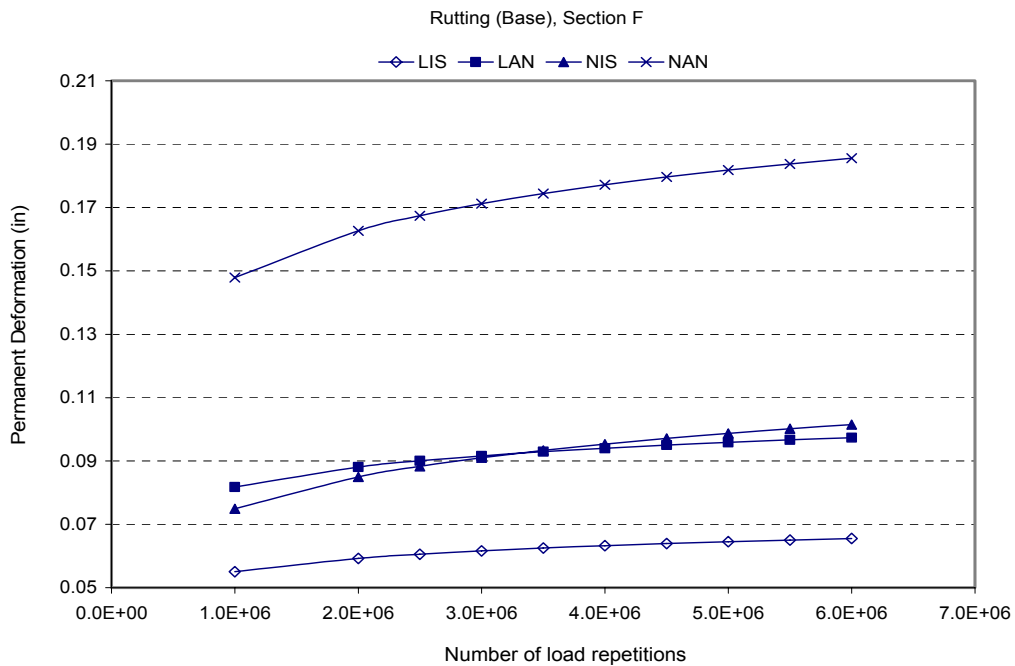
FIGURE B18 Base permanent deformation in section F using the AASHTO 2002 model.
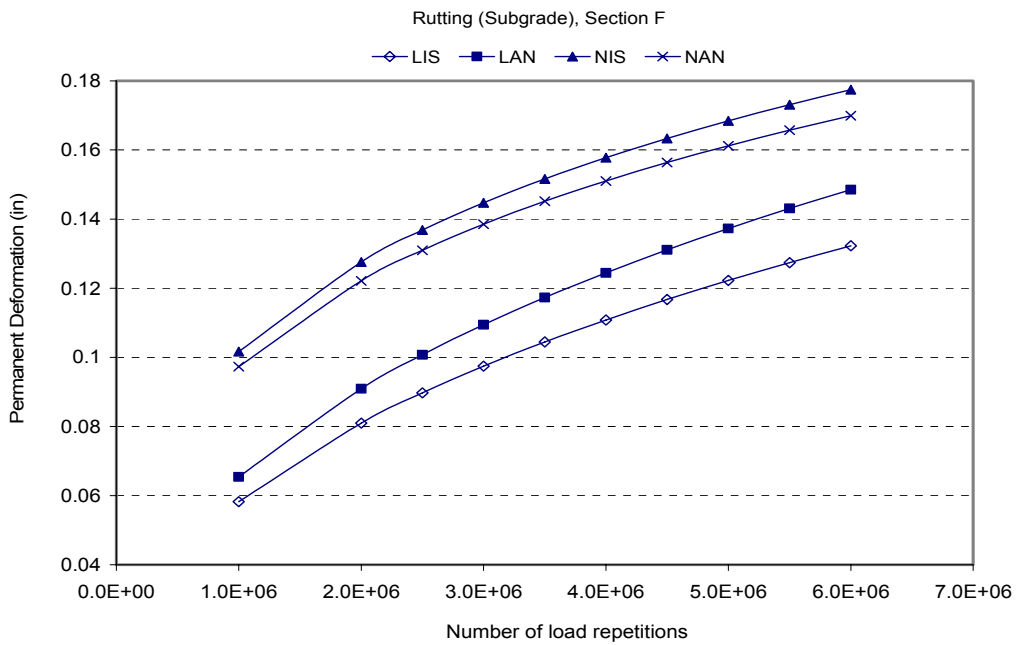
FIGURE B19 Subgrade permanent deformation in section F using the AASHTO 2002 model.
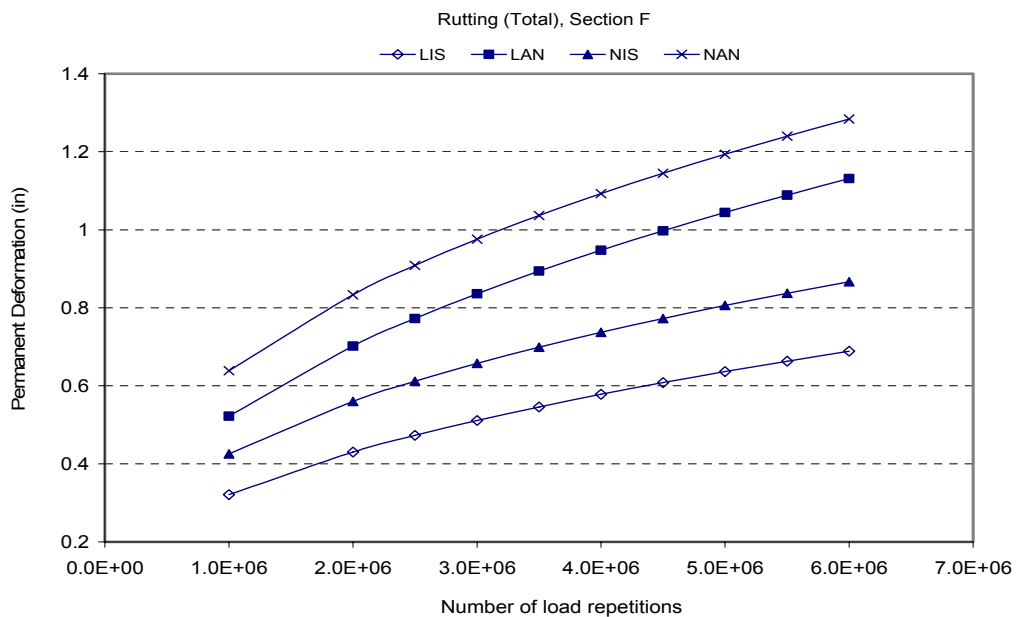
FIGURE B20 Total permanent deformation in section F using the AASHTO 2002 model.

APPENDIX C

TABLE C1 The Analysis Results of Asphalt Pavement with Binder Grade of PG58-28, Base Layer with Modulus of 42.0 ksi in Houston Under AADT of 3000

Thickness (in)		Material	Rutting (in)				Longitudinal Cracking(ft/mi)		Alligator Cracking (%)	IRI(in/mi)
HMA	Base	Subgrade	HMA	Base	Subgrade	Total	Surface	Depth=0.5	Bottom up cracking	
4	10	A-2-5 (28 ksi)	0.4896	0.0541	0.3126	0.8563	1170	514	87	195.5
8	10	A-2-5	0.3812	0.0287	0.2411	0.651	8420	7410	19.4	86.4
4	12	A-2-5	0.4112	0.0526	0.3113	0.7751	1160	519	86.7	189.2
8	12	A-2-5	0.3138	0.0309	0.3815	0.7262	8280	7230	18.1	82.5
4	15	A-2-5	0.4875	0.0679	0.2622	0.8176	1030	430	86.7	192.6
8	15	A-2-5	0.3829	0.0369	0.3639	0.7837	8290	7210	19.3	86.3
4	10	A-6 (18 ksi)	0.406	0.052	0.3334	0.7914	1500	713	90.8	247.9
8	10	A-6	0.366	0.0283	0.2551	0.6494	8200	7070	26.2	102.1
4	12	A-6	0.4065	0.0575	0.3115	0.7755	1250	568	90	236.3
8	12	A-6	0.3021	0.0304	0.2408	0.5733	7870	6630	23.7	97.4
4	15	A-6	0.4057	0.0653	0.2762	0.7472	1030	443	89.2	226.6
8	15	A-6	0.3735	0.0365	0.2247	0.6347	7750	6440	23.5	100.9
4	10	A-7-6 (8 ksi)	0.4749	0.0556	0.3692	0.8997	1300	588	93	307.3
8	10	A-7-6	0.3531	0.03	0.2714	0.6545	6080	4300	33.3	116.1
4	12	A-7-6	0.4758	0.0608	0.3406	0.8772	903	376	91.9	281.2
8	12	A-7-6	0.3593	0.0335	0.2556	0.6484	5480	3610	30.3	114.6
4	15	A-7-6	0.4766	0.0685	0.2962	0.8413	615	231	90.6	259.2
8	15	A-7-6	0.3672	0.0384	0.2338	0.6394	5000	3060	27.1	113.1

TABLE C2 The Analysis Results of Asphalt Pavement with Binder Grade of PG58-28, Base Layer with Modulus of 38.0 ksi in Houston Under AADT of 3000

Thickness (in)		Material	Rutting (in)				Longitudinal Cracking(ft/mi)		Alligator Cracking (%)	IRI(in/mi)
HMA	Base	Subgrade	HMA	Base	Subgrade	Total	Surface	Depth=0.5	Bottom up cracking	
4	10	A-2-5 (28 ksi)	0.4137	0.0524	0.3131	0.7792	1280	576	88.5	205.9
8	10	A-2-5	0.3107	0.0271	0.2406	0.5784	8550	7590	20.3	83.4
4	12	A-2-5	0.4143	0.0583	0.4149	0.8875	1230	545	88.5	205.2
8	12	A-2-5	0.3114	0.0304	0.3842	0.726	8500	7530	20.2	83.3
4	15	A-2-5	0.4122	0.0661	0.2629	0.7412	1170	508	88.3	204.2
8	15	A-2-5	0.4468	0.0378	0.3663	0.8509	8580	7600	23	87.1
4	10	A-6 (18 ksi)	0.4106	0.0515	0.3372	0.7993	1700	816	92.4	276.7
8	10	A-6	0.2971	0.0265	0.2553	0.5789	8330	7260	27.5	99.1
4	12	A-6	0.4108	0.0571	0.3155	0.7834	1450	671	91.8	264.4
8	12	A-6	0.2997	0.0298	0.2429	0.5724	8160	7020	26.2	98.6
4	15	A-6	0.4092	0.065	0.2799	0.7541	1220	535	91.1	252
8	15	A-6	0.3028	0.0345	0.2258	0.5631	7990	6770	24.8	97.9
4	10	A-7-6 (8 ksi)	0.4816	0.0549	0.3743	0.9108	1530	707	94.4	347.7
8	10	A-7-6	0.3505	0.0293	0.274	0.6538	6600	4900	36.5	117.9
4	12	A-7-6	0.4818	0.0602	0.346	0.888	1110	473	93.5	318.4
8	12	A-7-6	0.3563	0.0327	0.2586	0.6476	6100	4290	33.6	116.3
4	15	A-7-6	0.4814	0.068	0.3014	0.8508	778	302	92.4	291.3
8	15	A-7-6	0.3639	0.0376	0.2371	0.6386	5680	3760	30.3	114.6

TABLE C3 The Analysis Results of Asphalt Pavement with Binder Grade of PG58-28, Base Layer with Modulus of 35.0 ksi in Houston Under AADT of 3000

Thickness (in)		Material	Rutting (in)				Longitudinal Cracking(ft/mi)		Alligator Cracking (%)	IRI(in/mi)
HMA	Base	Subgrade	HMA	Base	Subgrade	Total	Surface	Depth=0.5	Bottom up cracking	
4	10	A-2-5 (28 ksi)	0.4962	0.0538	0.3164	0.8664	1470	662	91.1	243.1

TABLE C3 Continued

8	10	A-2-5	0.3759	0.0279	0.2428	0.6466	8830	7970	24.3	88.3
4	12	A-2-5	0.4182	0.0583	0.4174	0.8939	1440	651	90.7	234
8	12	A-2-5	0.3088	0.0301	0.3834	0.7223	8750	7870	22.8	84.3
4	15	A-2-5	0.493	0.0682	0.2651	0.8263	1410	621	91.1	243.6
8	15	A-2-5	0.3766	0.0362	0.3631	0.7759	8800	7920	24.4	88.3
4	10	A-6 (18 ksi)	0.4145	0.0513	0.34	0.8058	1890	912	93.5	304.3
8	10	A-6	0.3611	0.0273	0.2586	0.647	8640	7680	31.3	104.5
4	12	A-6	0.4146	0.057	0.3185	0.7901	1650	769	93	291.7
8	12	A-6	0.2976	0.0294	0.2447	0.5717	8390	7320	28.5	99.6
4	15	A-6	0.4128	0.0651	0.2832	0.7611	1420	636	92.5	279.6
8	15	A-6	0.3673	0.0356	0.2291	0.632	8360	7260	28.9	103.3
4	10	A-7-6 (8 ksi)	0.4872	0.0545	0.3786	0.9203	1750	822	95.3	388.8
8	10	A-7-6	0.348	0.0286	0.2762	0.6528	7010	5400	39.3	119.6
4	12	A-7-6	0.487	0.0599	0.3507	0.8976	1310	573	94.6	355
8	12	A-7-6	0.3535	0.0321	0.2611	0.6467	6610	4870	36.5	117.9
4	15	A-7-6	0.4859	0.0679	0.3063	0.8601	959	383	93.7	326.4
8	15	A-7-6	0.3606	0.0371	0.24	0.6377	6260	4410	33.4	116.2

TABLE C4 The Analysis Results of Asphalt Pavement with Binder Grade of PG58-28, Base Layer with Modulus of 31.5 ksi in Houston Under AADT of 3000

Thickness (in)		Material	Rutting (in)				Longitudinal Cracking(ft/mi)		Alligator Cracking (%)	IRI(in/mi)
HMA	Base	Subgrade	HMA	Base	Subgrade	Total	Surface	Depth=0.5	Bottom up cracking	
4	10	A-2-5 (28 ksi)	0.4213	0.0519	0.3181	0.7913	1660	764	92.3	261.6
8	10	A-2-5	0.3061	0.0261	0.2424	0.5746	8930	8130	25.1	85.3
4	12	A-2-5	0.4216	0.0581	0.4216	0.9013	1650	758	92.3	263
8	12	A-2-5	0.3061	0.0295	0.3866	0.7222	8930	8120	25.1	85.3

TABLE C4 Continued

4	15	A-2-5	0.4194	0.0662	0.2674	0.753	1640	749	92.4	264.2
8	15	A-2-5	0.4382	0.037	0.3692	0.8444	9070	8300	29.5	90
4	10	A-6 (18 ksi)	0.4195	0.0507	0.3437	0.8139	2120	1040	94.6	343.3
8	10	A-6	0.2931	0.0254	0.2586	0.5771	8710	7790	32.2	101.4
4	12	A-6	0.4195	0.0566	0.3224	0.7985	1900	901	94.3	329.2
8	12	A-6	0.2951	0.0288	0.2468	0.5707	8620	7640	31.2	100.9
4	15	A-6	0.4173	0.0647	0.2873	0.7693	1680	770	93.9	316.2
8	15	A-6	0.2974	0.0334	0.2303	0.5611	8520	7500	29.9	100.3
4	10	A-7-6 (8 ksi)	0.4949	0.0537	0.3838	0.9324	2040	1000	96.2	444.5
8	10	A-7-6	0.3453	0.0278	0.2789	0.652	7450	5950	42.6	121.8
4	12	A-7-6	0.4941	0.0592	0.3562	0.9095	1580	709	95.6	408.2
8	12	A-7-6	0.3504	0.0312	0.2641	0.6457	7120	5500	40	120
4	15	A-7-6	0.4921	0.0673	0.3119	0.8713	1200	495	95	374.3
8	15	A-7-6	0.357	0.0362	0.2434	0.6366	6840	5110	36.9	118.1

TABLE C5 The Analysis Results of Asphalt Pavement with Binder Grade of PG58-28, Base Layer with Modulus of 28.0 ksi in Houston Under AADT of 3000

Thickness (in)		Material	Rutting (in)				Longitudinal Cracking(ft/mi)		Alligator Cracking (%)	IRI(in/mi)
HMA	Base	Subgrade	HMA	Base	Subgrade	Total	Surface	Depth=0.5	Bottom up cracking	
4	10	A-2-5 (28 ksi)	0.4254	0.0515	0.3214	0.7983	1890	882	93.7	296.9
8	10	A-2-5	0.3034	0.0256	0.2439	0.5729	9090	8360	27.7	86.5
4	12	A-2-5	0.4257	0.0577	0.4261	0.9095	1910	894	93.8	300.3
8	12	A-2-5	0.3032	0.029	0.39	0.7222	9100	8370	27.9	86.5
4	15	A-2-5	0.4234	0.0659	0.2708	0.7601	1930	904	93.9	303.4
8	15	A-2-5	0.4334	0.0364	0.3733	0.8431	9260	8580	33	91.8
4	10	A-6 (18 ksi)	0.4254	0.0501	0.3477	0.8232	2400	1190	95.6	389.2
8	10	A-6	0.3554	0.026	0.2626	0.644	9020	8230	37.4	107.8

TABLE C5 Continued

4	12	A-6	0.4252	0.0561	0.3267	0.808	2200	1070	95.3	377.1
8	12	A-6	0.2923	0.0281	0.2491	0.5695	8830	7950	34.2	102.5
4	15	A-6	0.4227	0.0642	0.2918	0.7787	1990	941	95.1	362.6
8	15	A-6	0.36	0.0342	0.2344	0.6286	8870	8000	35.4	106.7
4	10	A-7-6 (8 ksi)	0.5039	0.0528	0.3894	0.9461	2380	1160	96.9	517
8	10	A-7-6	0.3422	0.0269	0.2817	0.6508	7850	6500	46.1	124.4
4	12	A-7-6	0.5024	0.0584	0.3622	0.923	1920	883	96.5	473.5
8	12	A-7-6	0.3469	0.0303	0.2674	0.6446	7600	6130	43.7	122.6
4	15	A-7-6	0.4995	0.0666	0.3182	0.8843	1510	647	96	434.8
8	15	A-7-6	0.3531	0.0352	0.2472	0.6355	7390	5820	40.8	120.6

TABLE C6 The Analysis Results of Asphalt Pavement with Binder Grade of PG76-22, Base Layer with Modulus of 42.0 ksi in Houston Under AADT of 3000

Thickness (in)		Material	Rutting (in)				Longitudinal Cracking(ft/mi)		Alligator Cracking (%)	IRI(in/mi)
HMA	Base	Subgrade	HMA	Base	Subgrade	Total	Surface	Depth=0.5	Bottom up cracking	
4	10	A-2-5 (28ksi)	0.2758	0.0479	0.3072	0.6309	1850	916	92.9	275.9
8	10	A-2-5	0.1988	0.0234	0.2323	0.4545	8770	7930	25.6	85.5
4	15	A-2-5	0.2752	0.061	0.2588	0.595	1630	779	92.6	268.8
8	15	A-2-5	0.1999	0.0307	0.3559	0.5865	8690	7810	25.2	85.4
4	10	A-6 (18ksi)	0.2733	0.0473	0.3294	0.65	2350	1210	95.3	372.3
8	10	A-6	0.1858	0.023	0.2462	0.455	8290	7250	33.8	102.3
4	15	A-6	0.2724	0.0601	0.2736	0.6061	1690	804	94.3	333.6
8	15	A-6	0.1907	0.0303	0.2186	0.4396	8050	6890	30.6	100.6
4	10	A-7-6 (8ksi)	0.3142	0.0507	0.3648	0.7297	2030	1000	96.6	485.6
8	10	A-7-6	0.2113	0.0257	0.2635	0.5005	5960	4230	45.5	124
4	12	A-7-6	0.3128	0.0558	0.337	0.7056	1510	686	96	434.8
8	12	A-7-6	0.216	0.0289	0.249	0.4939	5590	3790	42.2	121.5
4	15	A-7-6	0.3104	0.0632	0.2933	0.6669	1090	452	95.3	391.3

TABLE C7 The Analysis Results of Asphalt Pavement with Binder Grade of PG76-22, Base Layer with Modulus of 38.0 ksi in Houston Under AADT of 3000

Thickness (in)		Material	Rutting (in)				Longitudinal Cracking(ft/mi)		Alligator Cracking (%)	IRI(in/mi)
HMA	Base	Subgrade	HMA	Base	Subgrade	Total	Surface	Depth=0.5	Bottom up cracking	
4	10	A-7-6 (8ksi)	0.3199	0.0499	0.3697	0.7395	2350	1180	97.2	550.9
8	10	A-7-6	0.2095	0.0249	0.2658	0.5002	6410	4730	48.3	126.2
4	12	A-7-6	0.318	0.055	0.3422	0.7152	1810	847	96.7	495.3
8	12	A-7-6	0.2138	0.0281	0.2517	0.4936	6110	4360	45.2	123.7
4	15	A-7-6	0.3148	0.0625	0.2985	0.6758	1340	579	96.1	442.1
8	15	A-7-6	0.2195	0.0326	0.2318	0.4839	5940	4120	41.5	121

TABLE C8 The Analysis Results of Asphalt Pavement with Binder Grade of PG76-22, Base Layer with Modulus of 35.0 ksi in Houston Under AADT of 3000

Thickness (in)		Material	Rutting (in)				Longitudinal Cracking(ft/mi)		Alligator Cracking (%)	IRI(in/mi)
HMA	Base	Subgrade	HMA	Base	Subgrade	Total	Surface	Depth=0.5	Bottom up cracking	
4	10	A-2-5 (28ksi)	0.2812	0.0474	0.3104	0.639	2300	1160	94.9	342.6
8	10	A-2-5	0.1958	0.0226	0.2335	0.4519	9060	8340	29.7	87.4
4	15	A-2-5	0.2808	0.0609	0.2614	0.6031	2200	1100	94.9	342.6
8	15	A-2-5	0.1963	0.0298	0.3547	0.5808	9040	8310	29.6	87.4
4	10	A-6 (18ksi)	0.2802	0.0464	0.3355	0.6621	2860	1520	96.5	459.4
8	10	A-6	0.183	0.022	0.2491	0.4541	8630	7710	38	104.7
4	15	A-6	0.2785	0.0596	0.2805	0.6186	2250	1120	96	415.8
8	15	A-6	0.187	0.0293	0.2227	0.439	8480	7480	35.3	103.1
4	10	A-7-6 (8ksi)	0.3249	0.0493	0.3739	0.7481	2640	1350	97.6	618.7
8	10	A-7-6	0.2078	0.0243	0.2678	0.4999	6760	5160	50.6	128.3
4	12	A-7-6	0.3225	0.0546	0.3468	0.7239	2100	1000	97.3	555.8
8	12	A-7-6	0.2118	0.0275	0.254	0.4933	6520	4840	47.7	125.7

TABLE C9 The Analysis Results of Asphalt Pavement with Binder Grade of PG76-22, Base Layer with Modulus of 31.5 ksi in Houston Under AADT of 3000

Thickness (in)		Material	Rutting (in)				Longitudinal Cracking(ft/mi)		Alligator Cracking (%)	IRI(in/mi)
HMA	Base	Subgrade	HMA	Base	Subgrade	Total	Surface	Depth=0.5	Bottom up cracking	
4	10	A-7-6 (8ksi)	0.3312	0.0484	0.3788	0.7584	3000	1580	98	703.3
8	10	A-7-6	0.2059	0.0235	0.2701	0.4995	7140	5630	53.3	703.3
4	12	A-7-6	0.3285	0.0537	0.3521	0.7343	2460	1220	97.7	703.3
8	12	A-7-6	0.2096	0.0266	0.2568	0.493	6950	5360	50.6	128.3
4	15	A-7-6	0.3246	0.0615	0.3088	0.6949	1970	908	97.4	572.7
8	15	A-7-6	0.2145	0.0312	0.2377	0.4834	6860	5220	47.5	125.5

TABLE C10 The Analysis Results of Asphalt Pavement with Binder Grade of PG76-22, Base Layer with Modulus of 28.0 ksi in Houston Under AADT of 3000

Thickness (in)		Material	Rutting (in)				Longitudinal Cracking(ft/mi)		Alligator Cracking (%)	IRI(in/mi)
HMA	Base	Subgrade	HMA	Base	Subgrade	Total	Surface	Depth=0.5	Bottom up cracking	
4	10	A-7-6 (8ksi)	0.3384	0.0474	0.3841	0.7699	3420	1850	98.4	812.2
8	10	A-7-6	0.2039	0.0226	0.2726	0.4991	7500	6090	56	133.8
4	12	A-7-6	0.3353	0.0528	0.3579	0.746	2890	1480	98.2	737.2
8	12	A-7-6	0.2073	0.0257	0.2596	0.4926	7360	5880	53.7	131.2
4	15	A-7-6	0.331	0.0606	0.3149	0.7065	2390	1150	97.9	667
8	15	A-7-6	0.2118	0.0302	0.2411	0.4831	7300	5780	50.8	128.3
4	10	A-2-5	0.2876	0.0466	0.3161	0.6503	2860	1500	96.4	434.6
8	10	A-2-5	0.1923	0.0216	0.2361	0.45	9290	8660	34.1	89.7
4	15	A-2-5	0.2873	0.0601	0.2676	0.615	2910	1530	96.5	444.2
8	15	A-2-5	0.1919	0.0287	0.3618	0.5824	9300	8690	34.7	90
4	10	A-6 (18ksi)	0.289	0.0451	0.3427	0.6768	3510	1940	97.5	585.2
8	10	A-6	0.1799	0.0208	0.2525	0.4532	8930	8130	42.7	107.7
4	15	A-6	0.2865	0.0585	0.2887	0.6337	3020	1590	97.2	539.2

TABLE C11 The Analysis Results of Asphalt Pavement with Binder Grade of PG76-22 in New York City Under AADT of 3000

Thickness (in)		Material		Rutting (in)				Longitudinal Cracking(ft/mi)		Alligator Cracking (%)	
HMA	Base	Base	Subgrade	HMA	Base	Subgrade	Total	Surface	Depth=0.5	Bottom up cracking	IRI(in/mi)
4	10	A-1-a (42ksi)	A-7-6	0.135	0.0506	0.3116	0.4972	568	249	82.5	210.8
4	10	A-1-a	A-7-6	0.135	0.0506	0.3116	0.4972	568	249	82.5	210.8
8	10	A-1-a	A-7-6	0.097	0.0266	0.2276	0.3512	1340	589	17.3	129.7
4	15	A-1-a	A-7-6	0.1353	0.0622	0.2508	0.4483	231	86	75	183.7
4	15	A-1-a	A-6	0.1396	0.059	0.2405	0.4391	544	240	73.1	165.4
4	15	A-1-a	A-7-6	0.1353	0.0622	0.2508	0.4483	231	86	75	183.7
4	10	A-1-b (38ksi)	A-7-6	0.1396	0.0493	0.3243	0.5132	771	347	86.8	237.9
8	10	A-1-b	A-7-6	0.0963	0.0251	0.2337	0.3551	2000	1000	21.1	131.1
4	10	A-2-4 (35.0ksi)	A-7-6	0.1548	0.0462	0.3439	0.5449	1430	683	92.9	323.3
4	10	A-2-4	A-7-6	0.1548	0.0462	0.3439	0.5449	1430	683	92.9	323.3
8	10	A-2-4	A-7-6	0.0945	0.0221	0.2409	0.3575	3210	1870	27.4	133.8
4	15	A-2-4	A-7-6	0.1523	0.0566	0.2782	0.4871	850	366	90.2	273.5
4	15	A-2-4	A-6	0.1522	0.0545	0.2612	0.4679	1410	684	88.5	240.2
4	15	A-2-4	A-7-6	0.1523	0.0566	0.2782	0.4871	850	366	90.2	273.5
4	10	A-2-4(31.5 ksi)	A-7-6	0.1582	0.0452	0.3485	0.5519	1670	816	94	355.7
8	10	A-2-4	A-7-6	0.0935	0.0213	0.2429	0.3577	3630	2220	29.5	134.8
4	10	A-2-5 (28ksi)	A-7-6	0.1621	0.044	0.3535	0.5596	1960	1000	95	397.3
4	10	A-2-5	A-7-6	0.1621	0.044	0.3535	0.5596	1960	1000	95	397.3
8	10	A-2-5	A-7-6	0.0924	0.0204	0.2451	0.3579	4080	2610	31.8	135.9
4	15	A-2-5	A-7-6	0.1585	0.0548	0.2894	0.5027	1300	588	93.3	334.9
4	15	A-2-5	A-6	0.1567	0.0531	0.2693	0.4791	1930	1000	92	289
4	15	A-2-5	A-7-6	0.1585	0.0548	0.2894	0.5027	1300	588	93.3	334.9

TABLE C12 The Analysis Results of Asphalt Pavement with Binder Grade of PG58-28 in New York City Under AADT of 3000

Thickness (in)		Material		Rutting (in)				Longitudinal Cracking(ft/mi)		Alligator Cracking (%)	
HMA	Base	Base	Subgrade	HMA	Base	Subgrade	Total	Surface	Depth=0.5	Bottom up cracking	IRI(in/mi)
4	15	A-1-a	A-7-6	0.2116	0.066	0.2513	0.5289	126	46	55	152.5
4	15	A-2-4 (35.0ksi)	A-7-6	0.2328	0.061	0.2784	0.5722	469	187	80.5	201.6
4	15	A-2-5	A-7-6	0.24	0.0594	0.2895	0.5889	746	310	86.9	238.1
4	15	A-1-a	A-6	0.215	0.063	0.2411	0.5191	315	133	53	137.1
4	15	A-2-4 (35.0ksi)	A-6	0.2362	0.0591	0.2618	0.5571	834	376	78.2	179.4
4	15	A-2-5	A-6	0.2414	0.0579	0.27	0.5693	1170	543	84.8	209.7

TABLE C13 The Analysis Results of Asphalt Pavement with Binder Grade of PG76-22 in Washington State Under AADT of 3000

Thickness (in)		Material		Rutting(in)				Longitudinal Cracking(ft/mi)		Alligator Cracking (%)	
HMA	Base	Base	Subgrade	HMA	Base	Subgrade	Total	Surface	Depth=0.5	Bottom up cracking	IRI (in/mi)
4	10	A-1-a (42ksi)	A-7-6	0.1804	0.0529	0.3047	0.538	582	259	82.4	180.7
8	10	A-1-a	A-7-6	0.1511	0.0288	0.2203	0.4002	2080	1000	17.5	100.3
4	15	A-1-a	A-7-6	0.186	0.0648	0.2507	0.5015	225	83.8	75.2	155
8	15	A-1-a	A-7-6	0.16	0.0369	0.1952	0.3921	926	305	12.1	98.4
4	10	A-1-b	A-7-6	0.1821	0.0521	0.3109	0.5451	714	324	85.4	198.3
8	10	A-1-b	A-7-6	0.1485	0.0281	0.2225	0.3991	2360	1220	19.1	100.9
4	15	A-1-a	A-6	0.2013	0.0622	0.2395	0.503	536	236	74.2	150.5
4	10	A-1-a	A-6	0.1967	0.0499	0.2953	0.5419	928	449	78.8	164.1
8	10	A-1-a	A-6	0.1631	0.0265	0.2213	0.4109	5320	3890	12.4	96.9
4	10	A-1-b	A-6	0.1978	0.0493	0.2991	0.5462	1070	523	82.1	177.6

TABLE C13 Continued

4	10	A-2-4 (35.0ksi)	A-7-6	0.2021	0.0497	0.3447	0.5965	1390	674	93.1	299.9
8	10	A-2-4	A-7-6	0.1476	0.0248	0.2412	0.4136	4260	2750	29.3	105.3
4	15	A-2-4	A-7-6	0.2028	0.0605	0.2784	0.5417	811	349	90.5	252
4	15	A-2-4	A-6	0.2123	0.0587	0.2616	0.5326	1370	659	89.3	231.8
4	10	A-2-4	A-6	0.2106	0.0473	0.3139	0.5718	1860	957	91	255.5
4	10	A-2-4(31.5 ksi)	A-7-6	0.2053	0.0488	0.3494	0.6035	1630	805	94.3	335.7
8	10	A-2-4	A-7-6	0.1458	0.0239	0.2433	0.413	4810	3270	31.9	106.5
4	10	A-2-5 (28ksi)	A-7-6	0.2091	0.0477	0.3544	0.6112	1920	1000	95.3	382.4
8	10	A-2-5	A-7-6	0.1438	0.0229	0.2456	0.4123	5380	3840	34.7	108
4	15	A-2-5	A-7-6	0.2077	0.0588	0.2895	0.556	1230	558	93.7	316.1
4	15	A-2-5	A-6	0.2155	0.0575	0.2697	0.5427	1860	933	92.8	289.1
4	10	A-2-5	A-6	0.2149	0.0459	0.321	0.5818	2330	1230	93.7	315.5
8	10	A-2-5	A-6	0.1557	0.0216	0.2344	0.4117	7890	6830	26	102.1

TABLE C14 The Analysis Results of Asphalt Pavement with Binder Grade of PG58-28 in Washington State Under AADT of 3000

Thickness (in)		Material		Rutting(in)				Longitudinal Cracking(ft/mi)		Alligator Cracking(%)	
HMA	Base	Base	Subgrade	HMA	Base	Subgrade	Total	Surface	Depth=0.5	Bottom up cracking	IRI(in/mi)
4	15	A-2-5	A-7-6	0.342	0.0642	0.2898	0.696	691	285	87	209.2
4	15	A-1-a	A-7-6	0.3154	0.069	0.2515	0.6359	122	43.8	53.6	121.9
4	15	A-2-4	A-7-6	0.3382	0.0656	0.2787	0.6825	437	174	80.1	170.5

TABLE C15 The Analysis Results of Asphalt Pavement with Binder Grade of PG76-22 in Houston City Under AADT of 1500

Thickness (in)		Material		Rutting(in)				Longitudinal Cracking(ft/mi)		Alligator Cracking(%)	IRI (in/mi)
HMA	Base	Base	Subgrade	HMA	Base	Subgrade	Total	Surface	Depth=0.5	Bottom up cracking	
4	10	A-1-a (42ksi)	A-7-6	0.1978	0.0455	0.2853	0.5286	1430	678	92.3	286.1
4	15	A-1-a	A-7-6	0.194	0.0569	0.2292	0.4801	751	307	89.4	239.5
4	15	A-1-a	A-7-6	0.194	0.0569	0.2292	0.4801	751	307	89.4	239.5
4	10	A-1-a	A-7-6	0.1978	0.0455	0.2853	0.5286	1430	678	92.3	286.1
4	15	A-1-a	A-6	0.1955	0.0553	0.2389	0.4897	1170	542	87.7	210.9
4	10	A-2-4 (35.0ksi)	A-7-6	0.2051	0.0439	0.2924	0.5414	1900	931	94.5	348.8
4	15	A-2-4	A-6	0.1999	0.0546	0.2449	0.4994	1590	763	91	252
4	15	A-2-4	A-7-6	0.2005	0.0557	0.2371	0.4933	1140	492	92.5	291.2
4	15	A-2-4	A-7-6	0.2005	0.0557	0.2371	0.4933	1140	492	92.5	291.2
4	10	A-2-4	A-7-6	0.2051	0.0439	0.2924	0.5414	1900	931	94.5	348.8
4	15	A-2-5 (28ksi)	A-6	0.2057	0.0531	0.2522	0.511	2200	1100	93.8	314.5
4	15	A-2-5	A-7-6	0.2087	0.0537	0.2463	0.5087	1720	794	95	370.6
4	10	A-2-5	A-7-6	0.2143	0.0418	0.3004	0.5565	2520	1290	96.2	438.3
4	10	A-2-5	A-7-6	0.2143	0.0418	0.3004	0.5565	2520	1290	96.2	438.3
4	15	A-2-5	A-7-6	0.2087	0.0537	0.2463	0.5087	1720	794	95	370.6

TABLE C16 The Analysis Results of Asphalt Pavement with Binder Grade of PG76-22 in Houston City Under AADT of 5000

Thickness (in)		Material		Rutting(in)				Longitudinal Cracking(ft/mi)		Alligator Cracking(%)	
HMA	Base	Base	Subgrade	HMA	Base	Subgrade	Total	Surface	Depth=0.5	Bottom up cracking	IRI(in/mi)
4	10	A-1-a (42ksi)	A-7-6 (8ksi)	0.3519	0.0525	0.4315	0.8359	2600	1320	98.1	721.4
4	15	A-1-a	A-7-6	0.3452	0.0656	0.3474	0.7582	1450	619	97.3	566.5
4	15	A-1-a	A-6 (18ksi)	0.3478	0.0638	0.3007	0.7123	2180	1070	96.9	495.7
4	15	A-1-a	A-7-6	0.3452	0.0656	0.3474	0.7582	1450	619	97.3	566.5

TABLE C16 Continued

8	10	A-1-a	A-7-6	0.2249	0.0262	0.3116	0.5627	6300	4530	57.7	132
4	10	A-1-a	A-7-6	0.3519	0.0525	0.4315	0.8359	2600	1320	98.1	721.4
4	10	A-1-b (38ksi)	A-7-6	0.3589	0.0517	0.4373	0.8479	2970	1550	98.5	827.8
4	10	A-2-4 (35.0ksi)	A-7-6	0.3649	0.0511	0.4422	0.8582	3310	1770	98.7	929.4
8	10	A-2-4	A-7-6	0.2212	0.0249	0.3166	0.5627	7050	5440	62.4	138.6
4	15	A-2-4	A-7-6	0.3567	0.0648	0.3592	0.7807	2120	1000	98.2	738.3
4	15	A-2-4	A-6	0.3556	0.0635	0.3082	0.7273	2850	1470	97.8	631.1
4	15	A-2-4	A-7-6	0.3567	0.0648	0.3592	0.7807	2120	1000	98.2	738.3
4	10	A-2-4	A-7-6	0.3649	0.0511	0.4422	0.8582	3310	1770	98.7	929.4
4	10	A-2-4(31.5 ksi)	A-7-6	0.3726	0.0503	0.4479	0.8708	3720	2040	98.9	1064.9
4	10	A-2-5 (28ksi)	A-7-6	0.3812	0.0493	0.4541	0.8846	4170	2370	100	1231.8
8	10	A-2-5	A-7-6	0.2171	0.0232	0.3222	0.5625	7720	6320	67.1	146.6
4	15	A-2-5	A-7-6	0.3712	0.0634	0.3729	0.8075	3040	1530	98.8	999.6
4	15	A-2-5	A-6	0.3659	0.0626	0.3173	0.7458	3730	2060	98.5	839.2
4	15	A-2-5	A-7-6	0.3712	0.0634	0.3729	0.8075	3040	1530	98.8	999.6
4	10	A-2-5	A-7-6	0.3812	0.0493	0.4541	0.8846	4170	2370	100	1231.8

VITA

Sanaa Ahmad Masad was born in Kuwait on January 20, 1978. She received her Bachelor of Science in Civil Engineering from Jordan University of Science and Technology in June 2001. She worked as an engineer for Al-Zoabe Construction Company in Irbid, Jordan from August of 2001 to August of 2002. She started her Master of Science program in civil engineering at Washington State University in August 2002 and transferred to Texas A&M University in January 2003. Her permanent address is:

Sanaa Masad

Irbid-Jordan

Tel: 02 7 250 129